Findings from

retinal optical coherence tomography

in a large cohort, UK Biobank

Thesis submitted for degree of

Doctor of Philosophy at UCL

Fang Ko, MD

Supervisors

Professor Paul Foster

Mr Nicholas Strouthidis

Institutions

Institute of Ophthalmology, University College of London, London, UK

Moorfields Eye Hospital, London UK

SECTION I:

OVERVIEW

1.1 Declaration

I, Fang Ko, confirm that the work presented in this thesis is my own. Where information has been derived from other sources, I confirm that this has been indicated in the thesis.

Fang Ko, 3 March 2019

1.2 Abstract

Background: UK Biobank is a large prospective multi-center community-based study, which included macular optical coherence tomography (OCT) of 67,321 people. OCT is a mainstay of ophthalmic imaging and is a potential screening test for dementia.

Aim of research: Cross-sectional analysis examined retinal layers, to determine the range of findings in normal individuals, as well as describe associations with demographic and physiologic variation. Longitudinal analysis assessed associations with not only current cognitive function, but future cognitive decline.

Results: All layers showed progressive thinning with older age. As compared to white people, black ethnicity was associated with significantly thicker retinal pigment epithelium (RPE) (+3.35 µm; $p<0.001$), but thinner photoreceptor inner segment-outer segment (IS-OS), ganglion cell layer-inner plexiform layer complex (GCL-IPL), and macular retinal nerve fibre layer (mRNFL) (-3.76 µm, -4.29 µm, and -3.97 µm, respectively; $p<0.001$). Higher intraocular pressure was associated with thinner RPE (-0.04 µm per mmHg, $p<0.001$), but was not significant at GCL-IPL or mRNFL. Higher body mass index was associated with thinner photoreceptor IS-OS (-0.12 µm per kg/m^2, $p<0.001$). Asian and Chinese ethnicity, refractive error, height, sex, smoking, and blood pressure showed mixed results.

Socioeconomic deprivation, educational levels, and cognitive function were examined for GCL-IPL and mRNFL. Socioeconomic deprivation was associated with significantly

thinner GCL-IPL, but was not significant at mRNFL. In contrast, lower education was significantly associated with thinner mRNFL but was not significant at GCL-IPL. Thinner mRNFL was associated with worse baseline cognitive performance. Follow-up cognitive tests were performed for 1251 participants. Participants with mRNFL thickness in the two thinnest quintiles were almost twice as likely to have at least one test score worse at follow-up cognitive testing (quintile 1: odds ratio (OR) 1.92, 95% CI: 1.29, 2.85, $p<0.001$, quintile 2: OR: 2.08, 95% CI: 1.40, 3.08, $P< 0.001$). While there were some associations between GCL-IPL and baseline cognitive function, no association was detected for risk of future cognitive decline.

Significance: Retinal thickness is variable and dynamic. This work will inform interpretation of both past and future research, as physiologic and demographic variation is associated with thickness of each layer. Of note, I show an association between IOP and RPE but not mRNFL. Further, thinner mRNFL is associated with greater likelihood of cognitive decline in the future. These observations have implications for future research, as well as prevention and treatment of dementia.

1.3 Impact

This body of work represents a detailed exploration of retinal sub-layer thickness and its associations using OCT imaging from subjects recruited to UK Biobank, probably the largest database of its kind.

In the RPE, there is surprisingly little published normal data. A literature review showed histological studies with fewer than 100 eyes (Okubo et al 1999, Ramrattan RS et al 1994, Curcio C et al 2011). In vivo OCT studies have included fewer than 200 people (Karampelas M et al 2013, Kenmochi et al 2017, Demirkaya et al 2013). My results show that basic demographics such as ethnicity are significantly associated with differences in RPE thickness. This research suggests that differences in ethnicity need to be carefully considered in future work measuring RPE thickness. Further, there was an unexpected association between higher IOP and thinner RPE. Whether this is a statistical association or carries aetiological significance is unclear, but it is certainly novel, interesting and warrants further exploration.

In reviewing older literature, one may be surprised by published studies that have failed to take basic demographics into account. For instance, little has been described regarding the interaction between photoreceptor layer thickness and ethnicity. Results of the current study show significant differences among Chinese and blacks, with photoreceptor thickness at central subfield 1.84 µm thicker among Chinese as compared to whites, and -3.76 µm thinner among blacks as compared to whites, after controlling

for potential confounders. Future work should take this into account, and one may keep this in mind in critical re-interpretation of older work.

No previously published data were identified detailing an association between BMI and photoreceptor thickness. UK Biobank data show a negative association between BMI and photoreceptor thickness. The trend was visible even at “normal” BMI. One wonders whether weight control may have a generalized positive effect on photoreceptor thickness, and may be a potentially modifiable risk factor, to counteract the effects of thinning with older age.

RNFL and GCL-IPL have been more well-studied. Whilst there were clear associations with demographic and physiological variables, of more interest were the links with cognitive function. Results for GCL-IPL suggested possible association with cognitive function, but baseline results did not appear to predict future cognitive function. In contrast, RNFL showed not only an association with baseline cognitive performance, but also with future cognitive decline. At the time of the analysis, this finding appeared unique, especially as it was in a community cohort with no relevant reported disease. Part of the ability to detect an association may be due to the use of individual cognitive function tests, rather than a reliance on a battery of tests such as mini-mental status examination, which may be less sensitive in healthy individuals and early disease. This is a novel finding which may guide future research, with use of methodology that may aid development of future studies.

1.4 Table of Contents

1 SECTION I: OVERVIEW 2

1.1 Declaration 3

1.2 Abstract 4

1.3 Impact 6

1.4 Table of Contents 8

1.5 List of Figures 12

1.6 List of Tables 19

1.7 List of Abbreviations 23

1.8 Supporting Publications 25

1.9 Supporting Presentations 26

1.10 Acknowledgements 27

2 SECTION II: INTRODUCTION 28

2.1 UK Biobank 29

2.1.1 Purpose of UK Biobank 29

2.1.2 Structure and Timeline 30

2.1.3 Repeat Assessments 33

2.1.4 Ophthalmic Testing and Quality Control 34

2.1.5 Published work produced from UK Biobank resource 38

2.2 Optical Coherence Tomography 41

2.2.1 Imaging modality 41

2.2.2 Automated segmentation 44

2.3 Retinal Anatomy and Function 47

2.3.1 Retinal Layers 47

2.3.2 Retinal Pigment Epithelium 49

2.3.3 Photoreceptors 54

2.3.4 Outer Plexiform Layer and Inner Nuclear Layer 58

2.3.5 Ganglion Cell Layer and Inner Plexiform Layer 59

2.3.6 Retinal Nerve Fibre Layer 63

2.4 Cognitive Function 69

2.6 Plan of Research 74

3 SECTION III: MATERIALS AND METHODS 76

3.1 UK Biobank 77

3.2 Inclusion and Exclusion Criteria 79

3.3 Eye measures and OCT Imaging Protocol 82

3.4 Analysis of Macular Thickness 83

3.5 Manual re-grading 85

3.6 Cognitive Function 88

3.7 Statistical Analysis 93

4 SECTION IV: RESULTS 97

4.1 Retinal Pigment Epithelium 98

4.1.1 Contributors to Study of Retinal Pigment Epithelium 98

4.1.2 Results 99

4.2 Photoreceptor Inner and Outer Segments 123

4.2.1 Contributors to Study of Photoreceptors 123

4.2.2 Results 123

4.3 Ganglion Cell Layer – Inner Plexiform Layer Complex 152

4.3.1 Contributors to Study of GCL-IPL 152

4.3.2 Results 152

4.4 Retinal Nerve Fibre Layer 176

4.4.1 Contributors to Study of Retinal Nerve Fibre Layer 176

4.4.2 Results 176

4.5 Cognitive Function, Ganglion Cell Layer – Inner Plexiform Layer Complex, and Retinal Nerve Fibre Layer 194

4.5.1 Contributors to Study of Cognitive Function 194

4.5.2 Results 195

4.5.2.1 GCL-IPL and Cognitive Function 195

4.5.3.2 RNFL and Cognitive Function 207

5 SECTION V: CONCLUSIONS 217

5.1 Discussion 218

5.1.1 Retinal Pigment Epithelium 218

5.1.2 Photoreceptor inner and outer segments 222

5.1.3 Ganglion Cell Layer – Inner Plexiform Layer Complex 227

5.1.4 Retinal Nerve Fibre Layer 231

5.1.5 Cognitive Function 236

5.1.5.1 GCL-IPL and Cognitive Function 236

5.1.5.2 RNFL and Cognitive Function 238

5.2 Summary 246

5.3 Future Work 250

6 SECTION VI: REFERENCES 253

1.5 List of Figures

2.1	Map of approved UK Biobank research projects in the UK and internationally.	30
2.2	Map of UK Biobank assessment centers.	31
2.3	Graph showing operational duration and tests performed at each UK Biobank assessment center.	32
2.4	General layout of UK Biobank assessment center.	33
2.5	Reproduction of retinal and optic disc OCT and histology from the first publication describing OCT (Huang et al 1991).	42
2.6	Example of spectral domain OCT image acquired as part of UK Biobank.	43
2.7	Example of automated two-step segmentation.	46
2.8	Basic diagram of macula and fovea relative to optic nerve and vascular arcades.	47
2.9	Retinal layers in histologic preparation.	48
2.10	Optical coherence tomography and automated segmentation of retinal pigment epithelium.	50
2.11	Optical coherence tomography and automated segmentation of photoreceptors.	55
2.12	Optical coherence tomography and automated segmentation of ganglion cell layer – inner plexiform layer complex.	60

2.13		Optical coherence tomography and automated segmentation of retinal nerve fibre layer.	65
2.14		Diagram of nerve fibre layer distribution at retina.	65
3.1		Inclusion/exclusion criteria for macular RNFL SDOCT.	80
3.2		Segmentation boundaries of retinal layers.	85
3.3	A	Manual re-grading algorithm for reviewing images after automated segmentation, as well as application of inclusion/exclusion criteria.	86
	B	Example of an image discarded because of poor segmentation due to low image quality.	87
	C	Example of an image that passed manual re-grading.	87
3.4		Screen shot of image shown during prospective memory test.	89
3.5		Example of a participant playing pairs game, showing results of a mis-match.	90
3.6		Example of a participant performing reaction time test, with matching cards.	92
3.7		Example of a scatter plot of age and RNFL thickness at outer nasal subfield.	94
4.1		RPE-BM inclusion/exclusion criteria.	101
4.2	A	Histogram of central RPE-BM thickness.	102
	B	RPE-BM thickness at different retinal subfields.	102
	C	RPE-BM thickness in women and men, at different retinal subfields.	103

4.3		Mean RPE-BM thickness by age.	104
4.4		Mean RPE-BM thickness by race.	106
4.5		Mean RPE-BM thickness by refraction.	107
4.6		Mean central RPE-BM thickness by ethnicity and refraction.	109
4.7		Mean RPE-BM thickness of subfields by ethnicity and refraction.	109
4.8		Mean RPE-BM thickness by IOP.	112
4.9	A	Mean of central RPE-BM thickness by systolic blood pressure.	115
	B	Mean of central RPE-BM thickness by diastolic blood pressure.	115
4.10	A	Mean central RPE-BM thickness by body mass index.	117
	B	Mean central RPE-BM thickness by body mass index and ethnicity.	117
4.11		Mean RPE-BM thickness by height.	118
4.12		Inclusion/exclusion criteria for macular photoreceptor inner and outer segment SDOCT.	124
4.13	A	Histogram of central photoreceptor thickness.	126
	B	Photoreceptor thickness at different locations.	126
	C-D	Macular RNFL thickness in C) women and D) men, at different retinal subfields.	127
4.14		Mean photoreceptor thickness at subfields, by age.	128
4.15		Mean photoreceptor thickness at subfields, by ethnicity.	131
4.16		Mean photoreceptor thickness at subfields, by intraocular pressure.	134
4.17		Mean photoreceptor thickness at subfields, by refraction.	137
4.18		Mean photoreceptor thickness at subfields, by height.	140

4.19		Mean photoreceptor thickness at subfields, by smoking status.	142
4.20		Mean photoreceptor thickness at subfields, by systolic blood pressure.	145
4.21		Mean photoreceptor thickness at subfields, by diastolic blood pressure.	147
4.22		Mean photoreceptor thickness at subfields, by body mass index.	149
4.23		Inclusion/exclusion criteria for GCL-IPL complex.	153
4.24	A-B	Histogram of macular GCL-IPL thickness at A) central and B) inner nasal subfields.	156
	C	Macular GCL-IPL thickness at different locations.	156
	D-E	Macular GCL-IPL thickness in D) women and E) men, at different locations.	157
4.25		Mean GCL-IPL thickness at subfields, by age.	158
4.26		Mean GCL-IPL thickness at subfields, by ethnicity.	160
4.27		Mean GCL-IPL thickness at subfields, by intraocular pressure.	161
4.28		Mean GCL-IPL thickness at subfields, by spherical equivalent.	163
4.29		Mean GCL-IPL thickness at subfields, by height.	164
4.30		Mean GCL-IPL thickness at subfields, by education level.	166
4.31		Mean GCL-IPL thickness at subfields, by deprivation index.	167
4.32		Inclusion/exclusion criteria for macular RNFL SDOCT.	178

4.33	A-B	Histogram of macular RNFL thickness at A) central and B) outer nasal subfields.	180
	C	Macular RNFL thickness at different subfields.	180
	D-E	Macular RNFL thickness in D) women and E) men, at different subfields.	180
4.34		Mean RNFL thickness at subfields, by age.	182
4.35		Mean RNFL thickness at subfields, by ethnicity.	183
4.36		Mean RNFL thickness at subfields, by intraocular pressure.	185
4.37		Mean RNFL thickness at subfields, by refraction.	186
4.38		Mean RNFL thickness at subfields, by height.	187
4.39	A	Mean RNFL thickness and education.	189
	B	Mean RNFL thickness and Townsend deprivation index.	189
4.40		Inclusion in cognitive testing among those with clean GCL-IPL OCT data.	196
4.41		Prospective memory and GCL-IPL thickness at baseline.	198
4.42		Pairs matching and GCL-IPL thickness at baseline.	199
4.43		Numeric & verbal reasoning and GCL-IPL thickness at baseline.	199
4.44		Reaction time and GCL-IPL thickness at baseline.	200
4.45		Total number of tests with poor performance and GCL-IPL thickness at baseline.	201

4.46 Proportion (with 95% confidence intervals) of 33,040 UK Biobank participants with a cognitive deficit, set at threshold of A) 1 or more tests or B) 2 or more tests, according to quintile of retinal nerve fibre layer thickness measured in the outer nasal retinal subfield by optical coherence tomography (OCT). 203

4.47 The proportion of 1,251 UK Biobank participants who underwent cognitive testing at baseline and 3 years later who experienced a decline in cognitive function test results. 205

A 1 or more of a total of 4 cognitive tests deteriorating.

B 2 or more of a total of 4 cognitive tests deteriorating.

4.48 Total number of cognitive tests worse on follow-up testing as compared with baseline GCL-IPL. 207

4.49 Inclusion in cognitive testing among those with clean RNFL OCT data. 209

4.50 Prospective memory and retinal nerve fibre layer thickness at baseline. 211

4.51 Pairs matching and retinal nerve fibre layer thickness at baseline. 212

4.52 Numeric & verbal reasoning and retinal nerve fibre layer thickness at baseline. 212

4.53 Reaction time and retinal nerve fibre layer thickness at baseline. 213

4.54 Proportion of 32,038 UK Biobank participants with a cognitive deficit (failure of 2 or more of a panel of 4 tests), according to quintile of retinal nerve fibre layer thickness measured in the outer nasal retinal subfield by optical coherence tomography (OCT). 213

4.55 Number of cognitive tests worse on follow-up testing is significantly associated with baseline RNFL. 215

1.6 List of Tables

2.1	Training program for assessment center staff.	36
4.1	Basic demographics for those included in RPE-BM analysis.	101
4.2	Linear regression of RPE-BM thickness at subfields, by age.	105
4.3	Linear regression of RPE-BM thickness at subfields, by refraction.	108
4.4	Mean RPE-BM thickness at subfields by smoking status.	114
4.5	Linear regression of RPE-BM thickness at subfields, by systolic and diastolic blood pressure.	116
4.6	Linear regression of RPE-BM thickness at subfields, per unit increase in BMI (kg/m^2).	117
4.7	Univariable and multivariable regression of RPE-BM thickness at subfields, by sex and height.	119
4.8	Multivariable regression of central RPE-BM thickness separately for people 45 years and younger, versus people older than 45 years of age.	122
4.9	Basic demographics for those included in photoreceptor inner and outer segment analysis.	125
4.10	Univariable regressions of photoreceptor thickness at subfields with A) age ≤55 and B) age >55.	129
4.11	Univariable regressions of photoreceptor thickness at subfields by ethnicity.	132

4.12	Univariable regression of photoreceptor thickness and intraocular pressure.	135
4.13	Univariable regression of photoreceptor thickness and refractive error among A) all participants, B) myopes, and C) hyperopes.	138
4.14	Univariable regression of photoreceptor thickness and height.	141
4.15	Univariable regressions of photoreceptor thickness at subfields by smoking status.	143
4.16	Univariable regression of photoreceptor thickness and systolic blood pressure.	146
4.17	Univariable regression of photoreceptor thickness and systolic blood pressure.	148
4.18	Univariable regression of photoreceptor thickness and body mass index.	150
4.19	Multivariable regression modeling for photoreceptor thickness at central subfield.	151
4.20	Basic demographics for those included in GCL-IPL analysis.	155
4.21	Linear regression of GCL-IPL thickness at subfields, by ethnicity.	160
4.22	Linear regression of RNFL thickness at subfields, by intraocular pressure.	162
4.23	Linear regression of GCL-IPL thickness at subfields, by height.	165
4.24	Linear regression of GCL-IPL thickness at subfields, by education.	167
4.25	Linear regression of GCL-IPL thickness at subfields, by deprivation index.	168

4.26	Multivariable regression of GCL-IPL thickness at A) inner, B) outer, and C) central subfields.	172
4.27	Basic demographics for those included in RNFL analysis.	179
4.28	Linear regression of RNFL thickness at subfields, by ethnicity.	183
4.29	Linear regression of RNFL thickness at subfields, by intraocular pressure.	185
4.30	Linear regression of RNFL thickness at subfields, by height.	187
4.31	Multivariable regression of RNFL thickness at select subfields.	192
4.32	Characteristics at baseline (2009-2010) of all participants recruited with baseline OCT available for analysis, of those included in baseline, and of the subset with follow-up assessment in 2012-2013.	197
4.33	Multivariable logistic regression modeling of association between GCL-IPL thickness and risk of failing A) 1 or more cognitive tests (compared to 0) or B) 2 or more tests (compared to 0 or 1 test) at baseline, controlled for age, sex, height, race, refraction, IOP, socioeconomic deprivation, and education.	202
4.34	Multivariable logistic regression modeling of association between GCL-IPL thickness and risk of worsening follow-up cognitive tests, controlled for age, sex, height, race, refraction, IOP, socioeconomic deprivation, and education.	206
	A Worsening on 1 or more follow-up cognitive function tests.	
	B Worsening on 2 or more follow-up cognitive function tests.	

4.35 Characteristics at baseline (2009-2010) of all participants recruited with baseline OCT available for analysis, of those included in baseline analysis, and of the subset with follow-up cognitive function assessment in 2012-2013. 210

4.36 Multivariable logistic regression modeling of association between RNFL thickness and risk of failing 1 or more tests (compared to 0 tests) at baseline, controlled for age, sex, height, race, refraction, IOP, socioeconomic deprivation, and education. 214

4.37 Multivariable logistic regression modeling of association between RNFL thickness and risk of worsening on 1 or more follow-up cognitive function tests (compared to 0 tests), controlled for age, sex, height, race, refraction, IOP, socioeconomic deprivation, and education. 216

1.7 List of Abbreviations

95% CI	95% confidence interval
A-level	General Certificate of Education Advanced Level
AD	Alzheimer's disease
AIGS	Advanced Imaging for Glaucoma Study
BMI	Body mass index
BP	Blood pressure
CAMCOG	Cambridge Cognitive Examination
CSE	Certificate of Secondary Education
ETDRS	Early Treatment of Diabetic Retinopathy Study
GCL-IPL	Ganglion cell layer – inner plexiform layer complex
IOP	Intraocular pressure
IOP_G	Goldmann-equivalent intraocular pressure
IS-OS	Inner and outer segments
mRNFL	Macular retinal nerve fibre layer
MMSE	Mini-Mental State Examination
MS	Multiple sclerosis
OCT	Optical Coherence Tomography
O-level	General Certificate of Education Ordinary Level
Prof. qual.	Professional or vocational qualification
REF	Reference variable
RNFL	Retinal nerve fibre layer

RPE	Retinal pigment epithelium
RPE-BM	Retinal pigment epithelium – bruchs membrane
SDOCT	Spectral domain optical coherence tomography
SD	Standard deviation

1.8 Supporting Publications

1. **Ko F**, Muthy ZA, Gallacher J, Sudlow C, Rees G, Yang Q, Keane PA, Petzold A, Khaw PT, Reisman C, Strouthidis NG, Foster PJ, Patel PJ; UK Biobank Eye & Vision Consortium. Association of Retinal Nerve Fiber Layer Thinning with Current and Future Cognitive Decline: A Study Using Optical Coherence Tomography. ***JAMA Neurology***. 2018 June 25. [Epub ahead of print]

2. **Ko F**, Foster PJ, Strouthidis NG, Shweikh Y, Yang Q, Reisman CA, Muthy ZA, Chakravarthy U, Lotery AJ, Keane PA, Tufail A, Grossi CM, Patel PJ; UK Biobank Eye & Vision Consortium. Associations with Retinal Pigment Epithelium Thickness Measures in a Large Cohort: Results from the UK Biobank. ***Ophthalmology***. 2017 Jan;124(1):105-117.

3. Patel PJ, Foster PJ, Grossi CM, Keane PA, **Ko F**, Lotery A, Peto T, Reisman CA, Strouthidis NG, Yang Q; UK Biobank Eyes and Vision Consortium. Spectral-Domain Optical Coherence Tomography Imaging in 67 321 Adults: Associations with Macular Thickness in the UK Biobank Study. ***Ophthalmology***. 2016 Apr;123(4):829-40.

4. Shweikh Y, **Ko F**, Chan MP, Patel PJ, Muthy Z, Khaw PT, Yip J, Strouthidis N, Foster PJ; UK Biobank Eye and Vision Consortium. Measures of socioeconomic status and self-reported glaucoma in the U.K. Biobank cohort. ***Eye (Lond)***. 2015 Oct;29(10):1360-7.

1.9 Supporting Presentations

2017 World Glaucoma Congress (Faculty presenter)

"Getting the most out of big data: UK Biobank Experience"

2016 Alzheimer's Association International Conference (featured talk)

"Retinal nerve fiber layer thinning associated with poor cognition among a large cohort, UK Biobank"

2015 Association for Research in Vision and Ophthalmology (poster)

"Retinal nerve fiber layer thinning associated with poor cognition among a large cohort, UK Biobank"

2015 Association for Research in Vision and Ophthalmology (poster)

"Frequency of glaucoma and its associations in a large cohort, UK Biobank"

1.10 Acknowledgements

I would like to thank my advisors, Professor Paul Foster and Mr Nick Strouthidis for their wisdom, guidance, and patience. In addition to his work with Moorfields Eye Hospital and Institute of Ophthalmology at University College of London, Professor Foster leads UK Biobank Eye & Vision Consortium. It has been an honor and privilege to be allowed to participate in the work at UK Biobank. Mr Nick Strouthidis recruited me to Moorfields and made it possible for me to conduct research during my time here.

This research would have been impossible without Qi Yang and Charles Reisman, at Topcon Advanced Biomedical Imaging Laboratory. They performed automated segmentation of raw OCT images. After I applied inclusion/exclusion criteria, values at upper and lower extremes were sent to Qi, who performed manual re-grading of the images. In the process of analysis and manuscript writing, several people were important. Mr Praveen Patel was particularly attentive to the rigor of imaging, as well as thinking about the most effective way of performing manual re-grading of such a large dataset. John Gallacher and Axel Petzold provided expertise critical toward interpretation of cognitive function results. Cathie Sudlow contributed expertise in statistical analysis, particularly in regards to odds ratios. Professor Peng Khaw provided guidance on overarching concepts that might have particular impact in publication. Zaynah Muthy assisted in literature search of cognitive function introductory section.

I am grateful to all the participants of UK Biobank for volunteering their time.

SECTION II:

INTRODUCTION

2.1 UK Biobank

2.1.1 Purpose of UK Biobank

UK Biobank is a community-based cohort study in the United Kingdom of 500,000 volunteer participants age 40 – 69 years old, with the aim of improving prevention, diagnosis, and treatment of a wide range of illnesses (http://www.ukbiobank.ac.uk/). To our knowledge, this is the largest study of retinal imaging yet undertaken. High-quality imaging of eyes from 67,321 participants were acquired, in addition to other ocular measures, physical measurements, and tests of cognitive function. In addition to baseline measures, 20,000 participants have undertaken repeat measures.

UK Biobank is a non-profit charity. It was established by the Wellcome Trust medical charity, Medical Research Council, Department of Health, Scottish Government, and the Northwest Regional Development Agency. It has also received funding from the Welsh Government, British Heart Foundation, Cancer Research UK, and Diabetes UK. UK Biobank is supported by the National Health Service. The de-identified health data collected by UK Biobank is open to researchers in the United Kingdom and internationally, in both academia and industry (Figure 2.1). Upon completion of their work, researchers return their findings to UK Biobank, to benefit the broader scientific community.

Figure 2.1. Map of approved UK Biobank research projects in the UK (A) and internationally (B). (http://www.ukbiobank.ac.uk/approved-research-2/)

A) B)

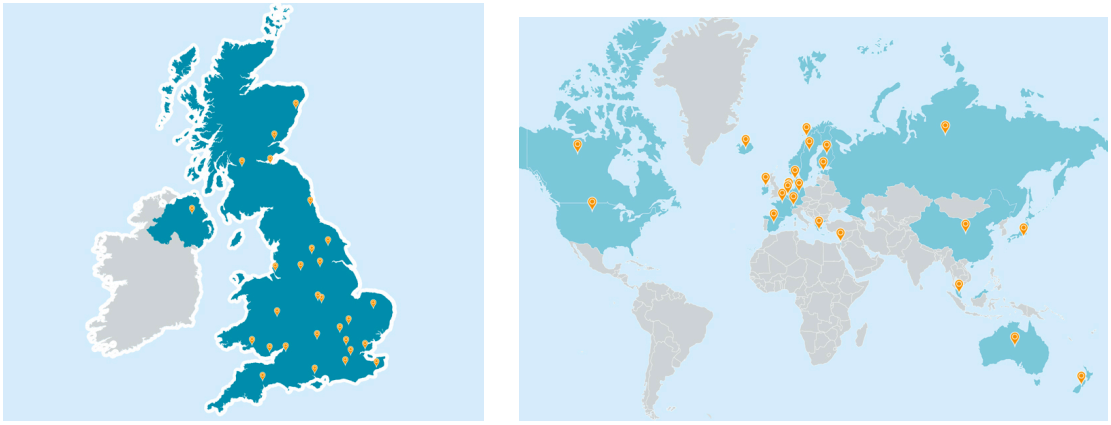

2.1.2 Structure and Timeline

There are 22 assessment centers located in Scotland, Wales, and England (Figure 2.2). The pilot phase began in March 2006, and the main phase began in April 2007, with the opening of the first assessment center. People aged 40-69 who were registered with the National Health Service were invited via mail. It was estimated that 5 million invitations would be needed in order to recruit the target number of 500,000 participants. Participants who attended assessment centers were asked to complete a touchscreen questionnaire, undergo a range of physical measures, and donate biological samples. In April 2009, cognitive function tests were added. Later that year, in August, eye measures were added to the study, including visual acuity, autorefraction, and intraocular pressure. Then in December 2009, optical coherence tomography (OCT) of the retina was added. Recruitment ended in July 2010.

Figure 2.2. Map of UK Biobank assessment centers. Stockport was the location of initial pilot testing and repeat assessment.

(http://biobank.ctsu.ox.ac.uk/crystal/exinfo.cgi?src=UKB_centres_map)

Eye measures were taken at assessment centers located in Liverpool, Hounslow, Sheffield, Croydon, Birmingham, and Swansea. In additional to these centers, Bristol, Nottingham, Middlesborough, and Wrexham locations were also used to obtain cognitive function testing (Figure 2.3). A map showing the generic layout of assessment centers is shown in Figure 2.4.

Figure 2.3. Graph showing operational duration and tests performed at each UK Biobank assessment center.

(http://biobank.ctsu.ox.ac.uk/~bbdatan/clinic_timelines.pdf)

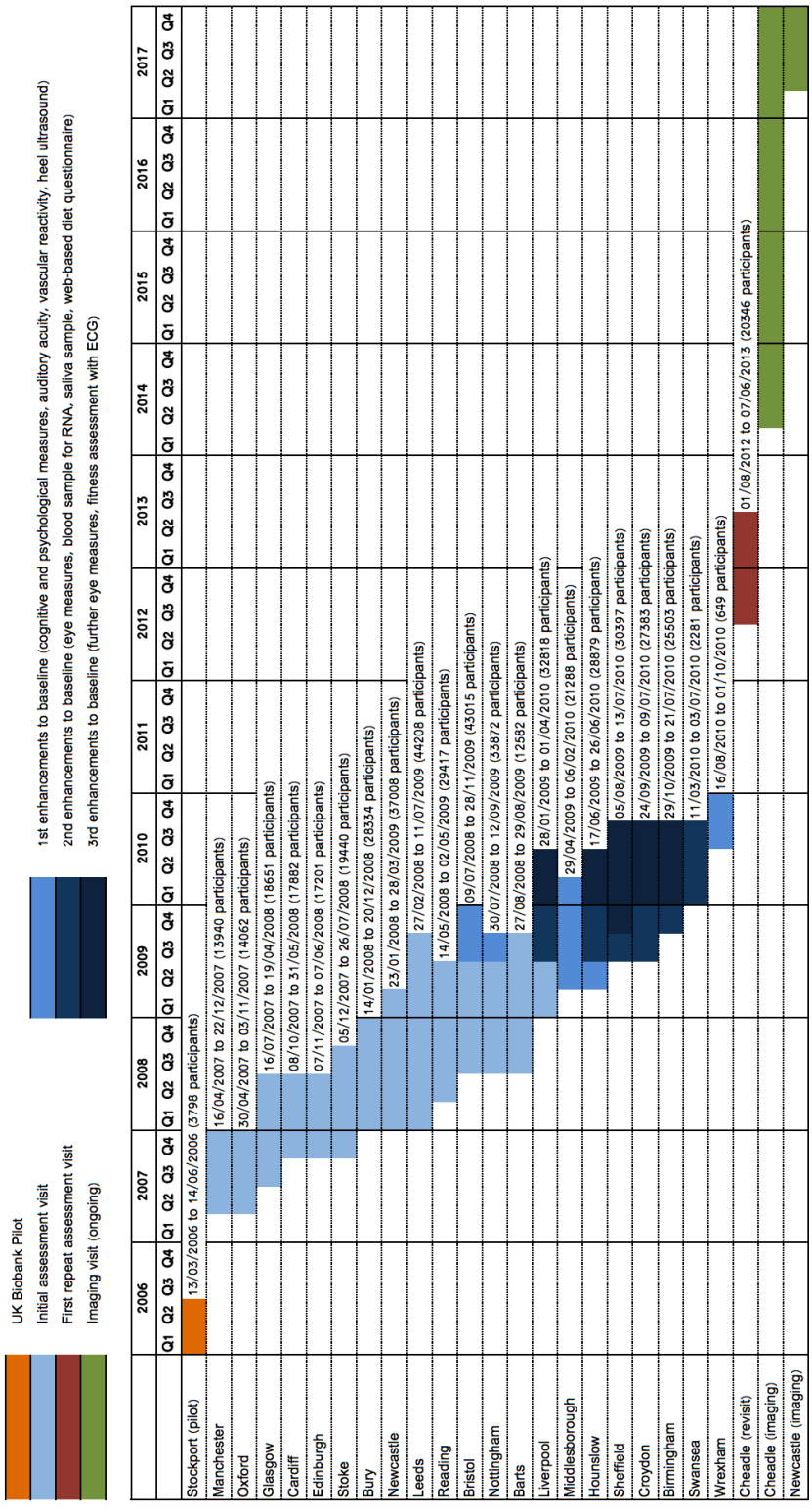

Figure 2.4. General layout of UK Biobank assessment center.

(http://biobank.ctsu.ox.ac.uk/crystal/exinfo.cgi?src=Clinic_layout)

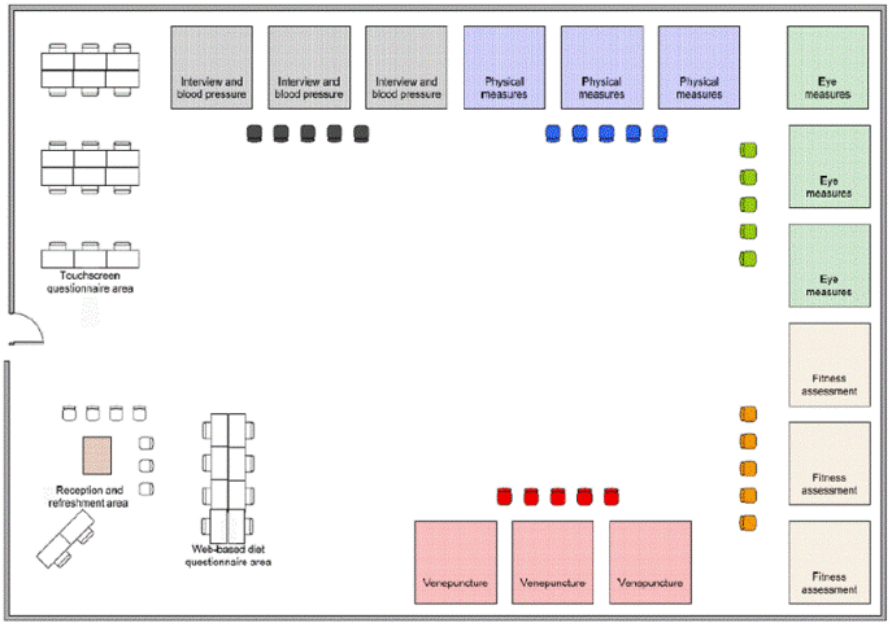

2.1.3 Repeat Assessments

Repeat assessments of 20,000 participants were carried out between August 2012 and June 2013. People who lived within 35 km of UK Biobank Co-ordinating Center in Stockport, UK were invited via email or letter, with an overall response rate of 21%. Participants underwent a repeat of the baseline assessment visit, including a participant's health and lifestyle questionnaire, cognitive function, eye measures, and OCT. Repeated measurements strengthened UK Biobank resource by producing more precise measures for the entire cohort by adjusting for regression dilution bias, which can be introduced through short-term biological variability (e.g., diurnal variation) or longer-term within-person variability (e.g., changes to diet or physical activity), with measurement error causing bias of the regression slope coefficient towards the null

hypothesis. Repeat measurements are not only a way of validating data, but also creating an opportunity for longitudinal comparison.

Demographics of those who attended repeat assessments did show some differences from baseline. According to UK Biobank tabulations, those who attended repeat assessments were more likely to be older, had lower body mass index (BMI), had fewer longstanding illnesses, disabilities, or infirmities, were more likely to rate their overall health as “excellent”, had higher educational attainment, had less socioeconomic deprivation, lived closer to UK Biobank Co-ordinating Center and were more likely to be never smokers as compared to those who declined or did not respond to an invitation (http://biobank.ctsu.ox.ac.uk/~bbdatan/repeat_assessment_characteristics_v1.pdf). Where pertinent to the current study, detailed demographic information comparing those who did and did not attend repeat assessment will be provided.

2.1.4 Ophthalmic Testing and Quality Control

The methods and protocol for the ocular portion of UK Biobank examination were designed by ophthalmologists from Moorfields Eye Hospital, London, UK (Keane et al 2016). Visual acuity at 3 meters was measured using with best-available refractive correction. Refractive error for each eye was assessed using an autorefractor (Tomey, Japan) (www.ukbiobank.ac.uk). Intraocular pressure and corneal biomechanics were simultaneously measured in both eyes using an Ocular Response Analyzer (Reichert Technologies, USA) (www.ukbiobank.ac.uk). Retinal images were captured with a retinal camera (TRC-NW6S, Topcon, Japan) and Spectral domain OCT (3D OCT-1000 Mark II,

Topcon, Japan) (www.ukbiobank.ac.uk). These ocular examinations were typically performed in around 11 minutes (Keane et al 2016). The North West Multi-centre Research Ethics Committee approved the study (REC Reference Number: 06/MRE08/65), in accordance with the principles of the Declaration of Helsinki. Written, informed consent was obtained for all participants in UK Biobank.

All assessment center staff underwent a formal interview to assess suitability and relevant experience (www.ukbiobank.ac.uk). Curriculum vitae and training record specifying procedures they were approved to undertake were maintained at the coordinating center and relevant assessment center. Core training for all staff spanned a period of 3-5 days, although staff were only required to attend days pertinent to their duties (Table 2.1).

Table 2.1. Training program for assessment center staff. Adapted from UK Biobank protocol, available at www.ukbiobank.ac.uk.

Sessions	Areas covered	Staff trained
Introduction	• Overview of UK purpose, assessment visit & IT system • Consent process • Participant welfare	All staff
Questionnaire	• Background to touch-screen and interview questionnaires • Use of touch-screen • Administration of interview	Nurses and all staff supervising touch-screens
Physical measurements	• Introduction to measurements • Maintenance and calibration of equipment • Workshop using all equipment	Nurses and technicians doing measurements
Practice sessions	• Q&A session with senior members of team • Practice runs of baseline assessment visit	All Staff

Technicians acquiring OCT images underwent a structured training program and competency exam to obtain certification (Keane et al 2016). This involved demonstrating that they had read and understood the standard operating procedure for image acquisition, as well as demonstrating the ability to acquire well-centered images with good signal strength. Additional training focused on pattern recognition to allow technitions to recognize 1) significant artifactitious variations in signal intensity (generally a sign of irregular media opacity or poor mydriasis), 2) artifactitious severe anomalies in retinal contour (generally a sign of severe refractive error), and 3) generalized reductions in OCT signal strength. All images from the first day of independent image acquisition were quality controlled by Moorfields Eye Hospital Reading Center ophthalmologists and a UK Biobank site duty manager. Additionally,

approximately 10% of OCT images were assessed for quality by certified graders at Moorfields Eye Hospital Reading Center. Re-training was provided for issues revealed during the real-time quality assurance review (Keane et al 2016).

The Clinical Trials Service Unit at the University of Oxford created custom software for live ongoing data monitoring during OCT image acquisition, using electronic direct data entry case report forms (Keane et al 2016). Visual acuity and refractive error were automatically imported into each case report form, and then the grader assessed each image set for overall image quality, image focus, centration relative to the fovea, and central macular thickness and accuracy of measurements. Image error was attributed to one of four possible categories: 1) participant, 2) operator, 3) equipment, or 4) indeterminate. Quality assessment feedback was then provided to each center on an ongoing basis.

OCT image sets were stored on UK Biobank servers in a central repository at Advanced Research Computing, University of Oxford (previously known as Oxford Supercomputing Centre (OSC)), adjacent to high performance computers (Keane et al 2016). This consisted of several 1000-core Linux servers, a Nvidia graphics processing unit (GPU) cluster, and a Windows 2012 server which created and managed a collection of Windows XP/Windows Vista/Windows 7 virtual machines. At the time of this analysis, UK Biobank data access rules and procedures for bulk data prohibited copying, storage, or removal of OCT source data outside of the Oxford computing system. Researchers were given access to computers at the central repository via remote secure login. A copy

of the stored OCT image file was fetched, analyzed through segmentation software, derived data extracted, and then OCT image file deleted.

2.1.5 Published work produced from UK Biobank resource

A great deal of work has been conducted through UK Biobank resource, spanning a wide range of body systems. Pubmed search at the time of this writing showed 453 articles with the keyword “UK Biobank.” Research ranges widely, including associations between cardiovascular disease and mode of transportation (eg, car versus public transport, cycling, or walking) (Panter et al 2018), genetic commonalities of asthma and allergic diseases (Zhu et al 2018), and associations between night shift work and type 2 diabetes (Vetter et al 2018).

In the field of ophthalmology, 68 new genomic loci associated with elevated intraocular pressure have been identified through UK Biobank resource (Khawaja et al 2018). Others have found associations with intraocular pressure including older age, male sex, systolic blood pressure, faster heart rate, higher myopia, and colder season ($p<0.001$) (Chan et al 2016). There may also be more complex associations with height, smoking, and diabetes, with opposite effects depending on whether the variable of interest is Goldmann-correlated intraocular pressure versus corneal-compensated intraocular pressure (Chan et al 2016). Further, an association with socioeconomic deprivation, measured by the Townsend deprivation index, has been shown with self-reported glaucoma (Shweikh et al 2015).

While progress has been made related to glaucoma, findings related to the retina and associated pathologies have been slower. In part, one issue has been speed of manual grading of >120,000 retinal photos from 60,000 people. One strategy has involved crowdsourcing, which has shown surprising accuracy in identifying retinal disease (Mitry et al 2016). However, a problem with crowdsourcing is cost, as there are thousands of images, and accuracy requires grading of each image by several people. Another approach is automated segmentation of images, which is particularly suitable for OCT images of the retina. Central macular retinal thickness has been shown to be positively associated with older age, female gender, higher myopia, smoking, body mass index, and white ethnicity ($P<0.001$) (Patel et al 2016). More detailed analysis of individual retinal layers and subfields are described in the current work.

Cognitive function has been another area of interest within UK Biobank. Research has identified an association between physical activity and grey matter volume on structural MRI among adults >60 years of age (Hamer et al 2018). This is supported by findings of markers of sedentary behaviors such as duration of television watching and driving time being positively associated with cognitive decline at follow-up (Bakrania et al 2018). Interestingly, the same study found computer-use time was inversely associated with cognitive decline, although this effect may be partially due to the use of computers to test cognitive function in UK Biobank (Bakrania et al 2018). One wonders whether physical activity stimulates cognitive function, or whether it is a general marker of vitality. Supporting the latter argument is the finding of an association between grip strength & cognitive function (Firth et al 2018), as one might not expect grip strength to

directly affect cognitive function, but rather that general good health might promote both strength and cognitive function.

Environmental exposures and cognitive function have been studied, such as coffee, alcohol, and medication intake. Habitual coffee intake showed no effect on cognitive function, measured as reaction time, pairs matching, reasoning, and prosective memory (Zhou et al 2018). In contrast, alcohol consumption was associated with slower reaction time when consumption exceeded 10 g/day (Piumatti et al 2018). Drugs with associations to poorer cognitive performance included those used for nervous system disorders, such as antiepileptics (eg, topiramate) and antipsychotics (e.g., risperidone); as well as those used for non-nervous system disorders, such as antihypertensives (e.g., amlodipine), antidiabetics (e.g., insulin), proton pump inhibitors (e.g., omeprazole), and laxatives (e.g., contact laxatives) (Nevado-Holgado et al 2016). Those used for nervous system disorders showed larger effect, with antiepileptics being associated with lower reasoning score of -0.65 (95% CI -1.05 to -0.24) and memory score -1.41 (95% CI -1.79 to -1.04) and antipsychotics with reaction time -33 msec (95% CI -46 to -20) (Nevado-Holgado et al 2016). This is in comparison to anti-hypertensives, which showed association with reasoning score -0.1 (95% CI -0.15 to -0.16), memory score -0.08 (95% CI -0.13 to -0.03), and reaction time -3 msec (95% CI -5 to -2); antidiabetics with reaction time -13 msec (95% CI -17 to -10); proton pump inhibitors with reasoning score -0.11 (95% CI -0.15 to -0.06), memory score -0.08 (95% CI -0.12 to -0.04), and reaction time -5 msec (95% CI -6 to -3); and laxatives with reaction time -13 msec (95% CI -19 to -8) (Nevado-Holgado et al 2016). Ibuprofen and glucosamine showed association towards a positive effect on cognitive function. Ibuprofen was associated with higher

reasoning score 0.05 (95% CI 0.02 to 0.08) and faster reaction time 4 msec (95% CI 3 to 5), and glucosamine was associated with higher reasoning score 0.09 (95% CI 0.03 to 0.14) and faster reaction time 5 msec (95% CI 3 to 6) (Nevado-Holgado et al 2016). One should interpret these results cautiously, as some of the associations may reflect the underlying diseases the medications were prescribed for.

Many of the studies conducted thus far through UK Biobank have focused on cross-sectional analysis. While this is helpful for identifying risk factors for certain conditions, it does not necessarily tell us about future risk. In my work, I not only perform cross-sectional analysis of associations with thickness of individual retinal layers and cognitive function, but also compare baseline measurements with future cognitive function.

2.2 Optical Coherence Tomography

2.2.1 Imaging modality

Optical coherence tomography (OCT) was first described in 1991 (Huang et al 1991). OCT extended the principle of low-coherence reflectometry to tomographic imaging, which directs a low-coherence light beam from an optical probe at a sample, which reflects light signals back to the interferometer. By knowing the coherence property of the light beam, time-of-flight delay information from the reflective boundary can be used to determine longitudinal location. Each point is recorded as a depth profile (A-scan),

which can be compiled together by scanning in a linear fashion across a sample to form a cross-sectional image (B-scan) (https://www.novacam.com/technology/how-lci-works/). OCT can be performed through a small aperture, as the coherence length of the light source is the main limitation to resolution, thus allowing high resolution of deep tissues through a small pupil (Huang et al 1991). Early techniques had a resolution of 10-15 µm (Huang et al 1991). A reproduction of retinal and optic disc OCT published in the first article describing OCT is shown (Figure 2.5).

Figure 2.5. Reproduction of retinal and optic disc OCT and histology from the first publication describing OCT (Huang et al 1991). BV = blood vessel, RPE = retinal pigment epithelium, SRF = subretinal fluid.

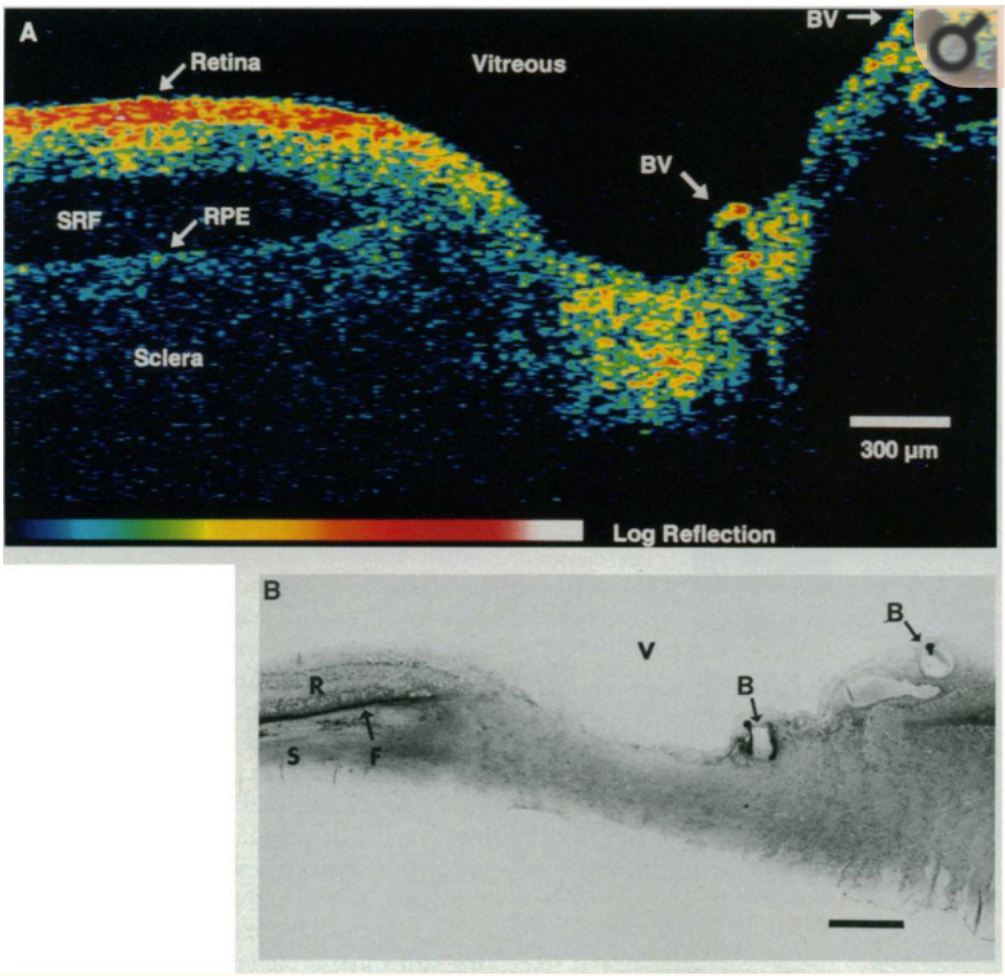

Since the first OCT devices were developed, resolution has improved from 10 µm to 3 µm and imaging speed has become faster, allowing higher-density raster scanning while minimizing motion artifacts (Forte et al 2009). The original time domain OCT obtained information based on longitudinal translation in time of the light signal. Newer spectral domain OCT measures the interferometric signal detected as a function of optical frequencies (Forte et al 2009). Put another way, the spectrometer detects relative amplitudes of many optical frequencies simultaneously, thus sampling many points at the same time. An example of spectral domain OCT image acquired as part of UK Biobank is shown (Figure 2.6).

Figure 2.6. Example of spectral domain OCT image acquired as part of UK Biobank.

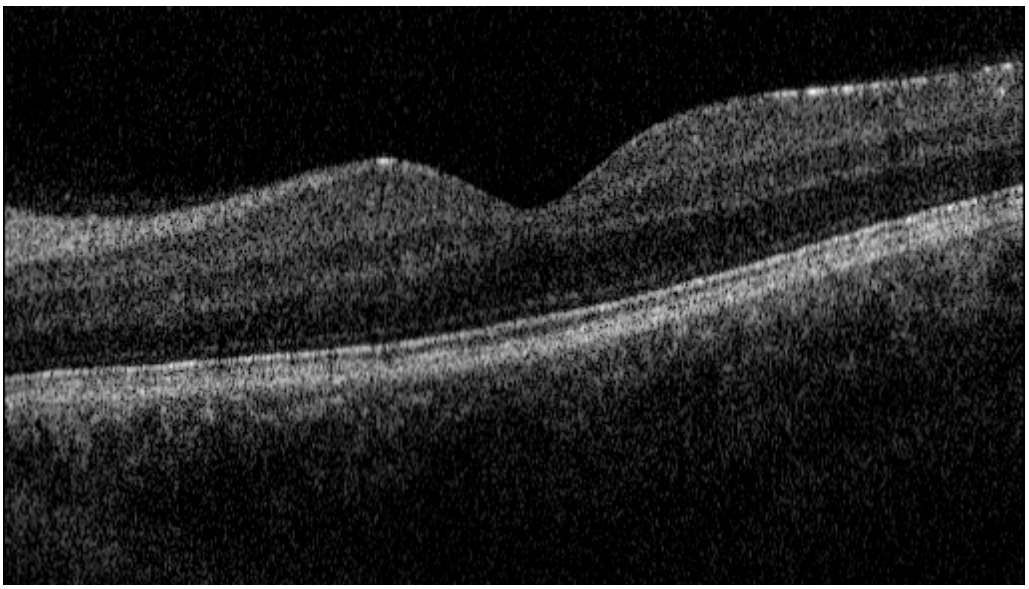

OCT has become an essential part of ophthalmic imaging, and has been the modality of choice in many research studies as well as in clinical practice (CATT Research Group et al 2011, Wang et al 2009, van Dijk et al 2009).

2.2.2 Automated Segmentation

The development of higher-quality and faster OCTs allowed clinicians and scientists to examine individual retinal layers with greater detail. Trained image graders can perform "segmentation," or delineation of boundaries of retinal layers to allow measurements. However, a hindrance to this process is the time required to manually assess images. In the case of UK Biobank, OCT imaging was acquired for both eyes of 67,316 participants. Even assuming a rate of 2 minutes per OCT, 4488 hours or the equivalent of 112 work weeks would be required to manually review all scans. For small studies, manual review of images is reasonable, and provides the benefits of accuracy and precision. For larger studies to be feasible, a more streamlined process is necessary. One mitigating strategy is to exclude images with obvious issues, such as image artifact or poor quality, although this may be inadequate if the study size is sufficiently large. Another solution is automated segmentation of images.

Automated segmentation has undergone several iterations. Challenges to automated segmentation include intrinsic speckle noise, presence of blood vessels, motion artifacts, and reduced illumination. Initial strategies were based on intensity variation (Ishikawa et al 2005, Shahidi et al 2005, Tan et al 2008, Koozekanani et al 2001, Cabrera et al 2005). Adaptive thresholding (Ishikawa et al 2005) and iterative refinement (Tan et al 2008, Cabrera et al 2005) have been proposed as improvements; however, the fundamental issue of intensity inconsistency and discontinuity, both within a single image or across images, remain problematic. Intensity thresholding tends to work adequately for

borders with high intensity and contrast, such as the internal limiting membrane or retinal pigment epithelium, but remain sub-optimal for other retinal layers.

More complex models incorporate gradient information in addition to intensity (Muiat et al 2005, Mishra et al 2009, Garvin et al 2008, Kajifi et al 2010). Gradient information has the advantage over intensity information in that segmentation will not be severely affected by local absolute intensity values as long as contrasts between layers remain. However, gradient information is correlated with intensity information, such that when blood vessels or artifacts are present, both local gradient and intensity information are degraded. This can result in errors in boundary detection. Yang et al (2011) noted that gradient information from a larger kernel can provide complementary information to local gradient or intensity signal, incorporating neighboring information to compensate for missing local information without losing other details. They utilize both global and local gradient information to gather edge information and optimize edges using shortest path search method, a type of dynamic programming (Yang et al 2011).

Yang et al (2011) developed a two-step segmentation algorithm. First, a customized Canny edge detector (Canny 1986) was used to create a map showing local main edges; as well, a complementary gradient map was acquired with a larger kernel. The Canny edge detector was customized using a low-value threshold to remove false edges, a high-value threshold to highlight significant edges, and a middle-value threshold to preserve other potential edges. The thresholds were set to constant values that varied by boundary. For high-contrast boundaries, such as the internal limiting membrane, the low-, middle-, and high-value thresholds are 0, 0, and 0.85, respectively. For low-

contrast boundaries such as the external limiting membrane, all three thresholds are set to 0. Other intraretinal boundaries have the low-, middle-, and high-value thresholds of 0.1, 0.55, and 0.8. The kernal size of each Canny edge detector is also varied proportionately to scan resolution. In the second step, a graph was built based on a combination of the Canny edge maps and axial intensity gradient. The layer boundary was then extracted by a shortest path search applied to the graph. An example of the two-step segmentation process is shown in figure 2.7.

Figure 2.7. Example of automated two-step segmentation. Reproduced from Yang et al 2011.

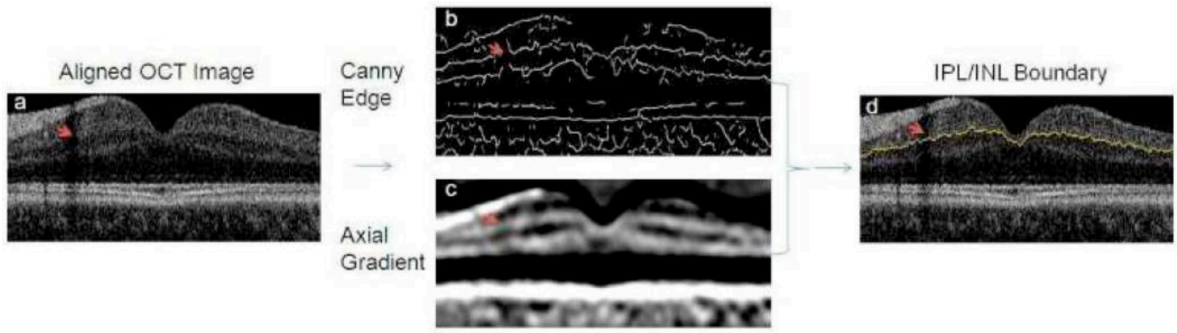

The execution time using this automated segmentation algorithm was 45 seconds for full nine layer detection using images acquired from Topcon 3D OCT-1000 machines, which has 128 frames covering a 6mm by 6 mm macular area with B-scan image size 480x512 (Yang et al 2011). Fast mode was also avilable, which required 16 seconds. In both modes, comparison between automated versus manual segmentation were within an axial resolution of 3.5 μm (Yang et al 2011).

2.3 Retinal Anatomy and Function

2.3.1 Retinal layers

The retina is important for collecting light, converting it to electrical signals, which are then sent to the brain for interpretation via nerve fibers. The macula is a particularly sensitive area of the retina with a high density of specialized cells for collecting light. It is usually 5-6 mm in diameter, centered vertically between the temporal vascular arcades, and is defined as the area with 2 or more layers of ganglion cells. The central 1.5 mm of the macula is referred to as the fovea, with unique anatomy and cellular composition. Here, there is a lack of blood vessels and inner retinal components, and an increased density of photoreceptor cells, allowing for high spatial acuity and colour vision (Figure 2.8) (Regillo et al 2010).

Figure 2.8. Basic diagram of macula (yellow dashed circle) and fovea (orange dashed circle) relative to optic nerve (yellow filled circle) and vascular arcades (red lines).

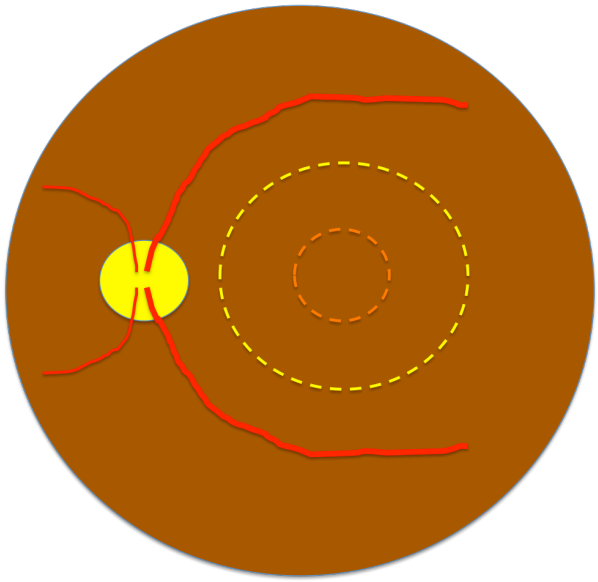

In histologic preparation, the retina appears as layers: internal limiting membrane (ILM), nerve fibre layer (NFL), ganglion cell layer (GCL), inner plexiform layer (IPL), inner nuclear layer (INL), outer plexiform layer (OPL), outer nuclear layer (ONL), external limiting membrane (ELM), photoreceptor inner and outer segments, and retinal pigment epithelium (RPE) (Figure 2.9).

Figure 2.9. Retinal layers in histologic preparation.

Adapted from https://www.memorangapp.com/flashcards/120774/Visual+System/

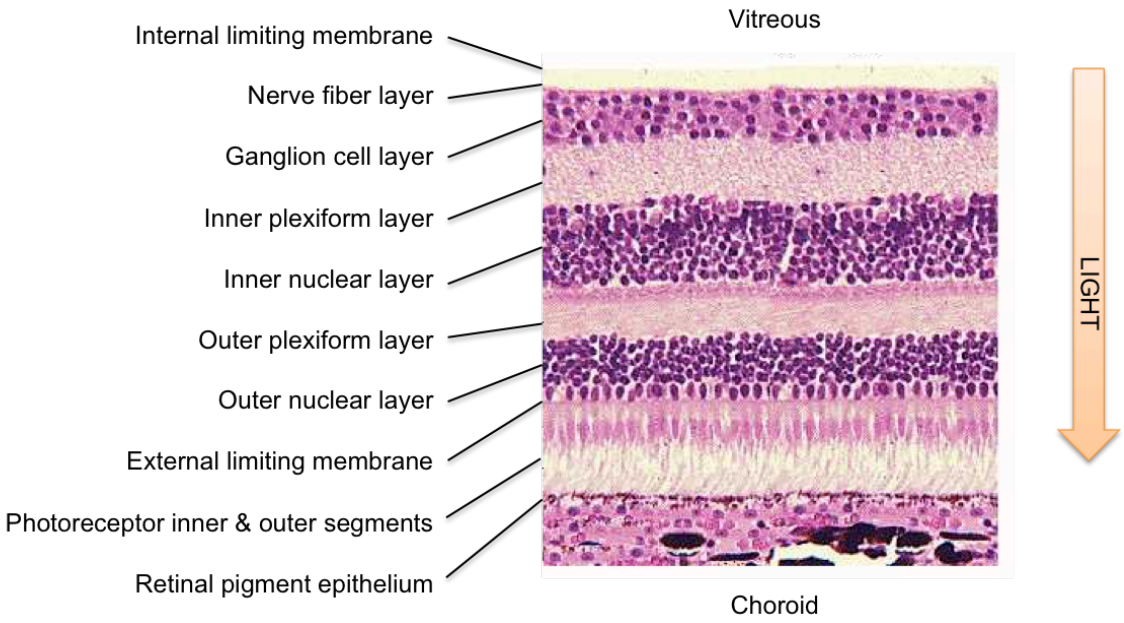

2.3.2 Retinal pigment epithelium

The retinal pigment epithelium (RPE) plays an important role in metabolic activity in the retina, and is critical in visual function (Strauss 2005). Failure of RPE function is involved in blinding disease such as age-related macular degeneration, the leading cause of blindness among caucasian people 65 years and older (Jonas JB 2014, Friedman DS et al 2004, Munoz et al 2000, Klaver et al 1998, Wang JJ et al 2000).

The retinal pigment epithelium derives from the neuroectoderm, forming a single layer of cuboidal cells between bruchs membrane and photoreceptors (Figure 2.10). The RPE cells are taller and denser at the macula than at the peripheral retina. Zonulae occludentes near the apices of the RPE cells form tight junctions that form the outer retinal blood-ocular barrier. The apical surface contains villous processes that interact with the outer segments of photoreceptor cells. The basal surface has infoldings of the plasma membrane.

Figure 2.10. Optical coherence tomography (upper image) and automated segmentation (bottom image) of retinal pigment epithelium. OS/RPE = boundary between photoreceptor outer segment and retinal pigment epithelium. BM/Choroid = boundary between bruchs membrane of retinal pigment epithelium and choroid. (Adapted from Yang et al 2010)

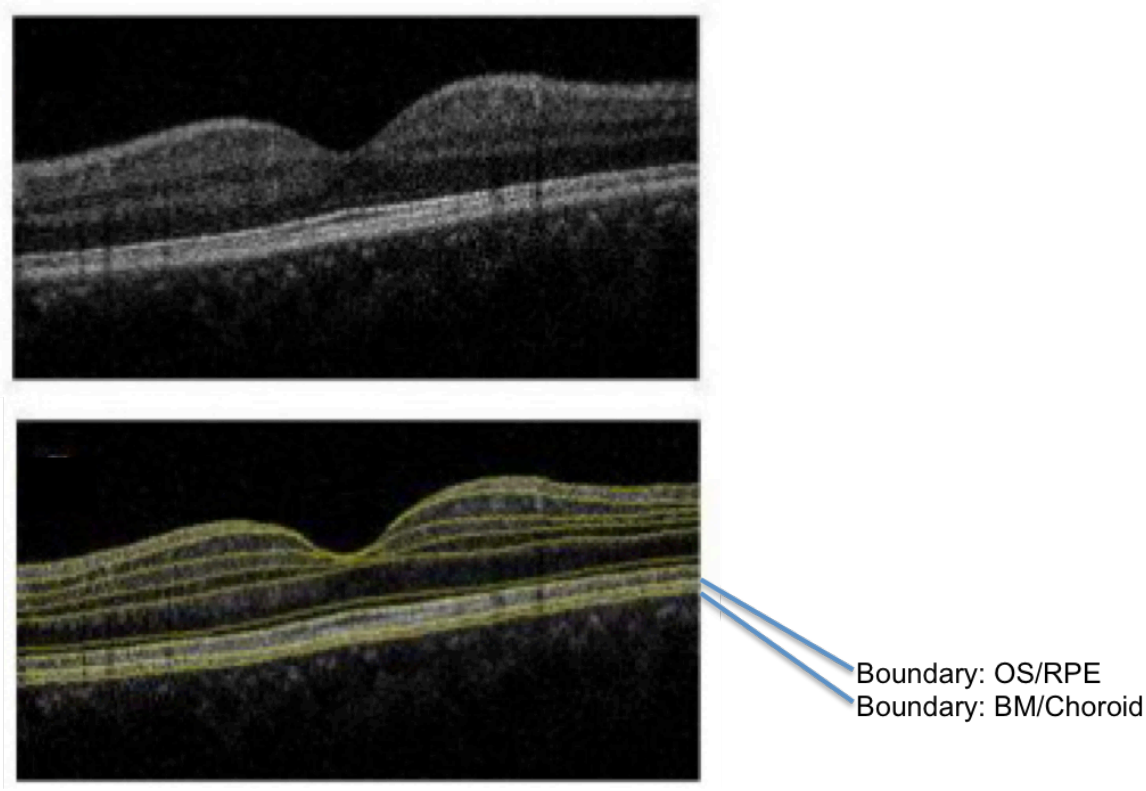

The RPE serves several functions, including forming the blood-ocular barrier, absorbing light, maintaining the subretinal space, phagocytosing rod and cone outer segments, participating in retinal and polyunsaturated fatty acid metabolism, and healing and scar tissue formation. Each RPE cell contains numerous melanosomes, which absorb light, with longer-wave blue light being absorbed more than red light. RPE has selective transport properties and a high capacity for fluid transport, preventing fluid

accumulation in the subretinal space. Apical processes of RPE cells envelope the outer segments of photoreceptors. RPE cells phagocytose the membranes, or discs, shed by the outer segments of photoreceptor cells. A diurnal rhythm occurs as discs are shed, phagocytosed, and renewed. Rod photoreceptors tend to shed discs at dawn, and cones at dusk. Lysosomes within the RPE produce enzymes that digest the outer segments. Retinal and polyunsaturated fatty acids from the outer segments are recycled. RPE cells contribute to photoreceptor function and metabolism by converting 11-*trans*-retinaldehyde to 11-*cis*-retinaldehyde. The latter is sensitive to light, and initiates the opsin signaling process in photoreceptor outer segments. Light photons stimulate 11-*cis*-retinaldehyde, which converts to *trans* configuration, and must be regenerated for continued visual signaling. Brief shortages of 11-*cis*-retinaldehyde can be experienced in healthy individuals, such as after a bright car light causes temporary inability to see at night due to depletion of 11-*cis*-retinaldehyde in rods. Conditions such as vitamin A deficiency can cause a disruption of this metabolic pathway, resulting in more serious visual pathology.

Disease states can result from abnormalities in RPE metabolism. For instance, Stargardt disease occurs when defective ABCR protein leads to accumulation of all-*trans*-retinol in the outer segment discs, stimulating formation of disproportionate amounts of A2E in RPE cells. A2E is a diretinal conjugate with ethanolamine, a constituent of lipofuscin. Components of lipofuscin can be toxic to RPE by inhibiting lysosomal protein degradation, producing reactive oxygen species and radicals, and inducing apoptosis of the RPE. Another disease linked with RPE dysfunction is vitelliform macular dystrophy, where yellowish subretinal material accumulates in the subretinal space, due to

separation of the photoreceptor outer segments from the RPE leading to decreased phagocytosis. Perhaps the most well-known disease related to RPE is macular degeneration, estimated to cause 6% of blindness worldwide (Bourne et al, WHO Vision 2020 GBVI – Global Cause Estimates.) In high income Western Europe and North America, AMD accounts for 11% of visual impairment (WHO Vision 2020 GBVI – Regional Summaries). In macular degeneration, RPE shows loss of melanin granules, formation of lipofuscin granules, and accumulation of residual bodies (Regillo et al 2010). Basal laminar deposits consisting of lipid-rich material and collagen fibers accumulate between the plasma membrane of the RPE and inner aspect of the basement membrane of the RPE (Regillo et al 2010). The overlying photoreceptor cells are subsequently reduced in density and distribution (Regillo et al 2010). Macular degeneration is an age-related disease, meaning that its prevalence increases with age (Rudnicka et al 2012), so one might expect the burden of disease to increase as the population ages. However, projections suggest that with the development of treatment options, prevalence may actually decrease (Delcourt et al 2018, Bourne et al 2018).

Despite its importance, little is known about the normal distribution of RPE thickness in the non-diseased state. Post-mortem histologic study suggests increases in RPE autofluorescence and Bruch's membrane (BM) thickness with age (Okubo et al 1999, Ramrattan RS et al 1994). Histologic study of 18 maculas showed mean RPE thickness of 14.1 μm and BM thickness of 4.7 μm at the foveal center (Curcio C et al 2011). Histological studies are limited in that they are post-mortem or utilize enucleated eyes and can be easily affected by artifact during handling of tissue. In vivo investigations have been made with spectral domain optical coherence tomography (OCT), but sample

sizes remain small. A study of 25 healthy individuals showed mean RPE-BM thickness of 22.7 μm at central subfield, and also suggests that the thickness increases with age (Karampelas et al 2013). Another study of 120 people age 18-81 also found increasing RPE thickness with older age (Demirkaya et al 2013). A separate study of 127 normal eyes found the opposite, reporting decreased thickness with older age (Kenmochi et al 2017). To our knowledge, there has been no large study examining the effects of other demographic factors, such as ethnicity, and its relationship with RPE thickness. Yet, one might expect ethnicity to play a role in RPE morphology, given the ethnic associations with macular degeneration, a disease with findings in the RPE (Fisher et al 2016, VanderBeek et al 2011). Understanding the physiologic changes of RPE may aid in research and development of therapeutic options.

2.3.3 Photoreceptors

Light entering the eye must pass through retina to reach the photoreceptors (Regillo et al 2010). The density, distribution, and type of photoreceptors vary depending on location within the retina. Cone photoreceptors are specialized for colour vision at higher light levels, and responsible for high spatial acuity. They predominantly occupy the fovea, with density over 140,000 cones/mm^2. Retinaldehyde molecules derived from vitamin A are bound to opsin apoproteins. Cones have three different opsins that are selectively sensitive to red, green, and blue light. Rod photoreceptors are specialized for vision at low light levels, with high sensitivity but low acuity. The opsin molecules of rods are known as rhodopsin. Rods predominantly occupy the peripheral retina, with greatest density approximately 20 degrees from fixation, and peak density of 160,000 rods/mm^2. Despite the high density, visual acuity remains low, as multiple rod responses are summated within each receptive field. The density of rod photoreceptors decreases toward the peripheral retina.

Photoreceptor cells appear to occupy three layers when viewed with OCT (Figure 2.11), as there are boundaries visible between the photoreceptor outer segment, photoreceptor inner segment, and photoreceptor cell bodies. However, the boundary between the photoreceptor cell bodies (also known as the outer nuclear layer) and the outer plexiform layer, is difficult to visualize on OCT. The next boundary that is readily visible is the one between the outer plexiform layer and the inner nuclear layer.

Figure 2.11. Optical coherence tomography (upper image) and automated segmentation (bottom image) of photoreceptors. INL/OPL = boundary between inner nuclear layer and outer plexiform layer. ELM = external limiting membrane. IS/OS = boundary between inner nuclear layer and photoreceptor outer segment. OS/RPE = photoreceptor outer segment and retinal pigment epithelium. (Adapted from Yang et al 2010)

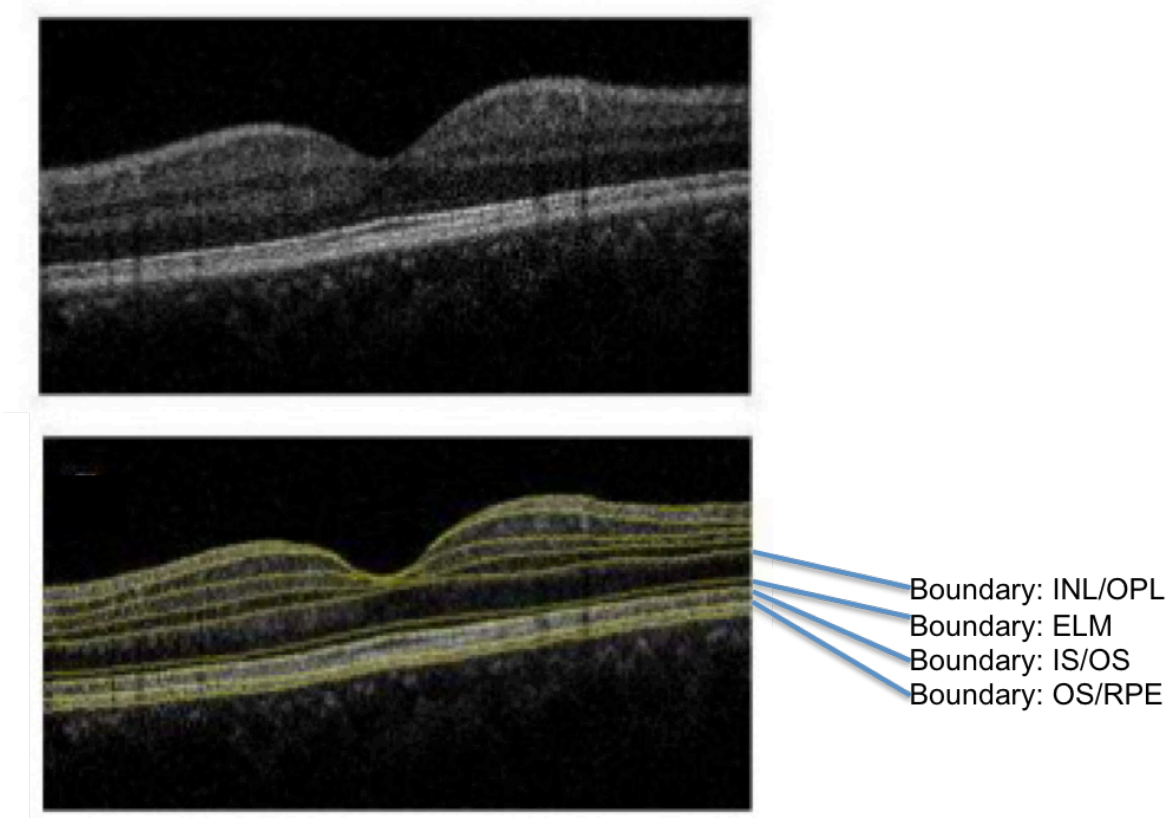

Each photoreceptor is composed of inner and outer segment containing unique structures with specialized functions, cell body containing a nucleus, and a synaptic terminal where neurotransmission occurs (Kolb et al 2012). The inner segment contains energy-generating mitochondria, protein-synthesizing ribosomes, and membranes

where opsin molecules are assembled. Opsins are then passed to the outer segment, where membrane evaginations and invaginations form discs. These discs detach and become free-floating within the outer segment rods, but remain attached to the outer segment membrane in cones. The opsin molecule binds 11-*cis*-retinaldhyde, which converts to *trans* formation upon absorption of a light photon, resulting in conformational changes that activate a cascade of events. Among these are the activation of the molecule rhodopsin to metarhodopsin II, which then activates the G-protein transducin, hydrolyzing cGMP-phosphodiesterase, leading to closing of a membrane bound cGMP-gated cation channel. In the dark, cation channels are open with a steady flow of current such that the photoreceptor is partially depolarized. The majority (80%) of cations are Na^{+}, but also consist of components of Ca^{2+} (15%) and Mg^{2+} (5%). Light-stimulated activation cascade causes closure of these cation channels, stopping the dark current and causing the photoreceptor membrane to hyperpolarize. The dark-state partially depolarized photoreceptor releases the amino acid glutamate, whereas light stops neurotransmitter release. This neurotransmitter release or cessation then affects second-order neurons.

The thickness of photoreceptor layer may be important. Thinner photoreceptor layer has been found to be linked to decreased visual sensitivity (Asaoka et al 2017), macular degeneration (Kenmochi et al 2017), and extreme hypertension (Lee et al 2017). Perhaps because of their critical role in visual function, much has been published regarding photoreceptors and physiologic changes, particularly with age. Histological studies show rod morphology changes beginning in the fourth decade, described as nodular swelling with increased diameter of 2.5-3.5 µm, initially in the perimacular

region, then extending to all areas of the macula with advanced age (Marshall et al 1979). By the seventh decade, 10-20% of rods were found to be involved (Marshall et al 1979). In contrast, cones have been described as accumulating refractile bodies of approximately 0.8 μm in size, particularly in eyes of women older than 40 years of age (Tucker GS 1986). Among men, refractile bodies were smaller, fewer in number, and involved fewer cones (Tucker GS 1986). Metabolic by-products such as lipofuscin have been described as accumulating in both rods and cones (Iwasaki and Inomata 1988). One might expect that the increase in accumulated byproducts might be associated with thickening of the photoreceptor layer. However, there is a reported 30% decline in rod density between mid-life and the 9th decade (Curcio et al 1993). A study of 55 normal eyes counted the number of photoreceptor inner segments on photographic images of histological slides found photoreceptor density decreased at a rate of 0.2% – 0.4% per year, with rods affected more than cones (Panda-Jonas et al 1995). Both increased accumulation of byproducts and swelling of photoreceptors, as well as gradual loss of rods and cones, may affect photoreceptor thickness.

Recent imaging techniques have allowed study of photoreceptor thickness *in vivo*. Despite the quantity of literature, much of it is conflicting with some groups reporting thinner photoreceptors with older age (Kenmoci et al 2017), whereas others report greater thickness with age (Wei et al 2017, Demirkaya et al 2013). The former study did not find an association with sex or refractive error (Kenmoci et al 2017), and the latter were underpowered for more detailed associations among subgroups (Wei et al 2017, Demirkaya et al 2013). The relatively small size of each of these studies, with 127 in the former (Kenmoci et al 2017), and 74 and 120 in the latter studies (Wei et al 2017,

Demirkaya et al 2013), may have been biased by outliers or demographic variation. For instance, Wei, et al. included 6 people who were white, 36 Asian, and 32 Hispanic but no effort was made to account for these ethnic differences in the statistical analysis.

2.3.4 Outer Plexiform Layer and Inner Nuclear Layer

Synapses between photoreceptors and second-order neurons occur in the outer plexiform layer. The outer plexiform layer and photoreceptor layers are distinct in histologic section (Figure 2.9), but cannot be reliably segmented with current OCT technology (Figure 2.11). The outer nuclear layer containing photoreceptor nuclei and outer plexiform layer containing synaptic connections appear together on OCT segmentation. The next visible boundary is that between the outer plexiform layer and inner nuclear layer. The latter contains the cell bodies of second-order neurons.

At the outer plexiform layer, photoreceptors synapse with bipolar cells and horizontal cells (Kolb et al 2012). A degree of integration of visual signaling occurs here, through successive ON and OFF pathways, splitting information into two channels: one for detecting objects lighter than background and another for objects darker than background. The signal interactions also create simultaneous contrast of visual objects through receptive field structure with a center contrasted to an inhibitory surround.

Each cone photoreceptor cell synpases 1-to-1 with a single bipolar cell known as the midget bipolar, whereas multiple rods converge on a single bipolar cell (Regillo et al

2010). Typically, 15 to 50 rods synapse with a single bipolar cell, depending on central versus peripheral location in the retina (Kolb et al 2012), but the number of rods synapsing on a single bipolar cell may exceed 100 (Regillo et al 2010). Bipolar cells, like photoreceptors, have a graded response with a change in polarization (Regillo et al 2010). Photoreceptors are in a depolarized state in the dark, and become hyperpolarized in light, which stimulates release of glutamate neurotransmitter. In contrast, bipolar cells may respond with either hyperpolarization or depolarization. The hyperpolarizing type are known as OFF-center cells, whereas depolarizing type are called ON-center cells (Kolb et al 2012). Bipolar cells will subsequently synapse with ganglion cells, which have a single type of excitatory channel; thus, the bipolar cell essentially determines the signal status that the ganglion cell will deliver to the brain.

Horizontal cells act as laterally interconnecting neurons in the outer plexiform layer (Kolb et al 2012). They are further connected by gap junctions, so they form a large interconnected cell network. The dendritic trees of horizontal cells vary in size, with smaller trees centrally and larger ones peripherally. Horizontal cells hyperpolarize in response to glutamate neurotransmitter from photoreceptors. They summate information from across a wide spatial area of the horizontal cell network, and provide a feedback response to photoreceptor and bipolar cells.

2.3.5 Ganglion Cell Layer and Inner Plexiform Layer

Bipolar cells synapse with ganglion cells at the inner plexiform layer, with signal modulation by amacrine cells (Kolb et al 2012, Regillo et al 2010). The cell bodies and

nuclei of ganglion cells lie in a layer of the same name. The inner plexiform layer and ganglion cell layers are distinct histologically (Figure 2.9), but are difficult to segment with current OCT imaging (Figure 2.12). Thus, they are often treated as a single complex in research studies using OCT.

Figure 2.12. Optical coherence tomography (upper image) and automated segmentation (bottom image) ganglion cell layer – inner plexiform layer complex. NFL/GCL = boundary between nerve fibre layer and ganglion cell layer. GCL-IPL = boundary between ganglion cell layer and inner plexiform layer. IPL/INL = boundary between inner plexiform layer and inner nuclear layer. (Adapted from Yang et al 2010)

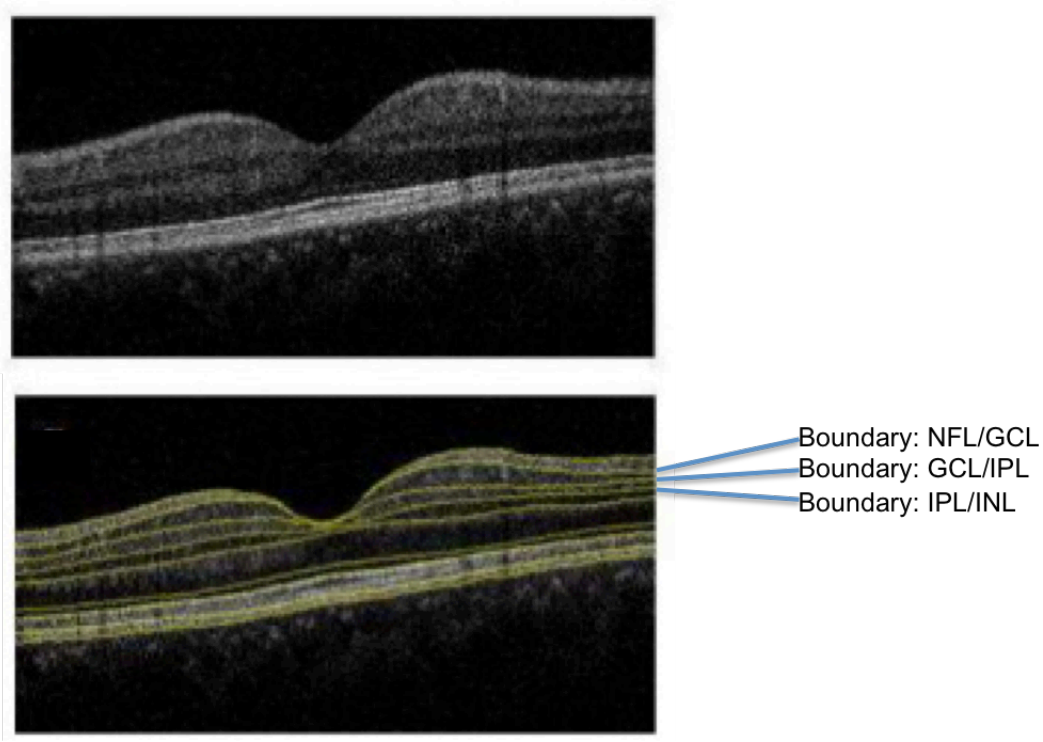

Amacrine cells may synapse with bipolar cells, ganglion cells, or other amacrine cells. They are classified based on morphology, including dendritic tree size (small, medium, large), branching characteristics (tufted, linear, beaded, etc), and stratification within the IPL. Cajal noted strata within the IPL, with cells being capable of making synaptic interactions within the same strata, but not across disparate strata (Cajal 1892). Amacrine cells produce inhibitory neurotransmitters, GABA and glycine, to further modulate visual signals (Kolb et al 2012).

Ganglion cells are classified according to cell body size, dendritic tree spread, branching patterns, and branching level in the strata of the IPL (Kohl et al 2012). They can be monostratified or bistratified. The size of ganglion cell dendritic trees varies depending on distance from the fovea, with the smallest dendritic trees near the fovea, and larger dendritic spread in the peripheral retina. The two most common types of ganglion cells in the human retina are the parasol and midget ganglion cells, which project to the magnocellular and parvocellular layers of the lateral geniculate nucleus, respectively. Parasol ganglion cells are also known as M-cells and are sensitive to luminance changes in dim illumination scotopic conditions, and have large dendritic fields (Cioffi et al 2010). They are primarily responsible for processing information related to motion, and are not responsive to colour. Midget cells, also known as P-cells, are concentrated in the central retina, have smaller dendritic fields, and smaller-diameter axons. Their conduction velocity is slower, and are specialized in colour vision under higher luminance conditions. They are important for discerning fine detail and colour vision.

Axons of ganglion cells form the nerve fibre layer, which will pass through the optic nerve to an area of the brain known as the dorsolateral geniculate nucleus (Regillo et al 2010). Disruptions of these pathways have been associated with glaucoma, the second leading cause of blindness worldwide (Kingman 2004). Measurements of the ganglion cell-inner plexiform layer complex have been shown to have utility in detecting glaucoma (Naghizdeh et al 2014, Na et al 2012, Sung et al 2012).

GCL-IPL thinning among different age groups is well established, both in histologic studies (Gao et al 1992) and imaging *in vivo* (Wei et al 2017, Demirkaya et al 2013, Harwerth and Wheat 2008, Zhang et al 2016, Altay et al 2017, Bloch et al 2017). A cross-sectional study of 74 people showed 0.21% per year (equivalent to 0.14 µm per year) difference in mean GCL-IPL thickness over a span of six decades (Wei et al 2017). A larger cross-sectional study of 623 Chinese adults showed an association of thinner GCL-IPL with older age ($\beta = -0.202$, $P < 0.001$) (Koh et al 2012). This is consistent with results from the Advanced Imaging for Glaucoma Study (AIGS), which provides both longitudinal and cross-sectional data, showing GCL-IPL thickness decreased 0.25 µm per year (SD 0.05, $P < 0.001$) in longitudinal analysis and 0.17 µm thinner per year of baseline age (SD 0.05, $P < 0.001$) in cross-sectional analysis (Zhang et al 2016). The Twins UK study analyzed 1657 healthy participants of European ancestry, conducting heritability analysis using maximum likelihood structural equation twin modeling, and found significant associations with age ($\beta = -0.14$, $P < 0.001$) (Bloch et al 2017).

While GCL-IPL thinning with age has been described by multiple sources, the associations with other variables are less well understood. A few groups with larger

study populations have attempted to study variables associated with GCL-IPL thickness. A Chinese group of 623 participants found an association between thinner GCL-IPL with female sex (β = −2.367, P < 0.001) and axial length (β = −1.279, P = 0.002) (Koh et al 2012). They found no significant association with IOP, central corneal thickness, or diabetes (Koh et al 2012). AIGS found no association with IOP (Zhang et al 2016). They did not attempt to identify associations with other demographic, ocular, or systemic factors. TwinsUK found BMI (β = -0.15, P = 0.001) and refractive spherical equivalence (β = 0.70, P <0.001) were significantly associated with GCL-IPL thickness in multivariable modeling (Bloch et al 2017). Intraocular pressure was not significant in any statistical model (Bloch et al 2017). Blood pressure, and diabetic indices were significant in univariable regressions, but not significant after controlling for other confounders (Bloch et al 2017). Sex was also not significant – but the study was underpowered due to the small number of men included (174 or 10.5%) (Bloch et al 2017). Several other studies were not able to find a significant association with sex and GCL-IPL thickness (Wang et al 2016, Mwanza et al 2011).

2.3.6 Retinal Nerve Fiber Layer

RNFL is a potential biomarker for detection and monitoring of ocular and neurologic diseases, such as glaucoma, multiple sclerosis, and dementia (Tuulonen and Airaksinen 1991, Fisher et al 2006, Garcia et al 2014, Coppola et al 2015). Changes in RNFL thickness correlate with optic nerve function measured by perimetry (Schuman et al

1995, Miglior et al 2007) and multifocal visual evoked potential (Hood et al 2007, Horn et al 2012). While peripapillary RNFL remains the clinical reference standard, there is emerging evidence that macular retinal nerve fiber layer (mRNFL), may add important additional information in monitoring diseases such as glaucoma. One reason for this is that it is less affected by anomalous optic disc anatomy (Rauscher et al 2009, Akashi et al 2013).

The retinal nerve fiber layer is composed of axons from ganglion cells as they pass toward the optic nerve. It appears as a well-demarcated hyperintense layer on OCT (Figure 2.13). The fibers are distributed in an arcuate pattern, arcing toward the superior and inferior portions of the retina before returning toward the midline and entering the optic nerve (Figure 2.14).

Figure 2.13. Optical coherence tomography (upper image) and automated segmentation (bottom image) of retinal nerve fiber layer. ILM = internal limiting membrane. NFL/GCL = boundary between nerve fiber layer and ganglion cell layer. (Adapted from Yang et al 2010)

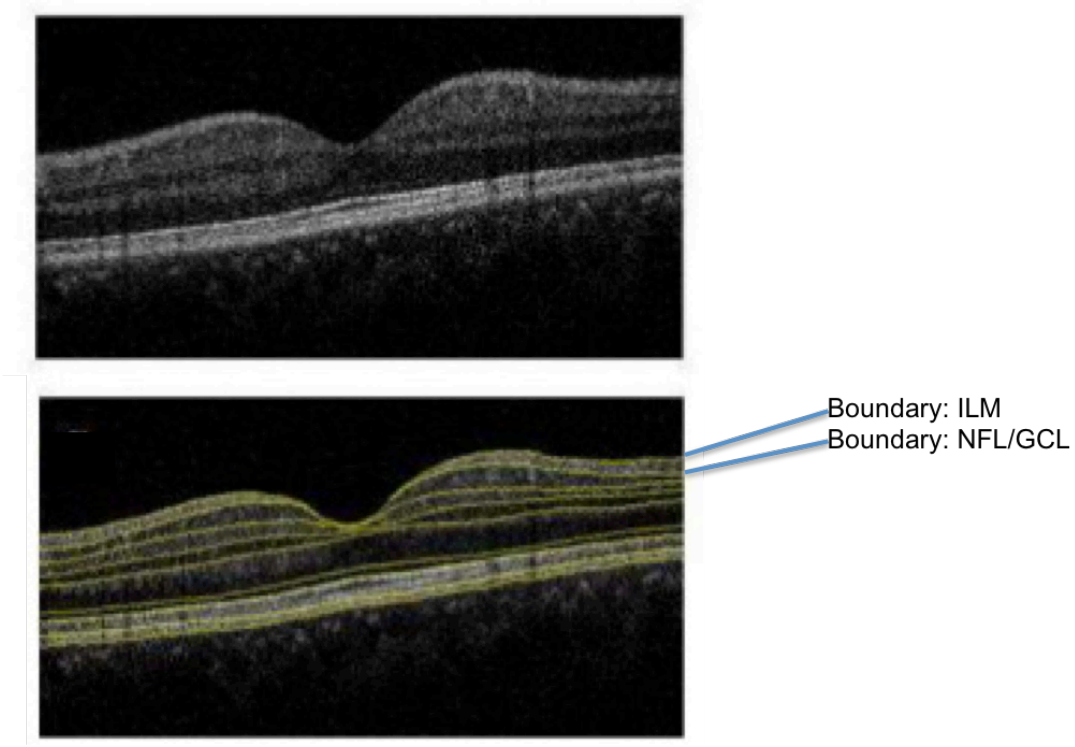

Figure 2.14. Diagram of nerve fiber layer distribution at retina of left eye. Yellow lines denote nerve fibers, yellow circle denotes optic nerve, red lines represent blood vessels.

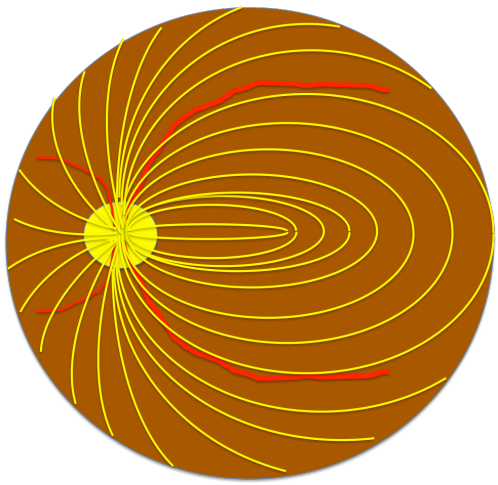

Physiologic changes such as age and ethnicity are associated with RNFL thickness (Schuman et al 1995). Understanding the distribution of normal mRNFL thickness values in the population is important in interpreting results of imaging tests. Histologic studies of the mRNFL show average thicknesses of 27, 34, 26, and 12 µm just superior, inferior, nasal, and temporal to the foveola, and show lower thicknesses in older people (Varma et al 1996). Observed cross-sectional differences between older and younger people on OCT (Sung et al 2009, Jampel et al 2009) suggest that RNFL does progressively thin with age. Evidence has also emerged suggesting that mRNFL is associated with ethnicity, with thinner RNFL seen among those of African descent (Tan et al 2009). The use of mRNFL in clinical management of disease remains limited by relatively small normative databases.

The connection between retinal nerve fibre layer defects and glaucoma has been well established. Changes in nerve fibre layer thickness measured by OCT have been shown to correlate with visual field defects ($p<0.001$) (Schuman et al 1995). In a comparative study of eyes with normal characteristics, ocular hypertension, and glaucoma, OCT showed peripapillary RNFL was significantly thinner among eyes with ocular hypertension (mean 72.8 µm, 95% CI 66.4-78.1 µm) and glaucoma (mean 44.4 µm, 95% CI 36.4-52.6 µm) as compared to normal eyes (85.8 µm, 95% CI 80.2-91.7 µm; $p<0.001$ for all diagnostic groups) (Bowd et al 2000). One study of people with ocular hypertension that converted to glaucoma, found the initial sign of glaucomatous damage could be either generalized thinning or localized RNFL thinning (Tuulonen et al 1991).

More recently, there has been interest in other diseases associated with RNFL damage, especially neurologic disease. Conceptually, the retina is often regarded as an extension of the central nervous system (Whitson et al 2015). The shared embryological origin of the retina and the brain means that retinal microvasculature and neuronal components offer a unique "window" on tissues that are closely allied to intracranial structures (Cheung et al 2014, Wong and Mitchell 2007, Liew et al 2009a, Lloyd et al 1995). If the eye is an extension of the brain, then it may be vulnerable to the same processes that cause neurodegenerative diseases (Whitson et al 2015). It has been suggested (Almarcegui et al 2010) that axonal damage in the brain will result in changes to the retinal nerve fibre layer (RNFL) (Frohman et al 2006). It is these defects that may be the earliest signs of neurological diseases like Alzheimer's disease (Garcia-Martin et al 2014, He et al 2012, Hinton et al 1986).

Several studies have investigated the association between RNFL and Alzheimer's disease, and suggested that such patients may have significantly thinner retina. Illustrating this, Gao *et. al.* (2015) found that patients with Alzheimer's disease and mild cognitive impairment showed significantly thinner RNFL compared to controls. In addition, they also found volume of the macula lutea in both patient groups were significantly reduced as compared to controls. A different study carried out by Garcia-Martin *et. al.* (2014) reported similar findings in patients with mild Alzheimer's. The data from this report proposed that the first affected area of the retina in mild Alzheimer's disease might be the macular area and that as the disease advances, deterioration of the RNFL becomes more evident. However, the authors were unable to ascertain whether the macula really is the first area that mild Alzheimer's disease affects, or

whether it is simply the first place with enough retinal ganglion cells present to see an effect. The findings above confirm previous reports that there may be reduced RNFL thickness and macular volume in patients with Alzheimer's disease and mild cognitive impairment (Iseri et al 2006, Kesler et al 2011, Marziani et al 2013, Paquet et al 2007, Danesh-Meyer et al 2006a, Parisi 2003, Parisi et al 2001, Valenti 2007, Shi et al 2014). As well as in the areas of general cognitive decline and AD, comparable results have been found in studies examining the association between retinal abnormalities and Parkinson disease (Inzelberg et al 2004, Moschos et al 2011), Lewy body dementia (Moreno-Ramos et al 2013) and multiple sclerosis (MS) (Parisi et al 1999, Saidha et al 2012, Tatrai et al 2012), though most of these studies were limited by small sample size (n=10-40).

Understanding RNFL is important toward current clinical use in managing diseases such as glaucoma, and may have future applications for cognitive function.

2.4 Cognitive Function

Cognitive function can be broadly defined as cerebral activities related to mental processes including knowledge, memory, reasoning, language, and attention. Defects in cognitive function are found in dementia such as Alzheimer's disease. Dementia is the largest neurodegenerative condition contributing to the global disease burden with an estimated prevalence of 45,956,000 patients world wide (Global Burden of Disease Study 2015 in Lancet 2017). In high-income North America, dementia is ranked top amongst other neurological diseases for disability-adjusted life-years (Global Burden of Disease Study 2015 in Lancet 2017, Saint Martin et al 2017, Hebert et al 2013). Prevalence of dementia increases with age, affecting 2-5%, 11%, 32%, and 82% of people aged over 60, 65, 75, and 85 years respectively (Ferri et al 2005, Hebert et al 2013). As the population ages, rates of dementia in Western countries are expected to increase, doubling every 20 years to 81.1 million worldwide by 2040 (Ferri et al 2005). Others project the prevalence of Alzheimer's Disease, the commonest form of dementia, may triple by 2050 (Global Burden of Disease Study 2015 in Lancet 2017, Hebert et al 2013, Hebert et al 2003). The World Health Organization estimated that dementia contributed to 11.2% of years lived with disability in people aged 60 and older, more than stroke (9.5%), cardiovascular disease (5.0%), and cancer (2.4%) (2003). Not only does dementia cause disability, but there is an economic burden as well, with an estimated $8.2 billion yearly in the United Kingdom for institutional care (Comas-Herrera et al 2005). Informal caregivers such as family members may need to cut back on work hours, costing an estimated $18 billion in the United States in 1998 (Langa et al

2001). Globally, an estimated 46 million people are living with dementia, a number that is expected to rise to 131 million by 2050 (Global Burden of Disease Study 2015 in Lancet 2017). However, if onset can be delayed by just 1 year, the projected global burden would decrease by 9 million (Brookmeyer et al 2007).

A hindrance to the development of new treatments to prevent dementia is the lack of markers that help predict who will be affected (Mormino et al 2014, Wirth et al 2013). One of the most common tests of cognitive function is the mini-mental state examination (MMSE). It is a 30-point questionnaire requiring 5-10 minutes, often used in clinical settings to detect early signs of dementia (Baek et al 2016). It has good sensitivity and specificity to detect mild to moderate stages of dementia (Baek et al 2016). However, it is less sensitive for mild cognitive impairment, particularly certain areas of cognitive function such as abstract reasoning (Baek et al 2016). It is affected by education levels, in that people with lower education or socioeconomic status have more false-positive errors, while those with higher education have a ceiling effect because of the low level of item difficulty (Baek et al 2016). Other tests have been developed, including the Cambridge Cognitive Examination (CAMCOG) used in the Rotterdam Study (Breteler et al 1994). The CAMCOG test is frequently used to evaluate for dementia and cognitive impairment, assessing orientation, language, memory, abstract thinking, perception, and calculation (Figueiredo and Salter 2009). It includes 67 items, though is sometimes shortened to 25 items in the revised Rotterdam CAMCOG, and requires 20-30 minutes to administer (Figueiredo and Salter 2009). It is not subject to ceiling effect of the MMSE but it is affected by education and social class (Huppert et

al 1995). Computerized cognitive function tests have also been developed, such as CogState (Falleti et al 2006). Each test has its strengths and weaknesses.

In selecting a test, one must consider the population of interest, including study size, time to administer test, expected level of cognitive function, and indices of interest. The first two are important toward practicalities of study design. For a study the size of UK Biobank, time to administer can be costly, upwards of 500,000 GBP per minute (personal correspondence, Paul Foster). Thus, one ought to consider what portions of the test are pertinent to the cognitive level of the study population. For instance, the clock-drawing portion of the MMSE can be a good test for delirium, but is unlikely to be positive in a largely healthy population presenting for voluntary out-patient study. One need not necessarily use an entire battery of tests, but may rather select specific portions that may be sensitive within the population of interest to identify relative differences and potential associations. UK Biobank used four main tests: prospective memory, pairs matching, numeric & verbal reasoning, and reaction time. These will be described further within methods section.

While testing cognitive function is critical in studying dementia, it can be limited in the time required for deficits to develop. Also, waiting for cognitive deficits to develop is necessarily after onset of disease. The ability to detect sub-clinical disease would be beneficial to increasing the speed of research, developing earlier treatment modalities, and public policy planning to identify at-risk populations. Magnetic resonance imaging (MRI) can identify certain structural changes that may be related to future risk of dementia, such as periventricular and subcortical white matter lesions, lacunar infarcts,

and atrophy (Kantarci 2005, Smith et al 2003, Vermeer et al 2003). However, MRI may not be useful in detecting early stages of disease, and is limited by issues of spatial resolution, time of image acquisition, motion artifact, and cost of imaging. As a result, the retina has become a candidate for detection of cognitive function and its deficits.

The retina shares similar embryologic origin as neural tissue of the brain (Regillo et al 2010). It is currently visualized and measured in standard ophthalmic practice, through direct examination, fundus photography, and imaging techniques such as OCT. The Rotterdam study found an association between retinopathy and prevalent dementia and Alzheimer's disease (Schrijvers et al 2012). Retinal venular widening has been associated with incident dementia (de Jog et al 2011). Larger retinal arteriolar and venular calibres have been associated with lower scores on memory tests (Ding et al 2011). Some have suggested that retinal branching patterns may be related to blood flow and ischemia (Tomita et al 2005, Hammes et al 2011). Decreased retinal vascular fractal dimension, a measure of the geometric branching complexity and density of retinal vessels, has been associated with worse scores on tests for cognitive dysfunction (Cheung et al 2014). However, measurement of retinal vascular calibre and branching can be time-consuming when done manually, and current software has not been able to fully automate the process. OCT has become useful as a measure of retinal thickness, with fast acquisition time, automated segmentation, and high resolution with ability to identify certain retinal sub-layers with good reliability. OCT is a non-invasive imaging tool that can produce three dimensional cross-sectional images of the retina and permits precise and accurate measurement of the thickness of individual retinal components (Huang et al 1991, Yang et al 2010).

The RNFL is thinner in people with early Alzheimer's Disease (AD) compared to normal, age-matched controls (Paquet et al 2007). Similar findings have been reported in studies of other neurodegenerative conditions associated with cognitive decline, such as Parkinson's disease and Lewy body dementia (Weil et al 2016, Moreno-Ramos et al 2013). More recently, studies using OCT imaging have shown that RNFL is thinner in people with early cognitive impairment (Cheung et al 2015, Garcia-Martin et al 2014, Coppola et al 2015). A cross-sectional association between retinal anatomy and cognitive function has been documented in two larger community-based studies (van Kookwijk et al 2009, Khawaja et al 2016). Only one small, prospective study has shown that a mixed cohort of 78 people with normal or mildly impaired cognition who suffered future cognitive decline also showed greater reduction of RNFL thickness measured by OCT over a 25 month period (Shi et al 2014). At the time of this writing, no major studies existed linking retinal structure and future cognitive function.

2.6 Plan of Research

The eye is unique as compared to the rest of the body, not only for its perceptive abilities, but also for the ease with which it can be perceived and examined. In its natural state, both the anterior and posterior segments of the eye can be directly visualized. With a slit lamp, or even a handheld device, the top three causes of blindness worldwide – cataracts, glaucoma, and macular degeneration – can largely be diagnosed by direct examination (World Health Organization, accessed 2018). Partially because of the ease of examination, the eye can be a site where pathology elsewhere in the body can be identified, sometimes as a direct result of the disease, such as retinopathy and diabetes; or through shared disease processes, such as hypertension causing both renal and retinal vascular changes (Cioffi et al 2010, Regillo et al 2010). Interest has developed in the associations between the eye and cognitive function (Global Burden of Disease Study 2015 in Lancet 2017, Paquet et al 2007, Weil et al 2016, Moreno-Ramos et al 2013). However, to understand pathology, or a deviation from normal, one must first understand the range of normal variation.

As part of UK Biobank, UK residents aged 40–69 years at enrolment underwent baseline OCT imaging of the retina, physical examination, and answered a health questionnaire. Eye examination included Goldmann-adjusted intraocular pressure (IOP) and refraction. Four basic cognitive tests were performed at baseline, then repeated in a subset of participants approximately 3 years later.

The current analysis includes eyes with high-quality OCT images, excluding those with eye disease or vision loss, history of ocular or neurological disease, or diabetes. Physiologic and demographic associations with RPE, photoreceptor IS-OS, GCL-IPL, and RNFL are explored. Additionally, associations are explored between inner retinal thickness and cognitive function. Further, the potential of RNFL and GCL-IPL thickness measurement to identify those at greater risk of cognitive decline in a large community cohort of healthy people are examined, using multivariable logistic regression modeling to control for demographic as well as physiologic and ocular variation.

SECTION III:

MATERIALS AND METHODS

3.1 UK Biobank

UK Biobank study is a multi-site community-based study of 502,656 UK residents aged 40–69 years who were registered with the National Health Service (NHS) from 22 study assessment centers between 2007-2010. UK Biobank was established by the Wellcome Trust medical charity, Medical Research Council, Department of Health, Scottish Government, and Northwest Regional Development Agency (https://www.ukbiobank.ac.uk/about-biobank-uk/). The North West Multi-center Research Ethics Committee approved the study (REC Reference Number: 06/MRE08/65), in accordance with the principles of the Declaration of Helsinki. This study was conducted under generic approval from the NHS National Research Ethics Service (Ref. 11/NW/0382). All participants gave written informed consent. Baseline assessments took place at 22 centres across England, Scotland and Wales between 2006 and 2010.

The overall study protocol (http://www.ukbiobank.ac.uk/resources/) and protocols for individual tests (http://biobank.ctsu.ox.ac.uk/crystal/docs.cgi) are available online. In brief, UK residents registered with the NHS received an invitation to participate by mail. Participants answered a touch-screen questionnaire of demographic, socioeconomic and health information. Health examination included blood pressure, body mass index, and blood samples, which were taken for biological markers. At the time of this study, blood sample results were unavailable for analysis. Eye data including visual acuity, autorefraction (Tomey RC5000, Erlangen-Tennenlohe, Germany), Goldmann-corrected intraocular pressure (IOP_G) and cornea-corrected IOP (IOP_{CC}) (Ocular Response Analyzer,

Reichert, Depew, NY, USA) were collected from 133,668 participants in 2010. Acquisition of retinal OCT measurements and was performed in 67,318 of these participants. Ophthalmic tests were performed at 6 centers distributed across the United Kingdom, including Croydon and Hounslow in Greater London, Liverpool and Sheffield in Northern England, Birmingham in the Midlands, and Swansea in Wales.

Participants identified their own ethnicity as either white, Chinese, Asian (in this cultural context, the majority were of Indian descent, but also included those of Pakistani, Bangladeshi, and others), black, mixed, or other. I combined the mixed and other categories into one group. The Townsend deprivation index was determined according to the participants' postcodes at recruitment and the corresponding output areas from the preceding national census. The index was calculated on the basis of the output area's employment status, home and car ownership, and household condition; the higher and more positive the index, the more deprived an area. Smoking status was determined by the participant's answer to “Do you smoke tobacco now?” Participants could answer “yes,” “on most or all days,” “only occasionally,” “no,” or “prefer not to answer.” Diabetes status was determined as those who answered yes to “Has a doctor ever told you that you have diabetes?” Glaucoma and macular degeneration status were determined as those who selected “glaucoma” or “macular degeneration” from a list of eye disorders to the question, “Has a doctor told you that you have any of the following problems with your eyes?”

3.2 Inclusion and Exclusion Criteria

People who underwent retinal thickness measurement through SDOCT imaging as part of UKBB were used as a starting point for analysis. Participants were excluded from the analysis if they withdrew consent. Images were excluded if missing thickness values from Early Treatment of Diabetic Retinopathy Study (ETDRS) subfields, poor OCT signal strength or image quality, poor centration certainty, or poor segmentation certainty (poorest 20% of images excluded based on each of the segmentation indicators). This led to the identification of the subset of people with good quality, well-centered images, and central, stable fixation during the OCT scan. Participants with high refractive error (>+6 or <-6 diopters), visual acuity <20/25, IOP ≥22 mmHg or ≤5 mmHg, self-reported ocular disorders (recent eye surgery, corneal graft, ocular injury, glaucoma, macular degeneration), diabetes, or neurodegenerative disease were excluded. Finally, if both eyes of one patient were eligible for inclusion in this analysis, one eye was chosen at random using randomization software in STATA/SE version 13.1 (StataCorp LP, College Station, Texas, USA) (Figure 3.1). At this point, analyses of associations between retinal thickness with demographic, physiologic, and ocular factors were performed. For associations between retinal thickness and cognitive function at baseline and 3-year follow-up, additional exclusion was performed based on whether cognitive function testing was performed. Of note, availability of follow-up cognitive testing was based on whether a participant was invited back; this number was chosen based on other facets of UK Biobank, rather than specifically on the requirements of the studies undertaken in this thesis.

Figure 3.1. Inclusion/exclusion criteria for macular RNFL SDOCT. Because data cleaning for individual layers was performed separately, manual regrading for individual layers were also performed separately.

* Exact numbers included differed for each retinal layer, due to ease of segmentation and imaging quality. Numbers for RNFL are shown here, as this was used in analysis of longitudinal data. For other layers, numbers are shown in the appropriate subsections.

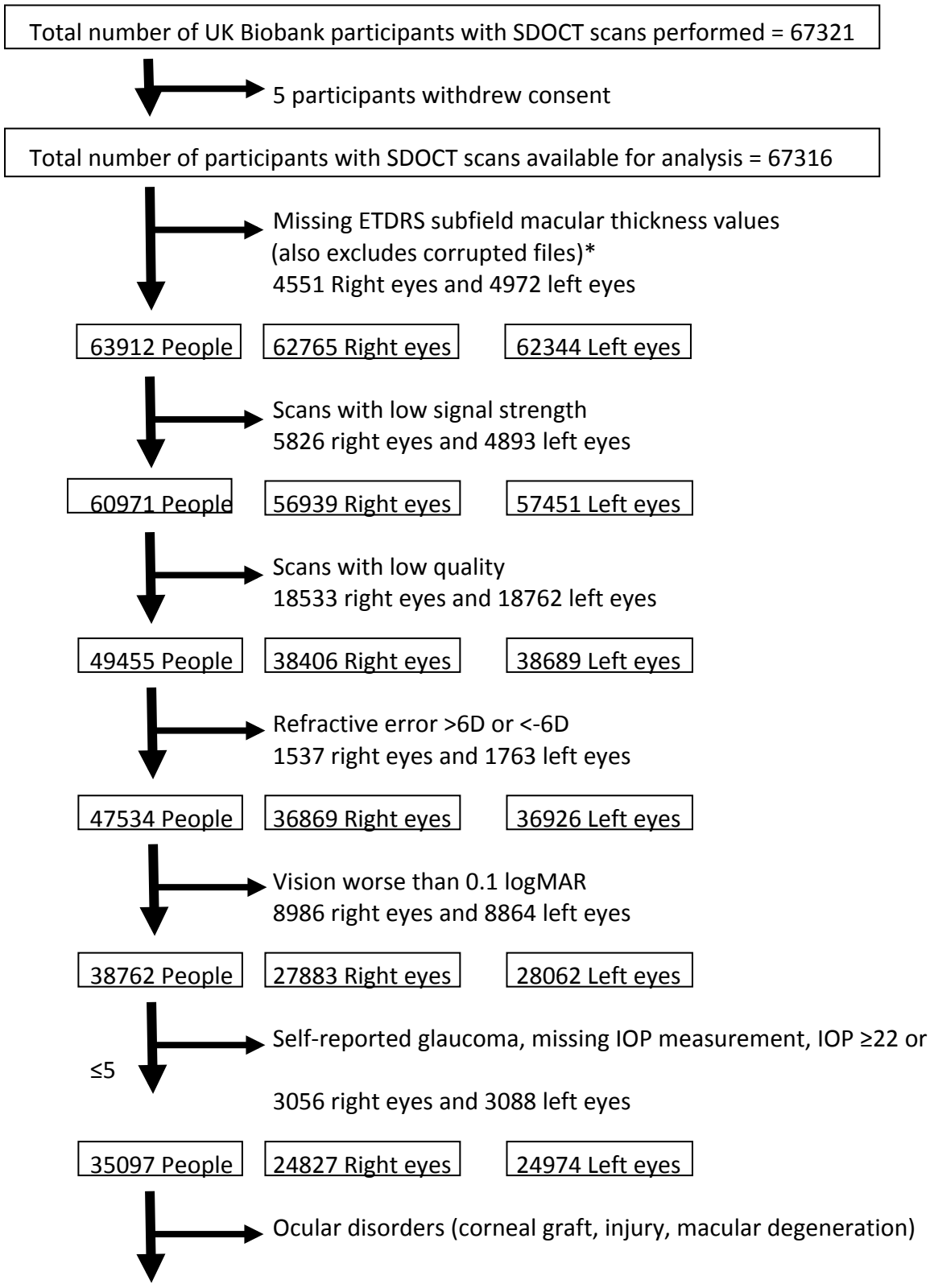

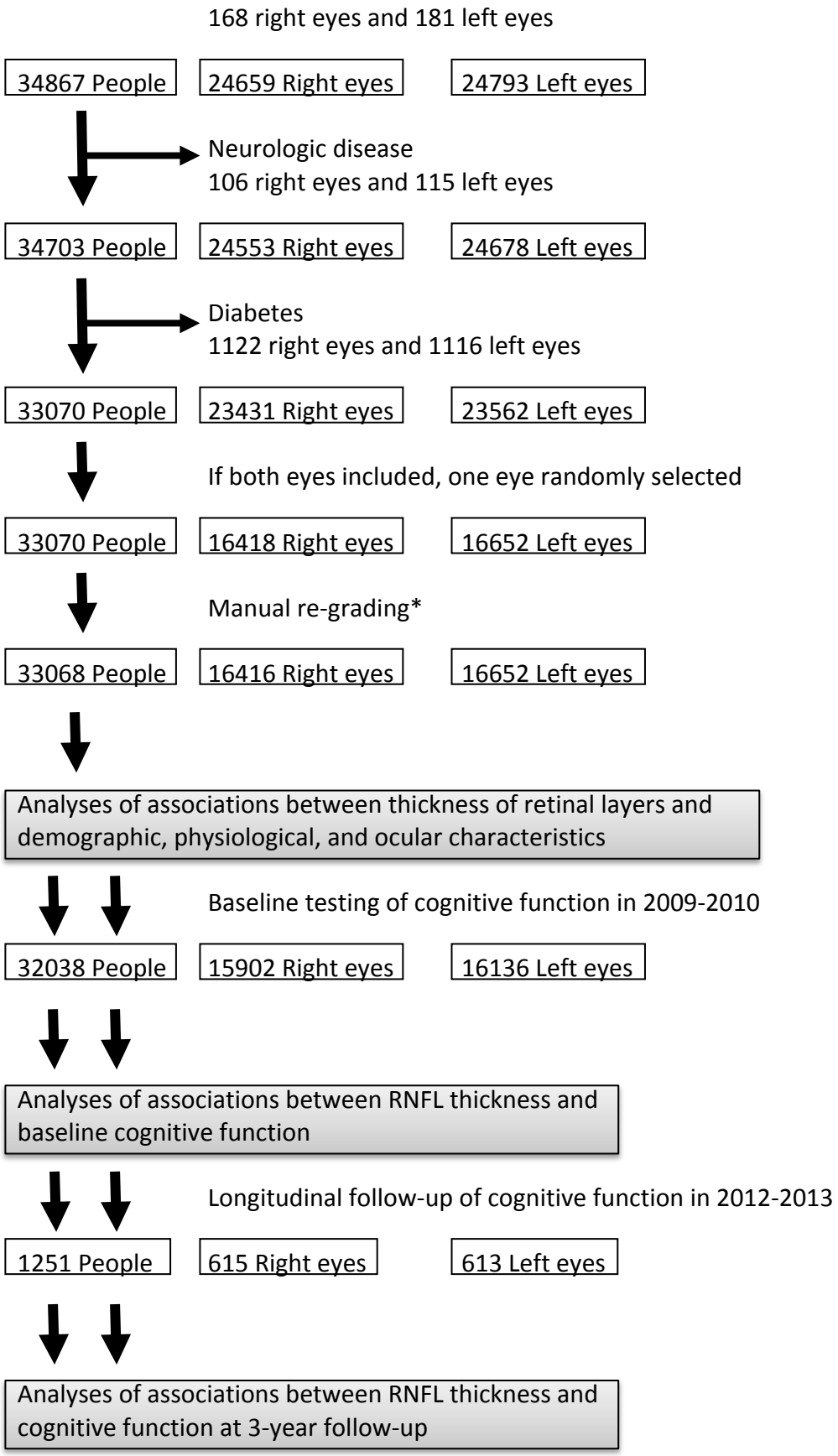
168 right eyes and 181 left eyes
34867 People
24659 Right eyes
24793 Left eyes
Neurologic disease
106 right eyes and 115 left eyes
34703 People
24553 Right eyes
24678 Left eyes
Diabetes
1122 right eyes and 1116 left eyes
33070 People
23431 Right eyes
23562 Left eyes
If both eyes included, one eye randomly selected
33070 People
16418 Right eyes
16652 Left eyes
Manual re-grading*
33068 People
16416 Right eyes
16652 Left eyes
Analyses of associations between thickness of retinal layers and demographic, physiological, and ocular characteristics
Baseline testing of cognitive function in 2009-2010
32038 People
15902 Right eyes
16136 Left eyes
Analyses of associations between RNFL thickness and baseline cognitive function
Longitudinal follow-up of cognitive function in 2012-2013
1251 People
615 Right eyes
613 Left eyes
Analyses of associations between RNFL thickness and cognitive function at 3-year follow-up

3.3 Eye measures and OCT Imaging Protocol

Eye data including visual acuity, autorefraction, Goldmann-corrected and cornea-corrected IOP (IOP_G and IOP_{CC}, respectively) were collected from 133,668 participants in 2009-2010. Participants were seated in a darkened room and asked if they had eye surgery, when, what type, and which eye. If a participant had surgery within the last 4 weeks, they were not permitted to continue with ocular measures. Visual acuity was assessed with the participant seated in a chair placed at 4-metres from a LogMar chart, and wearing their usual refractive correction. If the participant normally wears glasses/contacts, but has forgotten them, this fact was recorded. The right eye was measured first, followed by the left eye. The participant was asked to read letters aloud from the LogMar chart, with the test terminating when two out of five letters were incorrectly read. Next, an estimate of the participant's refractive error was obtained through the Tomey autorefractor. The participant's head was positioned within the autorefractor device, and standard protocol was followed to obtain measurement (http://biobank.ctsu.ox.ac.uk/crystal/docs/Refraction.pdf). The participant then proceeded to Reichert Ocular Response Analyzer for intraocular pressure measurement, and again standard protocol was used for device operation (http://biobank.ctsu.ox.ac.uk/crystal/docs/Intraocularpressure.pdf). If IOP was greater than 24, then the test was repeated, after checking the participant's head was correctly positioned, ensuring no air was in the way of the machine's air puff, and reminding participant to not blink. A maximum number of 3 attempts were made.

OCT imaging was performed using the Topcon 3D OCT 1000 Mk2 (Topcon Inc., Oakland, NJ, USA). Image acquisition was performed after visual acuity, autorefraction and IOP measurement had been completed. SDOCT imaging was carried out with lowest possible illumination conditions but without pharmacological dilation of the pupils. The scan protocol used was the 3-dimensional 6x6 mm^2 macular volume scan (512 horizontal A scans per B scan; 128 B scans in a raster pattern). The right eye was imaged first, then repeated for the left eye.

3.4 Analysis of Macular Thickness

All OCT images were stored as .fds image files on UK Biobank supercomputers in Oxford, UK. As part of the original UKBB data access rules and procedures for bulk data, the stored OCT files (source data) could not be copied, stored, or removed outside the local Oxford University network. Researchers were given access to computers at the central Biobank data repository via remote, secure log-in and could then install any analysis software needed on the UKBB computers. A copy of each preexisting 3-dimensional OCT scan file was retrieved from the UKBB database before running the segmentation analysis software. The derived data were then extracted, after which the OCT scan file was deleted. Up to 12 log-ins were implemented in parallel, increasing the processing throughput by a nearly proportional factor.

Version v1.6.1.1 of the Topcon Advanced Boundary Segmentation (TABS^{TM}) (Yang Q et al 2010) algorithm was used to identify the inner retinal surface and posterior boundary of the nerve fiber layer. Quality control measures recommended by Topcon included the image quality score (Q≥45), internal limiting membrane (ILM) indicator (≥7049.648), validity count (≥870), and motion indicators (minimum motion correlation ≥0.311721, maximum motion delta ≤5.484375, maximum motion factor ≤5.183594). The image quality score identified poor scan quality and/or segmentation failures. The ILM indicator was a measure of the minimum localized edge strength around the ILM boundary across the entire scan. It was useful for identifying blinks, scans that contain regions of severe signal attenuation, and/or segmentation errors. The validity count indicator was used to identify scans with a significant degree of clipping in the OCT scan's Z-axis dimension. The motion indicators utilize both the NFL and full retinal thicknesses, from which Pearson correlations and absolute differences between the thickness data from each set of consecutive B-scans were calculated. The lowest correlation and the highest absolute difference in a scan served as the resulting indicator scores. This last group of indicators served to identify blinks, eye motion artifacts, and segmentation failures. It should be noted that the various indicators, including the image quality score, tend to be highly correlated with one another.

Boundaries for segmentation of OCT images are shown in Figure 3.2. Of note, photoreceptor thicknesses were analyzed as inner segment and outer segment together, or external limiting membrane to OS/RPE boundary.

Figure 3.2. Segmentation boundaries of retinal layers.

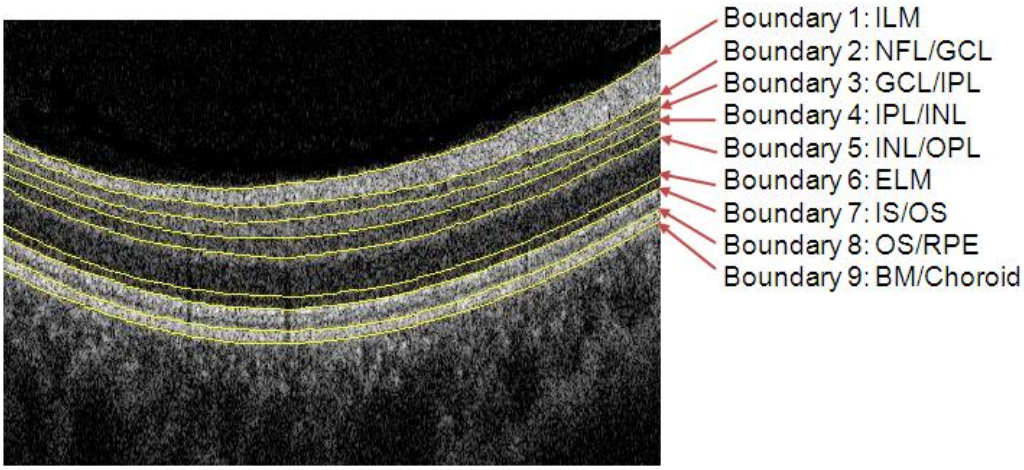

3.5 Manual Re-grading

After initial inclusion/exclusion criteria were applied, images at extremes of RNFL thickness were then submitted for manual re-grading to visually identify any errors in segmentation or abnormalities of retinal morphology. Because of the large size of the database, it was not feasible to manually re-grade every image. Rather, images were ordered according to thickness, and systematic manual re-grading performed in a stepwise manner (Figure 3.3). The image with the greatest thickness was reviewed first. Next, the image that was 1 standard deviation less than the thickest image was reviewed. If this image was abnormal (either abnormal morphology or segmentation error), then the next scan chosen for review was 1 standard deviation thinner. This was repeated until a normal scan could be identified. Once a normal scan was identified, the reviewer would choose 10 images at ½ standard deviation greater thickness than the normal image for review. If any of the 10 images were abnormal, the reviewer would

continue using the same algorithm until 10 normal images could be identified. This would be set as the cutoff when we felt we could confidently rely on automated segmentation. All images greater than this cutoff thickness were then discarded. This process was then repeated at the opposite end of the thickness spectrum, beginning with the thinnest image.

Figure 3.3a. Manual re-grading algorithm for reviewing images after automated segmentation, as well as application of inclusion/exclusion criteria.

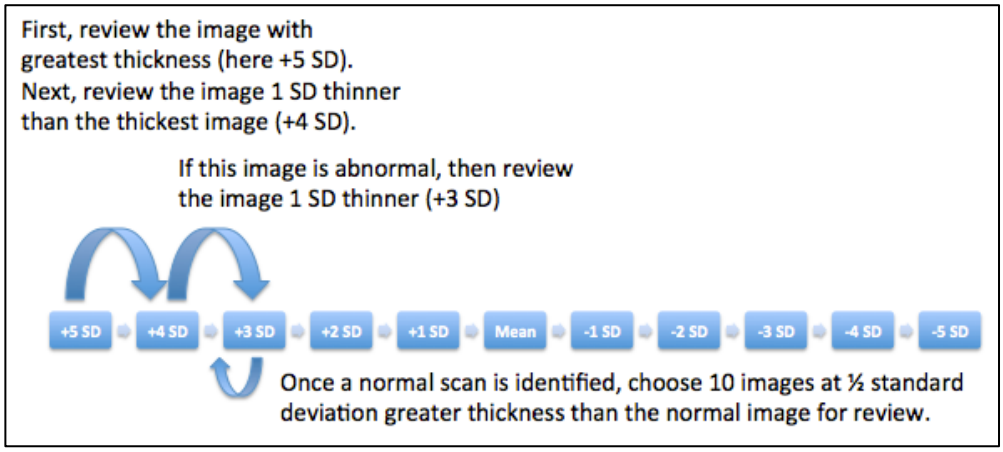

Figure 3.3b. Example of an image discarded because of poor segmentation due to low image quality.

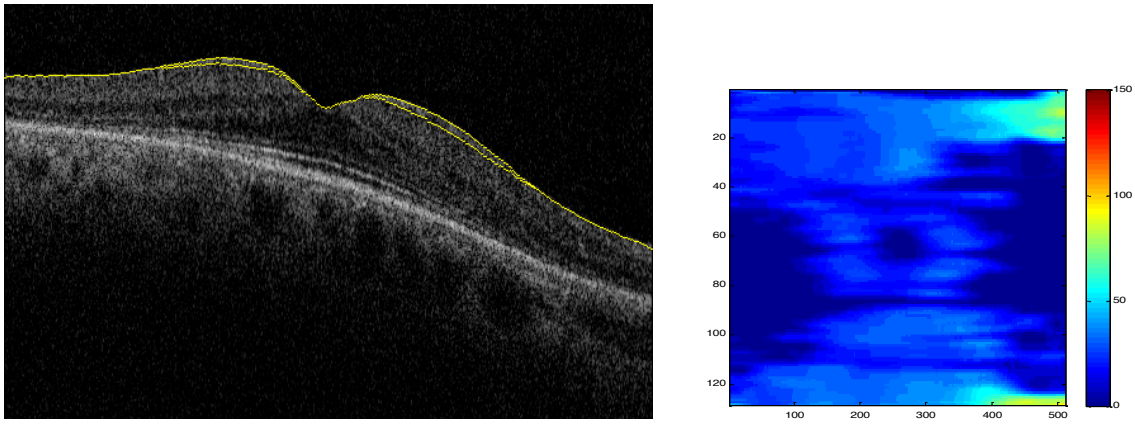

Figure 3.3c. Example of an image that passed manual re-grading.

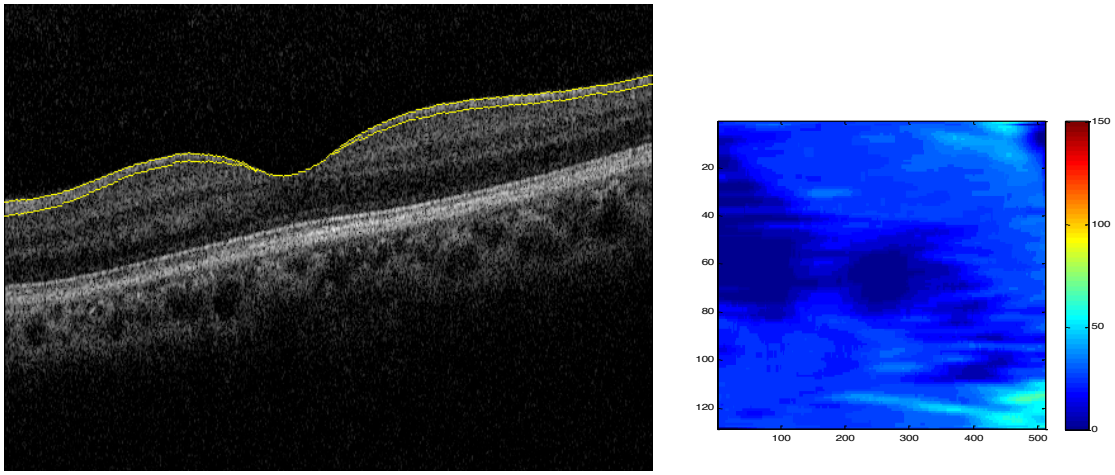

3.6 Cognitive Function

The cognitive tests included in UK Biobank are optimised for use at scale. The constraints of cognitive testing at scale include tests being brief, self-explanatory, and automated. At the inception of UKBB suitable tests did not exist and were developed specifically for this study. To maximize comparability with other datasets, for each test a standard and widely used test paradigm was employed as a template. For the tests reported in this study, prospective memory is an embedded task and comparable to that used in the CAMCOG interview. Reaction time used a stop-go paradigm. Reasoning included both verbal and numeric items as used in the AH4. The pairs test is a paired associates learning task designed to test episodic memory.

The distributions of test scores are available on UK Biobank data showcase website http://biobank.ctsu.ox.ac.uk/crystal/. As expected, reaction time was log-normally distributed and reasoning score was normally distributed. The pairs test showed a ceiling effect indicating a lack of sensitivity for high performers but good sensitivity for low performers. The distribution of the prospective memory test is relatively uninformative as it has a range of 3. Nevertheless, most individuals achieved the maximum score as might be expected in a normal population.

Reaction time has a monotonic inverse association with age indicating a constant slowing of processing speed with increasing age throughout the age range. Both

memory scales also decline monotonically with age. Reasoning is poorer only in older age groups indicating a substantial crystalized intelligence component.

Prospective Memory (http://biobank.ctsu.ox.ac.uk/crystal/field.cgi?id=20018).

For the Prospective Memory test, participants were asked to engage in a specific behavior later in the assessment: 'At the end of the games we will show you four coloured symbols and ask you to touch the blue square. However, to test your memory, we want you to actually touch the Orange Circle instead'. Participants were scored depending on whether they completed the task on first attempt, second attempt, or not at all. Below is a screen shot of the image shown to participants (Figure 3.4).

Figure 3.4. Screen shot of image shown during prospective memory test.

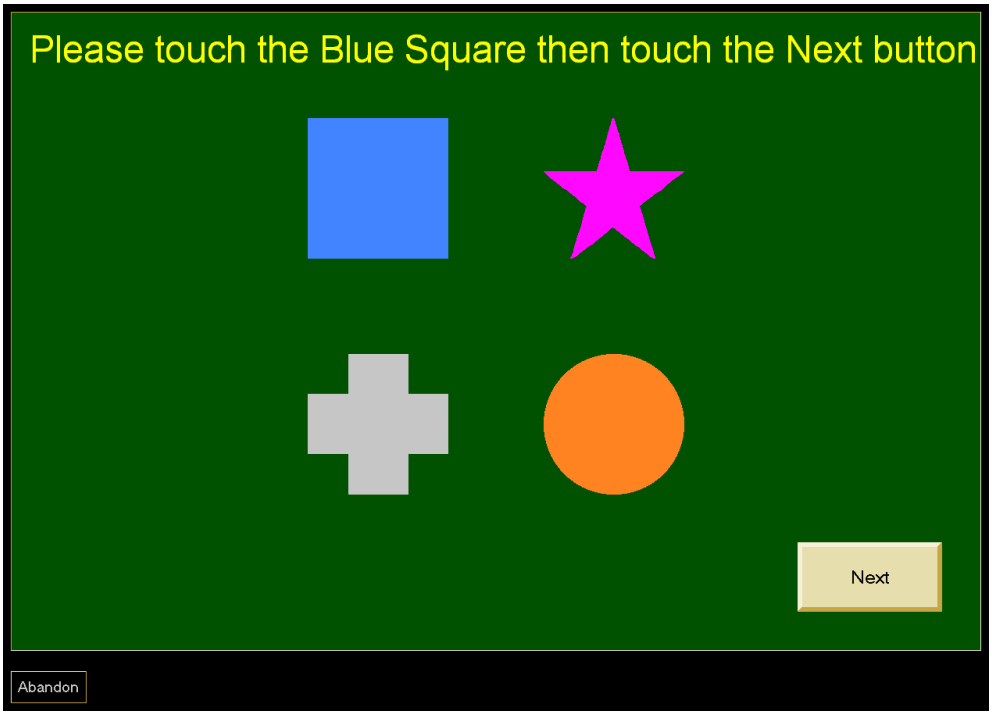

Pairs matching / Visual memory

(http://biobank.ctsu.ox.ac.uk/crystal/label.cgi?id=100030),

Memory was measured using a computerised 'pairs matching' game. There were three pairs of cards with matching simple symbols, arranged randomly in a grid, which were presented to participants on a computer screen for three seconds. The cards were then 'turned' face down. The participants were instructed to select, from recall and in the fewest number of attempts, the pairs of cards that had matching symbols. There was no time limit and the participants could make as many attempts as they needed to find all the pairs. Higher scores reflect poorer cognitive function. Figure 3.5 shows an example of a mis-match when participant is playing pairs game.

Figure 3.5. Example of a participant playing pairs game, showing results of a mis-match.

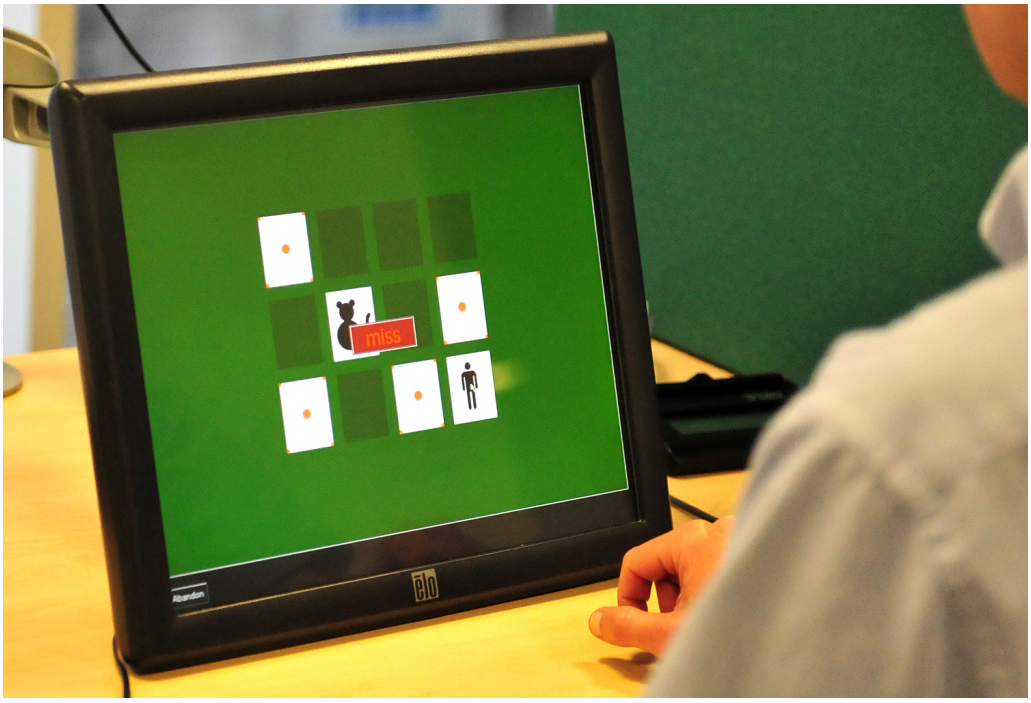

Numeric & Verbal Reasoning (http://biobank.ctsu.ox.ac.uk/crystal/field.cgi?id=20016)
A task with thirteen logic/reasoning-type questions and a two-minute time limit was labeled as 'fluid intelligence' in UK Biobank protocol but is hereafter referred to as 'verbal-numerical reasoning'. There were six verbal items. There were seven numerical items, involving sequence recognition and arithmetic. Participants were required to answer all the items within two minutes. All were multiple-choice. An example verbal item is: "Age is to years as height is to?" (answer options were, "Long/Deep/Top/Metres/Tall/Do not know/Prefer not to answer"). An example numerical item is: "150…137…125…114…104… what comes next?" (answer options were, "96/95/94/93/92/Do not know/Prefer not to answer"). The total score out of thirteen was recorded and used for the present study. The Cronbach alpha coefficient, a measure of internal consistency or how closely related items are as a group, for the thirteen items was 0.62. UK Biobank Field IDs (variable names) used in this test, with each one corresponding to each of the 13 items, were 4935, 4946, 4957, 4968, 4979, 4990, 5001, 5012, 5556, 5699, 5779, 5790, and 5866.

Reaction time (http://biobank.ctsu.ox.ac.uk/crystal/field.cgi?id=20023)
Participants completed a timed test of symbol matching, similar to the common card game 'Snap' conceptually similar to some 'Go/No-Go' reaction time tasks. Two cards with simple symbols (e.g. a square or equals sign) were presented to participants on a computer screen. Participants were instructed to push an adjacent button box as quickly as possible, using their dominant hand, if the two cards had identical symbols. After completing four practice trials, participants completed eight experimental trials, of which four included identical pairs; these four required a button to be pressed. Each

participant's reaction time score was calculated as the mean time (in msec) to push the button for the four trials in which the stimuli were identical. The score on this task was the mean response time in milliseconds across trials that contained matching pairs. Figure 3.6 shows an example of matching cards while participant is playing the game.

Figure 3.6. Example of participant performing reaction time test, with matching cards.

Of the people who were included in RNFL analysis, 32901 completed the prospective memory test, 32990 pairs matching, 32161 numeric & verbal reasoning, and 32752 reaction time at the baseline test of cognitive function in 2006-2010. Repeat assessment

was performed in 2012-2013, and of the participants analysed at baseline, 1256 received follow-up prospective memory test, 1256 pairs matching, 1254 numeric & verbal reasoning, and 1253 reaction time testing.

Test failure at baseline (2009-2010) was defined as an incorrect answer on first attempt of prospective memory, or doing worse than 95% of participants in pairs matching (>2 incorrect matches), numeric and verbal reasoning tests (score<3) or reaction time (>770 msec). Performance was considered worse on follow-up testing (2012-2013) if the number of attempts increased on prospective memory test, the number of incorrect matches increased on pairs matching, a decrease in the numeric and verbal reasoning test scores, or a reaction time slowed by at least 100 msec.

3.7 Statistical Analysis

Statistical analyses were performed using STATA/SE version 13.1 (StataCorp LP, College Station, Texas, USA). Descriptive statistics were used to report sub-layer thickness in all ETDRS subfields among all participants, subsets of different demographic variables, as well as ocular and systemic variables. For continuous variables, mean, standard error (SE), standard deviation (SD) and 95% confidence intervals were calculated. For categorical variables, proportions expressed as percentages and 95% CIs were calculated. Unpaired t-tests were performed to compare percentages and means.

Scatter plots were generated to further evaluate associations; however, given the large sample size, the density of scatter plots is difficult to interpret (Figure 3.7).

Figure 3.7. Example of a scatter plot of age and RNFL thickness at outer nasal subfield.

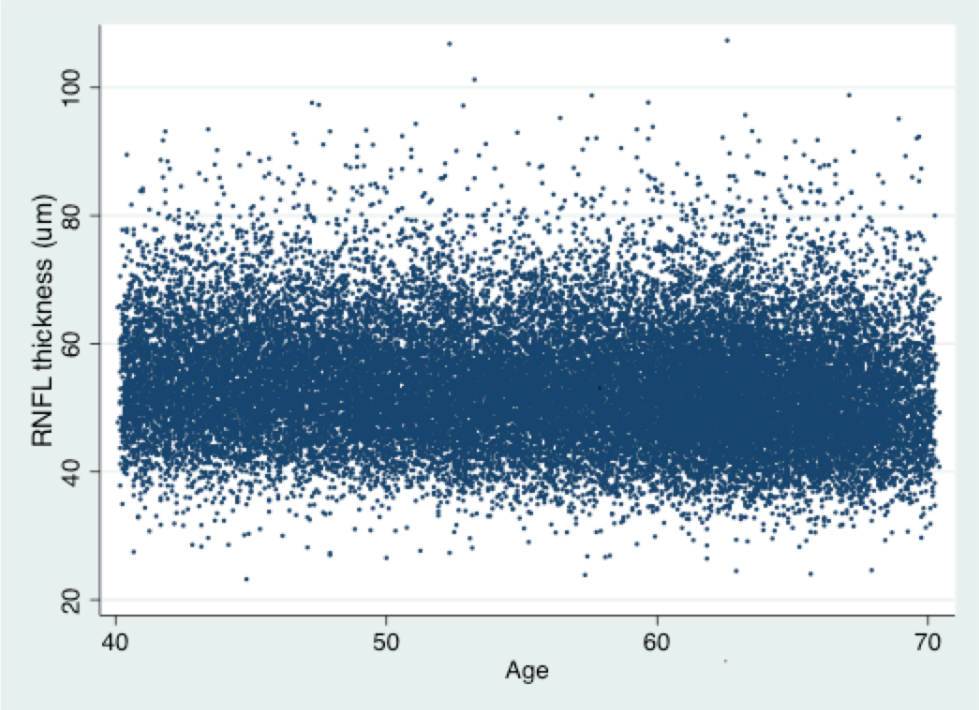

For associations with demographic, physiological, and ocular characteristics, univariable linear regression analyses were performed to assess associations of retinal sub-layer thickness in each ETDRS subfield with age, sex, height, ethnicity, intraocular pressure, refraction, blood pressure, body mass index, smoking status. Where appropriate, continuous variables were grouped into categories, such as 1-year or 5-year groupings of age. Variables found to be significant, or felt to be potential confounders, were included together in multivariable regression modeling. Variables such as systolic and

diastolic blood pressure, which were highly likely to have issues with covariance were analyzed individually, but not included together in multivariable regression modeling (in the example of blood pressure, only systolic blood pressure was included in multivariable modeling). Variables such as education and deprivation, which may be related but do not necessarily co-vary, where added to multivariable regression modeling separately before including together in a single model.

For cognitive function, linear regression analyses were first used to test associations between cognitive function and RNFL, both at baseline and on follow-up testing. Logistic regression was then used to determine odds ratio for cognitive deficit and decline for each quintile of retinal thickness. Further testing was performed to determine whether effects were additive; i.e., doing poorly on zero/one/two/three/four tests at baseline. Multivariable regression modeling was performed to adjust for potential confounders. Where appropriate, 2-sided hypothesis testing was performed. The null hypothesis was rejected if $p < 0.001$, with threshold chosen based on the formula (0.05 / number of tests performed).

Values were considered significant if $p < 0.001$. This threshold was partially based on the correction of α (0.05) divided by the number of tests performed. The number of analyses performed was calculated as 42 (4 retinal layers x 6 tests per layer [age, sex, race, height, refraction, IOP] + 2 retinal layers (photoreceptors and RPE) x 3 tests [blood pressure, smoking, BMI] + 2 retinal layers (GCL-IPL and RNFL) x 2 tests [education and deprivation] + 2 retinal layers (GCL-IPL and RNFL) x 4 types of cognitive function tests). For each retinal layer, 9 subfields were available for analysis. The thickest subfield of

each layer was chosen for determination of significance and drawing conclusions, as it was least likely to be subject to artefact. However, all subfields were analyzed to assess for consistency. For cognitive function, associations were assessed for whether they were consistent across multiple types of cognitive tests. Finally, results were compared with literature from other studies, where this information was available.

SECTION IV:

RESULTS

4.1 Retinal Pigment Epithelium

4.1.1 Contributors to Study of Retinal Pigment Epithelium

I am grateful to the following people for their contributions to this work. Paul Foster was critical to designing the eye portion of UK Biobank. He and Praveen Patel provided guidance in design and conception of the RPE section of this work. Carlota Grossi shared her own work on a related topic which was a great help at the beginning of analysis of this large dataset. Qi Yang and Charles Reisman performed automated segmentation of OCT images, without which this work would not have been possible. After automated segmentation of images were performed, I reviewed data to evaluate for outliers, and recommended images to Qi Yang for manual re-grading. These variables were then analyzed by myself. Paul Foster, Nick Strouthidis, Praveen Patel, and Andrew Lotery were involved in suggestions for improved methods of analysis as the work evolved. Paul Foster, Praveen Patel, Nick Strouthidis, Yusrah Shweikh, Qi Yang, Charles Reisman, Zaynah Muthy, Usha Chakravarthy, Andrew Lotery, Pearse Keane, and Adnan Tufail were involved in the reviewing and editing phase. With the exception of designing UK Biobank and performing automated segmentation, all work presented here was performed by me, though I remain grateful to the many contributors and collaborators who improved the quality of this work.

4.1.2 Results

67,321 people underwent OCT macular imaging, with 51,987 having high-quality images, among whom 34,752 people had refractive error within 6 diopters of emmetropia, vision ≥20/30, no self-reported ocular disorders, and no neurological disease or diabetes (Figure 4.1). Images at the upper and lower extremes were manually reviewed, with 288 images excluded, leaving 34,464 included for analysis (Figure 4.1).

Mean age was 56.0 years, with a slightly higher number of women (53.7%) than men. Mean height was shorter among women (163 cm) than men (176 cm, $p<0.001$). The majority of participants were white, with 129 Chinese, 898 Asians, 974 blacks, and 795 mixed/other. There were more left eyes than right. Mean visual acuity was -0.04 logMAR, mean refraction was -0.05 diopters, and mean IOP was 15 mmHg (Table 4.1).

Figure 4.1. RPE-BM inclusion/exclusion criteria.

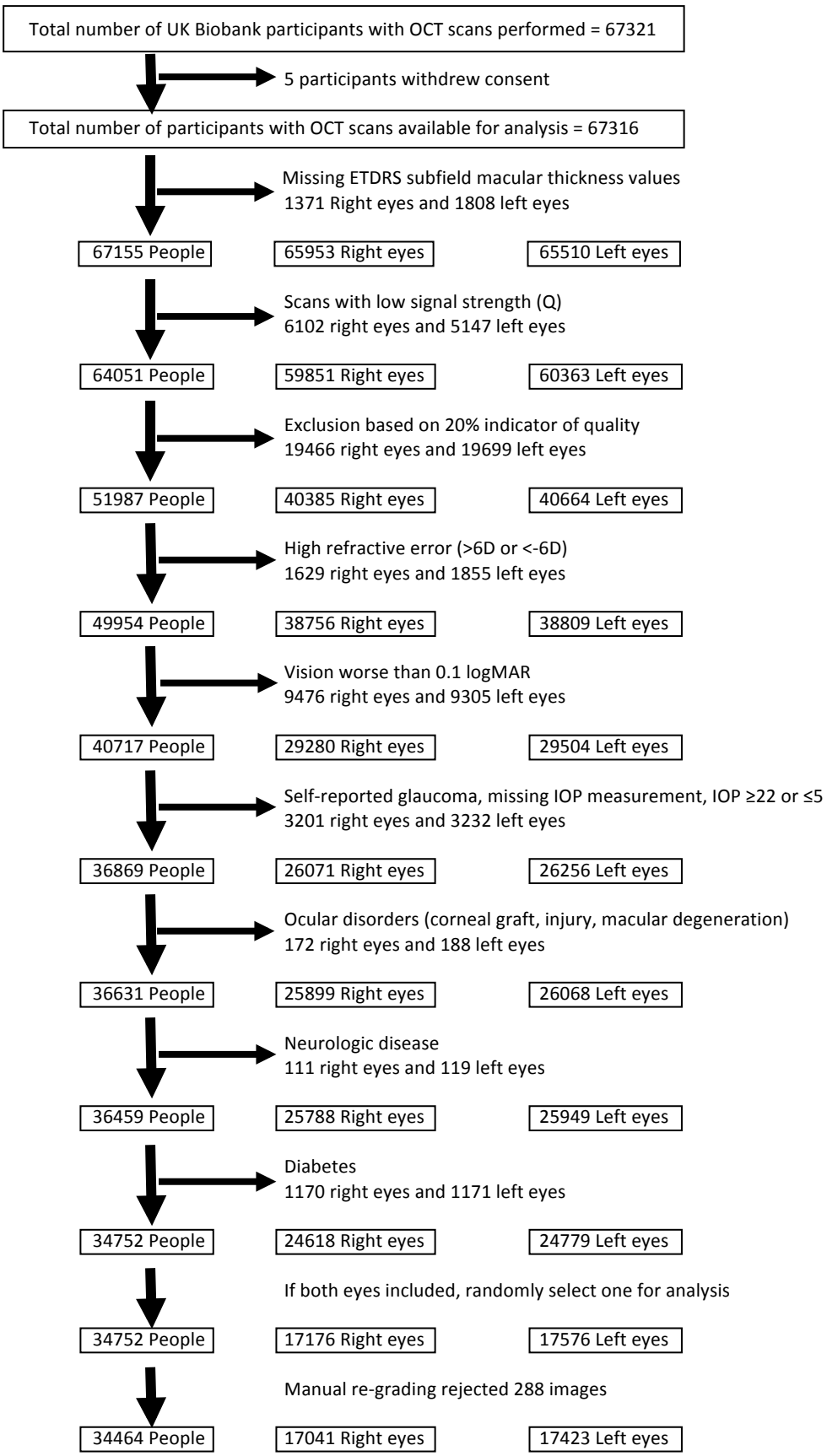

Table 4.1. Basic demographics for those included in RPE-BM analysis.

	Estimate (95% CI)	N = 34464
*** Age (mean years)**	56.0 (55.9 – 56.1)	SD = 8.2
+ Female Gender	53.7 (53.2 – 54.2)%	
*** Height (mean centimetres)**	169.2 (169.1 – 169.3)	SD = 9.2
Women	163.1 (163.0 – 163.2)	SD = 6.3
Men	176.3 (176.2 – 176.4)	SD = 6.8
+ Ethnicity		
White	91.8 (91.5 – 92.1)%	
Chinese	0.4 (0.3 – 0.4)%	
Asian	2.6 (2.5 – 2.8)%	
Black	2.8 (2.7 – 3.0)%	
Mixed/Other	2.3 (2.2 – 2.5)%	
+ Laterality = Right eye	49.4 (48.9 – 50.0)%	
*** Visual acuity (logMAR)**	-0.04 (-0.042 – -0.039)	SD = 0.157
*** Refraction**	-0.05 (-0.07 – -0.03)	SD = 1.91
*** IOP (Goldmann corrected)**	15.0 (15.0 – 15.1)	SD = 3.0

* mean (95% confidence interval)
+ percentage (95% confidence interval)
SD = standard deviation

A histogram of RPE-BM thickness (Figure 4.2a) shows mean thickness of 26.3 µm (SD = 4.8 µm) in the central subfield. Figure 4.2b shows mean RPE-BM thickness at ETDRS subfields, with nasal and temporal subfields significantly thicker than superior or inferior subfields ($p<0.001$). The thickest subfield is the inner nasal subfield. Results remained consistent for women and men (figure 4.2c). Furthermore, women had thicker RPE-BM in central and inner superior subfields ($p<0.001$), whereas men appeared to have thicker RPE-BM in all other subfields ($p<0.001$) except inner inferior subfield, which was not significant.

Figure 4.2a. Histogram of central RPE-BM thickness. Mean = 26.34 µm. Standard error = 0.02 µm. Standard deviation = 4.80 µm.

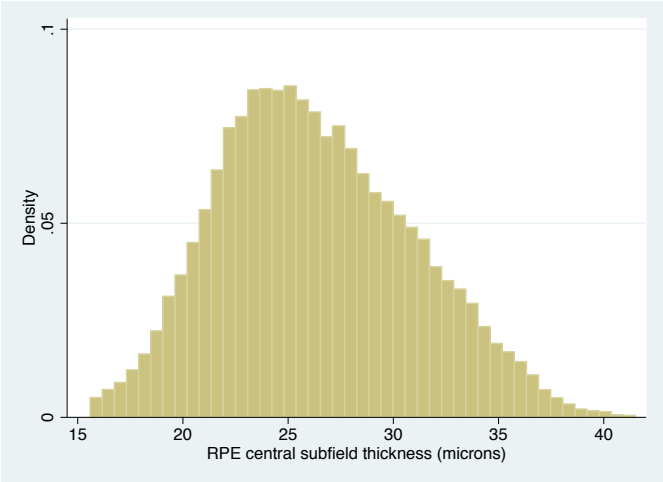

Figure 4.2b. RPE-BM thickness at different retinal subfields. Mean ± standard deviation (µm). P<0.001 for t-test of all subfields compared to central subfield.

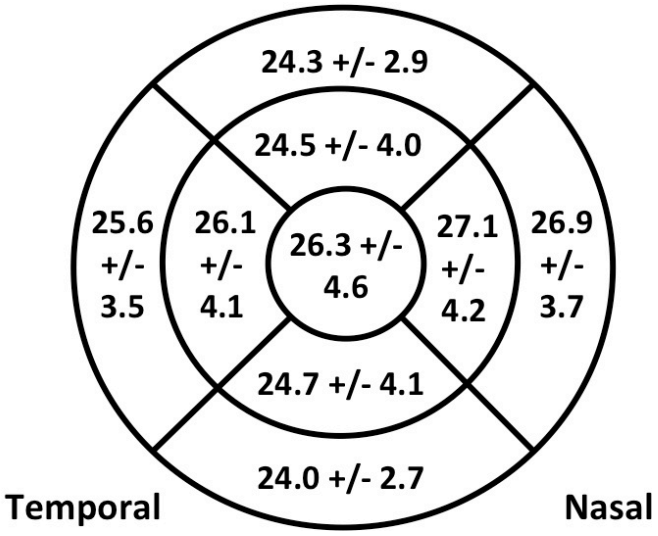

Figure 4.2c. RPE-BM thickness in women (pink) and men (blue), at different retinal subfields. Error bars represent 95% confidence intervals. T-test of women versus men, p<0.001 at all subfields except inner inferior (p=0.13).

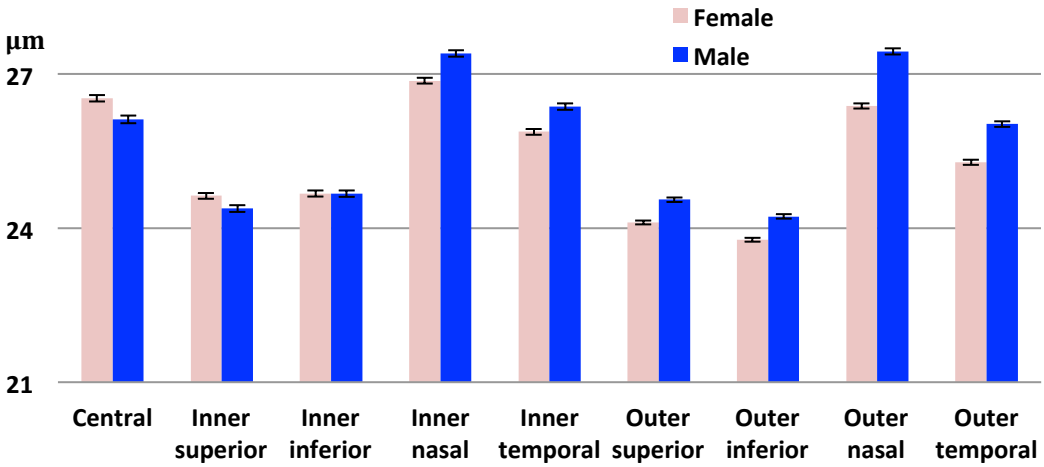

Figure 4.3a shows mean central RPE-BM thickness by age. Central macular subfield RPE-BM complex thickness shows no significant changes between ages 40-45; however, after age 46, mean thickness declines steadily at a rate of 0.10 µm per year (p<0.001). A similar trend is evident among all subfields (figure 4.3b-c), with linear regression showing no significant changes from ages 40-45 and negative slope after age 46 in every subfield (p<0.001) (Table 4.2). At all ages, nasal and temporal subfields are significantly thicker than superior and inferior subfields, with nasal subfields being the thickest (figures 4.3b-c).

Figure 4.3a. Mean central RPE-BM thickness by age. Linear regression for ages 45 and younger = 27.3 + 0.004 (per year), p=0.93. Linear regression for ages 46 and older = 31.74 - 0.10 (per year), p<0.001. Error bars = 95% confidence interval.

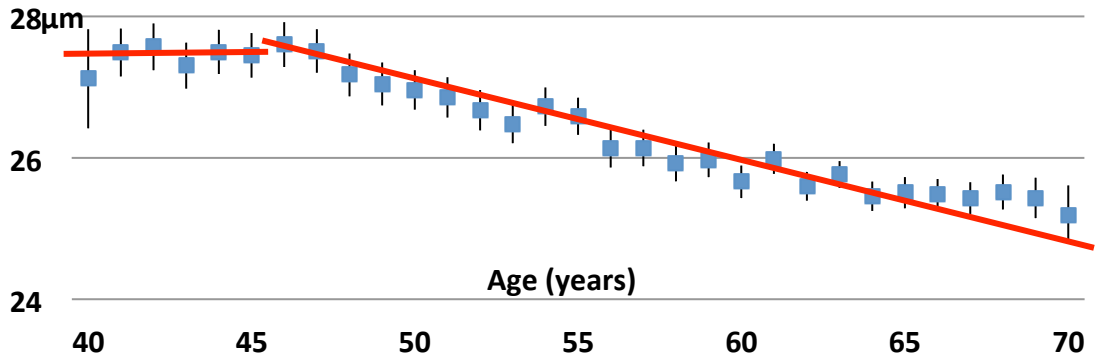

Figure 4.3b. Mean RPE-BM thickness of inner subfields by age. Error bars = 95% confidence interval.

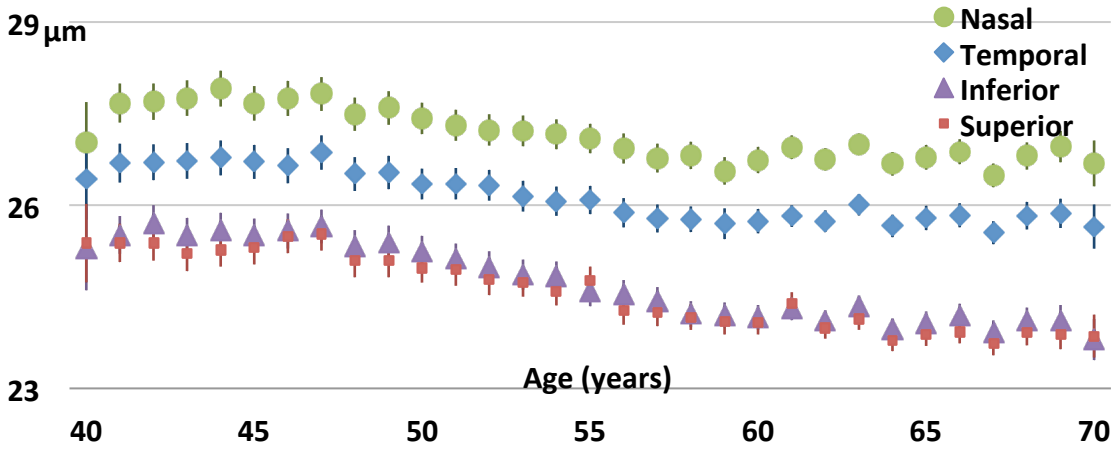

Figure 4.3c. Mean RPE-BM thickness of outer subfields by age. Error bars = 95% confidence interval.

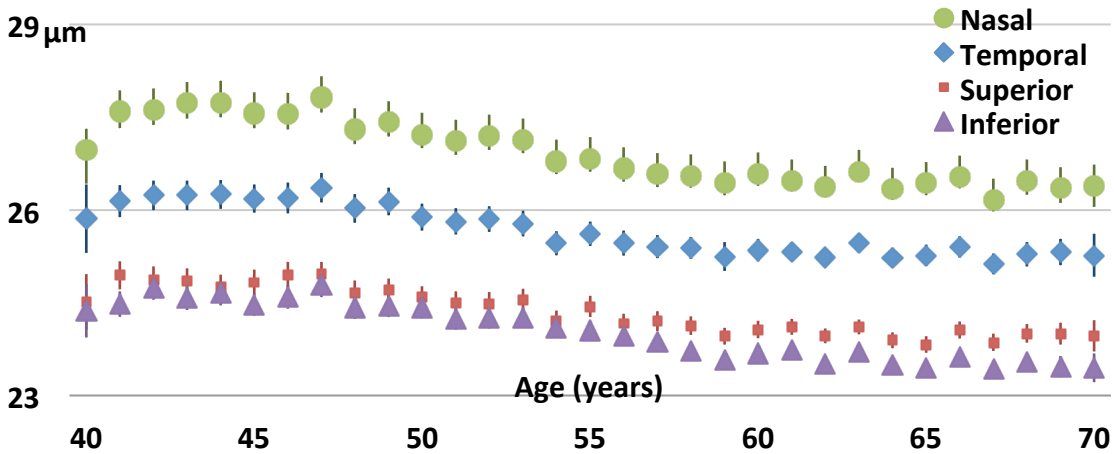

Table 4.2. Linear regression of RPE-BM thickness at subfields, by age. CI = confidence interval.

	Slope	95% CI		p-value
Age 40-45				
Central	0.004	-0.09	0.1	0.93
Inner Temporal	0.02	-0.06	0.11	0.59
Inner Superior	-0.02	-0.11	0.06	0.56
Inner Nasal	0.05	-0.03	0.14	0.24
Inner Inferior	0.001	-0.09	0.09	0.99
Outer Temporal	0.03	-0.04	0.1	0.48
Outer Superior	-0.01	-0.07	0.05	0.74
Outer Nasal	0.04	-0.04	0.11	0.32
Outer Inferior	-0.002	-0.06	0.05	0.94
Age 46-70				
Central	-0.1	-0.1	-0.09	<0.001
Inner Temporal	-0.04	-0.05	-0.04	<0.001
Inner Superior	-0.07	-0.08	-0.07	<0.001
Inner Nasal	-0.04	-0.05	-0.04	<0.001
Inner Inferior	-0.07	-0.08	-0.07	<0.001
Outer Temporal	-0.04	-0.05	-0.04	<0.001
Outer Superior	-0.04	-0.05	-0.04	<0.001
Outer Nasal	-0.06	-0.06	-0.05	<0.001
Outer Inferior	-0.06	-0.06	-0.05	<0.001

When RPE-BM thickness is compared amongst different ethnicities, black ethnicity shows significantly greater thickness at every subfield (Figure 4.4a-c). White, Chinese, and Asian ethnicities show similar central RPE-BM thickness. When RPE-BM thickness is analyzed by refraction, hyperopes show significantly thicker central RPE-BM, with linear regression estimating an increase of 0.2 μm/dioptre (figure 4.5a). A similar trend is seen for all subfields (figure 4.5b-c, Table 4.3).

Figure 4.4a. Mean central RPE-BM thickness by race. Error bars = 95% confidence interval.

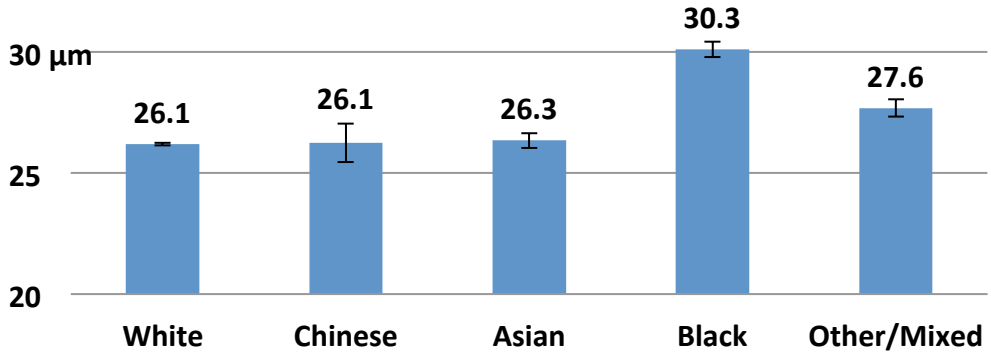

Figure 4.4b. Mean RPE-BM thickness of inner subfields by race. Error bars = 95% confidence interval.

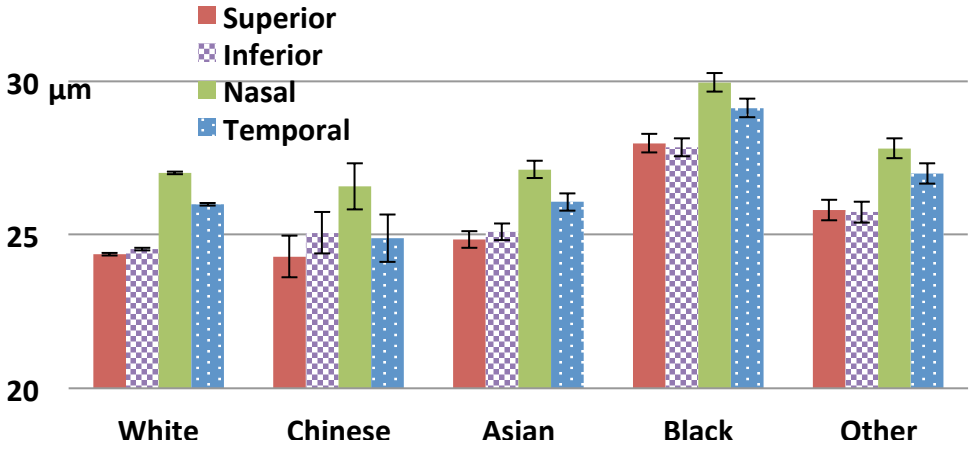

Figure 4.4c. Mean RPE-BM thickness of outer subfields by race. Error bars = 95% confidence interval.

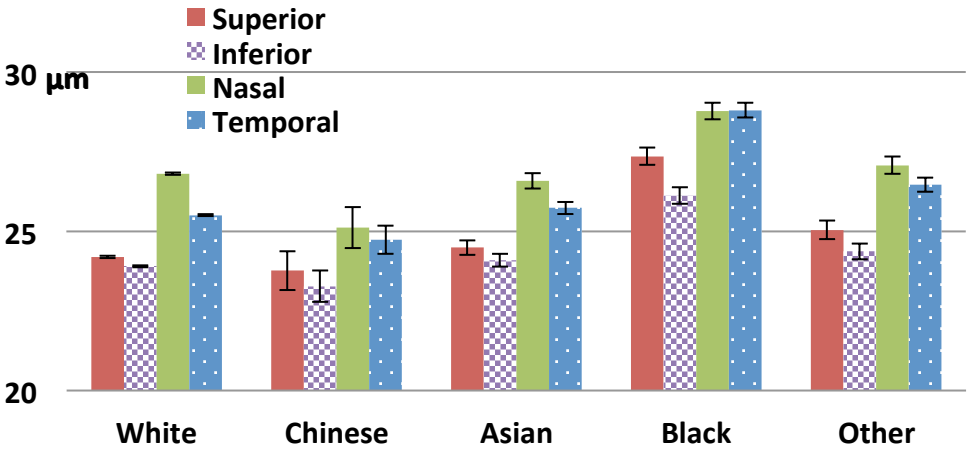

Figure 4.5a. Mean central RPE-BM thickness by refraction. Linear regression = 26.4 + 0.2 (per dioptre), p<0.001. Error bars = 95% confidence interval.

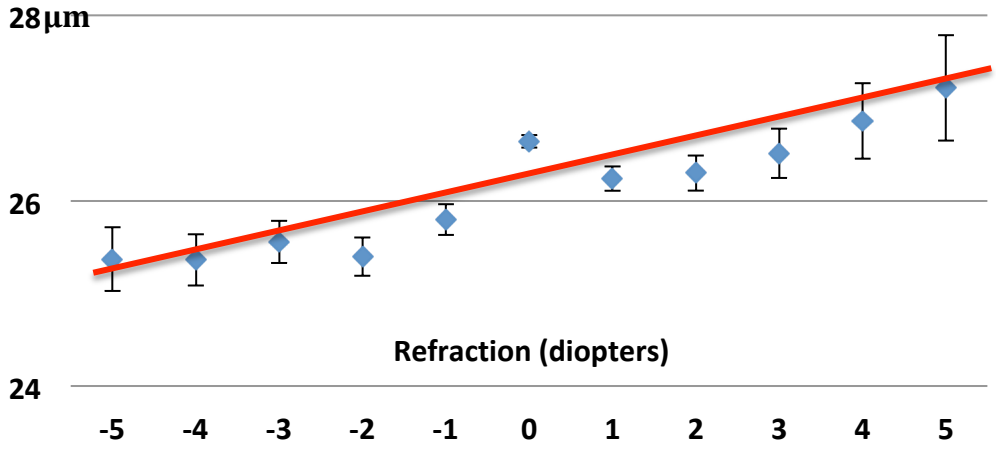

Figure 4.5b. Mean RPE-BM thickness of inner subfields by refraction. Error bars = 95% confidence interval.

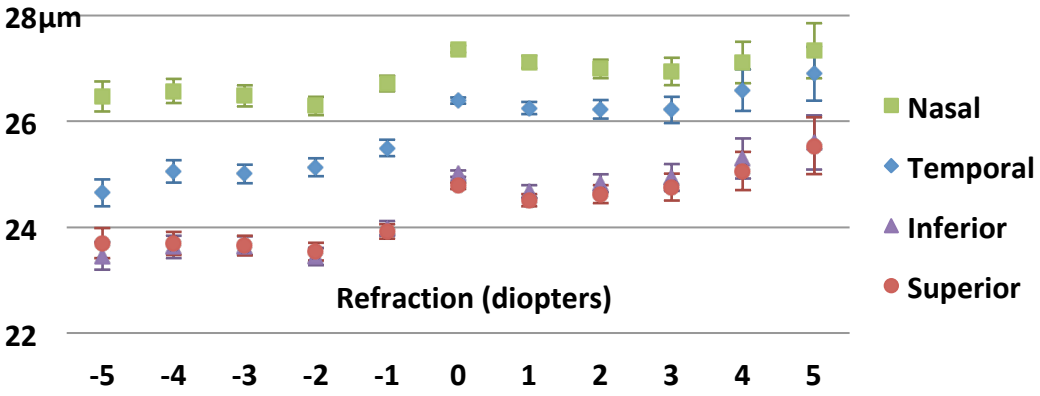

Figure 4.5c. Mean RPE-BM thickness of outer subfields by refraction. Error bars = 95% confidence interval.

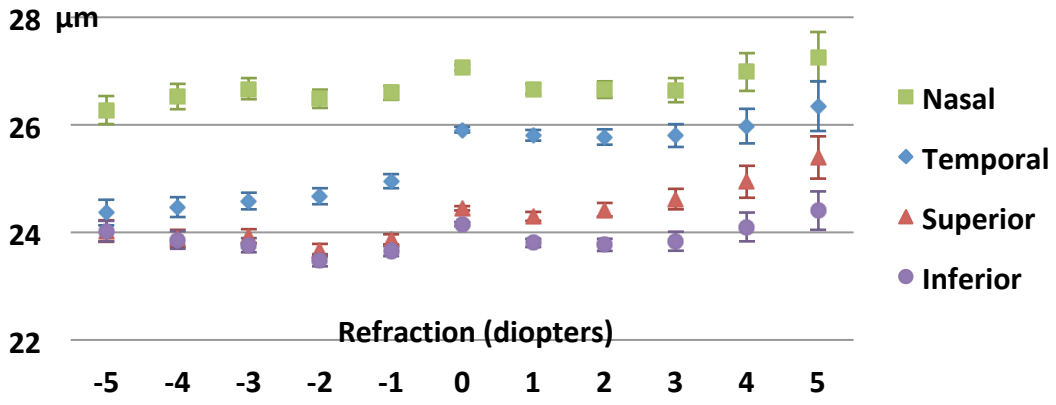

Table 4.3. Linear regression of RPE-BM thickness at subfields, by refraction.

	Slope	95% CI		p-value
Central	0.19	0.16	0.23	<0.001
Inner Temporal	0.25	0.22	0.28	<0.001
Inner Superior	0.20	0.18	0.23	<0.001
Inner Nasal	0.12	0.09	0.15	<0.001
Inner Inferior	0.26	0.23	0.28	<0.001
Outer Temporal	0.25	0.23	0.27	<0.001
Outer Superior	0.13	0.11	0.15	<0.001
Outer Nasal	0.05	0.03	0.08	<0.001
Outer Inferior	0.03	0.01	0.05	0.001

To determine whether race and refraction are potential confounders, RPE-BM thicknesses are plotted for both variables (figure 4.6; Chinese and mixed/other excluded due to small numbers in race/refraction sub-groups). At central subfield, black ethnicity continues to show the greatest RPE-BM thickness, with Asian and white ethnicity demonstrating similar RPE-BM thicknesses. Among whites, there continues to be a trend toward increasing central RPE-BM thickness per dioptre increase in refraction; however, this effect is small compared to ethnic differences. Among Asians and blacks, there is no trend in central RPE-BM thickness by refraction. The effects of ethnicity and refraction on RPE-BM thickness remain consistent for all subfields, with ethnicity effects overshadowing that of increased mean RPE thickness with increased hyperopia (Figure 4.7).

Figure 4.6. Mean central RPE-BM thickness by ethnicity and refraction. Linear regression for white ethnicity = 26.15 + 0.21 (per dioptre), p<0.001; Asian ethnicity = 26.39 + 0.11 (per dioptre), p>0.49; black ethnicity = 30.36 + 0.23 (per dioptre), p=0.22. Error bars = 95% confidence interval.

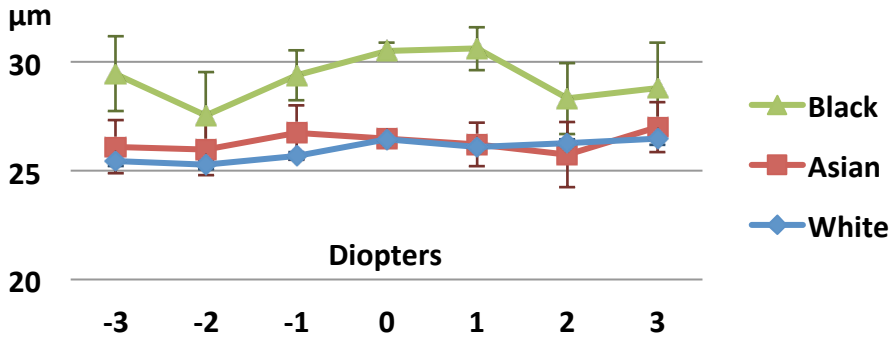

Figure 4.7a-h. Mean RPE-BM thickness of subfields by ethnicity and refraction. Error bars = 95% confidence interval.

a) Inner temporal subfield.

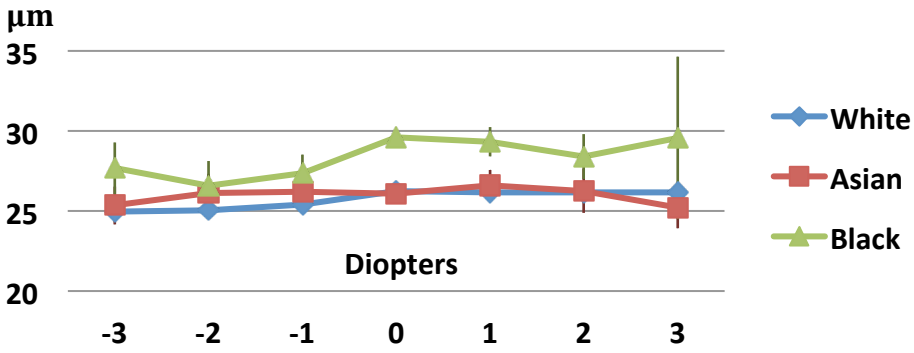

b) Inner superior subfield.

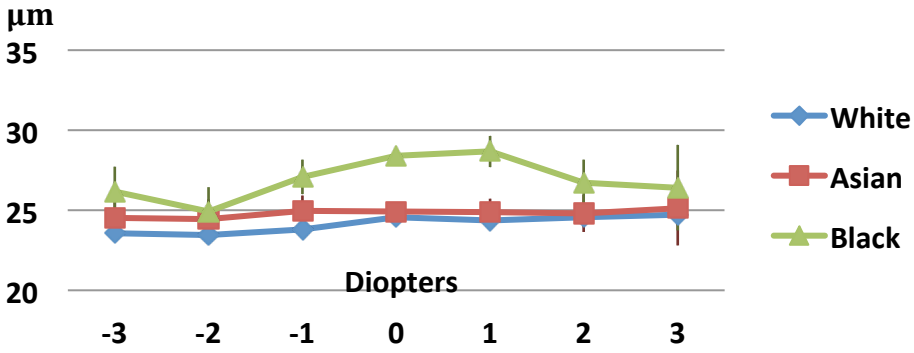

c) Inner nasal subfield.

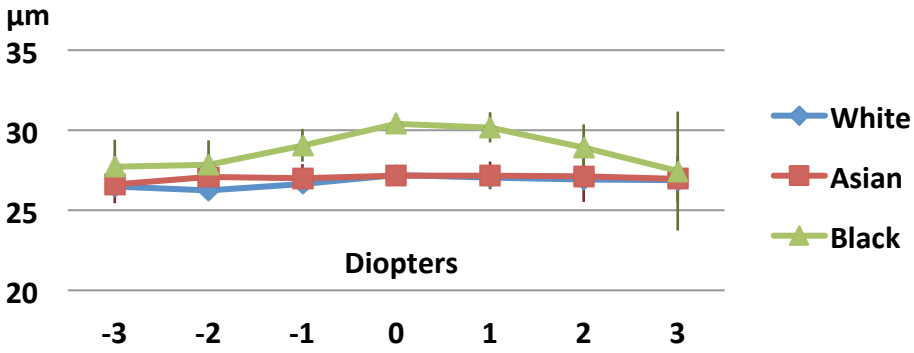

d) Inner inferior subfield.

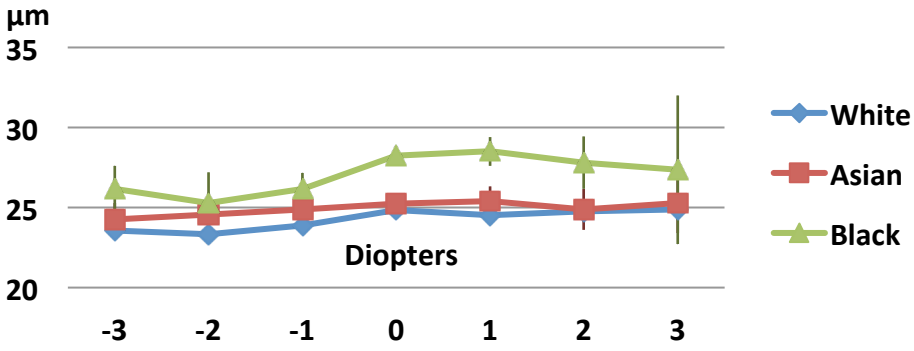

e) Outer temporal subfield.

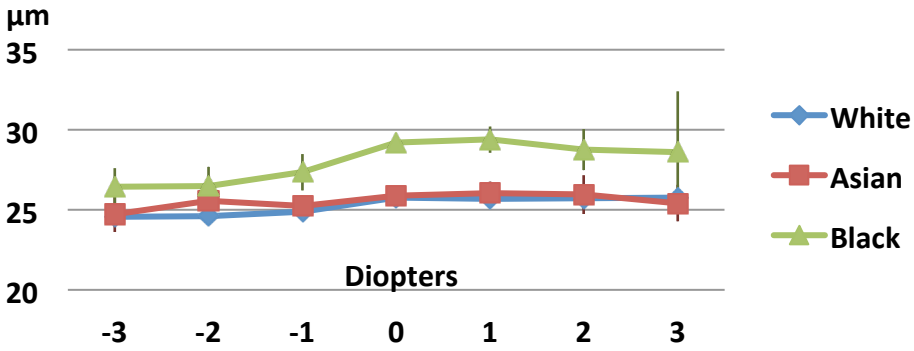

f) Outer superior subfield.

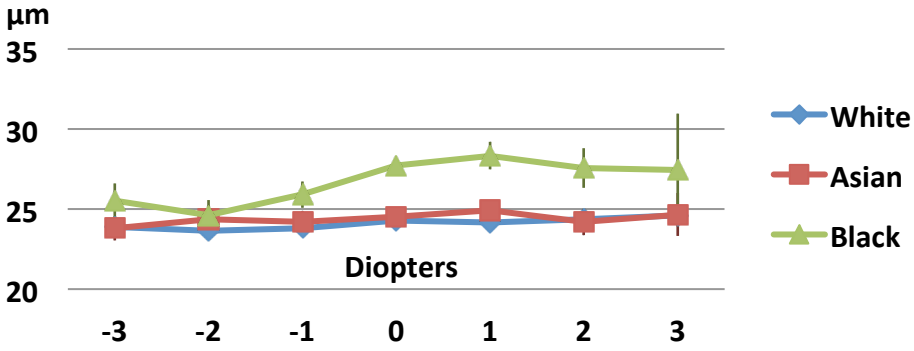

g) Outer nasal subfield.

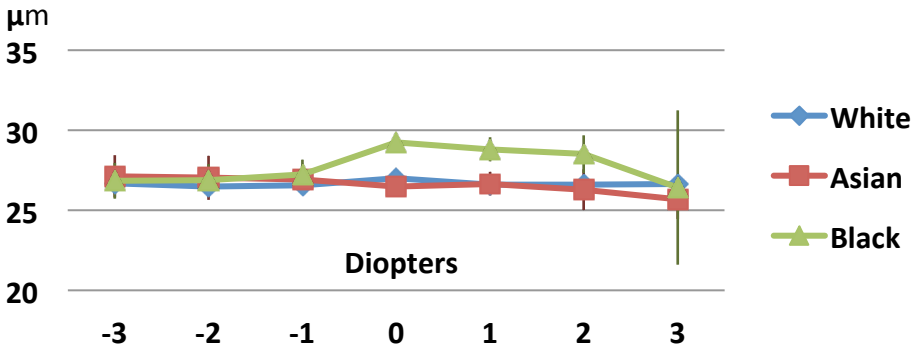

h) Outer inferior subfield.

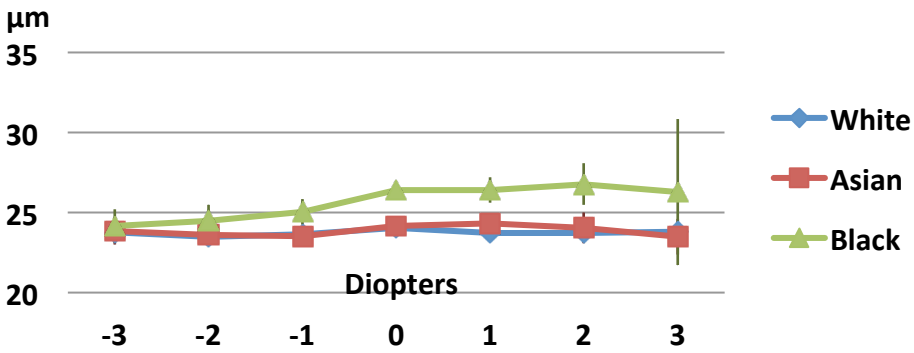

The relationship between RPE-BM thickness and IOP is illustrated in figure 6. In the central subfield, higher IOP is correlated with thinner RPE-BM thickness, with regression slope of -0.08 µm per mmHg ($p<0.001$) (figure 4.8a). This trend is consistent across all subfields (figure 4.8b-c).

Figure 4.8a. Mean central RPE-BM thickness by IOP. Linear regression for IOP 8mmHg and greater = 27.47 - 0.08 (per mmHg), p<0.001. Error bars = 95% confidence interval.

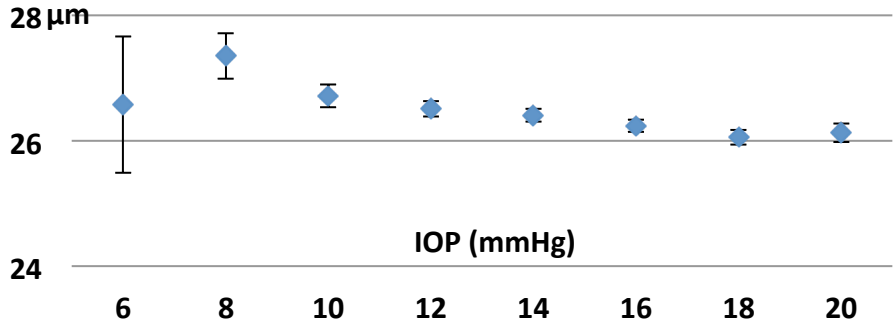

Figure 4.8b. Mean RPE-BM thickness of inner subfields by IOP. Error bars = 95% confidence interval.

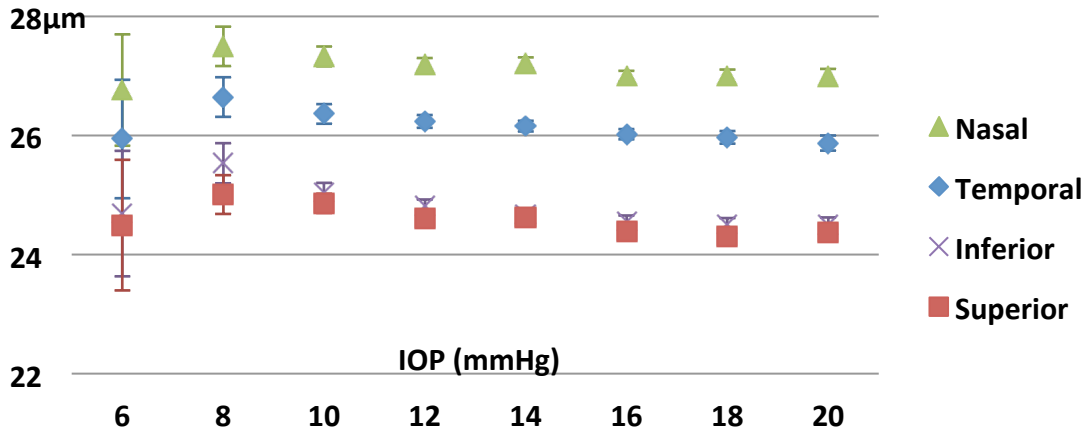

Figure 4.8c. Mean RPE-BM thickness of outer subfields by IOP. Error bars = 95% confidence interval.

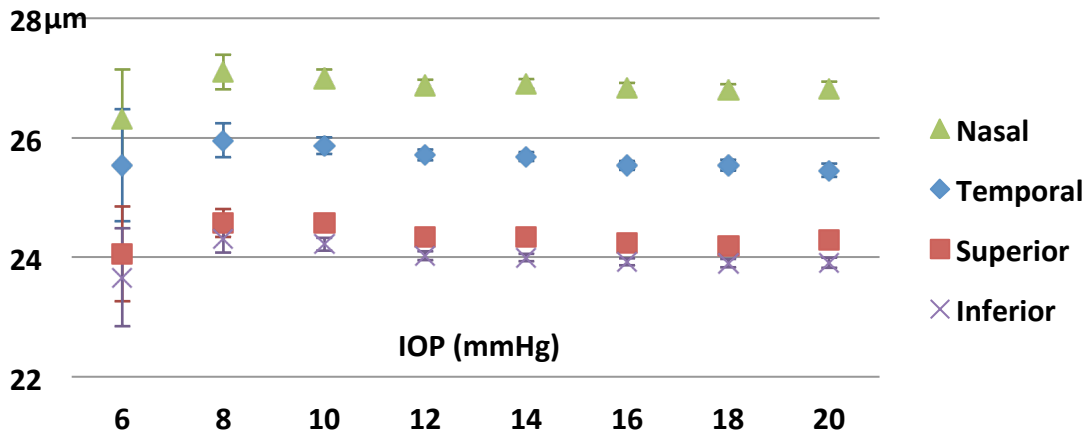

A dose response with smoking status was not observed but significant differences were detected between the different classes of smoking habit. Current smoking habit did not correlate with RPE-BM thickness (Table 4.4). Former smokers had significantly thinner RPE-BM than non-smokers (26.1 μm and 16.5 μm respectively, $p<0.001$) in the central subfield. Current smokers who classified themselves as regular smokers showed significantly thicker RPE-BM as compared to non-smokers at outer temporal ($p<0.001$) and outer inferior ($p<0.001$) subfields. Current smokers were not significantly different from non-smokers, regardless of whether they smoked occasionally or on most/all days for inner superior, inner nasal, and inner inferior subfields which showed the same trend (Table 4.4). Occasional smokers had significantly thicker RPE-BM at outer temporal ($p<0.001$), outer nasal ($p<0.001$), and outer inferior ($p<0.001$) subfields (Table 4.4).

Table 4.4. Mean RPE-BM thickness at subfields by smoking status. SE = standard error, CI = confidence interval.

Central	Mean	95% CI		P-value
No	26.47	26.40	26.53	Reference
Former smoker	26.11	26.02	26.19	<0.001
Yes, occasional	26.50	26.21	26.78	0.83
Yes, most or all days	26.36	26.17	26.55	0.32
Inner temporal				
No	26.11	26.05	26.17	Reference
Former smoker	26.02	25.95	26.1	0.07
Yes, occasional	26.23	25.98	26.48	0.38
Yes, most or all days	26.39	26.22	26.56	0.003
Inner superior				
No	24.57	24.51	24.63	Reference
Former smoker	24.38	24.30	24.45	<0.001
Yes, occasional	24.72	24.47	24.97	0.25
Yes, most or all days	24.63	24.46	24.8	0.5
Inner nasal				
No	27.15	27.09	27.21	Reference
Former smoker	27.04	26.97	27.12	0.02
Yes, occasional	27.18	26.92	27.45	0.81
Yes, most or all days	27.16	26.99	27.34	0.89
Inner inferior				
No	24.74	24.68	24.80	Reference
Former smoker	24.52	24.45	24.60	<0.001
Yes, occasional	24.83	24.57	25.08	0.52
Yes, most or all days	24.79	24.62	24.97	0.58
Outer temporal				
No	25.57	25.52	25.62	Reference
Former smoker	25.61	25.55	25.67	0.3
Yes, occasional	25.90	25.69	26.12	<0.001
Yes, most or all days	26.09	25.94	26.24	<0.001
Outer superior				
No	24.33	24.29	24.37	Reference
Former smoker	24.24	24.19	24.29	0.01
Yes, occasional	24.55	24.38	24.73	0.02
Yes, most or all days	24.47	24.34	24.59	0.04
Outer nasal				
No	26.84	26.79	26.89	Reference
Former smoker	26.83	26.76	26.89	0.73
Yes, occasional	27.20	26.97	27.43	<0.001
Yes, most or all days	27.13	26.98	27.29	<0.001
Outer inferior				
No	23.98	23.95	24.02	Reference
Former smoker	23.91	23.86	23.96	0.02
Yes, occasional	24.30	24.13	24.47	<0.001
Yes, most or all days	24.17	24.06	24.29	<0.001

There is no significant association between systolic blood pressure (Figure 4.9a, Table 4.5), diastolic blood pressure (Figure 4.9b, Table 4.5), or body mass index (Figure 4.10a, Table 4.6). Body mass index and ethnicity were considered together, and again no association was identified (Figure 4.10b).

Figure 4.9a. Mean of central RPE-BM thickness by systolic blood pressure. Error bars = 95% confidence interval.

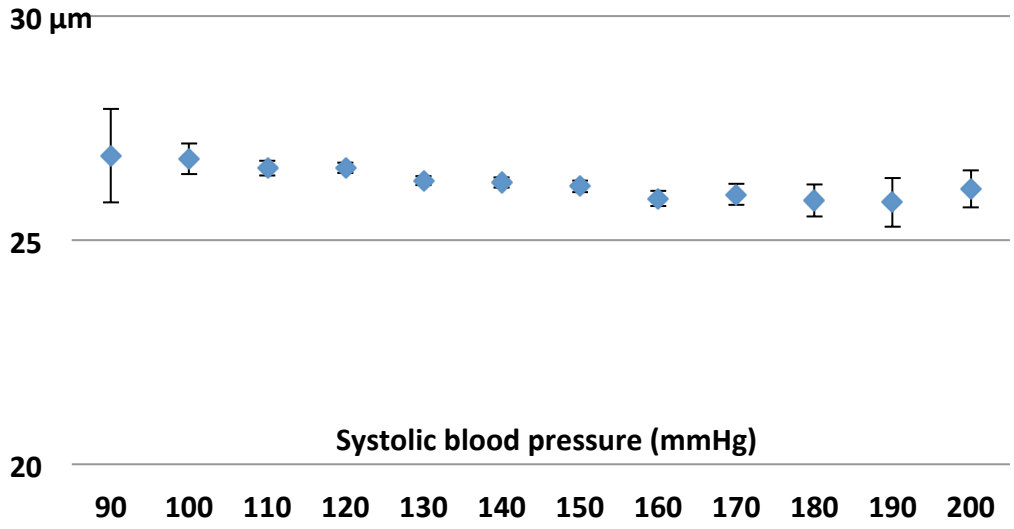

Figure 4.9b. Mean of central RPE-BM thickness by diastolic blood pressure. Error bars = 95% confidence interval.

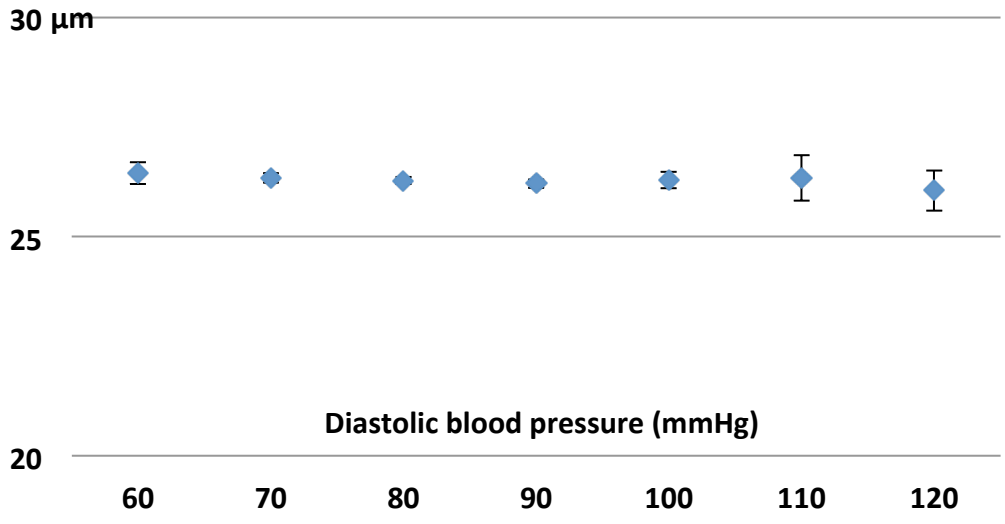

Table 4.5. Linear regression of RPE-BM thickness at subfields, by systolic and diastolic blood pressure. CI = confidence interval.

	Slope	95% CI		p-value
Systolic blood pressure (per mmHg)				
Central	-0.01	-0.02	-0.01	<0.001
Inner Temporal	0.00	0.00	0.00	0.06
Inner Superior	-0.01	-0.01	-0.01	<0.001
Inner Nasal	0.00	-0.01	0.00	0.01
Inner Inferior	-0.01	-0.01	-0.01	<0.001
Outer Temporal	0.00	0.00	0.00	0.88
Outer Superior	0.00	0.00	0.00	0.16
Outer Nasal	0.00	0.00	0.00	0.02
Outer Inferior	0.00	-0.01	0.00	<0.001
Diastolic blood pressure (per mmHg)				
Central	-0.01	-0.01	0.00	0.002
Inner Temporal	0.01	0.00	0.01	0.03
Inner Superior	0.00	-0.01	0.00	0.22
Inner Nasal	0.00	0.00	0.01	0.15
Inner Inferior	0.00	-0.01	0.00	0.22
Outer Temporal	0.01	0.01	0.01	<0.001
Outer Superior	0.00	0.00	0.01	0.002
Outer Nasal	0.01	0.00	0.01	0.001
Outer Inferior	0.00	0.00	0.01	0.01

Figure 4.10a. Mean central RPE-BM thickness by body mass index. Error bars = 95% confidence interval.

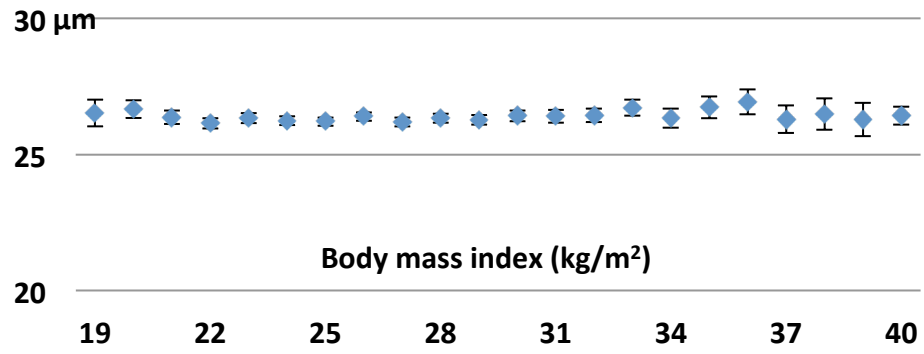

Figure 4.10b. Mean central RPE-BM thickness by body mass index and ethnicity. Chinese not shown due to small numbers

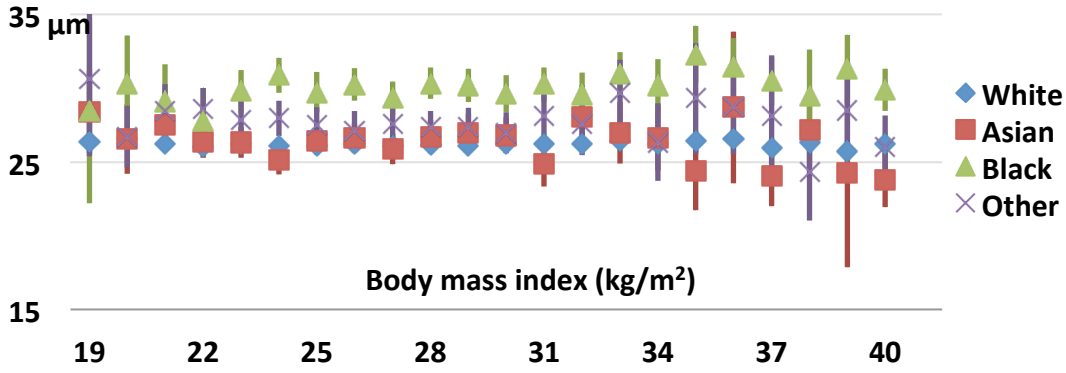

Table 4.6. Linear regression of RPE-BM thickness at subfields, per unit increase in BMI (kg/m^2). CI = confidence interval.

	Slope	95% CI		p-value
Central	0.01	0.00	0.02	0.02
Inner Temporal	0.03	0.02	0.04	<0.001
Inner Superior	0.00	-0.01	0.01	0.52
Inner Nasal	0.02	0.01	0.03	<0.001
Inner Inferior	0.01	0.00	0.02	0.20
Outer Temporal	0.02	0.02	0.03	<0.001
Outer Superior	0.00	-0.01	0.00	0.63
Outer Nasal	0.01	0.00	0.02	<0.001
Outer Inferior	0.00	-0.01	0.00	0.25

As height and sex may be potential confounders, the two variables were examined separately and together (Figure 4.11, Table 4.7a-b). When regression analysis was performed together for sex and height, changes in significance were noted at central subfield, which remained significantly thicker among women; inner inferior subfield, which was no longer statistically significant; and inner inferior subfield, which became significantly thicker among men.

Figure 4.11. Mean RPE-BM thickness by height. Error bars = 95% confidence interval.

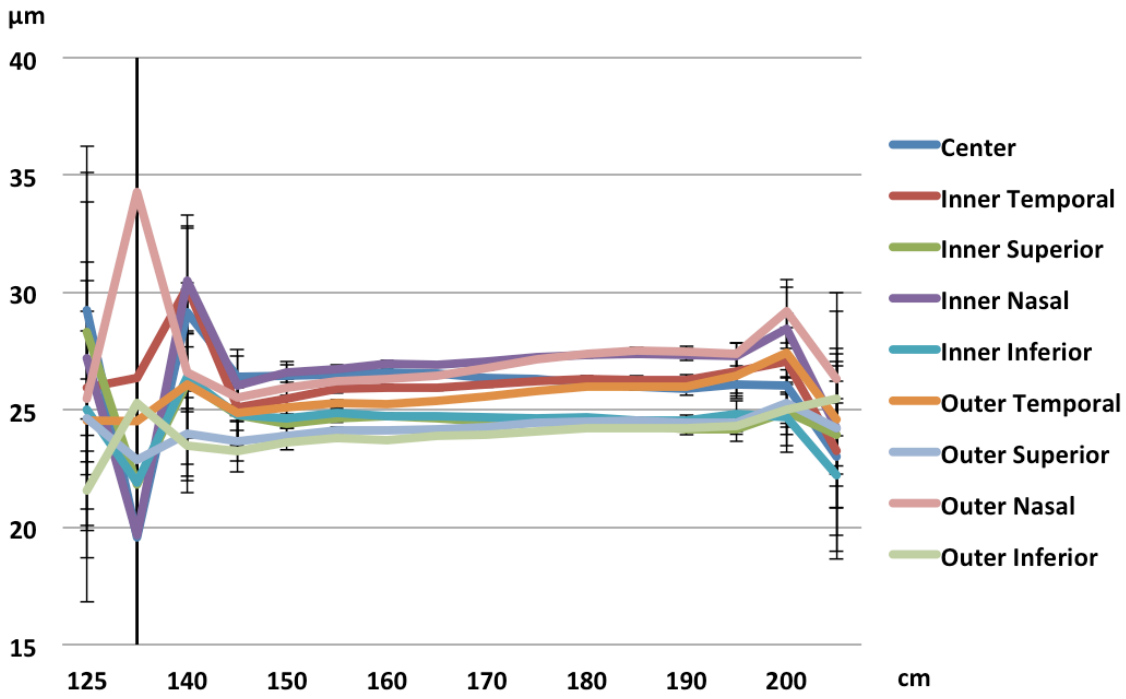

Table 4.7. Univariable and multivariable regression of RPE-BM thickness at subfields, by sex and height.

Table 4.7a. Univariable regression of RPE-BM thickness at subfields, by sex and height.

		Coefficient	95% CI		P-value
Center					
	Female (vs. Male)	0.41	0.32	0.51	<0.001
	Height (per cm)	-0.02	-0.03	-0.02	<0.001
Inner Temporal					
	Female (vs. Male)	-0.49	-0.58	-0.40	<0.001
	Height (per cm)	0.02	0.01	0.02	<0.001
Inner Superior					
	Female (vs. Male)	0.25	0.16	0.34	<0.001
	Height (per cm)	-0.01	-0.02	-0.01	<0.001
Inner Nasal					
	Female (vs. Male)	-0.53	-0.62	-0.44	<0.001
	Height (per cm)	0.02	0.02	0.03	<0.001
Inner Inferior					
	Female (vs. Male)	0.00	-0.09	0.09	0.98
	Height (per cm)	-0.01	-0.01	0.00	0.009
Outer Temporal					
	Female (vs. Male)	-0.75	-0.82	-0.68	<0.001
	Height (per cm)	0.03	0.03	0.03	<0.001
Outer Superior					
	Female (vs. Male)	-0.44	-0.50	-0.38	<0.001
	Height (per cm)	0.02	0.01	0.02	<0.001
Outer Nasal					
	Female (vs. Male)	-1.07	-1.14	-0.99	<0.001
	Height (per cm)	0.05	0.04	0.05	<0.001
Outer Inferior					
	Female (vs. Male)	-0.45	-0.51	-0.39	<0.001
	Height (per cm)	0.02	0.02	0.02	<0.001

CI = confidence interval.

Table 4.7b. Multivariable regression of RPE-BM thickness at subfields, combining sex and height.

		Coefficient	95% CI		P-value
Center					
	Female (vs. Male)	0.28	0.14	0.41	<0.001
	Height (per cm)	-0.01	-0.02	0.00	0.007
Inner Temporal					
	Female (vs. Male)	-0.54	-0.66	-0.42	<0.001
	Height (per cm)*	0.00	-0.01	0.00	0.31
Inner Superior					
	Female (vs. Male)*	0.10	-0.02	0.22	0.1
	Height (per cm)	-0.01	-0.02	0.00	0.001
Inner Nasal					
	Female (vs. Male)	-0.54	-0.67	-0.42	<0.001
	Height (per cm)*	0.00	-0.01	0.01	0.87
Inner Inferior					
	Female (vs. Male)*	-0.18	-0.3	-0.05	0.005
	Height (per cm)	-0.01	-0.02	-0.01	<0.001
Outer Temporal					
	Female (vs. Male)	-0.72	-0.82	-0.62	<0.001
	Height (per cm)*	0.00	0.00	0.01	0.37
Outer Superior					
	Female (vs. Male)	-0.47	-0.56	-0.39	<0.001
	Height (per cm)*	0.00	-0.01	0.00	0.4
Outer Nasal					
	Female (vs. Male)	-0.89	-1.00	-0.78	<0.001
	Height (per cm)	0.01	0.01	0.02	<0.001
Outer Inferior					
	Female (vs. Male)	-0.41	-0.49	-0.32	<0.001
	Height (per cm)*	0.00	0.00	0.01	0.12

CI = confidence interval.
*P-value becomes significant or p-value loses significance, as compared to Table 4.7a.

Variables found to be significant during analysis of individual variables were included in multivariable regression modeling of central RPE-BM thickness (Table 4.8). Central subfield was chosen for analysis, as it is the subfield with greatest clinical relevance. Also, due to the findings of different effects of age before and after 45 years in single variable analysis, with no effect before age 45 and gradual thinning evident at age 46 and above, separate models were performed for those ≤45 years old versus those >45 years old. For those aged 45 years and younger, only ethnicity (black or mixed/other) and refraction were significantly associated with increased RPE-BM thickness (Table 4.8a). In contrast, those older than 45 years of age showed RPE-BM was significantly thinner with older age (-0.1 μm/year, $p<0.001$), Black or mixed race (+3.26 and +0.75 μm vs. white, respectively, $p<0.001$), taller height (-0.02 μm /cm, $p<0.001$), higher intraocular pressure (-0.03 μm /mmHg, $p<0.001$), and greater myopia (-0.28 μm /diopter, $p<0.001$). Female sex, Chinese or Asian races, and smoking were not significant (Table 4.8b).

Table 4.8. Multivariable regression of central RPE-BM thickness separately for A) people 45 years and younger, versus B) people older than 45 years of age.

A) Multivariable regression of central RPE-BM thickness among those 45 years and younger.

	Coefficient	95% Confidence Interval		P-value
Age (per year)	0.02	-0.09	0.12	0.75
Female (vs male)	-0.32	-0.73	0.10	0.13
Height (per cm)	-0.02	-0.05	0.00	0.03
Race (vs white)				
Chinese	-0.84	-3.02	1.34	0.45
Asian	-0.12	-0.76	0.53	0.72
Black	3.61	2.95	4.27	<0.001
Mixed/other	1.77	0.95	2.59	<0.001
Refraction (per dioptre)	0.40	0.3	0.50	<0.001
IOP_G (per mmHg)	-0.04	-0.08	0.01	0.14
Smoke (vs. "No")				
Former	-0.09	-0.43	0.26	0.62
Occasional	-0.40	-1.10	0.30	0.27
Yes, most or all days	-0.37	-0.9	0.17	0.18

IOP_G = Goldmann-corrected intraocular pressure.

B) Multivariable regression of central RPE-BM thickness among those older than 45 years.

	Coefficient	95% Confidence Interval		P-value
Age (per year)	-0.10	-0.11	-0.09	<0.001
Female (vs male)	0.06	-0.09	0.21	0.41
Height (per cm)	-0.02	-0.03	-0.02	<0.001
Race (vs white)				
Chinese	-0.18	-1.06	0.71	0.70
Asian	-0.45	-0.82	-0.08	0.02
Black	3.26	2.88	3.63	<0.001
Mixed/other	0.75	0.35	1.15	<0.001
Refraction (per dioptre)	0.28	0.25	0.31	<0.001
IOP (per mmHg)	-0.03	-0.05	-0.02	<0.001
Smoke (vs. "No")				
Former	-0.10	-0.21	0.00	0.06
Occasional	-0.20	-0.52	0.12	0.22
Yes, most or all days	-0.27	-0.48	-0.05	0.02

IOP_G = Goldmann-corrected intraocular pressure.

4.2 Photoreceptor Inner and Outer Segments

4.2.1 Contributors to Study of Photoreceptors

With the exception of designing UK Biobank (by Paul Foster) and performing automated segmentation (by Topcon collaborators, Qi Yang and Charles Reisman), all work on photoreceptors was performed by me. I am grateful to Paul Foster and Nick Strouthidis for their overall guidance.

4.2.2 Results

67,321 people underwent OCT imaging, with 49,455 having high-quality images of the photoreceptor layer, as compared to 51,987 high-quality images of the RPE layer. After excluding those with high refractive error (< -6 D, > +6 D), poor vision (<20/30), self-reported ocular disorders or diabetes, manual re-grading was performed, and 32,677 OCT images were included for analysis (figure 4.12).

Figure 4.12. Inclusion/exclusion criteria for macular photoreceptor inner and outer segment SDOCT.

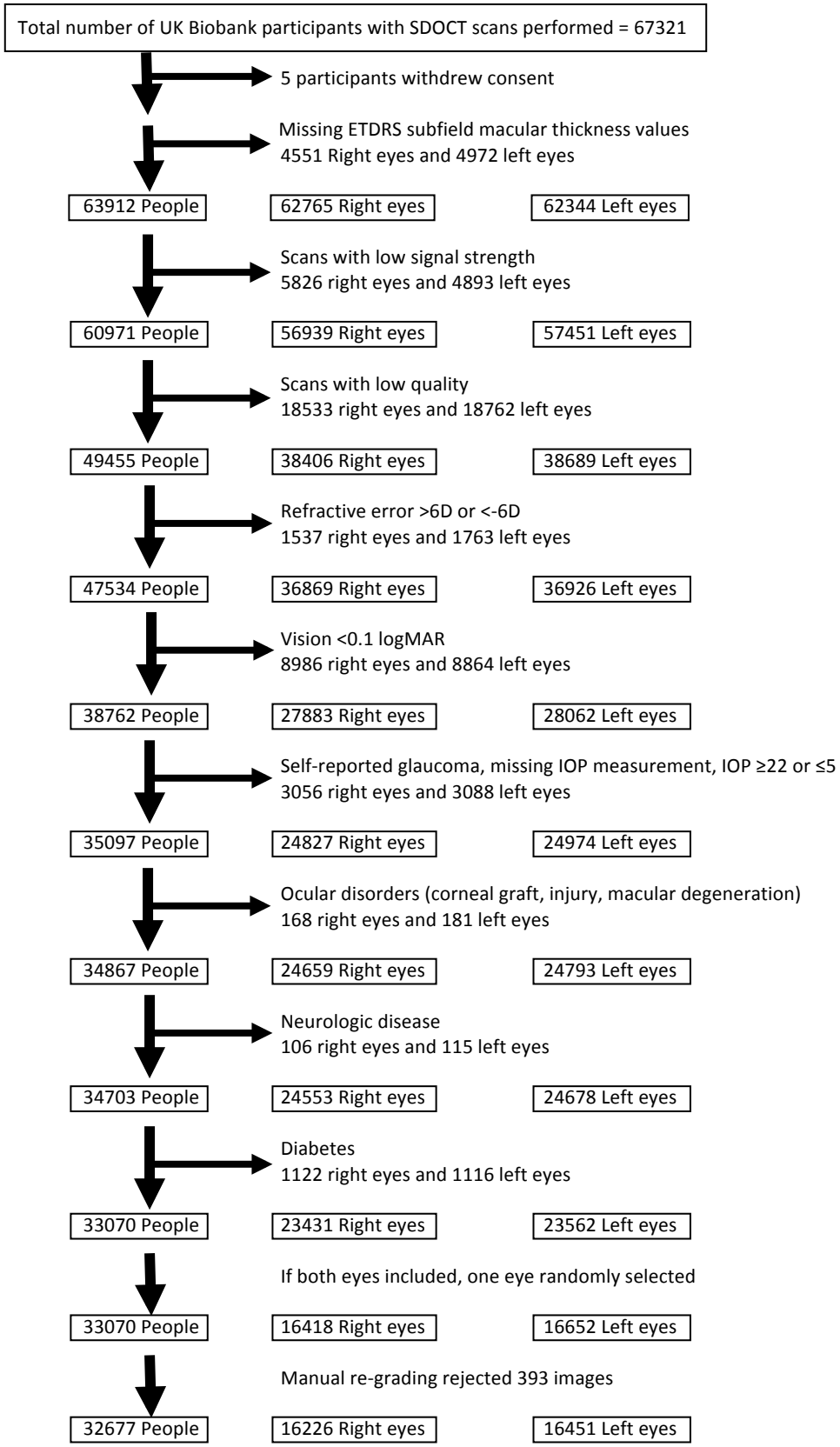

Mean age was 56.0 years, with a slightly higher number of women (53.6%) than men. Mean height was shorter amongst women (163 cm) than men (176 cm, p<0.001). The majority of participants were white (91.8%), with 0.4% Chinese, 2.6% Asians, 2.9% blacks, and 2.3% mixed/other. Chinese people were the smallest ethnic group, and included 119 participants. There were slightly more left eyes (50.3%) than right (49.7%). Mean visual acuity was -0.04 logMAR, mean refraction was -0.04 diopters, and mean IOP was 15 mmHg (Table 4.9).

Table 4.9. Basic demographics of those included in photoreceptor inner and outer segment analysis.

	Estimate (95% CI)	N = 33068
*** Age (mean years)**	56.0 (55.9 – 56.1)	SD = 8.2
+ Female Sex	53.6 (53.0 – 54.1)%	
*** Height (mean centimetres)**	169.2 (169.1 – 169.3)	SD = 9.23
Women	163.1 (163.0 – 163.2)	SD = 6.3
Men	176.3 (176.2 – 176.4)	SD = 6.7
+ Ethnicity		
White	91.8 (91.5 – 92.1)%	
Chinese	0.4 (0.3 – 0.4)%	
Asian	2.6 (2.5 – 2.8)%	
Black	2.9 (2.7 – 3.1)%	
Mixed/Other	2.3 (2.2 – 2.5)%	
+ Laterality = Right eye	49.7 (49.1 – 50.2)%	
*** Visual acuity (logMAR)**	-0.041 (-0.043 – -0.039)	SD = 0.16
*** Refraction**	-0.04 (-0.06 – -0.02)	SD = 1.90
*** IOP (Goldmann corrected)**	15.04 (15.01 – 15.07)	SD = 3.0

* mean (95% confidence interval)
+ percentage (95% confidence interval)
SD = standard deviation

A histogram of photoreceptor thickness (figure 4.13a) shows mean thickness of 71.7 µm (SD = 5.6 µm) in the central subfield. There was a slight plateau configuration centrally, with right skew. Figure 4.13b shows mean photoreceptor thickness at ETDRS subfields,

with inner subfields significantly thicker than corresponding outer subfields (p<0.001). The thickest subfield is the central subfield. Results remained consistent for women and men (figure 4.13c). Furthermore, women had thinner photoreceptor layer in all subfields (p<0.001), except central and outer superior, which were not statistically significant.

Figure 4.13a. Histogram of central photoreceptor thickness. Mean = 71.7 µm, standard error = 0.03 µm, standard deviation = 5.6 µm.

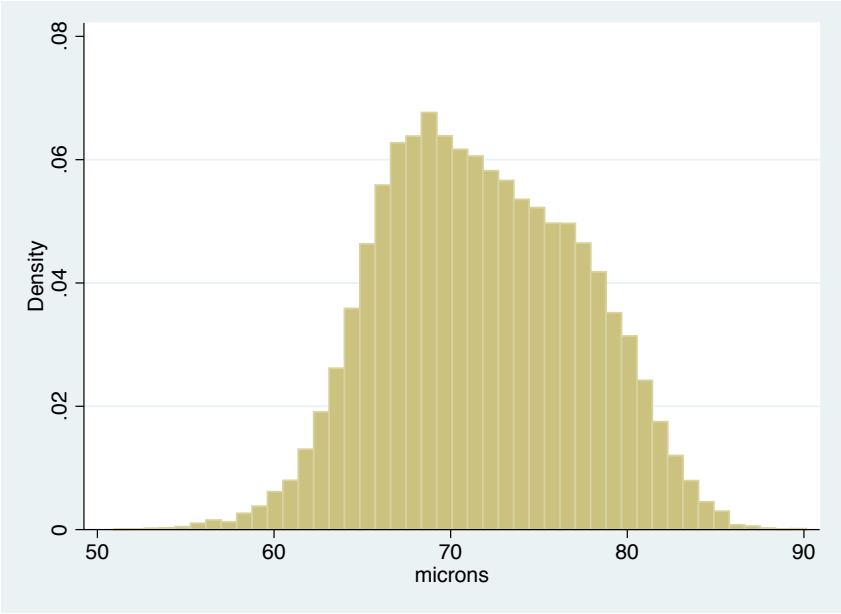

Figure 4.13b. Photoreceptor thickness at different locations. Mean (µm) ± standard deviation.

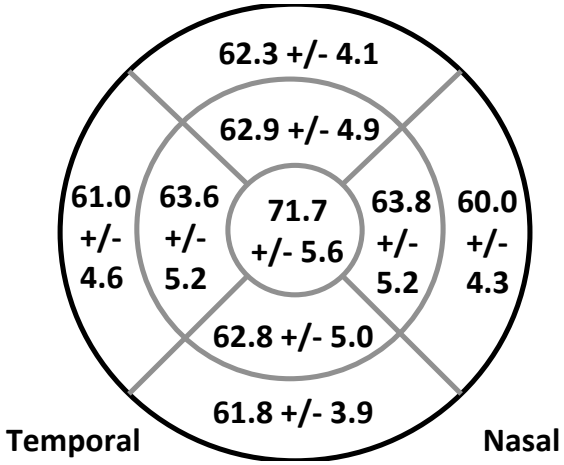

Figure 4.13c-d. Macular RNFL thickness in women (c) and men (d), at different retinal subfields. Mean (μm) ± standard deviation. T-test of women versus men, p<0.001 at all subfields except center (p=0.01) and outer superior (p=0.10).

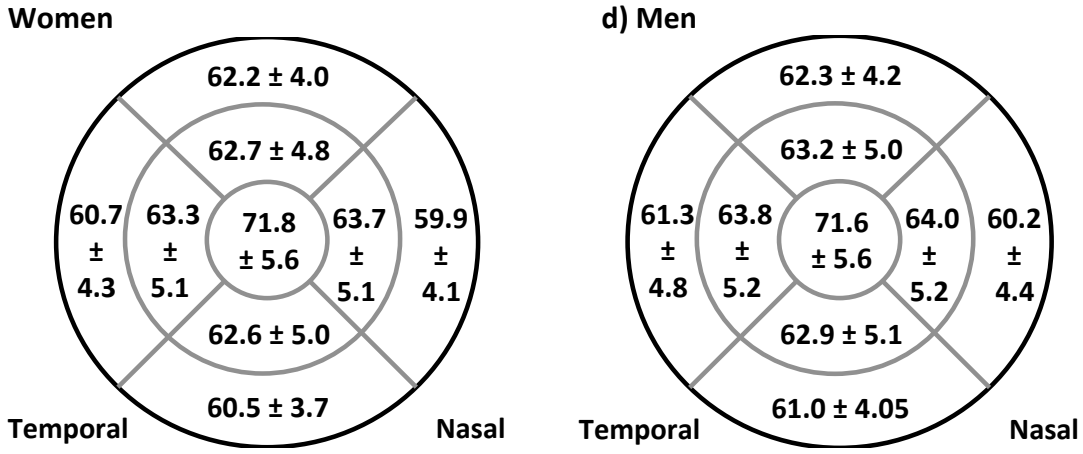

Figure 18 shows mean photoreceptor thickness by age. There is an inflection in direction of trend in thickness before and after age 55, visible graphically as a change from positive to negative slope (figure 4.14). Numerically, univariable regression coefficients are ≥0 at all subfields before age 55, and negative after age 55 (Table 4.10). The most dramatic shift is in the central subfield, with increased average thickness 0.05 μm per year among the younger group (95% CI 0.03 – 0.07, p<0.001), versus -0.19 μm per year among the older group (95% CI -0.12 – -0.17, p<0.001).

Figure 4.14. Mean photoreceptor thickness at subfields, by age.
Error bars = 95% confidence interval.

4.14a. Mean photoreceptor thickness at central subfield, by age.
Error bars = 95% confidence interval.

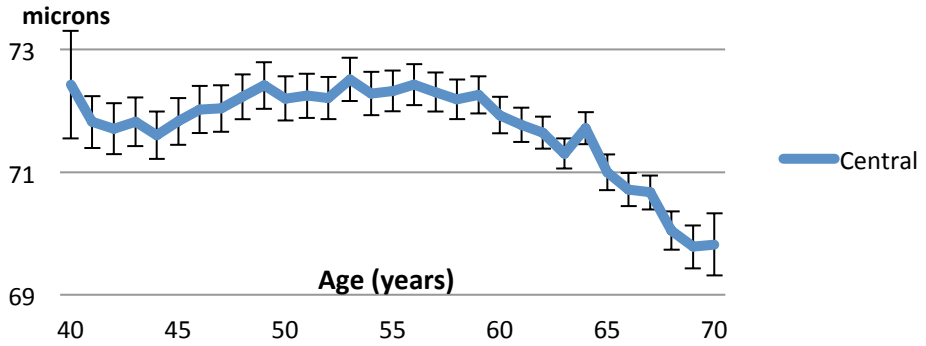

4.14b. Mean photoreceptor thickness at inner subfields, by age.
Error bars = 95% confidence interval.

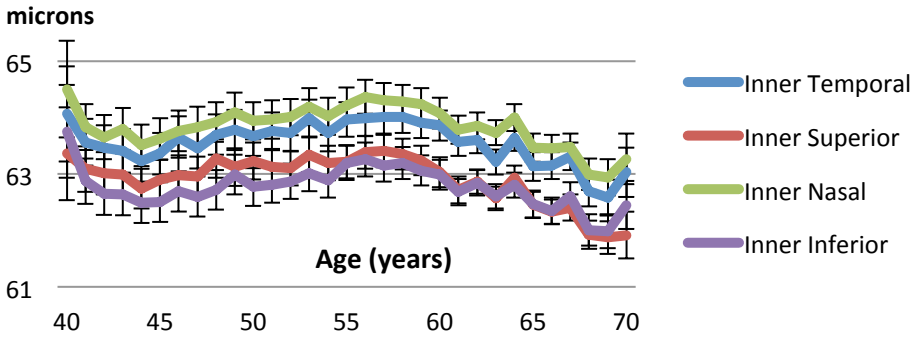

Figure 4.14c. Mean photoreceptor thickness at outer subfields, by age.
Error bars = 95% confidence interval.

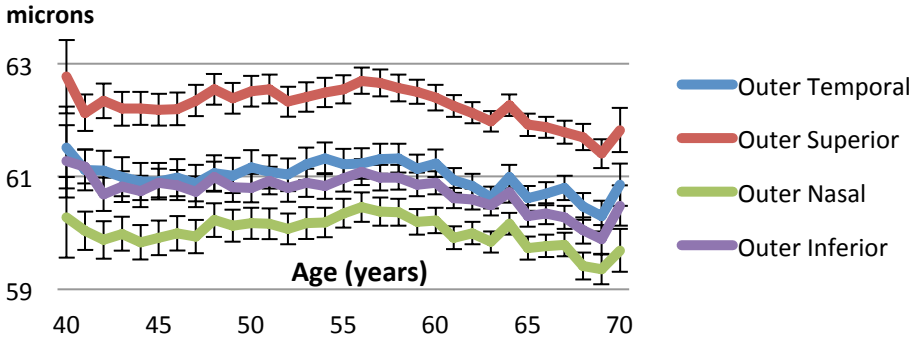

Table 4.10. Univariable regressions of photoreceptor thickness at subfields with A) age ≤55 and B) age >55.

Table 4.10a. Univariable regressions of photoreceptor thickness at subfields with age ≤55.

Photoreceptor subfield	Coefficient	95% CI		P>t
Central	0.05	0.03	0.07	<0.001
Inner Temporal	0.04	0.02	0.06	0.001
Inner Superior	0.02	0.00	0.04	0.03
Inner Nasal	0.03	0.01	0.05	0.001
Inner Inferior	0.03	0.01	0.05	0.01
Outer Temporal	0.01	0.00	0.03	0.11
Outer Superior	0.02	0.01	0.04	0.009
Outer Nasal	0.02	0.01	0.04	0.005
Outer Inferior	0.00	-0.02	0.01	0.92

Table 4.10b. Univariable regressions of photoreceptor thickness at subfields with age >55.

Photoreceptor subfield	Coefficient	95% CI		P>t
Central	-0.19	-0.21	-0.17	<0.001
Inner Temporal	-0.10	-0.12	-0.08	<0.001
Inner Superior	-0.11	-0.13	-0.10	<0.001
Inner Nasal	-0.10	-0.12	-0.08	<0.001
Inner Inferior	-0.09	-0.10	-0.07	<0.001
Outer Temporal	-0.06	-0.08	-0.05	<0.001
Outer Superior	-0.09	-0.1	-0.07	<0.001
Outer Nasal	-0.07	-0.09	-0.06	<0.001
Outer Inferior	-0.08	-0.09	-0.06	<0.001

When photoreceptor thickness was compared amongst different ethnicities, Chinese ethnicity showed significantly greater thickness at every subfield (figure 4.15, table 4.11). At central subfield, Chinese people had 2.37 µm thicker photoreceptors as compared to white people (95% CI 1.33 – 3.41, p<0.001). At inner subfields, average difference between Chinese and white people ranged from 1.89 µm at superior subfield (95% CI 0.96 – 2.82, p<0.001) to 2.59 µm at temporal subfield (95% CI 1.70 – 3.47,

p<0.001). At outer subfields, the difference ranged from 0.96 µm at inferior subfield (95% CI 0.22 – 1.70, p = 0.01) to 1.91 µm at temporal subfield (95% CI 1.15 – 2.67, p<0.001) (table 4.11).

In contrast, black people had the lowest photoreceptor thickness (figure 4.15, table 4.11). At central subfield, black people had -3.67 µm thinner photoreceptors as compared to white people (95% CI -4.08 – -3.26, p<0.001). At inner subfields, difference between black and white people ranged from -3.57 µm at nasal subfield (95% CI -3.95 – -3.18, p<0.001) to -3.36 µm at inferior subfield (95% CI -3.74 – -2.97, p<0.0001). At outer subfields, the difference ranged from -3.19 µm at nasal subfield (95% CI -3.51 – -2.86, p<0.001) to -2.04 µm at inferior subfield (95% CI -2.36 – -1.74, p<0.001) (table 4.11).

Asian people did not show significant association at p-value threshold of <0.001, which was selected based on the number of statistical tests performed. Photoreceptor layer thickness among those of mixed/other ethnicity was not statistically significant at central subfield, but did show thinner photoreceptor layer than white people at other subfields. At inner subfields, the difference ranged from -0.91 µm to -0.82 µm at superior and temporal subfields, respectively (95% CI -1.32 – -0.49 at superior subfield and -1.24 – -0.39 temporal subfield; p<0.001 for both) (table 4.11).

Figure 4.15. Mean photoreceptor thickness at subfields, by ethnicity.
Error bars = 95% confidence interval.

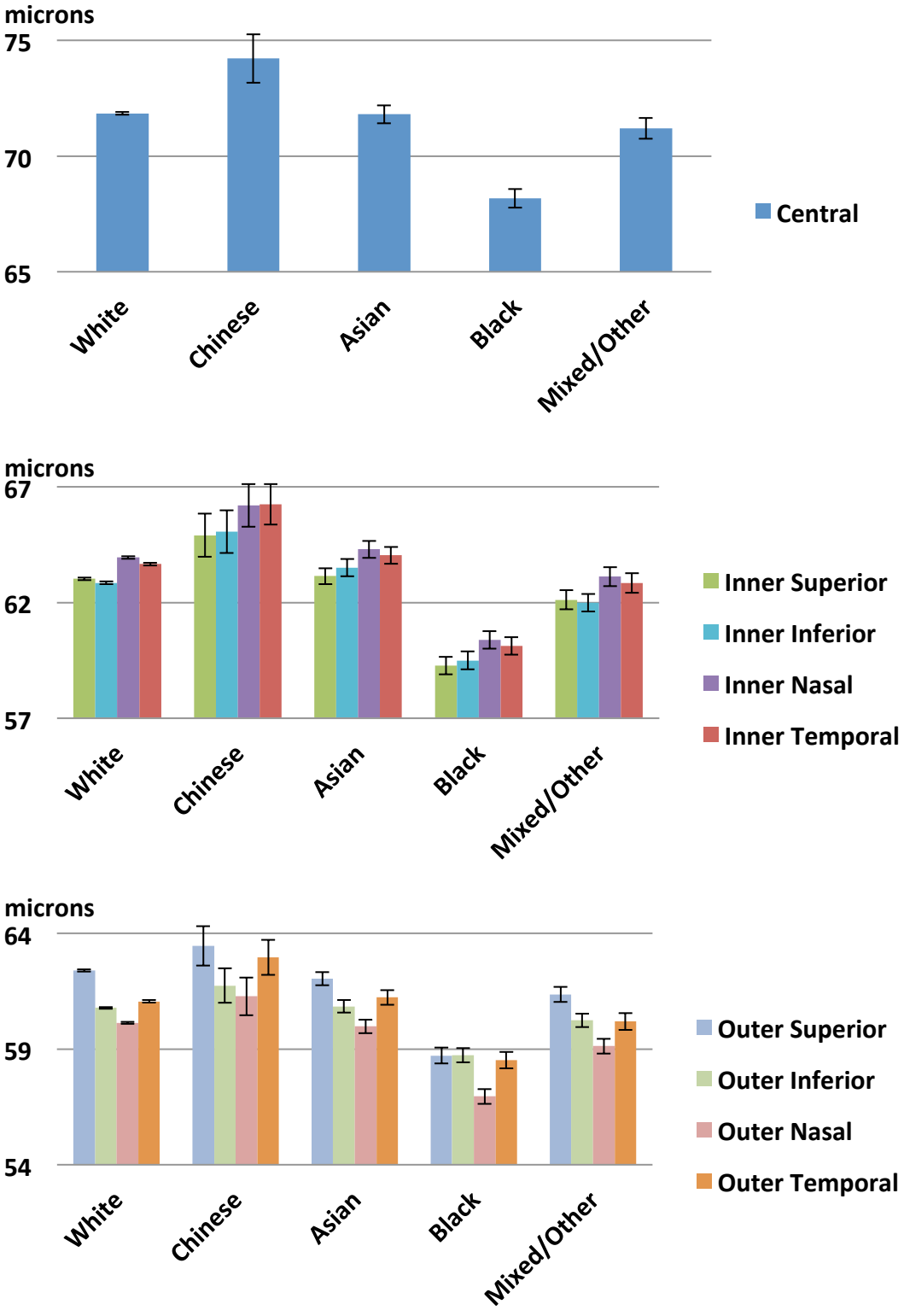

Table 4.11. Univariable regressions of photoreceptor thickness at subfields by ethnicity.

	Coefficient	95% CI		P-value
Central subfield				
White	(reference)			(reference)
Chinese	2.37	1.33	3.41	<0.001
Asian	-0.04	-0.43	0.35	0.85
Black	-3.67	-4.08	-3.26	<0.001
Mixed/Other	-0.64	-1.10	-0.19	0.006

	Coefficient	95% CI		P-value
Inner subfields				
Temporal				
White	(reference)			(reference)
Chinese	2.59	1.70	3.47	<0.001
Asian	0.38	0.01	0.75	0.04
Black	-3.55	-3.93	-3.16	<0.001
Mixed/Other	-0.82	-1.24	-0.39	<0.001
Superior				
White	(reference)			(reference)
Chinese	1.89	0.96	2.82	<0.001
Asian	0.12	-0.23	0.47	0.51
Black	-3.76	-4.14	-3.37	<0.001
Mixed/Other	-0.91	-1.32	-0.49	<0.001
Nasal				
White	(reference)			(reference)
Chinese	2.25	1.32	3.17	<0.001
Asian	0.35	-0.02	0.72	0.07
Black	-3.57	-3.95	-3.18	<0.001
Mixed/Other	-0.83	-1.24	-0.42	<0.001
Inferior				
White	(reference)			(reference)
Chinese	2.22	1.29	3.14	<0.001
Asian	0.66	0.28	1.04	0.001
Black	-3.36	-3.74	-2.97	<0.001
Mixed/Other	-0.86	-1.25	-0.47	<0.001

Table 4.11 (cont.). Univariable regressions of photoreceptor thickness at subfields by ethnicity.

	Coefficient	95% CI		P-value
Outer subfields				
Temporal				
White	(reference)			(reference)
Chinese	1.91	1.15	2.67	<0.001
Asian	0.17	-0.15	0.49	0.3
Black	-2.55	-2.91	-2.18	<0.001
Mixed/Other	-0.87	-1.24	-0.50	<0.001
Superior				
White	(reference)			(reference)
Chinese	1.07	0.22	1.93	0.01
Asian	-0.35	-0.64	-0.07	0.02
Black	-3.67	-4.02	-3.32	<0.001
Mixed/Other	-1.03	-1.36	-0.70	<0.001
Nasal				
White	(reference)			(reference)
Chinese	1.14	0.33	1.96	0.01
Asian	-0.16	-0.46	0.14	0.29
Black	-3.19	-3.51	-2.86	<0.001
Mixed/Other	-1.01	-1.34	-0.68	<0.001
Inferior				
White	(reference)			(reference)
Chinese	0.96	0.22	1.70	0.01
Asian	0.06	-0.22	0.33	0.67
Black	-2.04	-2.36	-1.73	<0.001
Mixed/Other	-0.54	-0.83	-0.26	<0.001

Intraocular pressure was associated with photoreceptor thickness (figure 4.16, table 4.12). At higher intraocular pressures, thicker photoreceptor layer measurements were observed, with regression coefficients ranging from 0.03 to 0.05 µm per mmHg difference in IOP (p<0.001, except inner superior subfield p=0.001) (table 4.12).

Figure 4.16. Mean photoreceptor thickness at subfields, by intraocular pressure (Goldmann-corrected). Error bars = 95% confidence interval.

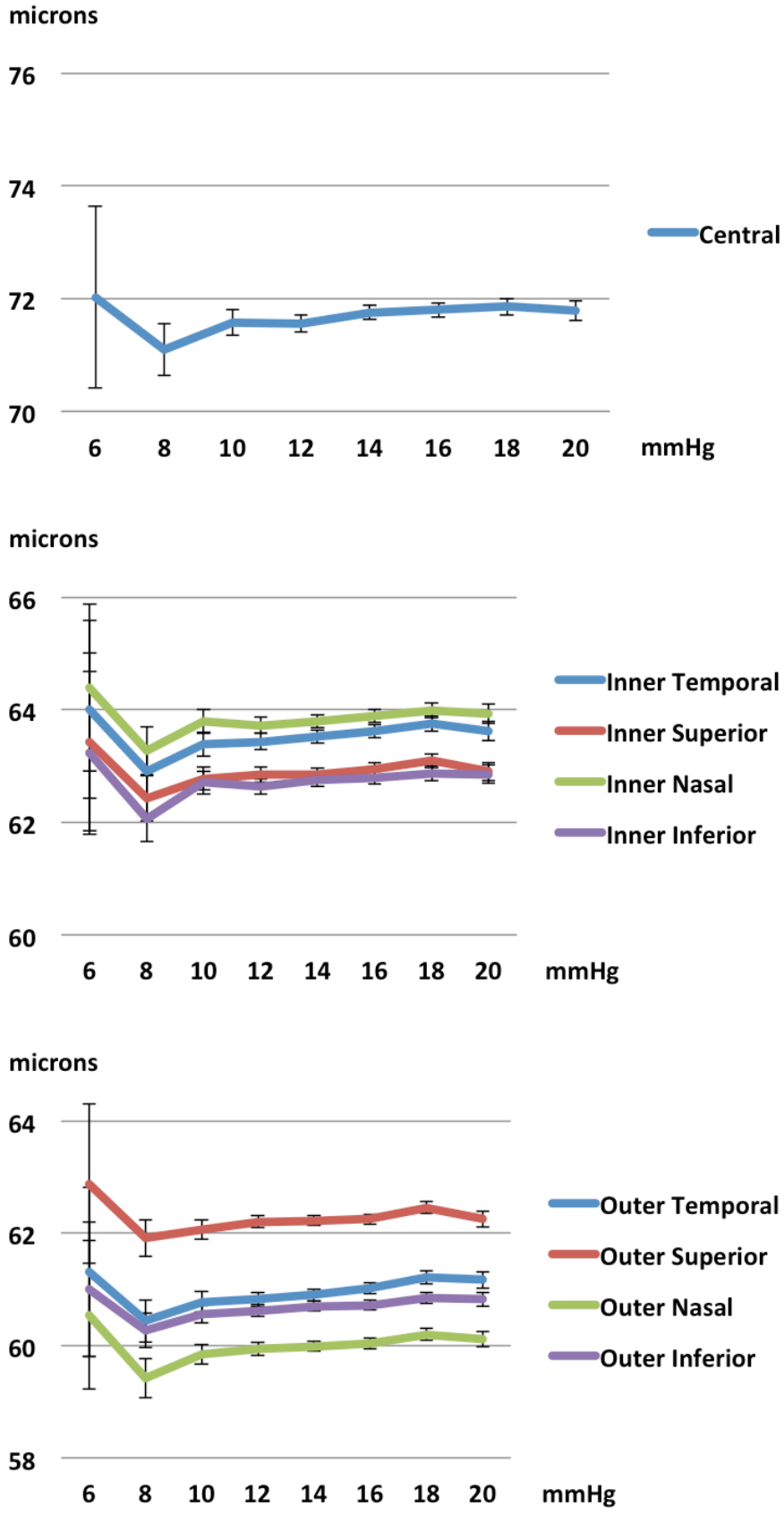

Table 4.12. Univariable regression of photoreceptor thickness and intraocular pressure (Goldmann-corrected).

	Coefficient	95% CI		p-value
Central	0.04	0.02	0.06	<0.001
Inner Temporal	0.04	0.02	0.06	<0.001
Inner Superior	0.03	0.01	0.05	0.001
Inner Nasal	0.03	0.02	0.05	<0.001
Inner Inferior	0.03	0.01	0.05	<0.001
Outer Temporal	0.05	0.04	0.07	<0.001
Outer Superior	0.03	0.01	0.04	<0.001
Outer Nasal	0.04	0.02	0.06	<0.001
Outer Inferior	0.03	0.02	0.05	<0.001

Refractive error is significantly associated with photoreceptor thickness, though the relationship is not linear (figure 4.17). If treated as a continuous variable, there appears to be a negative relationship, with thicker photoreceptor layer among myopes and thinner photoreceptor layer among hyperopes (table 4.13a). However, if analysis is done separately for those with refractive error ≤0 and >0, then a more nuanced relationship is evident (tables 4.13b-c). Among myopes, there is a negative regression coefficient; i.e., those with higher myopia have thicker photoreceptor layer and those closer to emmetropia have thinner photoreceptor layer (table 4.13b). The regression coefficient ranges from -0.56 µm per diopter at the outer temporal subfield (95% CI -0.60 – -0.51, p<0.001) to -0.12 µm per diopter at central and inner nasal subfields (95% CI -0.17 – -0.06, p<0.001) (table 4.13b).

Among hyperopes, there is a positive rather than negative association between photoreceptor thickness and refractive error, suggesting that photoreceptor layer thickness increases as refractive error approaches emmetropia, similar to myopes (table 4.13c). Of note, although the positive association was consistent across all subfields in

the hyperopic group, it was not significant at outer temporal, outer superior, or outer inferior subfields, where p-values did not reach the significance threshold of <0.001. Among the subfields that were significantly associated with photoreceptor thickness, the regression coefficient ranged from 0.16 μm per diopter at central subfield (95% CI 0.09 – 0.24, p<0.001) to 0.29 at inner temporal and inner nasal subfields (95% CI 0.22 – 0.35, p<0.001) (table 4.13c).

Figure 4.17. Mean photoreceptor thickness at subfields, by refraction. Error bars = 95% confidence interval.

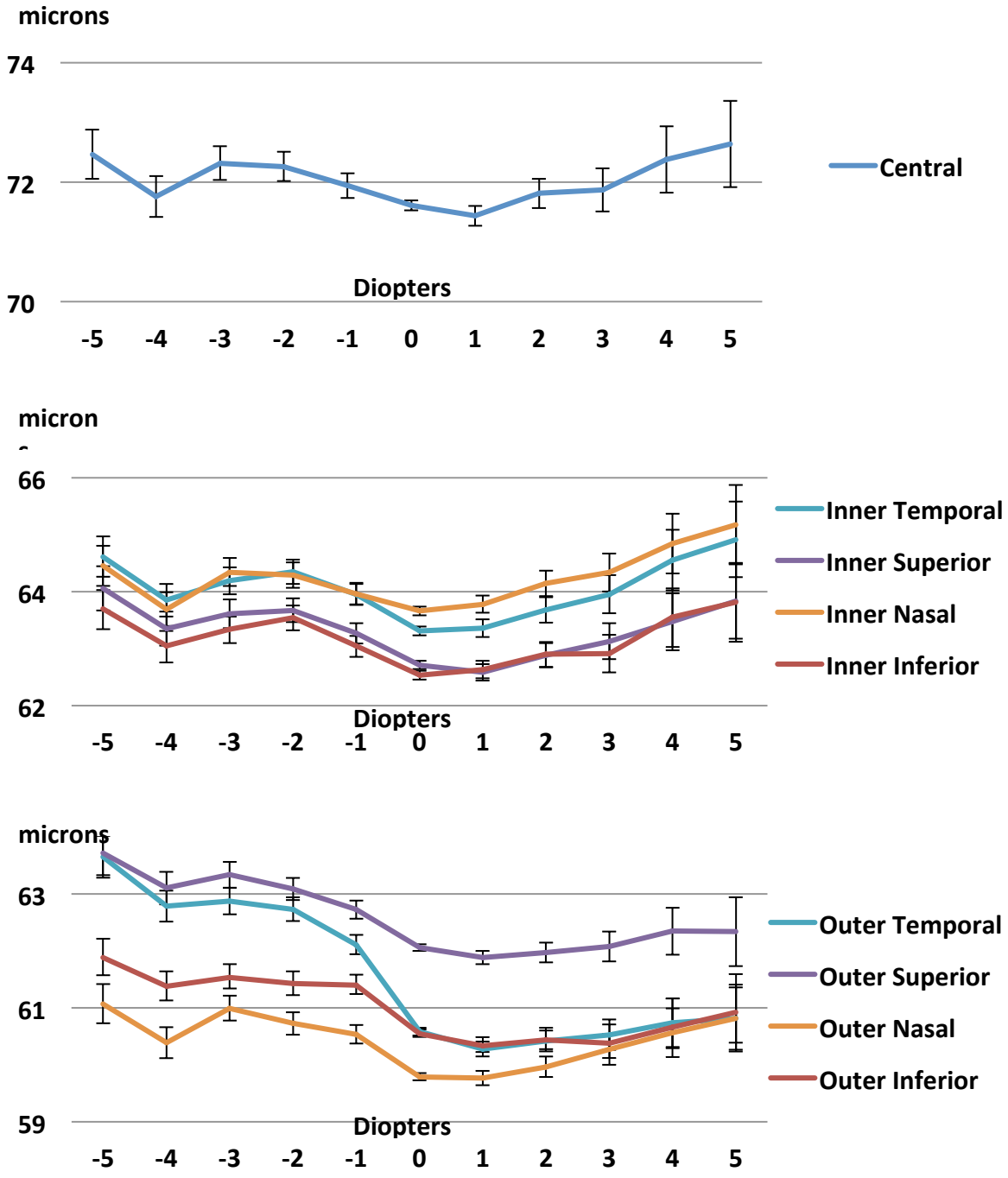

Table 4.13. Univariable regression of photoreceptor thickness and refractive error, among A) all participants, B) myopes, and C) hyperopes.

Table 4.13a. Univariable regression of photoreceptor thickness and refractive error among all participants.

	Coef.	95% CI		p-value
Central	-0.07	-0.10	-0.04	<0.001
Inner Temporal	-0.09	-0.11	-0.06	<0.001
Inner Superior	-0.12	-0.15	-0.10	<0.001
Inner Nasal	-0.01	-0.04	0.02	0.57
Inner Inferior	-0.08	-0.11	-0.05	<0.001
Outer Temporal	-0.42	-0.45	-0.40	<0.001
Outer Superior	-0.21	-0.23	-0.18	<0.001
Outer Nasal	-0.13	-0.16	-0.11	<0.001
Outer Inferior	-0.19	-0.21	-0.17	<0.001

Table 4.13b. Univariable regression of photoreceptor thickness and refractive error ≤0.

	Coefficient	95% CI		p-value
Central	-0.12	-0.17	-0.06	<0.001
Inner Temporal	-0.21	-0.26	-0.16	<0.001
Inner Superior	-0.21	-0.26	-0.16	<0.001
Inner Nasal	-0.12	-0.17	-0.07	<0.001
Inner Inferior	-0.21	-0.26	-0.17	<0.001
Outer Temporal	-0.56	-0.60	-0.51	<0.001
Outer Superior	-0.29	-0.34	-0.24	<0.001
Outer Nasal	-0.22	-0.27	-0.18	<0.001
Outer Inferior	-0.22	-0.26	-0.18	<0.001

Table 4.13c. Univariable regression of photoreceptor thickness and refractive error >0.

	Coefficient	95% CI		p-value
Central	0.16	0.09	0.24	<0.001
Inner Temporal	0.29	0.22	0.35	<0.001
Inner Superior	0.19	0.12	0.25	<0.001
Inner Nasal	0.29	0.22	0.36	<0.001
Inner Inferior	0.23	0.16	0.30	<0.001
Outer Temporal	0.07	0.02	0.13	0.01
Outer Superior	0.07	0.01	0.12	0.02
Outer Nasal	0.20	0.15	0.26	<0.001
Outer Inferior	0.04	-0.01	0.09	0.16

Height was analyzed as an individual variable, but also for the purposes of multivariable modeling, as it is a potential confounder with sex. There was a positive association between photoreceptor thickness and height at all subfields except central subfield, which did not reach the threshold for statistical significance (figure 4.18, table 4.14). At remaining subfields, univariable regression coefficients ranged between 0.02 to 0.03 µm per centimeter taller height ($p<0.001$) (table 4.14).

Figure 4.18. Mean photoreceptor thickness at subfields, by height. Error bars = 95% confidence interval.

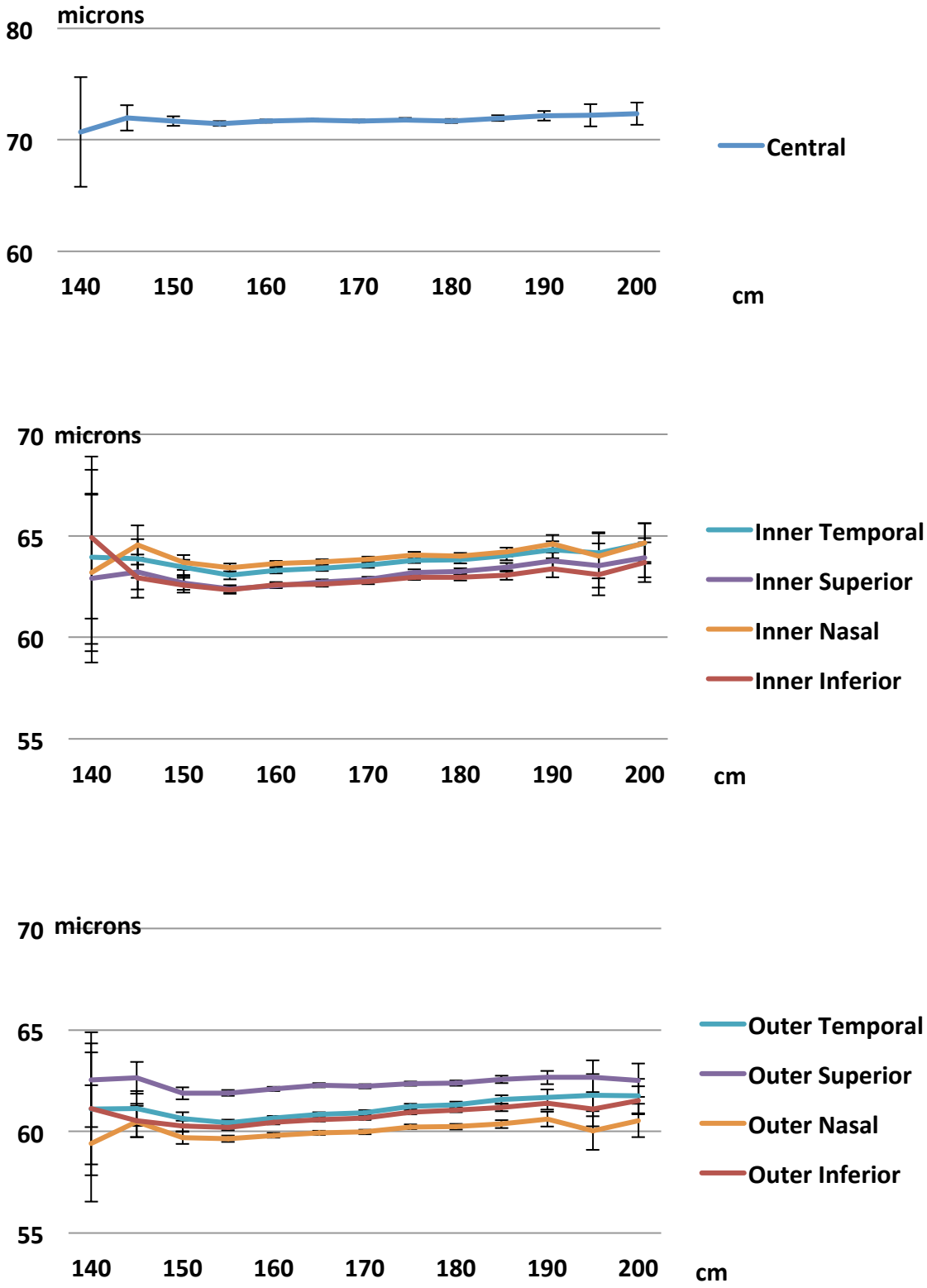

Table 4.14. Univariable regression of photoreceptor thickness and height.

	Coefficient	95% CI		p-value
Central	0.01	0.00	0.02	0.004
Inner Temporal	0.03	0.02	0.03	<0.001
Inner Superior	0.03	0.03	0.04	<0.001
Inner Nasal	0.02	0.02	0.03	<0.001
Inner Inferior	0.02	0.02	0.03	<0.001
Outer Temporal	0.03	0.03	0.04	<0.001
Outer Superior	0.02	0.01	0.02	<0.001
Outer Nasal	0.02	0.02	0.03	<0.001
Outer Inferior	0.03	0.03	0.03	<0.001

As with RPE, photoreceptor layer did not show a dose-specific response with smoking (figure 4.19). People who reported occasional smoking may have slightly thicker photoreceptor layer; however, this was not statistically significant. There was a consistent finding of thinner photoreceptor layer among people who smoked all or most days as compared to non-smokers. The smallest difference was at the central subfield, where people who smoked all or most days had -0.74 μm thinner photoreceptor layer than non-smokers (95% CI -0.98 – -0.49, p<0.001). The largest difference was at the outer temporal subfield, with regular smokers having -1.07 μm thinner photoreceptor layer than non-smokers (95% CI -1.27 – -0.86, p<0.001) (table 4.15). One must be careful interpreting these results, as direction of association changes depending on how smoking is categorized.

Figure 4.19. Mean photoreceptor thickness at subfields, by smoking status.
Error bars = 95% confidence interval.

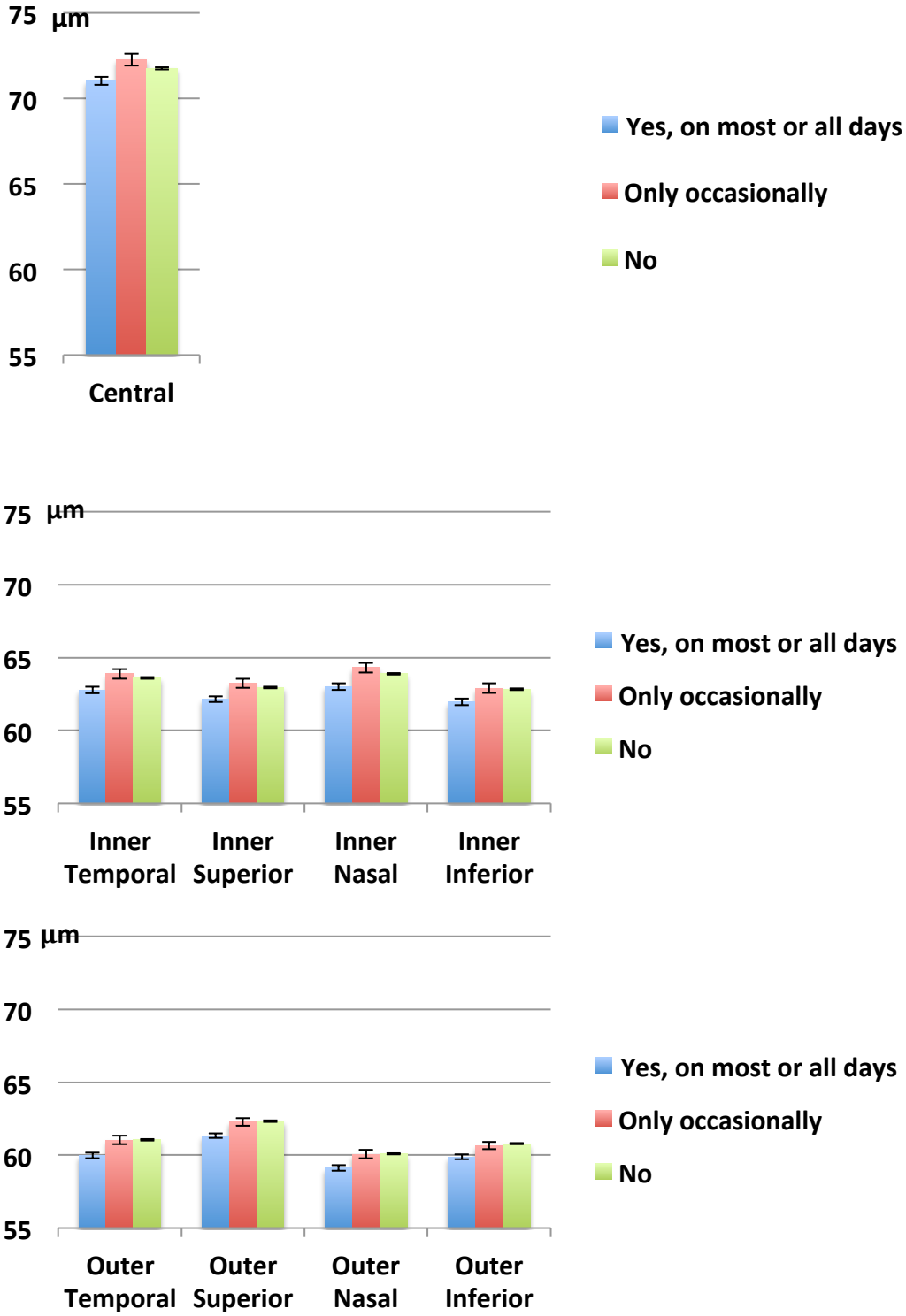

Table 4.15. Univariable regressions of photoreceptor thickness at subfields by smoking status.

	Coefficient	95% CI		P-value
Central subfield				
No	(reference)			(reference)
Occasional	0.52	0.15	0.88	0.005
All or most days	-0.74	-0.98	-0.49	<0.001
Inner subfields				
Temporal				
No	(reference)			(reference)
Occasional	0.28	-0.06	0.62	0.1
All or most days	-0.83	-1.06	-0.61	<0.001
Superior				
No	(reference)			(reference)
Occasional	0.28	-0.04	0.61	0.09
All or most days	-0.80	-1.02	-0.59	<0.001
Nasal				
No	(reference)			(reference)
Occasional	0.42	0.07	0.77	0.02
All or most days	-0.89	-1.12	-0.67	<0.001
Inferior				
No	(reference)			(reference)
Occasional	0.08	-0.26	0.42	0.63
All or most days	-0.86	-1.08	-0.64	<0.001
Outer subfields				
Temporal				
No	(reference)			(reference)
Occasional	-0.02	-0.32	0.28	0.89
All or most days	-1.07	-1.27	-0.86	<0.001
Superior				
No	(reference)			(reference)
Occasional	-0.05	-0.31	0.22	0.74
All or most days	-0.99	-1.17	-0.81	<0.001
Nasal				
No	(reference)			(reference)
Occasional	-0.02	-0.31	0.26	0.88
All or most days	-0.97	-1.16	-0.78	<0.001
Inferior				
No	(reference)			(reference)
Occasional	-0.11	-0.37	0.15	0.4
All or most days	-0.90	-1.06	-0.73	<0.001

Blood pressure, both systolic and diastolic, was associated with photoreceptor thickness, with higher blood pressure associated with thinner photoreceptor layer (figures 4.20-21). At the central subfield, there was -0.11 μm thinner photoreceptor layer per 10 mmHg higher systolic blood pressure (95% CI -0.14 – -0.08, p<0.001) and -0.12 μm thinner photoreceptor layer per 10 mmHg higher diastolic blood pressure (95% CI -0.17 – -0.06, p<0.001) (tables 4.16-17). This trend was consistent at all subfields, but was only statistically significant at central, inner superior, and outer subfields for systolic blood pressure (table 4.16). For diastolic blood pressure, the association was significant at central, outer superior, outer nasal, and outer inferior subfield (table 4.17).

Figure 4.20. Mean photoreceptor thickness at subfields, by systolic blood pressure.
Error bars = 95% confidence interval.

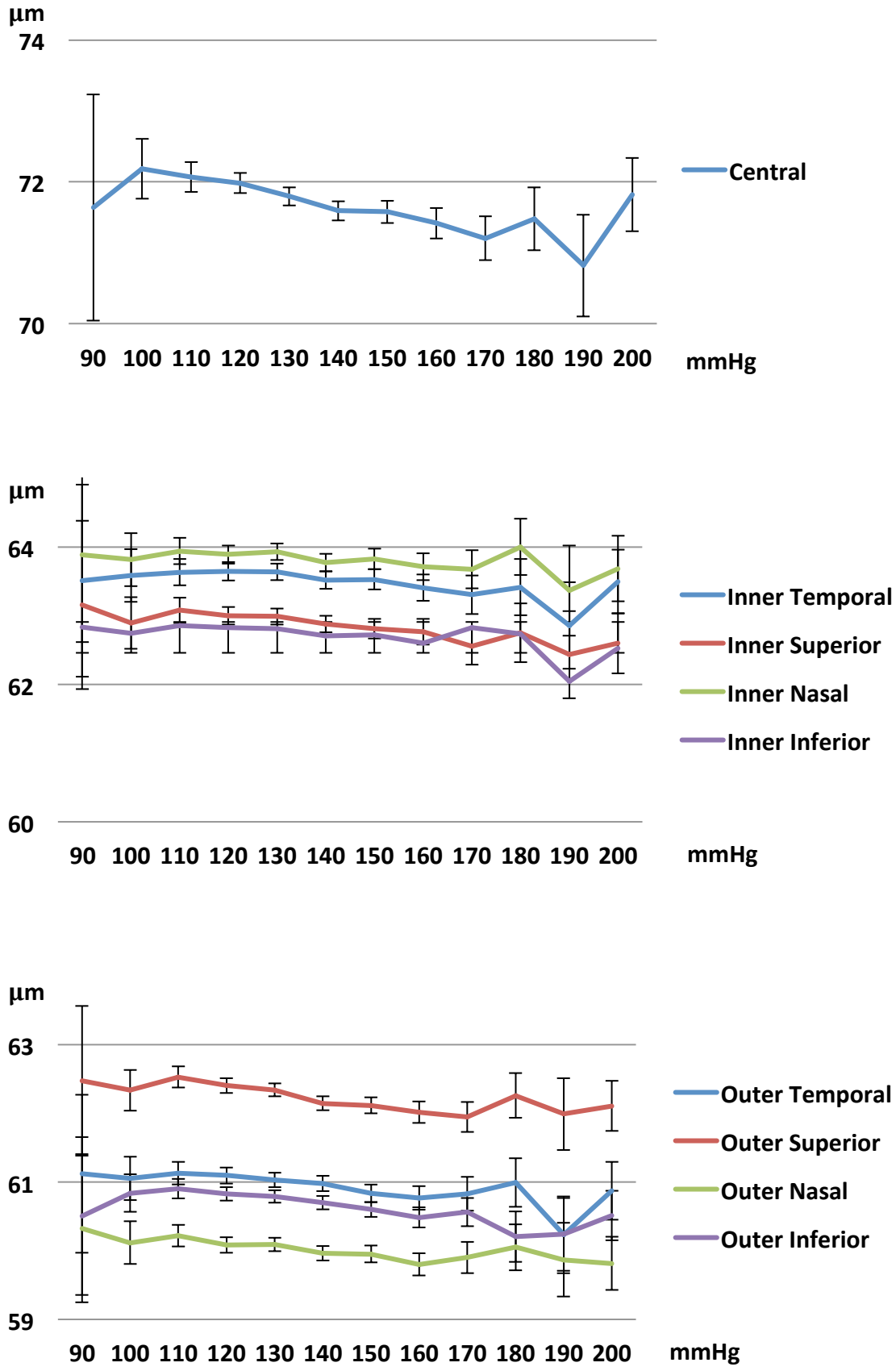

Table 4.16. Univariable regression of photoreceptor thickness and systolic blood pressure. Regression coefficient represents difference in photoreceptor thickness per 10 mmHg blood pressure.

	Coefficient	95% CI		p-value
Central	-0.11	-0.14	-0.08	<0.001
Inner Temporal	-0.04	-0.07	-0.02	0.002
Inner Superior	-0.06	-0.09	-0.03	<0.001
Inner Nasal	-0.03	-0.06	0.00	0.03
Inner Inferior	-0.03	-0.06	-0.01	0.02
Outer Temporal	-0.05	-0.08	-0.03	<0.001
Outer Superior	-0.07	-0.09	-0.05	<0.001
Outer Nasal	-0.05	-0.07	-0.02	<0.001
Outer Inferior	-0.07	-0.09	-0.05	<0.001

Figure 4.21. Mean photoreceptor thickness at subfields, by diastolic blood pressure.
Error bars = 95% confidence interval.

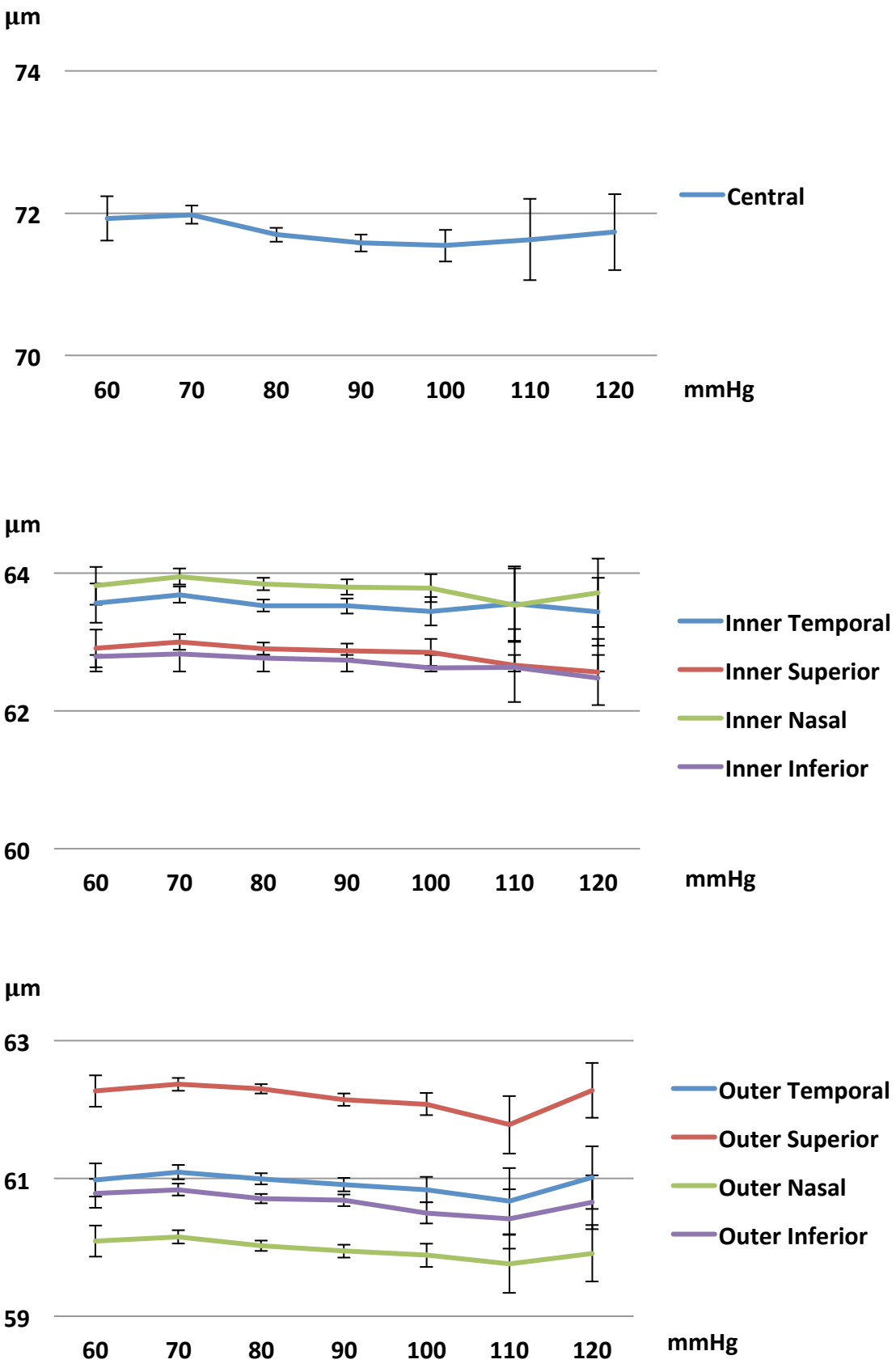

Table 4.17. Univariable regression of photoreceptor thickness and diastolic blood pressure. Regression coefficient represents difference in photoreceptor thickness per 10 mmHg blood pressure.

	Coefficient	95% CI		p-value
Central	-0.12	-0.17	-0.06	<0.001
Inner Temporal	-0.05	-0.10	0.00	0.05
Inner Superior	-0.05	-0.10	0.00	0.03
Inner Nasal	-0.05	-0.10	0.00	0.05
Inner Inferior	-0.05	-0.10	0.00	0.04
Outer Temporal	-0.06	-0.11	-0.02	0.007
Outer Superior	-0.08	-0.12	-0.04	<0.001
Outer Nasal	-0.07	-0.12	-0.03	<0.001
Outer Inferior	-0.07	-0.11	-0.03	<0.001

There was a significant association between BMI and photoreceptor layer thickness, with heavier BMI being associated with thinner photoreceptor layer (figure 4.22). At central subfield, photoreceptor layer was found to be -0.13 µm thinner per kg/m^2 increase in BMI (95% CI -0.14 – -0.12, p<0.001) (table 4.18). This trend was consistent across all subfields (p<0.001) (table 4.18).

Figure 4.22. Mean photoreceptor thickness at subfields, by body mass index. Error bars = 95% confidence interval.

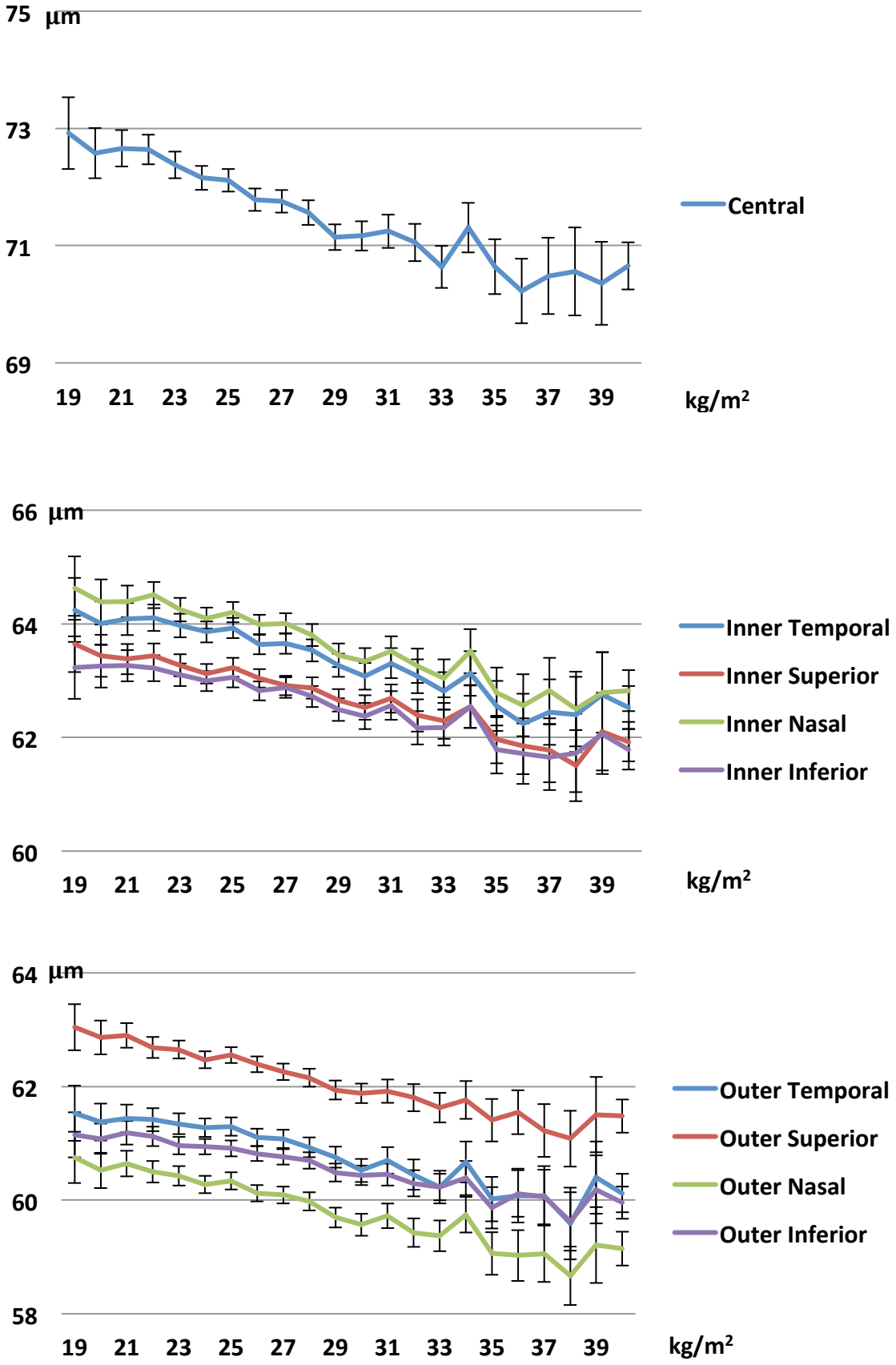

Table 4.18. Univariable regression of photoreceptor thickness and body mass index.

	Coefficient	95% CI		p-value
Central	-0.13	-0.14	-0.12	<0.001
Inner Temporal	-0.10	-0.11	-0.08	<0.001
Inner Superior	-0.09	-0.10	-0.08	<0.001
Inner Nasal	-0.10	-0.11	-0.09	<0.001
Inner Inferior	-0.09	-0.10	-0.08	<0.001
Outer Temporal	-0.08	-0.10	-0.07	<0.001
Outer Superior	-0.09	-0.10	-0.08	<0.001
Outer Nasal	-0.09	-0.10	-0.08	<0.001
Outer Inferior	-0.07	-0.08	-0.06	<0.001

Multivariable regression modeling of photoreceptor layer thickness at central subfield was performed, including variables found to be significant in single variable analyses (table 4.19). Older age remained significantly associated with thinner photoreceptor layer (-0.06 µm per year, 95% CI -0.07 – -0.06, p<0.001). Chinese people had significantly thicker photoreceptor layer than whites (1.84 µm, 95% CI 0.79 – 2.89, p<0.0001), whereas black people had significantly thinner photoreceptor layer (-3.76 µm, 95% CI -4.18 – -3.34, p<0.001). Mixed/other ethnicity showed intermediate results, but remained thinner as compared to whites (-0.87 µm, 95% CI -1.33 – -0.41, p<0.001). Intraocular pressured showed a positive association with photoreceptor layer thickness, of 0.05 µm per mmHg (95% CI 0.03 – 0.07, p<0.001). Those who smoked all or most days had -0.87 µm thinner photoreceptor layer than non-smokers (95% CI -1.12 – -0.63, p<0.001). Body mass index showed a significant negative association with photoreceptor layer thickness, at -0.12 µm thinner per kg/m^2 (95% CI -0.13 – -0.1, p<0.001) (table 19). After controlling for potential confounders, sex, height, Asian ethnicity, refractive error, occasional smoking, and systolic blood pressure were not significant.

Table 4.19. Multivariable regression modeling for photoreceptor thickness at central subfield. BP = blood pressure.

	Coef.	95% CI		P>t
Age (per year)	-0.06	-0.07	-0.06	<0.001
Female (vs. male)	0.15	-0.03	0.33	0.10
Race (vs. white)				
Chinese	1.84	0.79	2.89	<0.001
Asian	-0.42	-0.81	-0.02	0.04
Black	-3.76	-4.18	-3.34	<0.001
Mixed/Other	-0.87	-1.33	-0.41	<0.001
Refraction (per diopter)	0.00	-0.03	0.04	0.78
IOP_G (per mmHg)	0.05	0.03	0.07	<0.001
Height (per cm)	0.01	0.00	0.02	0.09
Smoking (vs. non-smoker)				
Occasional	0.42	0.06	0.78	0.02
All or most days	-0.87	-1.12	-0.63	<0.001
Systolic BP (per 10mmHg)	0.03	-0.01	0.06	0.14
Body mass index (per kg/m^2)	-0.12	-0.13	-0.10	<0.001

4.3 Ganglion Cell Layer – Inner Plexiform Layer Complex

4.3.1 Contributors to Study of GCL-IPL

With the exception of designing UK Biobank (by Paul Foster) and performing automated segmentation (by Topcon collaborators, Qi Yang and Charles Reisman), all work on GCL-IPL was performed by me. I am grateful to Paul Foster and Nick Strouthidis for their overall guidance.

4.3.2 Results

Of the 67321 people who underwent OCT testing, 33070 had high-quality images, good visual acuity, IOP between 6 – 21 mmHg, and reported no ocular, neurologic, or diabetic disease. This number was initially the same as that for RNFL layer. The difference was that only one image was rejected after manual re-grading, resulting in 33069 people available for analysis (Figure 4.23).

Figure 4.23. Inclusion/exclusion criteria for GCL-IPL complex

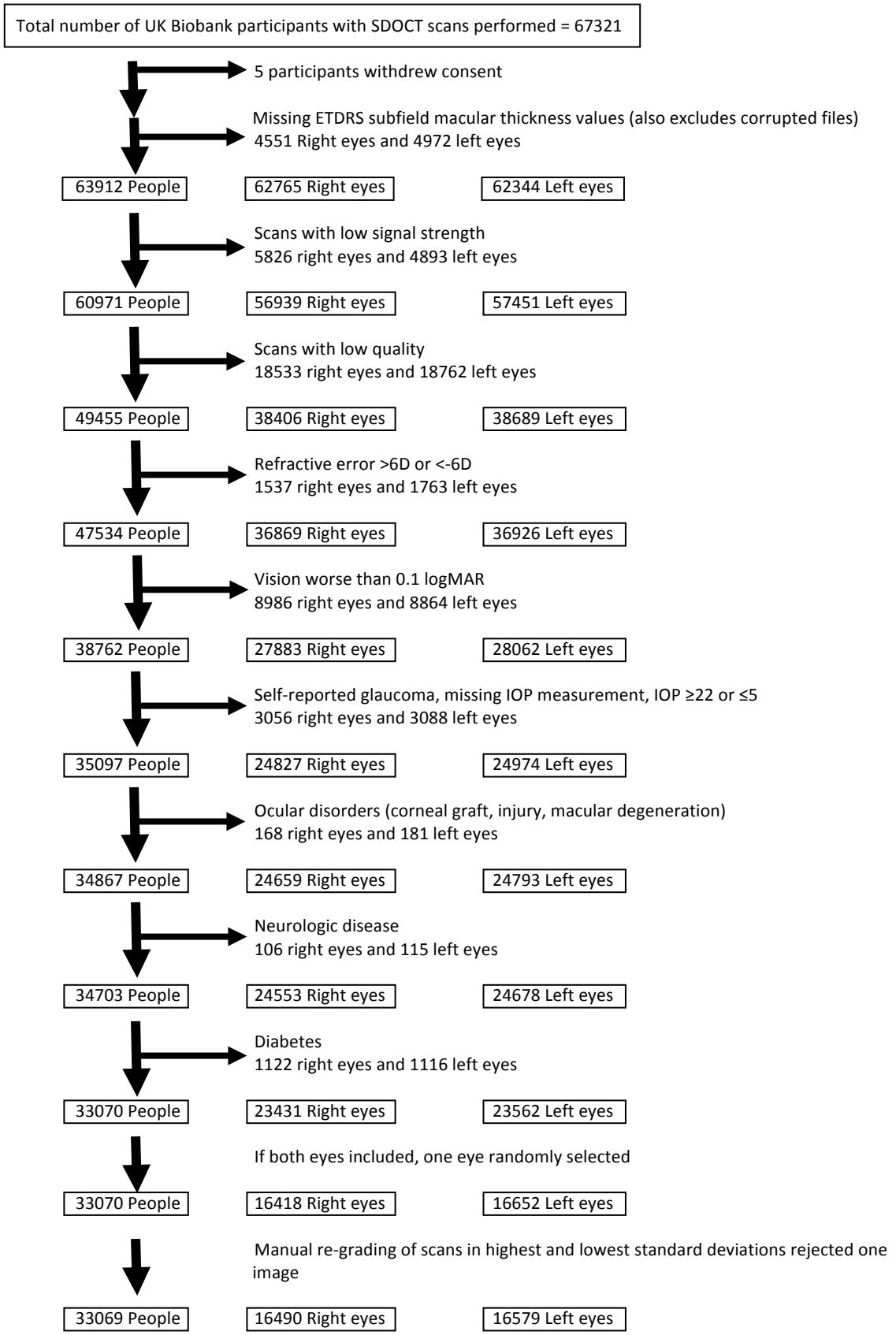

Mean age of participants was 56.0 years, with more women (53.5%) than men. Mean height was shorter among women (163.1 cm) as compared to men (176.3 cm). The majority of participants were white (91.8%). Blacks (2.9%), Asian (2.6%), and mixed/other ethnicity (2.3%) were the next largest groups. There were fewer people who identified as Chinese ethnicity (0.4%). Random selection of right vs. left eyes resulted in 49.9% of the former, and slightly more of the latter (50.1%). Mean visual acuity was -0.07 logMAR, mean refraction was -0.06 diopters, and mean IOP was 15 mmHg (Table 4.20).

Table 4.20. Basic demographics for those included in GCL-IPL analysis.

	Estimate (95% CI)	N = 33069
*** Age (mean years)**	56.0 (55.9 – 56.1)	SD = 8.2
+ Female Sex	53.5 (53.0 – 54.1)%	
*** Height (mean centimetres)**	169.2 (169.1 – 169.3)	SD = 9.2
Women	163.1 (163.0 – 163.2)	SD = 6.3
Men	176.3 (176.2 – 176.4)	SD = 6.7
+ Ethnicity		
White	91.8 (91.5 – 92.1)%	
Chinese	0.4 (0.3 – 0.4)%	
Asian	2.6 (2.4 – 2.8)%	
Black	2.9 (2.7 – 3.1)%	
Mixed/Other	2.3 (2.2 – 2.5)%	
+ Laterality = Right eye	49.9 (49.3 – 50.4)%	
*** Visual acuity (logMAR)**	-0.07 (-0.075 – -0.07)	SD = 0.09
*** Refraction**	-0.06 (-0.08 – -0.04)	SD = 1.91
*** IOP (Goldmann corrected)**	15.0 (15.01 – 15.07)	SD = 3.0
+ Educational attainment		
College degree	37.1 (36.6 – 37.6)%	
Prof. qual. or A-level	23.6 (23.1 – 24.0)%	
O-level	21.4 (21.0 – 21.9)%	
CSE	5.8 (5.6 – 6.1)%	
Lower than CSE	12.0 (11.7 – 12.4)%	
*** Townsend deprivation index**	-1.13 (-1.16 – -1.10)	SD = 2.93

* mean (95% confidence interval)
+ percentage (95% confidence interval)
SD = standard deviation
IOP (Goldmann equivalent) was measured using Reichert Ocular Response Analyser (ORA)
Prof. qual. = Professional or vocational qualification (including higher national diploma)
A-Level = General Certificate of Education Advanced Level, typically taken at age 18
O-Level = General Certificate of Education Ordinary Level, typically taken at age 16
CSE = Certificate of Secondary Education a less demanding exam usually taken at age 16

Mean GCL-IPL thickness at the central subfield was 53.2 µm (SD = 11.3 um). Histogram (Figure 4.24a) showed a slight right skew. At the inner nasal subfield, mean thickness was 92.0 µm (SD = 8.39 µm) (Figure 4.24b). Mean thickness of each subfield is shown in Figure 4.24c, with the thinnest being the central subfield and thickest being the inner nasal subfield. Inner subfields were thicker than outer subfields ($p<0.001$). This was in

contrast with the RNFL layer, shown in the next section, where outer subfields were thicker than inner. Women and men followed this same pattern, though when the two sexes were compared to each other, women had thicker average GCL-IPL at outer subfields than men ($p<0.001$), and men had thicker average inner subfields than women ($p<0.001$), with the exception of the inner superior subfield, which was not significant (Figure 4.24d).

Figure 4.24a-b. Histogram of macular GCL-IPL thickness at A) central and B) inner nasal subfields. Central subfield mean = 53.2 µm, standard error = 0.06 µm, standard deviation = 11.3 µm. Inner nasal subfield mean = 92.0 µm, standard error = 0.04 µm, standard deviation = 8.39 µm.

a) **b)**

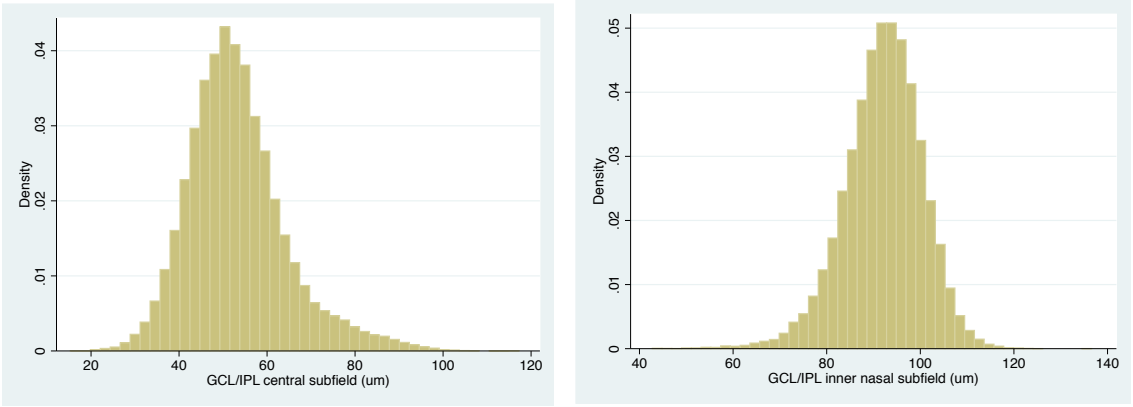

Figure 4.24c. Macular GCL-IPL thickness at different locations. Mean (µm) ± standard deviation.

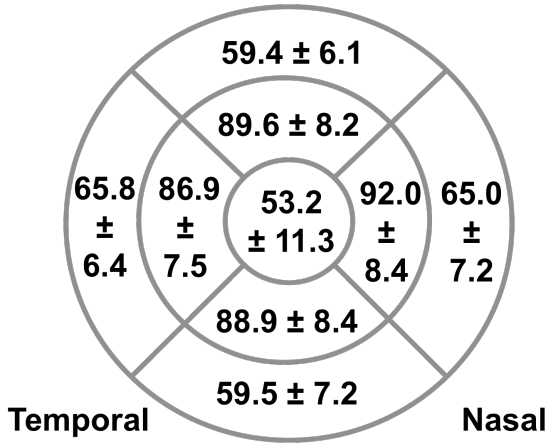

Figure 4.24d-e. Macular GCL-IPL thickness in women (d) and men (e), at different locations. Mean (μm) ± standard deviation. T-test of women versus men, p<0.001 at all subfields except inner superior (p=0.04).

d) **e)**

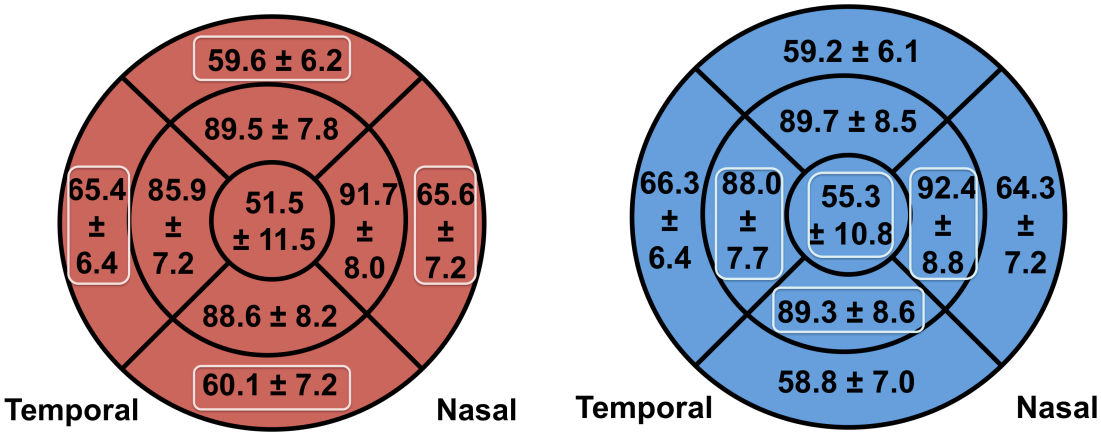

GCL-IPL appears\ed thinner with older age (Figure 4.25). This was statistically significant at all subfields (p<0.001) except the central subfield (p=0.24). The regression coefficient was highest among the inner subfields, which were also the thickest, ranging from -0.22 μm/year at the inner nasal subfield (p<0.001) to -0.14 μm/year at the inner temporal subfield (p<0.001). Outer subfields ranged from -0.14 μm/year at the outer nasal subfield to -0.07 year at the outer temporal subfield (p<0.001).

Figure 4.25. Mean GCL-IPL thickness at subfields, by age. Regression coefficients and p-values are shown. Error bars = 95% confidence interval.

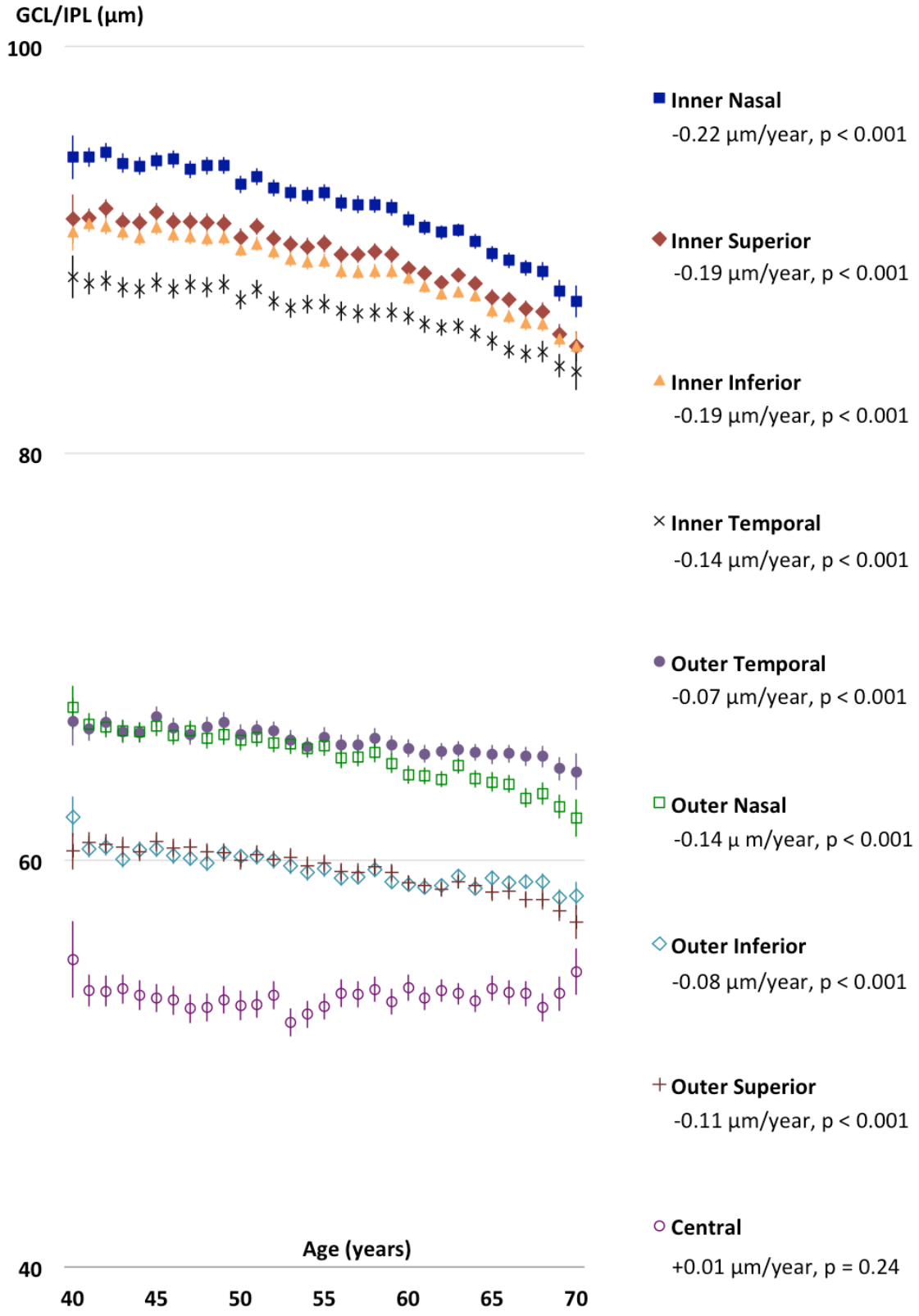

GCL-IPL thickness by ethnicity was examined (Figure 4.26, Table 4.21). Whites, being the largest group, were treated as the reference. The two largest defined ethnic groups, blacks and Asians, were explored first. Ethnicity trends were different between the inner and outer subfields. At the inner subfields, blacks and Asians showed thinner GCL-IPL as compared to whites. The largest difference was visible at the inner nasal subfield, where blacks had -3.45 μm thinner average GCL-IPL ($p<0.001$) as compared to whites, and Asians had -2.28 μm thinner average GCL-IPL ($p<0.001$). In contrast, at outer subfields, blacks had *thicker* average GCL-IPL than whites, ranging from 2.02 μm ($p<0.001$) at the outer inferior subfield to 1.12 μm ($p<0.001$) at the outer superior subfield. Outer temporal subfield showed no significant association when comparing blacks and whites. When considering outer subfields among Asians, only the outer temporal subfield was significant, and showed thinner GCL-IPL than whites (-1.32 μm, $p<0.001$). At the central subfield, both blacks (-7.69 μm, $p<0.001$) and Asians (-3.54 μm, $p<0.001$) had significantly thinner GCL-IPL as compared to whites.

Amongst Chinese people, the only subfield that showed a statistically significant difference at threshold $p<0.001$ was the outer nasal subfield, where GCL-IPL was 3.40 μm thicker as compared to white people. Inner superior, outer inferior, and outer superior subfields were also thicker among Chinese as compared to whites, but did not reach the threshold for considering the difference statistically significant.

In this study population, people of mixed/other ethnicity showed significantly thicker GCL-IPL at outer nasal (1.79 μm), outer inferior (1.66 μm), and outer superior (1.12 μm)

subfields (p<0.001). Outer temporal subfield (0.64 µm as compared to whites, p=0.008) followed this trend, but was not statistically significant. At central subfield, mixed/other ethnicity showed significantly thinner GCL-IPL (-4.98 µm, p<0.001) as compared to whites. Remaining subfields were not statistically significant.

Figure 4.26. Mean GCL-IPL thickness at subfields, by ethnicity. Error bars = 95% confidence interval.

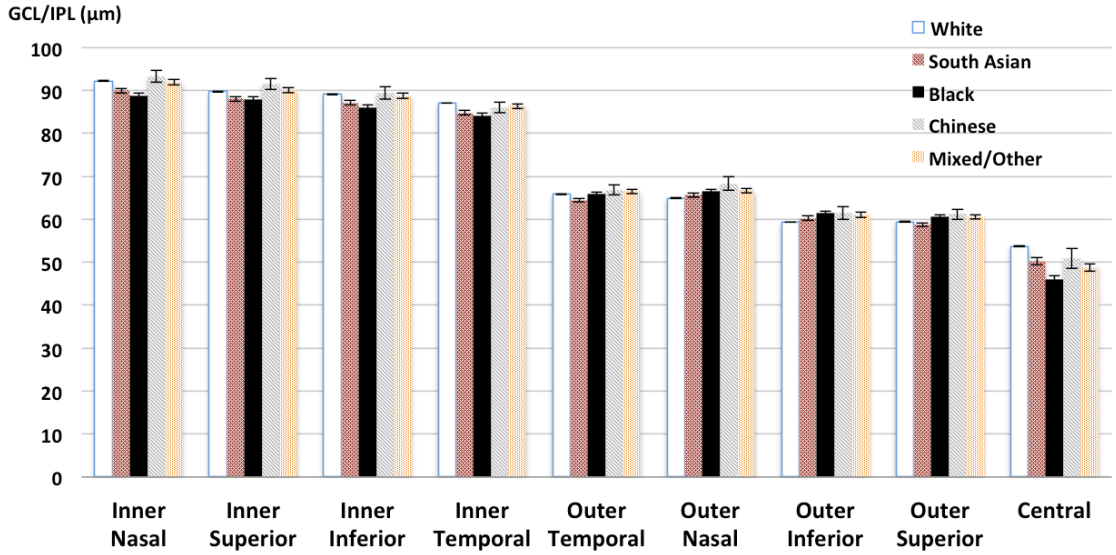

Table 4.21. Linear regression of GCL-IPL thickness at subfields, by ethnicity. Ref. = reference, Coef = coefficient.

	White (ref)	Asian		Black		Chinese		Mixed/Other	
		Coef	P-value	Coef	P-value	Coef	P-value	Coef	P-value
Inner Nasal	92.21	-2.28	<0.001	-3.45	<0.001	1.05	0.15	-0.38	0.25
Inner Superior	89.68	-1.69	<0.001	-1.72	<0.001	1.76	0.006	0.37	0.24
Inner Inferior	89.07	-1.94	<0.001	-3.12	<0.001	0.32	0.67	-0.3	0.37
Inner Temporal	87.02	-2.28	<0.001	-2.88	<0.001	-0.96	0.14	-0.73	0.02
Outer Temporal	65.80	-1.32	<0.001	0.08	0.72	1.01	0.1	0.64	0.008
Outer Nasal	64.87	0.74	0.003	1.70	<0.001	3.40	<0.001	1.79	<0.001
Outer Inferior	59.33	0.87	0.001	2.02	<0.001	2.08	0.007	1.66	<0.001
Outer Superior	59.40	-0.67	0.002	1.12	<0.001	1.75	0.005	1.12	<0.001
Central	53.69	-3.54	<0.001	-7.69	<0.001	-2.78	0.02	-4.98	<0.001

Intraocular pressure showed a small but significant association with GCL-IPL thickness at multiple subfields (Figure 4.27 and Table 4.22). Specifically, for each mmHg of higher intraocular pressure, there was a corresponding associated decrease in GCL-IPL thickness at all subfields except central subfield, and was statistically significant at inner superior (-0.06 µm/mmHg), inner inferior (-0.06 µm/mmHg), outer temporal (-0.09 µm/mmHg), outer nasal (-0.14 µm/mmHg), outer inferior (-0.15 µm/mmHg), and outer superior (-0.12 µm/mmHg) subfields ($p<0.001$). Inner nasal (-0.04 µm/mmHg, $p=0.007$) followed this trend, and approached statistical significance, but did not reach the strict threshold set for this study. Of note, the strongest associations were evident at the outer subfields (-0.12 to -0.09 µm/mmHg), rather than the thicker inner subfields, different from aging, where inner subfields showed more dramatic changes.

Figure 4.27. Mean GCL-IPL thickness at subfields, by intraocular pressure (IOPg – Goldmann equivalent). Error bars = 95% confidence interval.

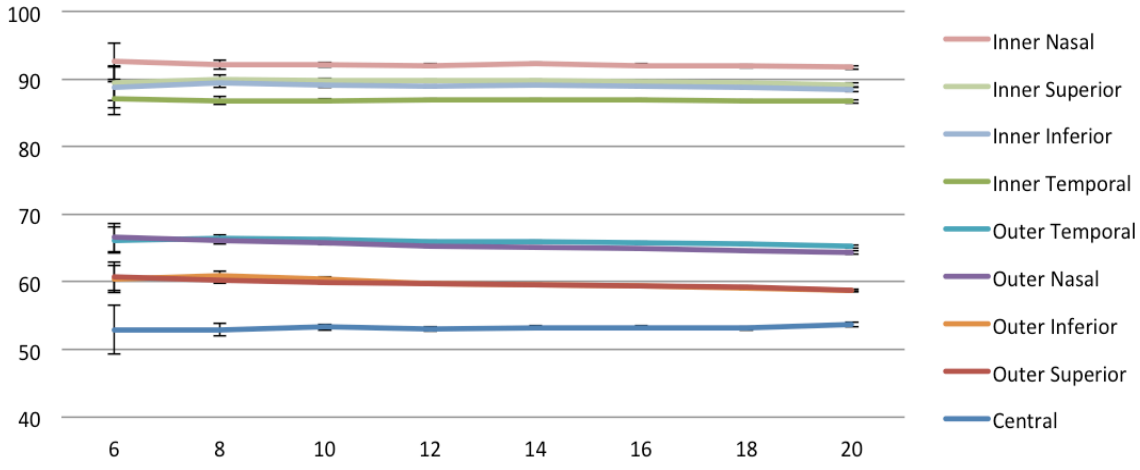

Table 4.22. Linear regression of RNFL thickness at subfields, by intraocular pressure (Goldmann equivalent).

	Constant	Change (per mmHg)	95% Confidence Interval		p-value
Inner Nasal	92.68	-0.04	-0.07	-0.01	0.007
Inner Superior	90.55	-0.06	-0.09	-0.03	<0.001
Inner Inferior	89.79	-0.06	-0.09	-0.03	<0.001
Inner Temporal	87.18	-0.02	-0.05	0.01	0.13
Outer Temporal	67.18	-0.09	-0.12	-0.07	<0.001
Outer Nasal	67.07	-0.14	-0.16	-0.11	<0.001
Outer Inferior	61.76	-0.15	-0.18	-0.13	<0.001
Outer Superior	61.24	-0.12	-0.14	-0.10	<0.001
Central	52.76	0.03	-0.01	0.07	0.13

Refraction was significantly associated with GCL-IPL thickness, and the direction of association varied for inner, outer, and central subfields (Figure 4.28). At inner subfields, only inner superior subfield reached statistical significance (+0.25 µm/diopter, p<0.001), although this may be an oversimplification, as the graph (Figure 4.28) shows greater mean thickness as one moves from myopia to emmetropia, with an inflection point at emmetropia, and thinner again as one moves toward hyperopia. Remaining inner subfields follow this trend, but the trend was not statistically significant.

At outer subfields, there was a positive association with all subfields, ranging from +0.76 µm/diopter at outer superior and temporal subfield, to +0.96 µm/diopter at outer nasal subfield (p<0.001). Outer inferior subfield showed a positive association of +0.94 µm/diopter (p<0.001). In contrast, central subfield showed significant negative association of -0.42 µm/diopter (p<0.001).

Figure 4.28. Mean GCL-IPL thickness at subfields, by spherical equivalent. Error bars = 95% confidence interval. Linear regression performed for all variables.

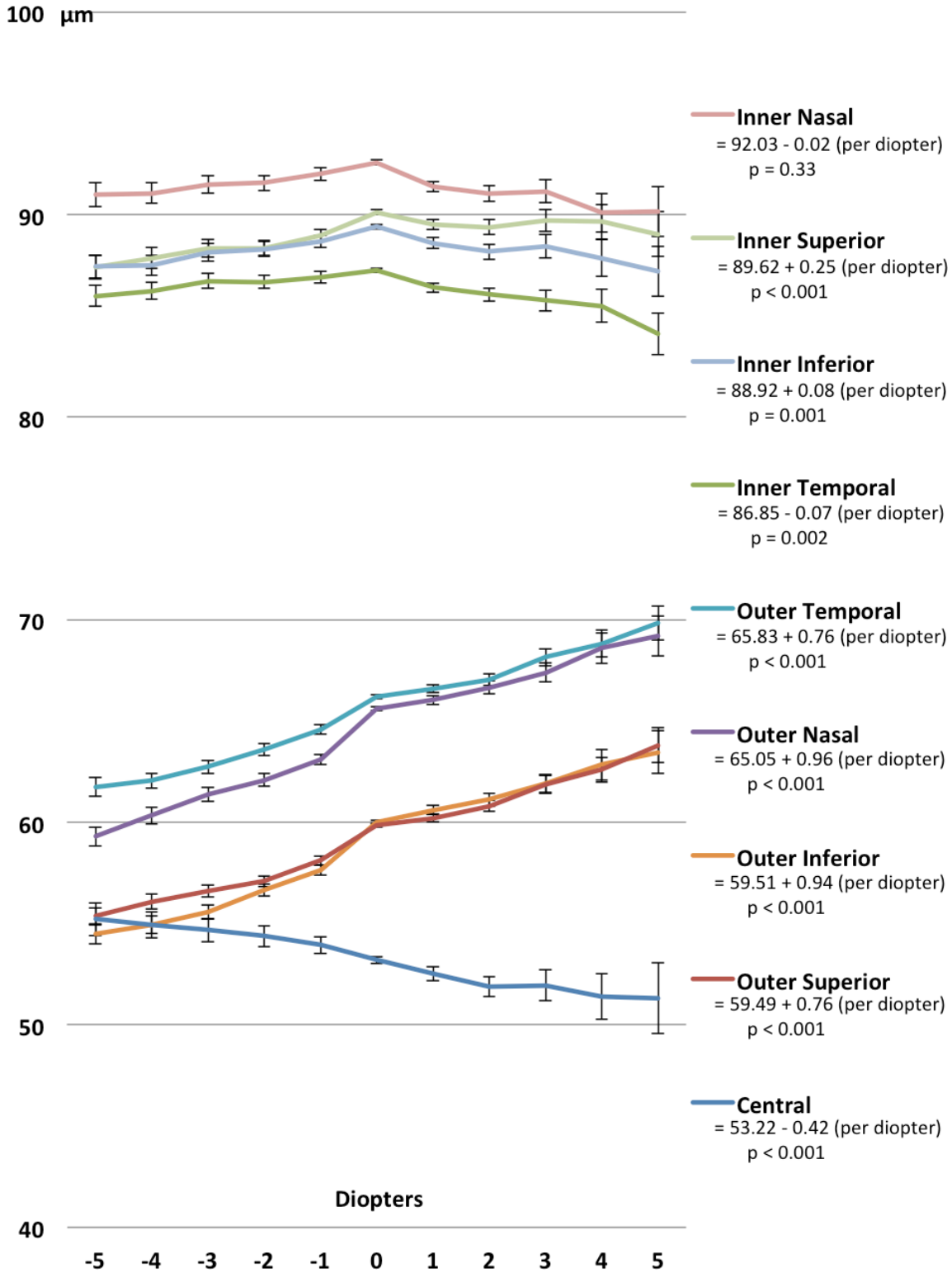

Height was associated with GCL-IPL thickness, with most subfields showing thicker GCL-IPL as mean height increased (Figure 4.29, Table 4.23). The greatest effect was visible at central subfield, with +0.18 µm/cm, followed by inner temporal subfield (+0.14 µm/cm), inner nasal and inner inferior subfields (+0.08 µm/cm for both), inner superior subfield (+0.05 µm/cm), and outer temporal subfield (+0.04 µm/cm) ($p<0.001$). Outer nasal (-0.05 µm/cm) and outer inferior (-0.06 µm/cm) showed thinner GCL-IPL with increased height ($p<0.001$). Outer superior subfield was not significant.

Figure 4.29. Mean GCL-IPL thickness at subfields, by height. Error bars = 95% confidence interval.

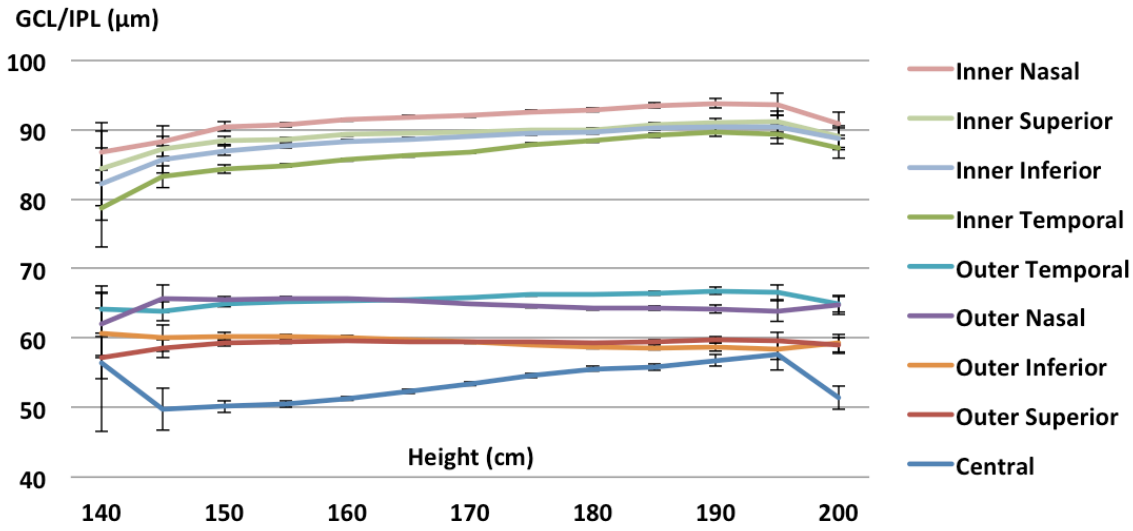

Table 4.23. Linear regression of GCL-IPL thickness at subfields, by height.

	Change (per cm)	95% Confidence Interval		p-value
Inner Nasal	0.08	0.07	0.09	<0.001
Inner Superior	0.05	0.04	0.06	<0.001
Inner Inferior	0.08	0.07	0.09	<0.001
Inner Temporal	0.14	0.13	0.14	<0.001
Outer Temporal	0.04	0.04	0.05	<0.001
Outer Nasal	-0.05	-0.06	-0.04	<0.001
Outer Inferior	-0.06	-0.06	-0.05	<0.001
Outer Superior	0.00	-0.01	0.00	0.54
Central	0.18	0.17	0.19	<0.001

Educational attainment showed statistically significant associations with GCL-IPL thickness, but not necessarily in a specific pattern or dose-related trend (Figure 4.30 and Table 4.24). For instance, being in the lowest category for educational attainment was associated with significantly thinner GCL-IPL as compared to people who attained a college degree (-1.97 µm, p<0.001). This appeared true for most subfields, but there was an exception at outer inferior subfield, which showed thicker GCL-IPL amongst those with lowest education as compared to people with college degrees (+0.47 µm, p<0.001). At the outer temporal and outer superior subfields, the relationship between education and GCL-IPL thickness approached statistical significance but did not reach pre-set threshold, and in the central subfield there was not a statistically significant relationship.

Those with a professional qualification or A-level had significantly thinner GCL-IPL at inner nasal (-0.54 µm, p<0.001) and inner temporal (-0.61 µm, p<0.001) subfields as compared to those with college degrees. Those with O-level qualifications had significantly thinner GCL-IPL at inner temporal subfield (-0.52 µm, p<0.001), but

significantly thicker GCL-IPL at outer nasal subfield (+0.45 µm, p<0.001). In contrast, CSE qualifications were significantly associated with thicker GCL-IPL at outer nasal (+1.05 µm, p<0.01), outer inferior (+0.68 µm, p<0.001), and outer superior (+0.71 µm, p<0.001) subfields. Remaining subfields were not statistically significant.

Figure 4.30. Mean GCL-IPL thickness at subfields, by education level. Inset shows the inner nasal subfield in greater detail. Error bars represent 95% confidence intervals.

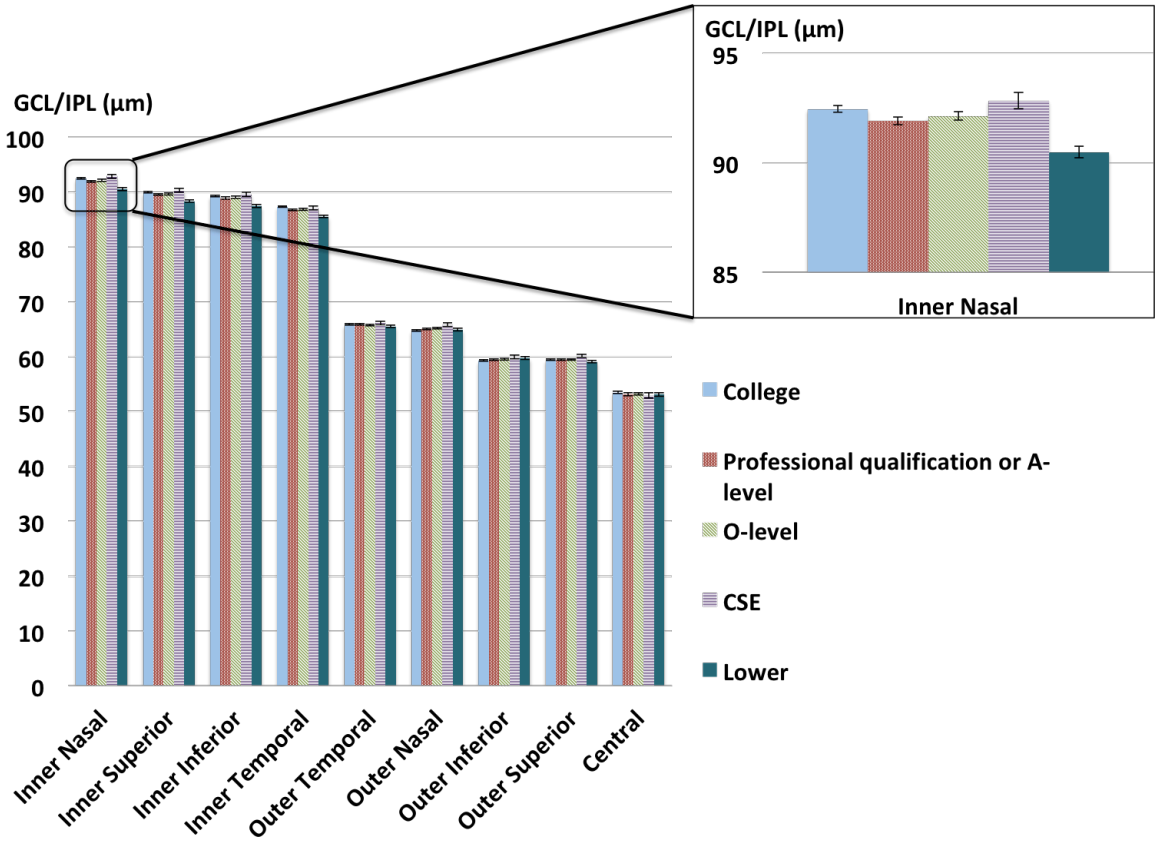

Prof. qual. = Professional or vocational qualification (including higher national diploma)
A-Level = General Certificate of Education Advanced Level, typically taken at age 18
O-Level = General Certificate of Education Ordinary Level, typically taken at age 16
CSE = Certificate of Secondary Education a less demanding exam usually taken at age 16

Table 4.24. Linear regression of GCL-IPL thickness at subfields, by education. REF = reference, coef. = coefficient

	College degree (REF)	Professional qualification or A-level		O-level		CSE		Lower	
		Coef.	P-value	Coef.	P-value	Coef.	P-value	Coef.	P-value
Inner Nasal	92.46	-0.54	<0.001	-0.33	0.008	0.39	0.06	-1.97	<0.001
Inner Superior	89.92	-0.38	0.002	-0.28	0.02	0.34	0.08	-1.56	<0.001
Inner Inferior	89.27	-0.39	0.001	-0.24	0.05	0.29	0.16	-1.82	<0.001
Inner Temporal	87.35	-0.61	<0.001	-0.52	<0.001	-0.28	0.13	-1.80	<0.001
Outer Temporal	65.86	-0.03	0.74	-0.17	0.07	0.24	0.14	-0.35	0.003
Outer Nasal	64.75	0.26	0.02	0.45	<0.001	1.05	<0.001	0.16	0.23
Outer Inferior	59.24	0.19	0.08	0.29	0.01	0.68	<0.001	0.47	<0.001
Outer Superior	59.42	0.03	0.73	0.06	0.5	0.71	<0.001	-0.35	0.002
Central	53.47	-0.37	0.02	-0.26	0.13	-0.55	0.05	-0.35	0.10

Prof. qual. = Professional or vocational qualification (including higher national diploma)
A-Level = General Certificate of Education Advanced Level, typically taken at age 18
O-Level = General Certificate of Education Ordinary Level, typically taken at age 16
CSE = Certificate of Secondary Education, a less demanding exam usually taken at age 16

Socioeconomic deprivation, measured by the Townsend Deprivation Index, was considered together with GCL-IPL thickness (Figure 4.31 and Table 4.25). Significantly thinner GCL-IPL was noted at the inner inferior (-0.66 µm, p<0.001) and inner temporal (-0.65 µm, p<0.001) subfields among those who were most deprived, as compared to those who were least deprived. However, the opposite was found at the outer nasal (+0.45 µm, p<0.001) and outer inferior (+0.58 µm, p<0.001) subfields, with those who were most deprived having significantly thicker GCL-IPL as compared to those who were least deprived.

Figure 4.31. Mean GCL-IPL thickness at subfields, by deprivation index. Inset shows the inner nasal subfield in greater detail. Error bars represent 95% confidence intervals.

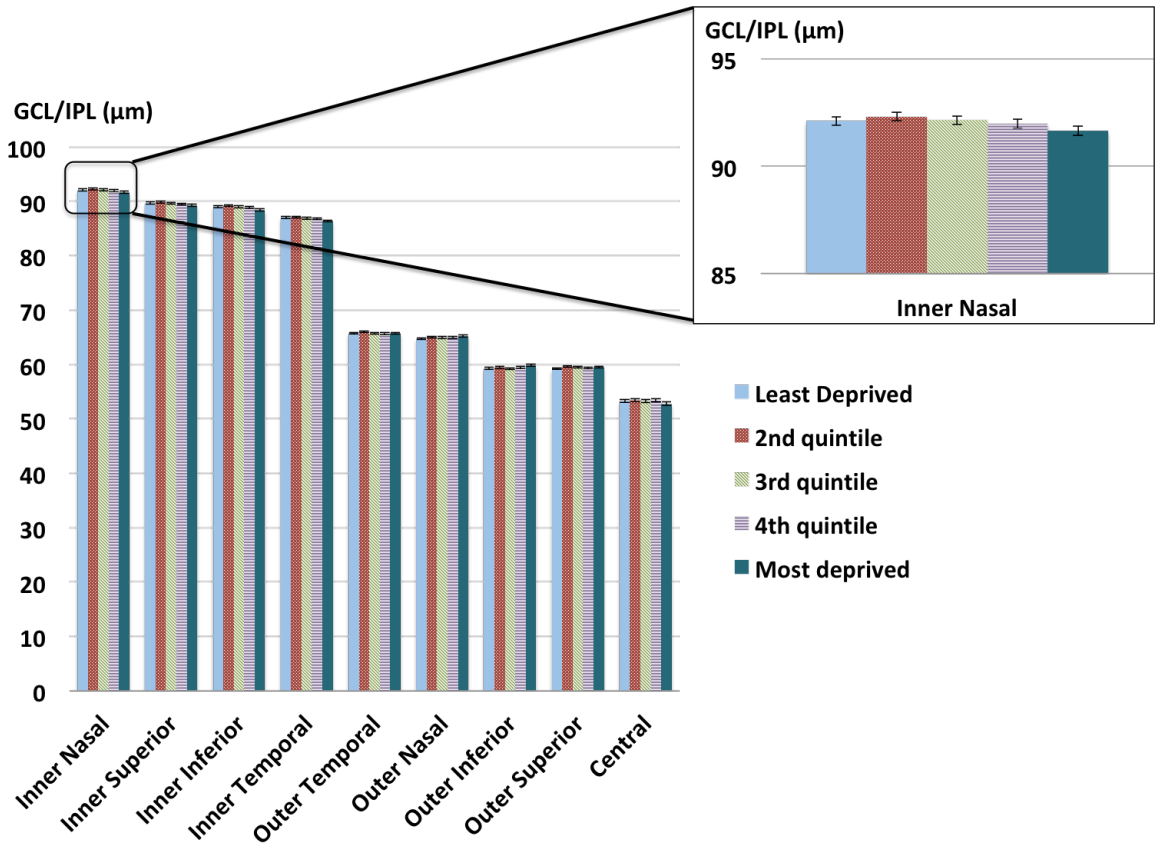

Table 4.25. Linear regression of GCL-IPL thickness at subfields, by deprivation index. REF = reference, coef. = coefficient, P = p-value.

	Least deprived (REF)	2nd quintile		3rd quintile		4th quintile		Most deprived	
		Coef.	P	Coef.	P	Coef.	P	Coef.	P
Inner Nasal	92.1	0.21	0.15	0.04	0.77	-0.13	0.37	-0.46	0.002
Inner Superior	89.68	0.2	0.15	-0.03	0.83	-0.16	0.26	-0.42	0.003
Inner Inferior	89.05	0.16	0.26	-0.03	0.83	-0.15	0.31	-0.66	<0.001
Inner Temporal	87.03	0.09	0.49	-0.13	0.3	-0.19	0.13	-0.65	<0.001
Outer Temporal	65.78	0.25	0.02	-0.05	0.67	-0.13	0.25	-0.06	0.62
Outer Nasal	64.78	0.29	0.02	0.17	0.18	0.19	0.13	0.45	<0.001
Outer Inferior	59.28	0.17	0.17	-0.03	0.79	0.15	0.22	0.58	<0.001
Outer Superior	59.27	0.35	0.001	0.21	0.05	0.08	0.45	0.24	0.02
Central	53.31	0.13	0.49	-0.06	0.74	0.1	0.62	-0.52	0.01

Multivariable regression modeling of GCL-IPL thickness was performed to quantify the impact of all variables

together. This was performed first for inner subfields, which were the thickest, and showed similar trends in single variable analyses (Table 4.26a). At all inner subfields, thinner GCL-IPL was significantly associated with older age (range -0.15 μm/year at inner temporal subfield to -0.24 μm/year at inner nasal subfield, p<0.001), Asian or Black ethnicity as compared to white ethnicity (range for Asians -2.34 μm at inner superior subfield to -3.15 μm at inner nasal subfield; range for Blacks -2.41 μm at inner superior subfield to -4.29 μm at inner nasal subfield; p<0.001), lower refraction (i.e., greater myopia or lower hyperopia) (range 0.11 μm/diopter at inner temporal subfield to 0.48 μm/diopter at inner superior subfield, p<0.001), shorter height (range 0.05 μm/cm at inner nasal, superior, and inferior subfields to 0.08 μm/cm at inner temporal subfield, p<0.001), and greater socioeconomic deprivation (range -0.16 μm per quintile at inner temporal subfield to -0.20 μm per quintile at inner superior and inner inferior subfields, p<0.001). Chinese ethnicity was associated with *thicker* GCL-IPL as compared to whites at inner superior subfield only (2.25 μm, p<0.001). Mixed/other ethnicity was significantly thinner than white ethnicity at inner nasal subfield only (-1.19 μm, p<0.001), but approached significance at inner inferior (-0.98 μm, p=0.004) and inner temporal subfields (-0.88 μm, p=0.003). Lower educational attainment was significantly associated with thinner GCL-IPL at inner superior (-0.13 μm per lower category of attainment, p<0.001), inner inferior (-0.14 μm per lower category of attainment, p<0.001), and inner temporal (-0.17 μm per lower category of attainment, p<0.001) subfields. At the inner nasal subfield, educational attainment approached significance (-0.12 μm per lower category of attainment, p=0.001), but did not reach the pre-set threshold for statistical significance. Women showed significantly thinner GCL-IPL as compared to men at inner temporal subfield only (-1.02 μm, p<0.001), although inner

superior subfield did also approach significance, albeit in the opposite direction (+0.38 µm, p=0.003). Of note, after controlling for other factors, IOP was not significantly associated with GCL-IPL thickness at any of the inner subfields.

Multivariable regression at outer subfields were considered next, as they showed different trends from inner subfields on several of the single variable analyses (Table 4.26b). The variables that showed completely consistent trends between inner and outer subfields were older age and refraction. Older people showed significantly thinner GCL-IPL, ranging from -0.11 µm/year (outer temporal subfield, p<0.001) to -0.19 µm/year (outer nasal subfield, p<0.001). Refraction, measured as spherical equivalent, was positively associated with GCL-IPL thickness; i.e., those with greater myopia had thinner GCL-IPL, and those with higher hyperopia had thicker GCL-IPL (range from +0.89 µm/diopter at outer temporal subfield to +1.12 µm/diopter, p<0.001).

Asian ethnicity showed similar trends within 2 out of 4 outer subfields being significantly thinner compared to whites (-1.23 µm at outer superior subfield, -1.71 µm at outer temporal subfield, p<0.001). Chinese people had thicker GCL-IPL as compared to whites, and this was significant at outer nasal (+3.73 µm, p<0.001) and outer superior (+2.30 µm, p<0.001) subfields. At outer inferior (+2.28 µm, p=0.002) and outer temporal (+1.72 µm, p=0.005), this trend was evident, but did not reach the threshold for statistical significance.

Women had significantly thicker GCL-IPL compared to men at three out of four outer subfields (range +0.42 µm at outer superior subfield to +1.03 µm at outer nasal subfield,

p<0.001); however, at outer temporal subfield, women had significantly thinner GCL-IPL as compared to men (-0.82 µm, p<0.001).

Interestingly, although IOP did not show any significant associations with GCL-IPL thickness at inner subfields, at outer subfields there was a significant association of thinner GCL-IPL with higher IOP, of -0.05 µm/mmHg at outer superior subfield (p<0.001), -0.06 µm/mmHg at outer nasal subfield (p<0.001), and -0.09 µm/mmHg at outer inferior subfield (p<0.001). The association with outer temporal subfield was not statistically significant, but did show a consistent trend (-0.04 µm/mmHg, p = 0.001).

Education (-0.16 µm per category lower in educational attainment, p<0.001) and deprivation (-0.09 µm per quintile of greater deprivation, p<0.001) were significant only at the outer temporal subfield. Height was not a significant factor at outer subfields.

Central subfield GCL-IPL multivariable regression results differed from those of inner and outer subfields (Table 4.26c). Most notably, age was not significant at central subfield, and refraction showed opposite effect at central subfield as compared to other subfields (-0.41 µm/diopter, p<0.001), with higher myopes having thicker GCL-IPL and hyperopes thinner. All ethnicities had thinner GCL-IPL as compared to whites, with the exception of Chinese, in which the association was not significant (regression coefficients for Asians -3.49 µm, blacks -7.67 µm, and mixed/other -4.60 µm as compared to whites, p<0.001). Women showed significantly thinner GCL-IPL as compared to men (regression coefficient -2.82 µm as compared to men, p<0.001). Those who were taller had thicker

GCL-IPL (+0.07 µm/cm, p<0.001). Associations with IOP, education, and deprivation were not significant.

Table 4.26a. Multivariable regression of GCL-IPL thickness at inner subfields.
95% CI = 95% confidence interval, IOP = intraocular pressure.

	Coefficient	95% CI		P-value
Inner Nasal				
Age (per year)	-0.24	-0.26	-0.23	<0.001
Ethnicity (vs. White) Asian	-3.15	-3.70	-2.59	<0.001
Black	-4.29	-4.95	-3.62	<0.001
Chinese	1.16	-0.24	2.57	0.10
Mixed/other	-1.19	-1.83	-0.55	<0.001
Female (vs. Male)	-0.16	-0.42	0.11	0.25
Refraction (per dioptre)	0.22	0.17	0.27	<0.001
IOP (per mmHg)	0.01	-0.02	0.04	0.39
Height (per cm)	0.05	0.03	0.06	<0.001
Education (per category)	-0.12	-0.19	-0.05	0.001
Deprivation index (per quintile)	-0.18	-0.24	-0.12	<0.001
Inner Superior				
Age (per year)	-0.22	-0.23	-0.2	<0.001
Ethnicity (vs. White) Asian	-2.34	-2.89	-1.79	<0.001
Black	-2.41	-3.01	-1.80	<0.001
Chinese	2.25	1.03	3.46	<0.001
Mixed/other	-0.30	-0.91	0.31	0.34
Female (vs. Male)	0.38	0.13	0.64	0.003
Refraction (per dioptre)	0.48	0.43	0.52	<0.001
IOP (per mmHg)	-0.001	-0.03	0.03	0.95
Height (per cm)	0.05	0.04	0.06	<0.001
Education (per category)	-0.13	-0.20	-0.07	<0.001
Deprivation index (per quintile)	-0.20	-0.26	-0.14	<0.001
Inner Inferior				
Age (per year)	-0.21	-0.22	-0.20	<0.001
Ethnicity (vs. White) Asian	-2.60	-3.22	-1.99	<0.001
Black	-3.82	-4.49	-3.15	<0.001
Chinese	0.68	-0.69	2.04	0.33
Mixed/other	-0.98	-1.64	-0.31	0.004
Female (vs. Male)	-0.13	-0.39	0.14	0.36
Refraction (per dioptre)	0.30	0.25	0.35	<0.001
IOP (per mmHg)	-0.01	-0.04	0.02	0.59
Height (per cm)	0.05	0.04	0.07	<0.001
Education (per category)	-0.14	-0.21	-0.07	<0.001
Deprivation index (per quintile)	-0.20	-0.27	-0.14	<0.001

Table 4.26a. (continued)

	Coefficient	95% CI		P-value
Inner Temporal				
Age (per year)	-0.15	-0.16	-0.14	<0.001
Ethnicity (vs. White) Asian	-2.54	-3.08	-2.00	<0.001
Black	-3.20	-3.79	-2.60	<0.001
Chinese	-0.14	-1.39	1.10	0.82
Mixed/other	-0.88	-1.46	-0.29	0.003
Female (vs. Male)	-1.02	-1.25	-0.79	<0.001
Refraction (per dioptre)	0.11	0.07	0.16	<0.001
IOP (per mmHg)	0.01	-0.02	0.04	0.45
Height (per cm)	0.08	0.07	0.10	<0.001
Education (per category)	-0.17	-0.24	-0.11	<0.001
Deprivation index (per quintile)	-0.16	-0.22	-0.10	<0.001

Table 4.26b. Multivariable regression of GCL-IPL thickness at outer subfields.
95% CI = 95% confidence interval, IOP = intraocular pressure.

	Coefficient	95% CI		P-value
Outer Nasal				
Age (per year)	-0.19	-0.19	-0.18	<0.001
Ethnicity (vs. White) Asian	-0.03	-0.5	0.44	0.90
Black	0.81	0.33	1.28	0.001
Chinese	3.73	2.31	5.16	<0.001
Mixed/other	0.80	0.27	1.33	0.003
Female (vs. Male)	1.03	0.82	1.24	<0.001
Refraction (per dioptre)	1.12	1.08	1.16	<0.001
IOP (per mmHg)	-0.06	-0.08	-0.03	<0.001
Height (per cm)	-0.02	-0.03	0.00	0.01
Education (per category)	0.02	-0.04	0.07	0.56
Deprivation index (per quintile)	-0.06	-0.12	-0.01	0.02

Table 4.26b. (continued)

	Coefficient	95% CI		P-value
Outer Superior				
Age (per year)	-0.15	-0.16	-0.14	<0.001
Ethnicity (vs. White) Asian	-1.23	-1.64	-0.82	<0.001
Black	0.44	0.01	0.87	0.05
Chinese	2.30	1.18	3.43	<0.001
Mixed/other	0.48	0.01	0.95	0.05
Female (vs. Male)	0.42	0.24	0.60	<0.001
Refraction (per dioptre)	0.91	0.88	0.94	<0.001
IOP (per mmHg)	-0.05	-0.07	-0.03	<0.001
Height (per cm)	0.01	0.00	0.02	0.03
Education (per category)	-0.08	-0.13	-0.03	0.001
Deprivation index (per quintile)	-0.07	-0.12	-0.03	0.002
Outer Inferior				
Age (per year)	-0.12	-0.13	-0.11	<0.001
Ethnicity (vs. White) Asian	0.37	-0.14	0.89	0.16
Black	1.36	0.85	1.87	<0.001
Chinese	2.28	0.83	3.74	0.002
Mixed/other	0.86	0.29	1.43	0.003
Female (vs. Male)	0.95	0.73	1.17	<0.001
Refraction (per dioptre)	1.04	1.00	1.08	<0.001
IOP (per mmHg)	-0.09	-0.11	-0.06	<0.001
Height (per cm)	-0.02	-0.03	0.00	0.009
Education (per category)	-0.01	-0.07	0.05	0.74
Deprivation index (per quintile)	0.002	-0.05	0.06	0.94
Outer Temporal				
Age (per year)	-0.11	-0.12	-0.1	<0.001
Ethnicity (vs. White) Asian	-1.71	-2.14	-1.27	<0.001
Black	-0.27	-0.74	0.20	0.25
Chinese	1.72	0.52	2.92	0.005
Mixed/other	0.28	-0.20	0.76	0.25
Female (vs. Male)	-0.82	-1.02	-0.63	<0.001
Refraction (per dioptre)	0.89	0.85	0.92	<0.001
IOP (per mmHg)	-0.04	-0.06	-0.02	0.001
Height (per cm)	0.01	0.002	0.02	0.02
Education (per category)	-0.16	-0.21	-0.11	<0.001
Deprivation index (per quintile)	-0.09	-0.14	-0.04	<0.001

Table 4.26c. Multivariable regression of GCL-IPL thickness at central subfields.
95% CI = 95% confidence interval, IOP = intraocular pressure.

	Coefficient	95% CI		p-value
Central				
Age (per year)	0.00	-0.01	0.02	0.78
Ethnicity (vs. White) Asian	-3.49	-4.36	-2.61	<0.001
Black	-7.67	-8.57	-6.77	<0.001
Chinese	-2.15	-4.55	0.24	0.08
Mixed/other	-4.60	-5.44	-3.76	<0.001
Female (vs. Male)	-2.82	-3.17	-2.47	<0.001
Refraction (per dioptre)	-0.41	-0.47	-0.34	<0.001
IOP (per mmHg)	-0.01	-0.05	0.03	0.69
Height (per cm)	0.07	0.05	0.09	<0.001
Education (per category)	0.02	-0.07	0.12	0.61
Deprivation index (per quintile)	0.13	0.05	0.22	0.003

4.4 Retinal Nerve Fibre Layer

4.4.1 Contributors

Paul Foster was central to designing the eye portion of UK Biobank. Paul Foster, Praveen Patel, and Nick Strouthidis provided guidance when planning the analysis. Qi Yang and Charles Reisman performed automated segmentation of OCT images. After automated segmentation of images were performed, I reviewed data to evaluate for outliers, and recommended images to Qi Yang for manual re-grading. These variables were then analyzed by me. Paul Foster, Praveen Patel, Peng Khaw were involved in suggestions for improved approach to analysis as the work evolved. Paul Foster, Peng Khaw, Praveen Patel, Nick Strouthidis, Qi Yang, Charles Reisman, Anthony Khawaja, David Garway-Heath, James Morgan, Yusrah Shweikh, and Zaynah Muthy were helpful during review and editing phase. Although there were many collaborators in this work, to whom I am grateful, the analysis and writing was performed entirely by me.

4.4.2 Results

33,068 high-quality OCT images from 16,416 right eyes and 16,652 left eyes from people without self-reported ocular disorders, diabetes, or neurodegenerative diseases were included for analysis (Figure 4.32). Participants included in the study are described in Table 4.27. Mean age was 56.0 years (95% CI 55.9-56.1%, SD 8.2). There were more women (53.5%) than men. The majority of participants were white (91.8%); however,

the number of participants from different ethnicities was sufficiently high to perform statistical testing, and included 123 Chinese, 857 Asians, 946 blacks, and 761 mixed/other. Mean visual acuity was LogMar -0.04 (SD 0.16) and mean refraction was -0.06 D (SD 1.91). Mean IOP was 15.0 mmHg (95% CI 15.01-15.07, SD 3.0).

Figure 4.32. Inclusion/exclusion criteria for macular RNFL SDOCT.

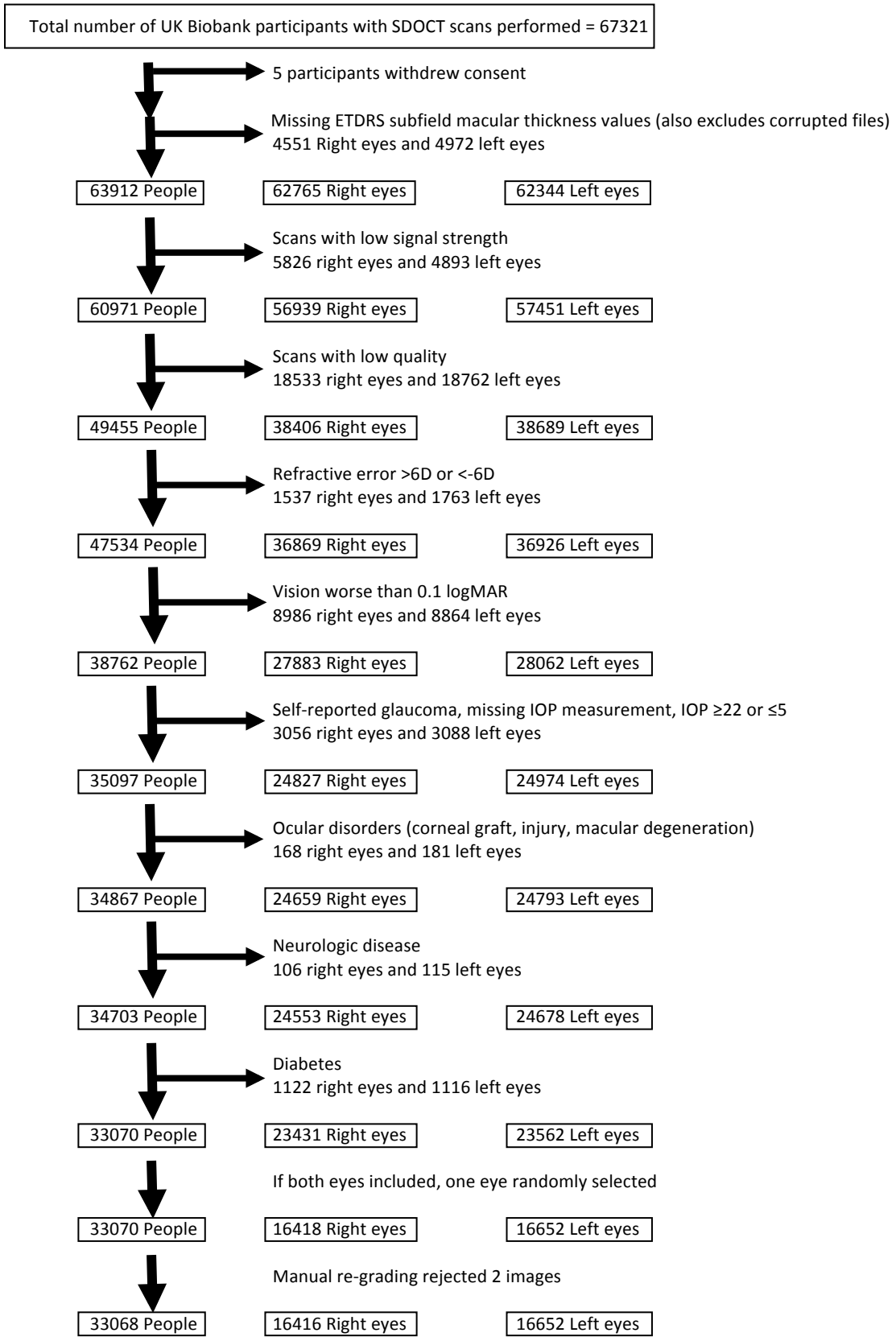

Table 4.27. Basic demographics for those included in RNFL analysis.

	Estimate (95% CI)	
*** Age (mean years)**	56.0 (55.9 – 56.1)	SD = 8.2
+ Female Sex	53.5 (53.0 – 54.1)%	
+ Ethnicity		
White	91.8 (91.5 – 92.1)%	
Chinese	0.4 (0.3 – 0.4)%	
Asian	2.6 (2.4 – 2.8)%	
Black	2.9 (2.7 – 3.1)%	
Mixed/Other	2.3 (2.2 – 2.5)%	
+ Laterality = Right eye	49.6 (49.1 – 50.2)%	
*** Visual acuity (logMAR)**	-0.04 (-0.042 – -0.039)	SD = 0.16
*** Refraction**	-0.06 (-0.08 – -0.04)	SD = 1.91
*** IOP_G**	15.0 (15.01 – 15.07)	SD = 3.0

* mean (95% confidence interval)
+ percentage (95% confidence interval)
SD = standard deviation
IOP_G (Goldmann equivalent) was measured using the Reichert Ocular Response Analyser

mRNFL thickness at each subfield is shown in Figure 4.33. The central subfield was thinnest at 8.3 µm (SD 4.2) and the outer nasal was thickest at 53.3 µm (SD 9.0). Superior and inferior subfields were of intermediate thickness, with outer subfields being thicker than inner subfields. There was a slight right skew toward higher RNFL thickness (figures 4.33a-b). Women and men had different distribution of mRNFL thicknesses (figures 4.33d-e), with women showing greater thickness at outer subfields, and men showing greater thickness at inner and central subfields ($p<0.001$ at all subfields except inner superior subfield).

Figure 4.33a-b. Histogram of macular RNFL thickness at A) central and B) outer nasal subfields. Central subfield mean = 8.26 µm, standard error = 0.02 µm, standard deviation = 4.20 µm. Outer nasal subfield mean = 53.28 µm, standard error = 0.05 µm, standard deviation = 8.90 µm.

a) **b)**

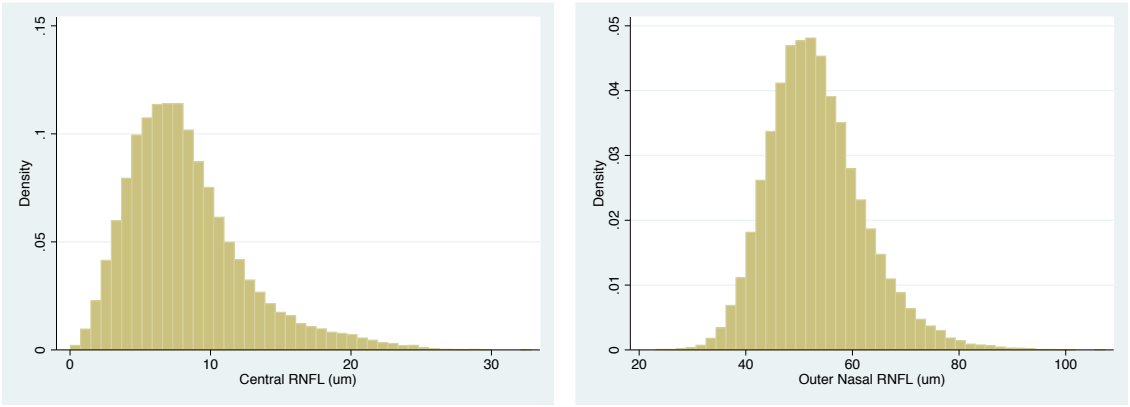

Figure 4.33c. Macular RNFL thickness at different subfields. Mean (µm) ± standard deviation.

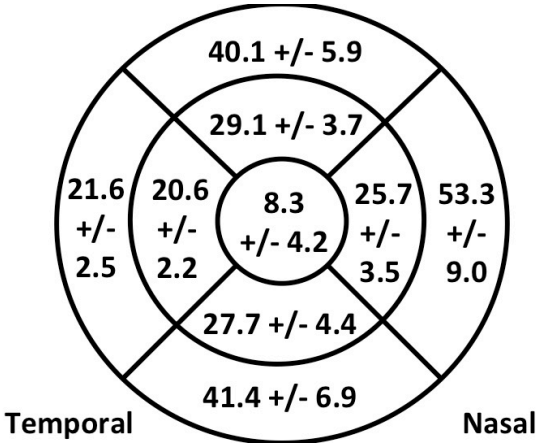

Figure 4.33d-e. Macular RNFL thickness in D) women and E) men, at different subfields. Mean (µm) ± standard deviation. T-test of women versus men, p<0.001 at all subfields except inner superior (p=0.36).

d) **e)**

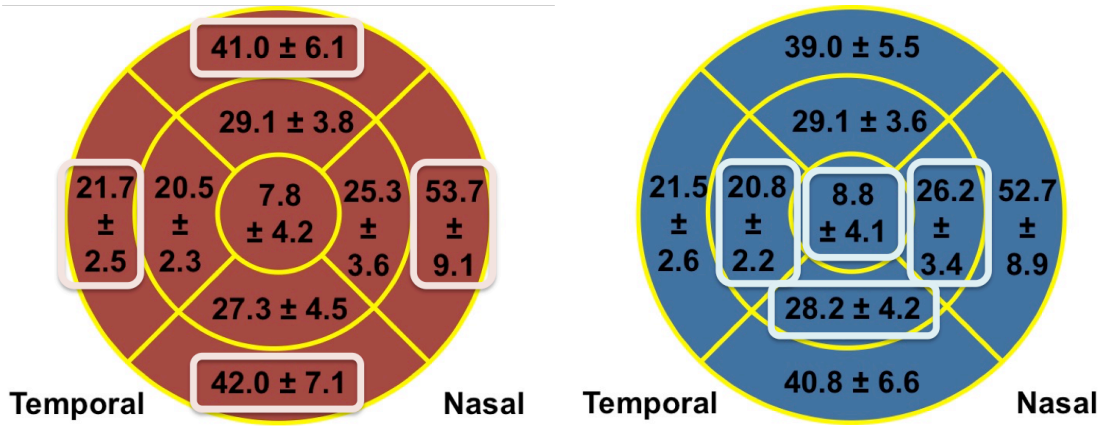

Regression analyses were performed to determine potential associations with mRNFL thickness with individual variables, including age, ethnicity, IOP, refraction, height, education, and Townsend deprivation index. There was significant association between thinner mRNFL and older age, with the most obvious being the outer nasal subfield, decreasing 0.12 µm per year (95% CI -0.13 – -0.11 µm per year, $p<0.001$) (figure 4.34). This relationship was consistent for all subfields except central subfield, which showed a positive association of +0.02 µm per year (95% CI 0.01 – 0.02 µm per year, $p<0.001$).

Figure 4.34. Mean RNFL thickness at subfields, by age. Regression coefficients and p-values are shown. Error bars = 95% confidence interval.

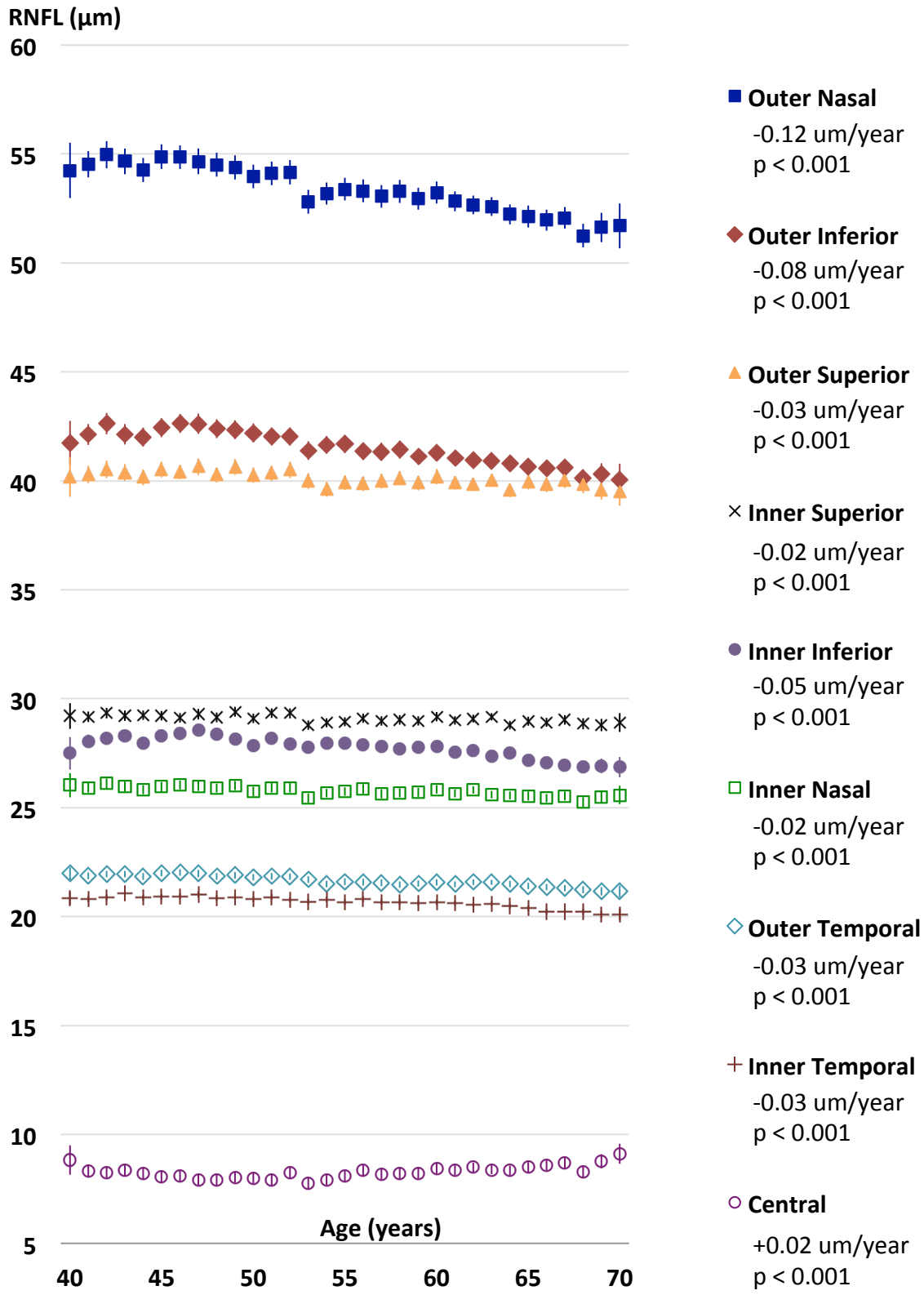

As compared to whites, black people had significantly thinner mRNFL in all subfields, and Asians were thinner in most subfields (Figure 4.35 and Table 4.28). Chinese and mixed/other ethnicities showed mixed results, with thinner RNFL at some subfields and thicker RNFL at other subfields, with no clear pattern or trend.

Figure 4.35. Mean RNFL thickness at subfields, by ethnicity. Error bars = 95% confidence interval.

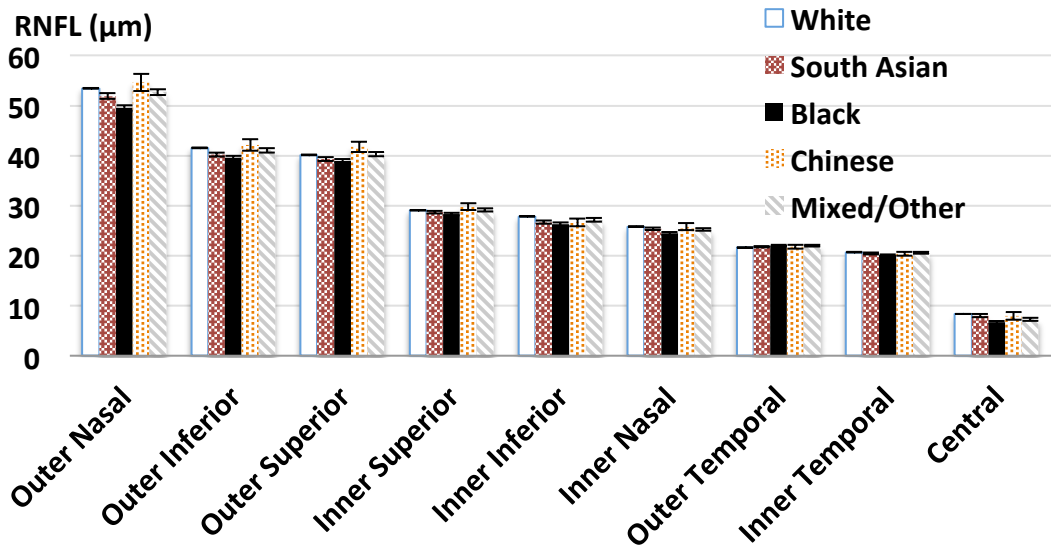

Table 4.28. Linear regression of RNFL thickness at subfields, by ethnicity. Ref = reference, Coef = coefficient, P = P-value.

	White (ref)	Asian		Black		Chinese		Mixed/Other	
		Coef.	P	Coef.	P	Coef.	P	Coef.	P
Outer Nasal	53.45	-1.53	-3.93	-3.93	<0.001	1.18	0.17	-0.74	0.02
Outer Inferior	41.55	-1.35	-1.98	-1.98	<0.001	0.56	0.35	-0.46	0.06
Outer Superior	40.12	-0.81	-1.13	-1.13	<0.001	1.62	0.002	0.17	0.41
Inner Superior	29.10	-0.44	-0.77	-0.77	<0.001	0.68	0.04	0.02	0.88
Inner Inferior	27.83	-1.15	-1.51	-1.51	<0.001	-1.20	0.002	-0.68	<0.001
Inner Nasal	25.79	-0.42	-1.38	-1.38	<0.001	-0.01	0.98	-0.54	<0.001
Outer Temporal	21.60	0.20	0.47	0.47	<0.001	0.19	0.37	0.41	<0.001
Inner Temporal	20.68	-0.27	-0.58	-0.58	<0.001	-0.29	0.16	-0.11	0.21
Central	8.35	-0.35	-1.68	-1.68	<0.001	-0.37	0.36	-1.08	<0.001

Ocular factors considered included IOP and refraction. No association was identified between mRNFL thickness and IOP_G (Figure 4.36). In fact, regression analysis showed 0.0 µm change for multiple subfields (Table 4.29), including outer inferior, outer superior, and central subfields (p-values 0.89, 0.69, and 0.73, respectively). The outer nasal subfield, which previously showed the most obvious thinness with age and ethnicity, showed a slight positive association with IOP_G (0.04 µm per mmHg, 95% CI 0.01 – 0.08, p=0.01). Inner inferior (0.02 µm per mmHg, 95% CI 0.01 – 0.04, p=0.004) and inner nasal (0.02 µm per mmHg, 95% CI 0.01 – 0.03, p=0.005) subfields also showed slight positive associations. There was a slight negative association at outer temporal (-0.04 µm per mmHg, 95% CI -0.05 – -0.03, p<0.001) and inner temporal (-0.01 µm per mmHg, 95% CI -0.02 – 0.00, p=0.01) subfields.

Figure 4.36. Mean RNFL thickness at subfields, by intraocular pressure (Goldmann-corrected). Error bars = 95% confidence interval.

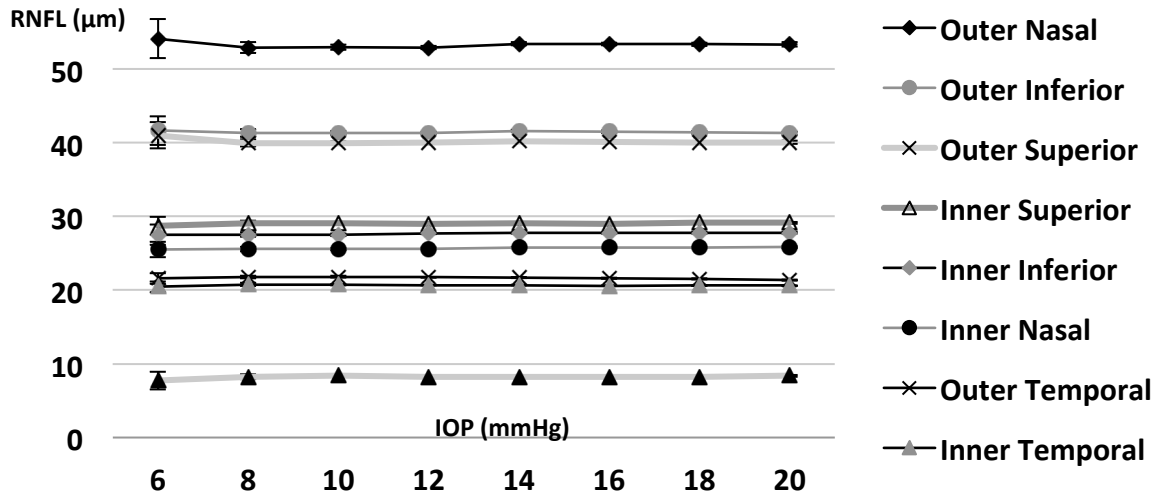

Table 4.29. Linear regression of RNFL thickness at subfields, by intraocular pressure (Goldmann-corrected).

	Constant	Change (per mmHg)	95% Confidence Interval		p-value
Outer Nasal	52.62	0.04	0.01	0.08	0.01
Outer Inferior	41.47	0.00	-0.03	0.02	0.89
Outer Superior	40.01	0.00	-0.02	0.03	0.69
Inner Superior	28.99	0.01	-0.01	0.02	0.43
Inner Inferior	27.38	0.02	0.01	0.04	0.004
Inner Nasal	25.45	0.02	0.01	0.03	0.005
Outer Temporal	22.25	-0.04	-0.05	-0.03	<0.001
Inner Temporal	20.82	-0.01	-0.02	0.00	0.01
Central	8.22	0.00	-0.01	0.02	0.73

In contrast, refraction was significantly associated with mRNFL thickness, with thicker mRNFL for each diopter of myopia and thinner mRNFL for each diopter of hyperopia (Figure 4.37). The most dramatic association was at the outer nasal subfield, which showed 1.33 µm change per diopter refraction (95% CI -1.38 – -1.28, p<0.001). The one exception was the outer temporal subfield, which was thicker among hyperopes.

Figure 4.37. Mean RNFL thickness at subfields, by refraction. Error bars = 95% confidence interval. Linear regression performed for all variables.

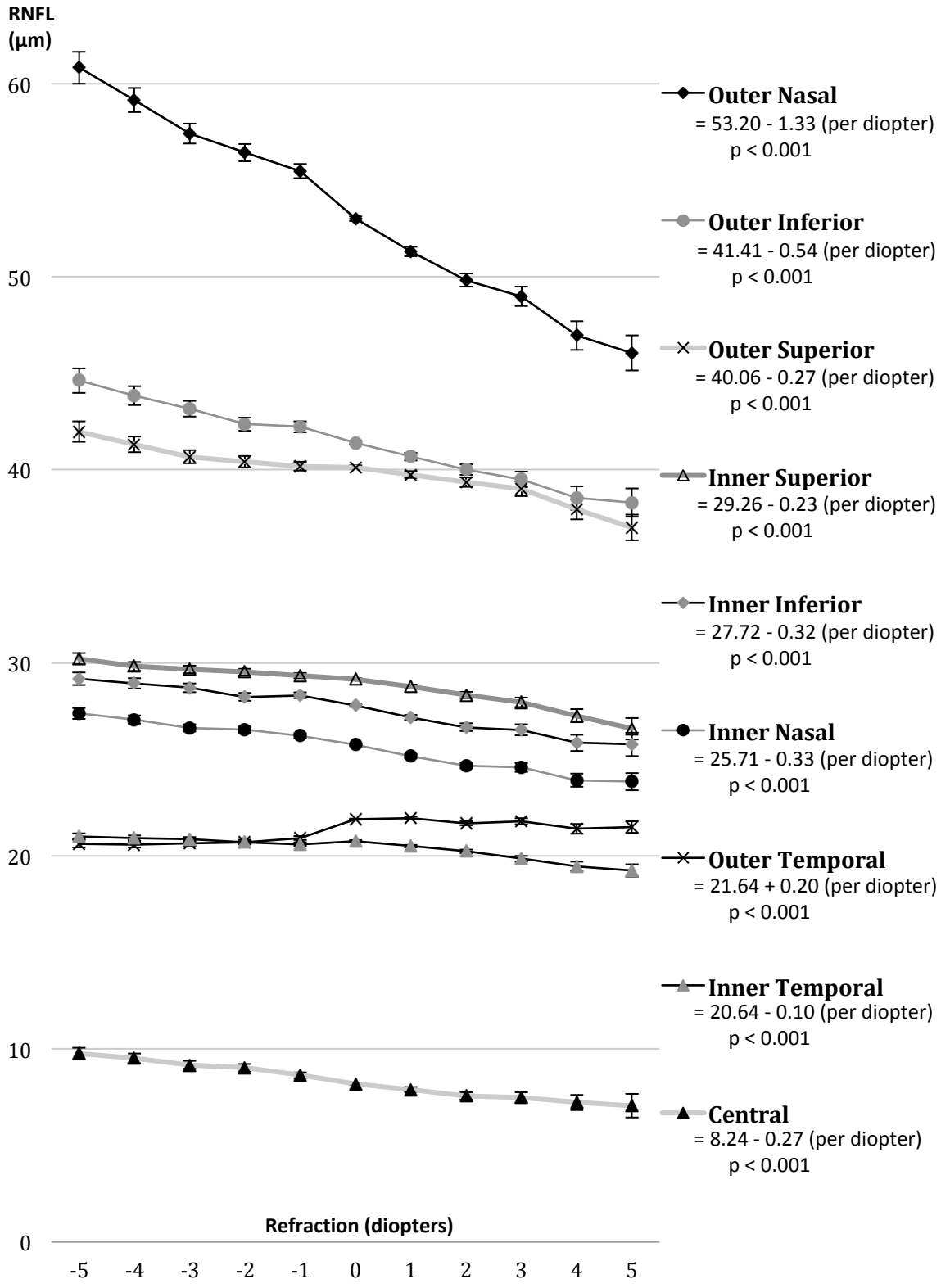

Height, a potential confounder with sex and refractive error, was considered as well (Figure 4.38 and Table 4.30). For most subfields, there was a small positive association, ranging from 0.01 to 0.06 µm per cm (Table 4.30). The exceptions were the outer superior subfield where there was a small but statistically significant association of -0.05 µm per cm. (95% CI -0.06 – -0.04, p<0.001), and outer inferior and outer temporal subfields, which were not significant.

Figure 4.38. Mean RNFL thickness at subfields, by height. Error bars = 95% confidence interval.

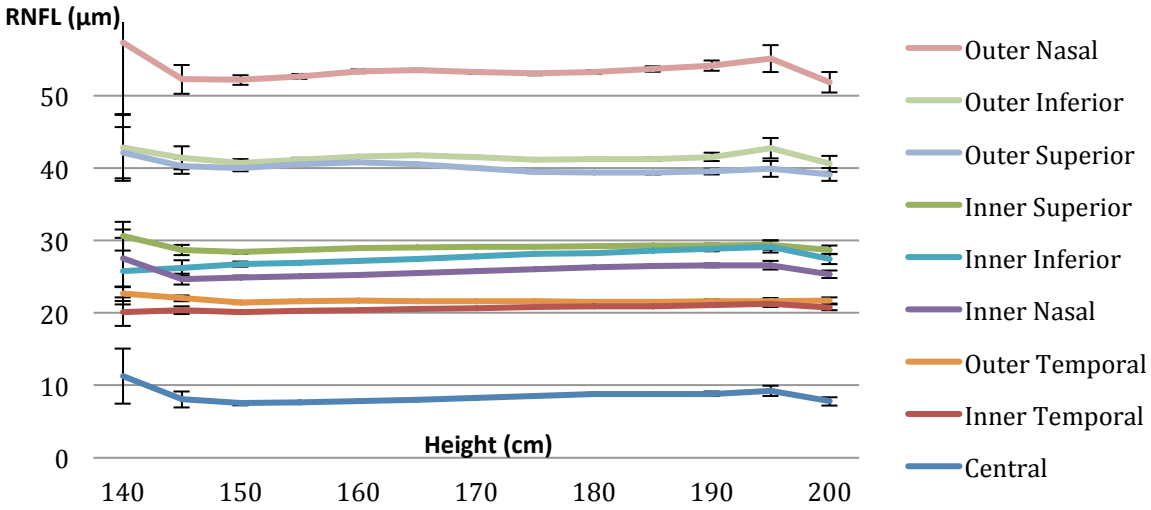

Table 4.30. Linear regression of RNFL thickness at subfields, by height.

	Change (per cm)	95% Confidence Interval		p-value
Outer Nasal	0.01	0.00	0.03	0.01
Outer Inferior	-0.01	-0.02	0.00	0.05
Outer Superior	-0.05	-0.06	-0.04	<0.001
Inner Superior	0.02	0.01	0.02	<0.001
Inner Inferior	0.06	0.05	0.06	<0.001
Inner Nasal	0.05	0.04	0.05	<0.001
Outer Temporal	0.00	-0.01	0.00	0.05
Inner Temporal	0.02	0.02	0.03	<0.001
Central	0.04	0.03	0.04	<0.001

Given the recorded associations between mRNFL and cognitive function, education and Townsend deprivation index (Figure 4.39) were included in multivariate analysis. Those with lower educational attainment (less than O-level) had significantly thinner mRNFL in all subfields, except the two thinnest subfields (inner temporal and central). The most dramatic finding was at the outer nasal subfield, which showed 0.65 µm thinner mRNFL for each category lower in educational attainment (95% CI -0.72 – -0.58, p<0.001). Townsend deprivation index, a measure of later life socioeconomic relative deprivation, showed a trend toward greater deprivation and thinner mRNFL, though the findings were not as large as educational attainment and was not statistically significant (Figure 4.39). At the outer nasal subfield, those with greater deprivation had 0.11 µm thinner mRNFL per quintile worse deprivation (95% CI -18 – -0.05 µm, p=0.002).

Figure 4.39. Mean RNFL thickness. Inset shows the outer nasal subfield in greater detail. A) mRNFL thickness and education (Regression at outer nasal subfield of -0.65 um per category lower education, 95% CI -0.72 - -0.58, p<0.001) and B) mRNFL thickness and Townsend deprivation index, a measure of socioeconomic deprivation (Regression at outer nasal subfield of -0.11 um per quintile of worsened deprivation, 95% CI -0.18 - -0.04, p=0.002). Error bars represent 95% confidence intervals.

A)

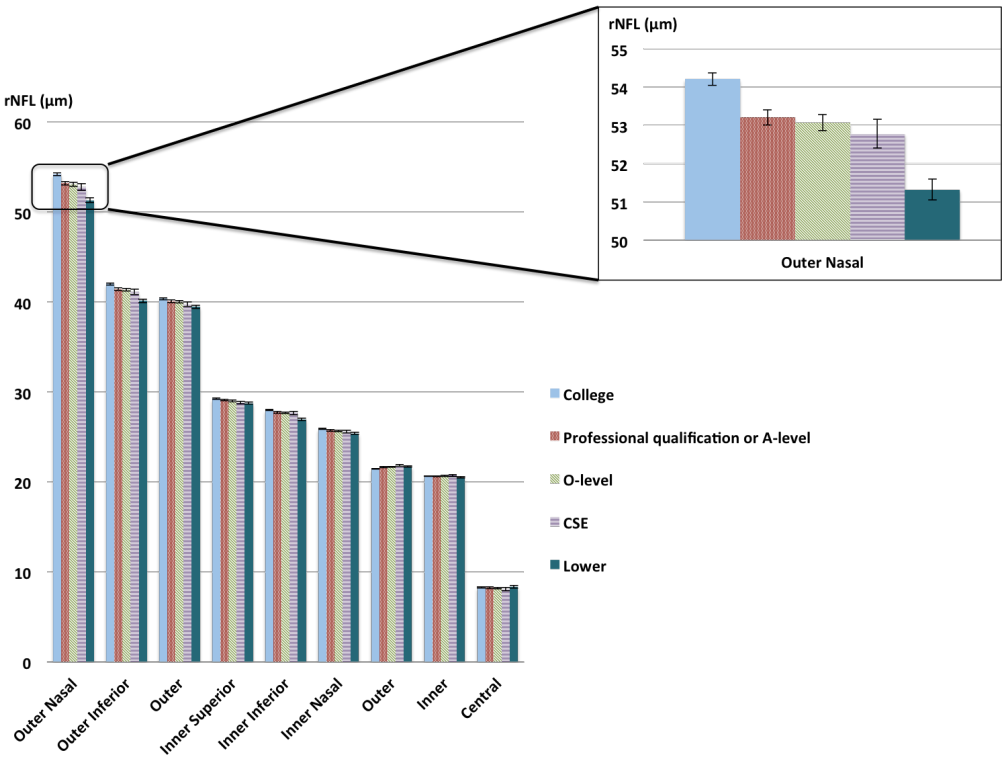

B)

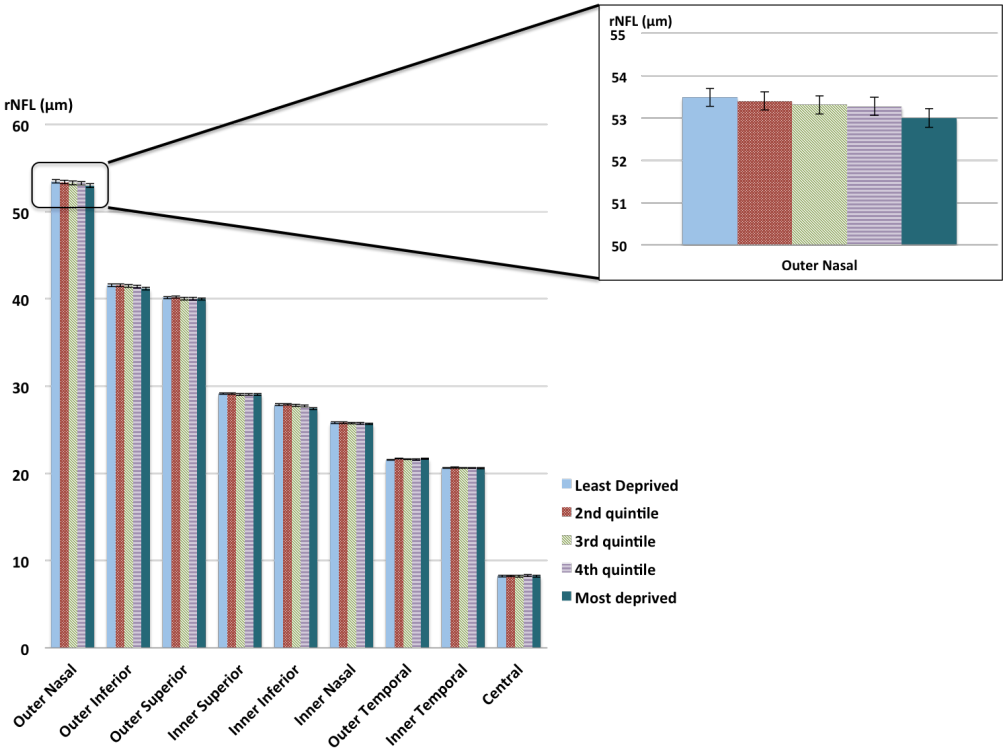

To quantify the relative impact of all variables together, multivariable regression modeling was performed for mRNFL thickness at outer nasal, outer inferior, outer superior, and central subfields (Table 4.31). The first three subfields were the ones with thickest mRNFL and largest trends in single variable analysis, whereas central subfield had thinnest mRNFL. Outer nasal subfield showed significantly thinner mRNFL in older age (-0.06 µm per year, 95% CI -0.07 – -0.05, p<0.001); Asian (-1.79 µm, 95% CI -2.36 – -1.22, p<0.001), black (-3.97 µm, 95% CI -4.54 – -3.40, p<0.001), or mixed/other (-0.78 µm, 95% CI -1.41 – -0.15, p=0.01) ethnicities compared with whites; higher hypermetropia (or lower myopia) (-1.23 µm per diopter, 95% CI -1.29 - -1.18, p<0.001); lower education attainment (-0.28 µm per category lower education, 95% CI -0.35 – -0.21, p<0.001); and greater socioeconomic deprivation (-0.08 µm, 95% CI -0.15 – -0.01, p=0.02). In contrast, women had a thicker RNFL than men (1.82 µm, 95% CI 1.55 – 2.09, p<0.001), including controlling for height (0.05 µm per cm (95% CI 0.04 – 0.07, p<0.001). There was no significant association between outer nasal macular RNFL thickness and Chinese ethnicity or intraocular pressure. Outer inferior and outer superior subfield regression modeling showed consistent results with those described above for the outer nasal subfield, with the exception of Chinese ethnicity (1.35 µm as compared to whites, 95% CI 0.30 – 2.39, p=0.01), which showed a significant positive association with outer superior RNFL. Central subfield RNFL multivariable regression modeling showed positive association with older age (0.03 µm per year, 95% CI 0.02 – 0.03, p<0.001), lower education (0.05 µm, 95% CI 0.02 – 0.09, p=0.02), and greater socioeconomic deprivation (0.07 µm, 95% CI 0.03 – 0.10, p=0.002); and negative association with female sex (-0.78 µm compared to men, 95% CI -0.91 – -0.65, p<0.001), black or mixed/other ethnicities (-1.50 µm and -0.99 µm compared to whites, 95% CI -1.81 – -1.19 and -1.29 – -0.69,

respectively, p<0.001), and higher refractive error (-0.30 µm per diopter, 95% CI -0.32 – -0.27, p<0.001). There was no significant association with Chinese or Asian ethnicity, or height. For all subfields, there was no significant association with intraocular pressure (IOP_G).

Table 4.31. Multivariable regression of RNFL thickness at select subfields.
95% CI = 95% confidence interval, IOP_G = Goldmann-corrected intraocular pressure.

		Coefficient	95% CI		P-value
Outer Nasal					
Age (per year)		-0.06	-0.07	-0.05	<0.001
Female (vs. Male)		1.82	1.55	2.09	<0.001
Ethnicity (vs. White)	**Asian**	-1.79	-2.36	-1.22	<0.001
	Black	-3.97	-4.55	-3.40	<0.001
	Chinese	-0.02	-1.66	1.62	0.98
	Mixed/other	-0.78	-1.41	-0.15	0.02
Refraction (per dioptre)		-1.23	-1.29	-1.18	<0.001
IOP_G (per mmHg)		0.03	0.00	0.06	0.08
Height (per cm)		0.05	0.04	0.07	<0.001
Education (per category)		-0.28	-0.35	-0.21	<0.001
Deprivation index (per quintile)		-0.08	-0.15	-0.01	0.02
Outer Inferior					
Age (per year)		-0.06	-0.07	-0.05	<0.001
Female (vs. Male)		1.86	1.64	2.07	<0.001
Ethnicity (vs. White)	**Asian**	-1.42	-1.84	-1.00	<0.001
	Black	-2.05	-2.47	-1.64	<0.001
	Chinese	0.06	-1.11	1.22	0.93
	Mixed/other	-0.57	-1.05	-0.08	0.02
Refraction (per dioptre)		-0.47	-0.51	-0.43	<0.001
IOP_G (per mmHg)		0.00	-0.02	0.03	0.76
Height (per cm)		0.04	0.03	0.06	<0.001
Education (per category)		-0.25	-0.3	-0.19	<0.001
Deprivation index (per quintile)		-0.09	-0.14	-0.04	0.001
Outer Superior					
Age (per year)		-0.01	-0.02	0.00	0.06
Female (vs. Male)		2.53	2.34	2.71	<0.001
Ethnicity (vs. White)	**Asian**	-0.58	-0.98	-0.19	0.004
	Black	-0.97	-1.34	-0.59	<0.001
	Chinese	1.35	0.30	2.39	0.01
	Mixed/other	0.15	-0.26	0.57	0.48
Refraction (per dioptre)		-0.24	-0.27	-0.20	<0.001
IOP_G (per mmHg)		0.01	-0.02	0.03	0.56
Height (per cm)		0.04	0.03	0.05	<0.001
Education (per category)		-0.13	-0.18	-0.08	<0.001
Deprivation index (per quintile)		-0.04	-0.09	0.00	0.07

Table 4.31. (continued)

		Coefficient	95% CI		P-value
Central					
Age (per year)		0.03	0.02	0.03	<0.001
Female (vs. Male)		-0.78	-0.91	-0.65	<0.001
Ethnicity (vs. White)	**Asian**	-0.32	-0.63	-0.01	0.05
	Black	-1.50	-1.81	-1.19	<0.001
	Chinese	-0.32	-1.14	0.49	0.44
	Mixed/other	-0.99	-1.29	-0.69	<0.001
Refraction (per dioptre)		-0.30	-0.32	-0.27	<0.001
IOP_G (per mmHg)		-0.01	-0.03	0.00	0.07
Height (per cm)		0.01	0.00	0.02	0.003
Education (per category)		0.05	0.02	0.09	0.004
Deprivation index (per quintile)		0.07	0.03	0.10	<0.001

4.5 Cognitive Function, Ganglion Cell Layer-Inner Plexiform Layer Complex, and Retinal Nerve Fibre Layer

4.5.1 Contributors to Study of Cognitive Function

Paul Foster, Praveen Patel, and John Gallacher were involved during design phase of the study. Qi Yang and Charles Reisman performed automated segmentation and manual review of OCT images. All analyses were performed by me, with suggestions from Paul Foster and Cathie Sudlow to improve statistical methodology. John Gallacher provided significant expertise in understanding cognitive function. Zaynah Muthy assisted in literature search. Paul Foster, Cathie Sudlow, John Gallacher, Peng Khaw, Praveen Patel, Nick Strouthidis, Qi Yang, Charles Reisman, Geraint Rees, Pearse Keane, Axel Petzold, and Zaynah Muthy were helpful during review and editing phase. Although I performed all analyses and writing, my collaborators elevated the quality of this work to the level you see here, and I am grateful for their contributions.

4.5.2 Results

4.5.2.1 GCL-IPL and Cognitive Function

To test for potential link between inner retinal layers and cognitive function, GCL-IPL and RNFL thickness were examined together with cognitive function tests. The first section will focus on GCL-IPL. RNFL results are shown in the next section. Between 2009-10, 67,321 people underwent OCT imaging. Of these, 32,069 people had high quality OCT imaging, all cognitive tests, and reported no neurological or ocular disease, and no diabetes (Figure 4.40). 1,251 people with high quality OCT scans and full additional data at baseline completed follow-up cognitive testing in 2012-13. Table 4.32 summarizes demographic, morphometric, and ophthalmic variables at baseline (2009-2010) for all participants with an OCT measure, the 32,069 included in this study, and the subset of those who also underwent follow-up assessment in 2012-2013. Compared to all participants recruited with OCT measurements available, participants included in this study were less economically deprived, more highly educated, had lower refractive error and were less ethnically diverse. The subset of participants with follow up data were slightly older, included more people of white ethnicity, had higher educational attainment and included more non-smokers when compared to the 32,069 included at baseline.

Mean age of the participants included in this study was 56.0 years (95% CI 55.9-56.1, SD 8.21 years) with a higher percentage of women (53.5%, 95% CI 53.0-54.1) than men. Mean age for those who received follow-up testing was 58.1 years (95% CI 57.7-58.5),

with approximately equal numbers of women and men. There was a predominance of white participants at both baseline and follow-up (91.8% and 98.6%, 95% CI 91.5-92.1 and 97.8-99.2, respectively). Mean Townsend deprivation index was -1.13 at baseline (95% CI -1.16—-1.10; more positive scores indicate greater deprivation, UK average: 0). Those included at follow-up were less disadvantaged than the UK average, and less so than those at baseline (mean Townsend deprivation index -2.49, 95% CI -2.63—-2.36). Over one-third of participants at baseline had a degree and another quarter had a professional qualification or A-levels. Of participants undergoing follow-up cognitive testing, almost half (47.7%, 95% CI 45.0-50.5) reported having a degree, less than one-quarter had a professional qualification or A-levels (23.2% 95% CI 21.0-25.6); and the remainder had GCSE's or lower.

Figure 4.40. Inclusion in cognitive testing among those with clean GCL-IPL OCT data.

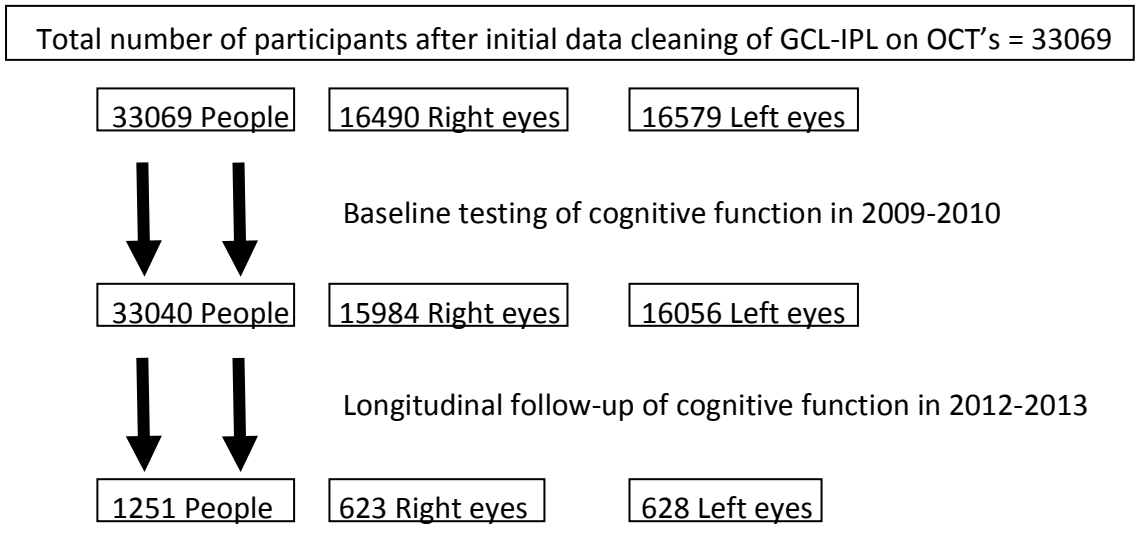

Table 4.32. Characteristics at baseline (2009-2010) of all participants recruited with baseline OCT available for analysis, of those included in baseline analysis, and of the subset with follow-up assessment in 2012-2013.

		All participants recruited with OCT available in 2009-2010			Participants with OCT included in this study			Participants with follow-up in 2012-2013		
		N=67316	95% CI		N=32069	95% CI		N=1251	95% CI	
* Age (years)		57.3	57.2	57.3	56.0	55.9	56.1	58.1	57.7	58.5
+ Female sex		54.4%	54.8	54.0%	53.5%	53.0	54.1%	51.1%	53.9	48.3%
+ Ethnicity	White	90.6%	90.4	90.8%	91.8%	91.5	92.1%	98.6%	97.8	99.2%
	Chinese	4.6%	4.1	5.2%	0.4%	0.3	0.4%	0.2%	0.0	0.6%
	Asian	3.3%	3.1	3.4%	2.2%	2.1	2.4%	0.2%	0.0	0.6%
	Black	3.2%	3.1	3.3%	2.6%	2.4	2.8%	0.2%	0.1	0.7%
	Mixed/Other	2.5%	2.3	2.6%	2.1%	2	2.3%	0.8%	0.4	1.5%
* Townsend deprivation index		-1.01	-1.03	-0.99	-1.13	-1.16	-1.10	-2.49	-2.63	-2.36
+ Education	College degree	35.7%	35.3	36.0%	37.1%	36.6	37.6%	47.7%	45.0	50.5%
	Prof. qual. or A-level	23.4%	23.1	23.7%	23.6%	23.1	24.0%	23.2%	21.0	25.6%
	GCSE or O-level	21.1%	20.8	21.4%	21.4%	21.0	21.9%	20.3%	18.1	22.6%
	CSE	5.6%	5.4	5.8%	5.8%	5.6	6.1%	3.1%	2.3	4.2%
	Lower than CSE	14.3%	14.0	14.6%	12.0%	11.7	12.4%	5.7%	4.5	7.1%
+ Laterality = right eye		N/A	N/A	N/A	49.9%	49.3	50.4%	49.8%	47.0	52.6%
* Visual acuity (logMAR)		° 0.02	0.02	0.03	-0.07	-0.08	-0.07	-0.05	-0.06	-0.04
* Intraocular pressure (mmHg)		° 15.8	15.8	15.8	15.0	15.0	15.1	15.2	15.0	15.3
* Refraction (diopters)		° -0.37	-0.39	-0.35	-0.06	-0.08	-0.04	-0.09	-0.20	0.03
* Height (mean cm)		168.7	168.6	168.8	169.2	169.1	169.3	170.0	169.5	170.5
	Women	162.7	162.6	162.8	163.1	163.0	163.2	163.5	163.1	164.0
	Men	175.8	175.7	175.9	176.3	176.2	176.4	176.7	176.2	177.2

* Mean

+ Percentage

° For those excluded, random selection of right/left eyes was not performed; thus, for the "all participants recruited" category, visual acuity, intraocular pressure, and refraction were calculated for right eyes only.

95% CI = 95% confidence interval.

SD = standard deviation

Prof. qual. = Professional or vocational qualification (including higher national diploma)

A-Level = General Certificate of Education Advanced Level, typically taken at age 18

GCSE = General Certificate of Secondary Education (formerly O-Level), typically taken at age 16)

O-Level = General Certificate of Education Ordinary Level, typically taken at age 16

CSE = Certificate of Secondary Education, a less demanding exam usually taken at age 16

Thinner baseline GCL-IPL was associated with worse performance on every cognitive test assessed (Figures 4.41 – 44). On prospective memory testing (Figure 4.41), for each quintile thinner GCL-IPL, there was an associated increase in number of attempts needed (-0.02 attempts per quintile, $p<0.001$). A similar effect was seen with remaining cognitive tests, with each quintile thinner GCL-IPL corresponding with greater number of

incorrect matches at pairs matching (-0.03 incorrect matches per quintile, p<0.001, Figure 4.42), worse score on numeric and verbal reasoning tests (0.08 per quintile, p<0.001, Figure 4.43), and slower reaction time (-9.43 msec per quintile, p<0.001, Figure 4.44). After controlling for potential confounders (age, sex, height, race, refraction, IOP, socioeconomic deprivation, and education), pairs matching (-0.01 incorrect/quintile, p<0.001) and reaction time (-2.97 msec/quintile, p<0.001) remained significant, whereas prospective memory (p-0.04) and numeric and verbal reasoning (p=0.001) were no longer significant at the pre-set threshold.

Figure 4.41. Prospective memory and GCL-IPL thickness at baseline. (A greater number of attempts indicate worse performance.) Regression coefficient -0.02 (95% CI -0.02 – -0.01, p<0.001). After controlling for potential confounders (age, sex, height, race, refraction, IOP, socioeconomic deprivation, and education), regression coefficient -0.004 (95% CI -0.008 – 0.0002, p=0.04).

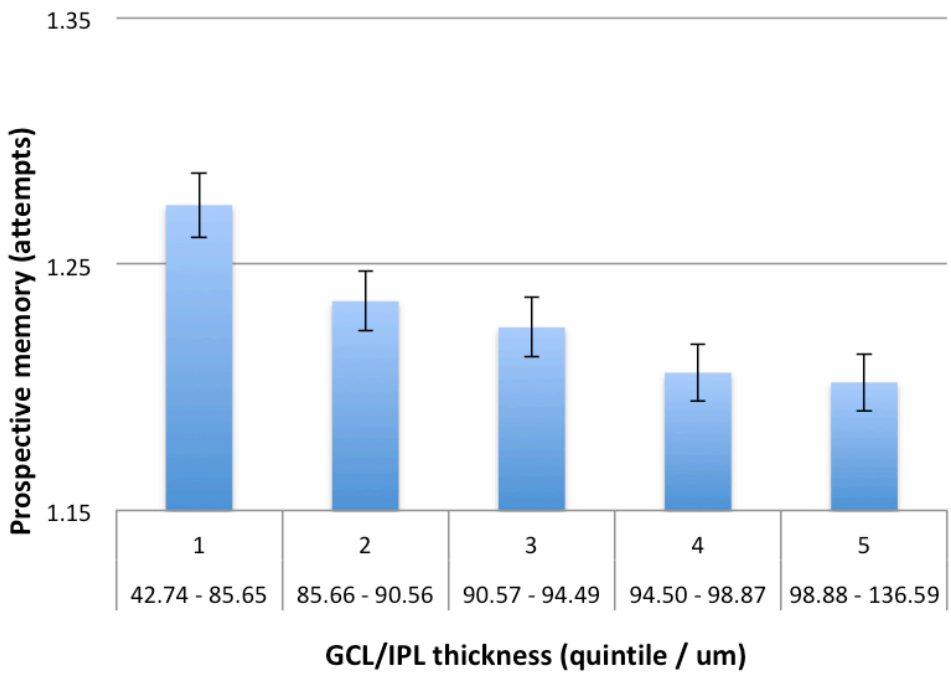

Figure 4.42. Pairs matching and GCL-IPL thickness at baseline. (A greater number of incorrect matches indicates worse performance.) Regression coefficient -0.03 (95% CI -0.04 – -0.03, p<0.001). After controlling for potential confounders (age, sex, height, race, refraction, IOP, socioeconomic deprivation, and education), regression coefficient -0.01 (95% CI -0.02 – -0.006, p<0.001).

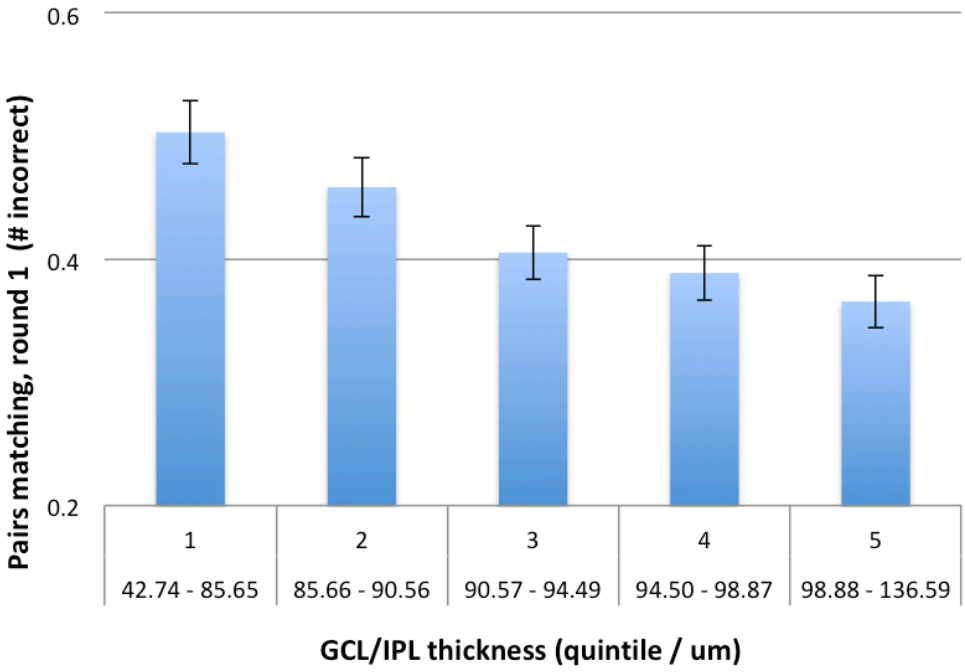

Figure 4.43. Numeric & verbal reasoning and GCL-IPL thickness at baseline. (Lower score indicates worse performance.) Regression coefficient 0.08 (95% CI 0.06 – 0.09, p<0.001). After controlling for potential confounders (age, sex, height, race, refraction, IOP, socioeconomic deprivation, and education), regression coefficient +0.02 (95% CI 0.01 – 0.04, p=0.001).

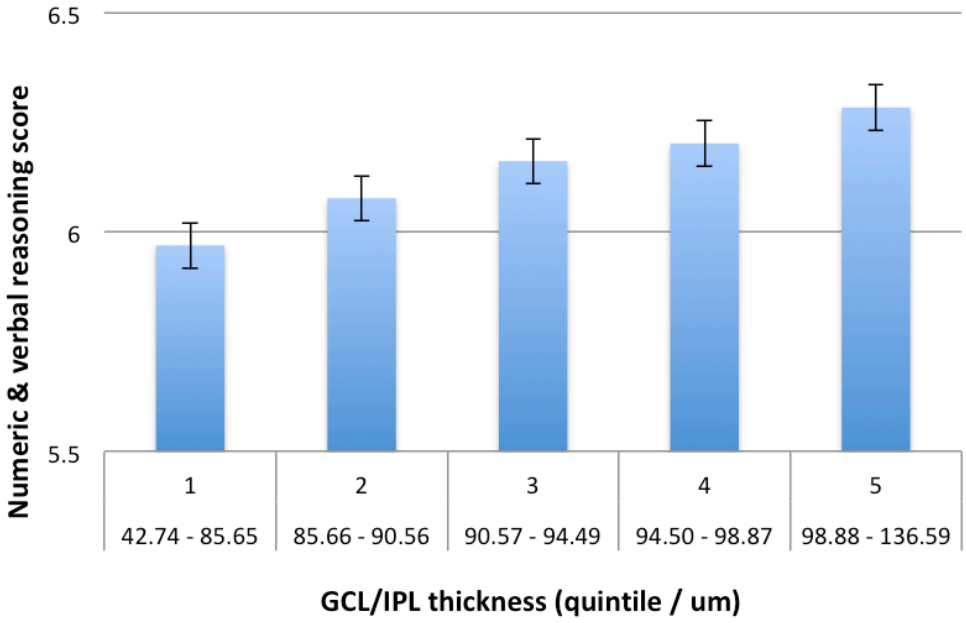

Figure 4.44. Reaction time and GCL-IPL thickness at baseline. (Longer reaction time indicates worse performance.) Regression coefficient -9.43 (95% CI -10.31 – -8.56, p<0.001). After controlling for potential confounders (age, sex, height, race, refraction, IOP, socioeconomic deprivation, and education), regression coefficient -2.97 (95% CI -3.84 – -2.10, p<0.001).

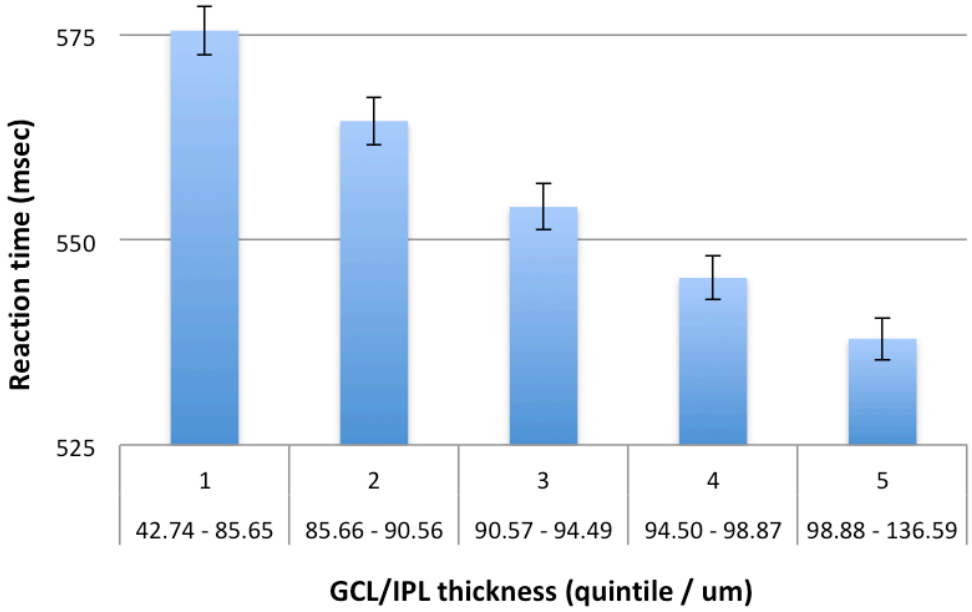

Furthermore, GCL-IPL thickness was associated with total number of tests with poor performance, defined as doing worse than 95% of participants, or an incorrect answer on first attempt of prospective memory. For each quintile thinner GCL-IPL, there was a corresponding increase in the number of cognitive tests with poor performance (-0.03 per quintile, p<0.001) (Figure 4.45). After controlling for potential confounders, regression coefficient decreased but remained significant (-0.01 tests with poor performance per quintile, p<0.001).

Figure 4.45. Total number of tests with poor performance and GCL-IPL thickness at baseline. Regression coefficient -0.03 (95% CI -0.04 – -0.03, p<0.001). After controlling for potential confounders (age, sex, height, race, refraction, IOP, socioeconomic deprivation, and education), regression coefficient -0.01 (95% CI -0.02 – -0.007, p<0.001).

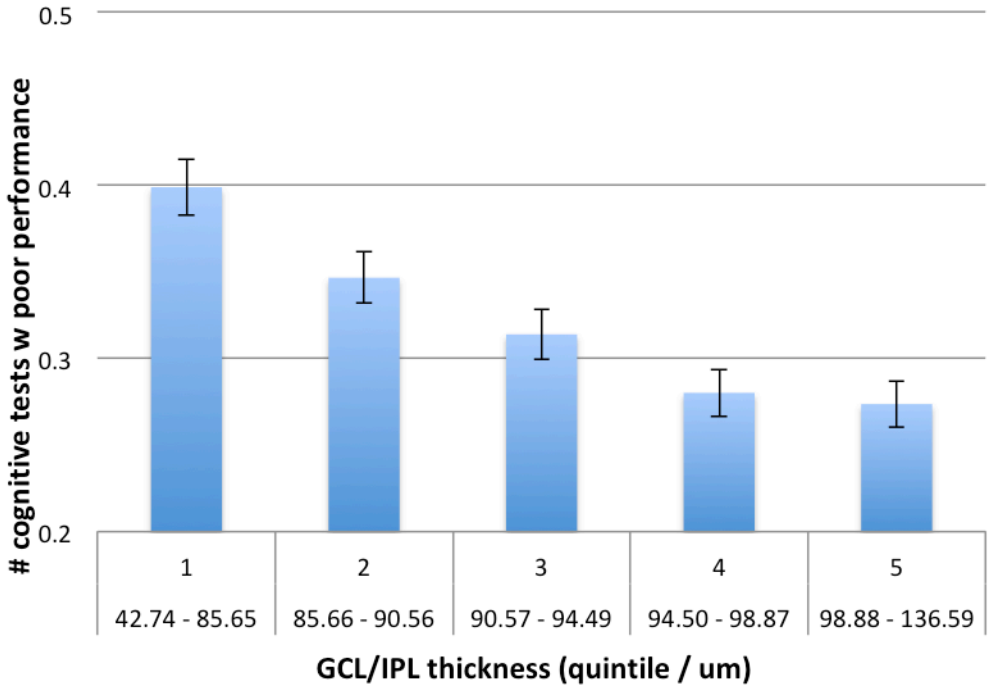

To better interpret risk, threshold was set at failure of either 1 or 2 cognitive tests, and regression analysis was performed, controlling for age, sex, height, race, refraction, IOP, socioeconomic deprivation, and education (Table 4.33). Those with thinnest GCL-IPL were at 14% increased risk of failing at least one test and 27% increased risk of failing at least two tests, as compared to those with thickest GCL-IPL; however, while this approached statistical significance (p=0.003 and p=0.007, respectively), it did not meet the statistical threshold set for the current study. When this was examined graphically (Figure 4.46), one can certainly appreciate a trend of greater cognitive deficit among those with thinner GCL-IPL. After controlling for potential confounders, regression

shows odds ratio 1.04 per quintile (p<0.001) at threshold of failing 1 or more tests, and 1.07 per quintile (p=0.001) at threshold of failing 2 or more tests.

Table 4.33. Multivariable logistic regression modeling of association between GCL-IPL thickness and risk of failing A) 1 or more cognitive tests (compared to 0) or B) 2 or more tests (compared to 0 or 1 test) at baseline, controlled for age, sex, height, race, refraction, IOP, socioeconomic deprivation, and education.

A) Risk of failing 1 or more cognitive tests (compared to 0).

GCL-IPL (µm)	Odds Ratio	95% CI		P-value
<=85.65	1.14	1.05	1.24	0.003
85.66 – 90.56	1.08	0.99	1.17	0.09
90.57 – 94.49	1.00	0.92	1.09	0.92
90.50 – 98.87	0.92	0.85	1.01	0.07
>=98.88	reference			reference

B) Risk of failing 2 or more cognitive tests (compared to 0 or 1).

GCL-IPL (µm)	Odds Ratio	95% CI		P-value
<=85.65	1.27	1.07	1.51	0.007
85.66 – 90.56	1.07	0.89	1.28	0.47
90.57 – 94.49	1.11	0.93	1.33	0.25
90.50 – 98.87	0.92	0.76	1.11	0.4
>=98.88	reference			reference

Figure 4.46. Proportion (with 95% confidence intervals) of 33,040 UK Biobank participants with a cognitive deficit, set at threshold of A) 1 or more tests or B) 2 or more tests, according to quintile of retinal nerve fibre layer thickness measured in the inner nasal retinal subfield by optical coherence tomography (OCT).

A) Threshold of 1 or more tests, according to quintile of retinal nerve fibre layer thickness measured in the inner nasal retinal subfield by optical coherence tomography (OCT). After controlling for potential confounders (age, sex, height, race, refraction, IOP, socioeconomic deprivation, and education), odds ratio 1.04 per quintile, p<0.001.

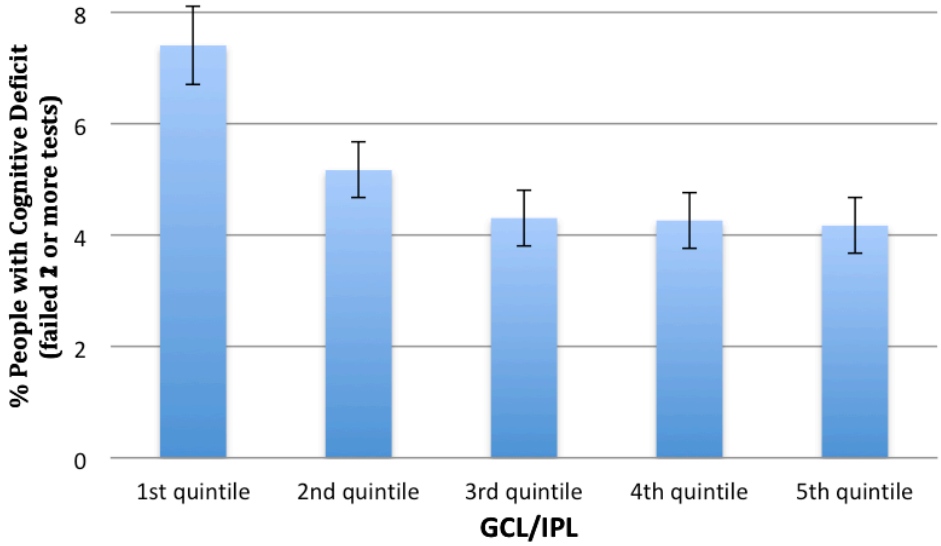

B) Threshold of 2 or more tests, according to quintile of retinal nerve fibre layer thickness measured in the inner nasal retinal subfield by optical coherence tomography (OCT). After controlling for potential confounders (age, sex, height, race, refraction, IOP, socioeconomic deprivation, and education), odds ratio 1.07 per quintile, p=0.001.

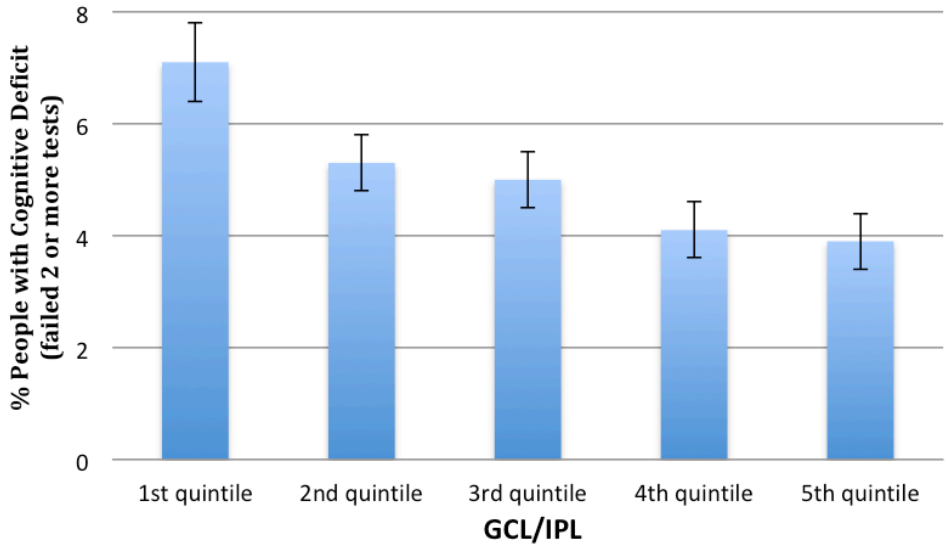

Baseline GCL-IPL thickness (collected 2009-2010) was analysed together with cognitive testing at follow-up (2012-2013). This was tested in several ways, with threshold of 1 or more cognitive tests worse on follow-up (Figure 4.47a, Table 3.34a), 2 or more cognitive tests worse on follow-up (Figure 4.47b, Table 3.34b), and total number of cognitive tests worse on follow-up (Figure 4.48). Results were examined graphically, as well as through regression analyses. While some trends were visible, none met the strict threshold set for statistical significance.

Figure 4.47. The proportion of 1,251 UK Biobank participants who underwent cognitive testing at baseline and 3 years later who experienced a decline in cognitive function test results. Rates are plotted against quintile of GCL-IPL thickness measured in the inner nasal retinal subfield by optical coherence tomography (OCT).

A) 1 or more of a total of 4 cognitive tests deteriorating.

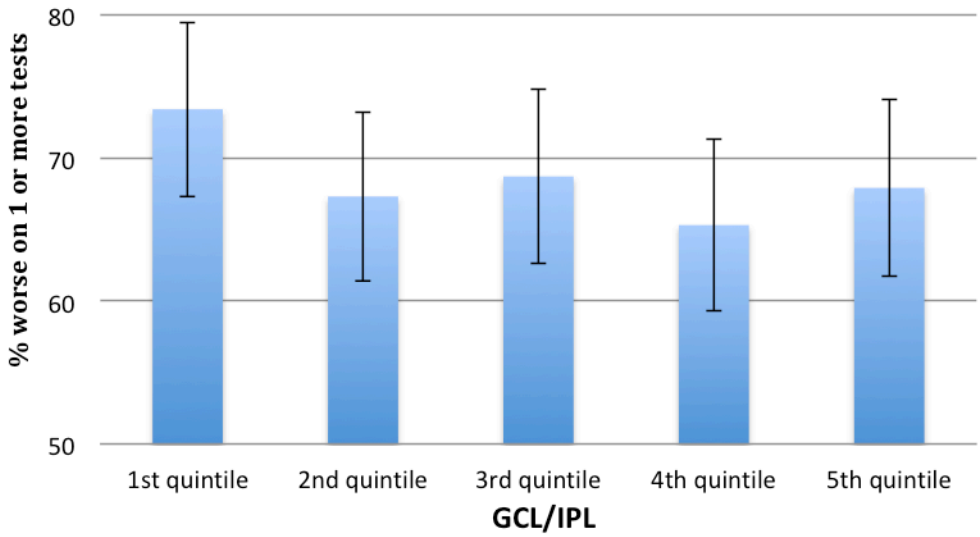

B) 2 or more of a total of 4 cognitive tests deteriorating.

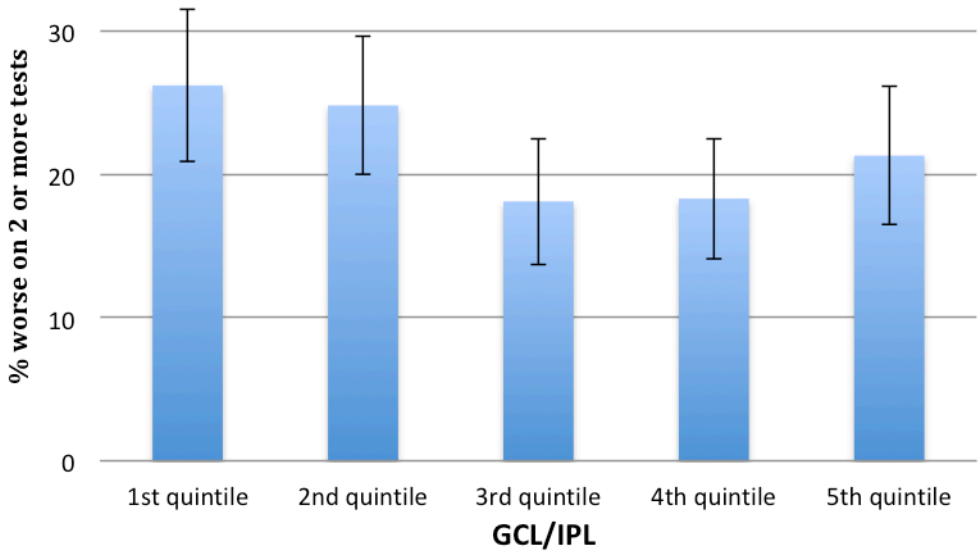

Table 4.34. Multivariable logistic regression modeling of association between GCL-IPL thickness and risk of worsening on A) 1 or more follow-up cognitive function tests (compared to 0 tests) or B) 2 or more follow-up cognitive tests (compared to 1 or 2 tests), controlled for age, sex, height, race, refraction, IOP, socioeconomic deprivation, and education.

A) Worsening on 1 or more follow-up cognitive function tests (compared to 0 tests).

GCL-IPL quintile (μm)	Odds Ratio	95% CI	P-value
<=85.65	1.28	0.85 1.93	0.24
85.66 – 90.56	0.98	0.67 1.44	0.93
90.57 – 94.49	1.02	0.69 1.51	0.91
90.50 – 98.87	0.88	0.60 1.29	0.52
>=98.88	reference		reference

GCL-IPL	Odds Ratio	95% CI	P-value
Per quintile	1.06	0.97 1.16	0.21

B) Worsening on 2 or more follow-up cognitive function tests (compared to 0 or 1 tests).

GCL-IPL quintile (μm)	Odds Ratio	95% CI	P-value
<=85.65	1.25	0.80 1.96	0.33
85.66 – 90.56	1.27	0.83 1.95	0.27
90.57 – 94.49	0.82	0.52 1.30	0.39
90.50 – 98.87	0.84	0.54 1.33	0.46
>=98.88	reference		reference

GCL-IPL	Odds Ratio	95% CI	P-value
Per quintile	1.1	0.99 1.21	0.08

Figure 4.48. Number of cognitive tests worse on follow-up testing as compared with baseline GCL-IPL. Regression coefficient 0.65 µm per each test failed, p=0.03. After controlling for potential confounders, including age, sex, race, ethnicity, Townsend deprivation index, height, refraction, and intraocular pressure, regression coefficient 0.58 µm per each test failed, p=0.04.

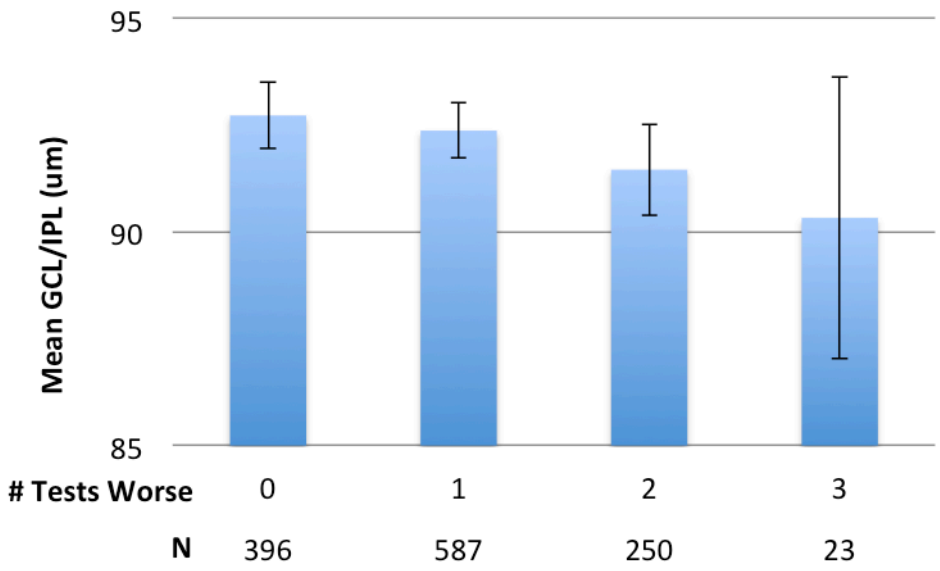

4.5.2.2 RNFL and Cognitive Function

Between 2009-10, 67,321 people underwent OCT imaging. Of these, 32,038 people had high quality OCT imaging, all cognitive tests, and reported no neurological or ocular disease, and no diabetes (Figure 4.49). 1,251 people with high quality OCT scans and full additional data at baseline completed follow-up cognitive testing in 2012-13. Table 4.35 summarizes demographic, morphometric, and ophthalmic variables at baseline (2009-2010) for all participants with an OCT measurement, the 32,038 included in this study, and the subset of those who also underwent follow-up assessment in 2012-2013. Compared to all participants recruited with OCT measurements available, participants included in this study were less economically deprived, more highly educated, had lower refractive error and were less ethnically diverse. The subset of participants with follow

up data were slightly older, included more people of white ethnicity, had higher educational attainment and included more non-smokers when compared to the 32,038 included at baseline.

Mean age of the participants included in this study was 56.0 years (95% CI 55.9-56.1, SD 8.21 years) with a higher percentage of women (53.6%, 95% CI 52.0-54.1) than men. Mean age at second visit was 58.1 years (95% CI 57.7-58.5), with approximately equal numbers of women and men. There was a predominance of white participants at both baseline and follow-up (92.7% and 98.6%, 95% CI 92.4-92.9 and 97.8-99.2, respectively). Mean Townsend deprivation index was -1.18 at baseline (95% CI -1.21—-1.14; interquartile range 4.23; more positive scores indicate greater deprivation, UK average: 0). Those included at follow-up were less disadvantaged than the UK average, and less so than those at baseline (mean Townsend deprivation index -2.49, 95% CI -2.63—-2.36; interquartile range 2.619). Over one-third of participants at baseline had a degree and another quarter had a professional qualification or A-levels. Of participants undergoing follow-up cognitive testing, almost half (47.7%, 95% CI 45.0-50.5) reported having a degree, less than one-quarter had a professional qualification or A-levels (23.2% 95% CI 21.0-25.6); and the remainder had GCSEs or lower.

Figure 4.49. Inclusion in cognitive testing among those with clean RNFL OCT data.

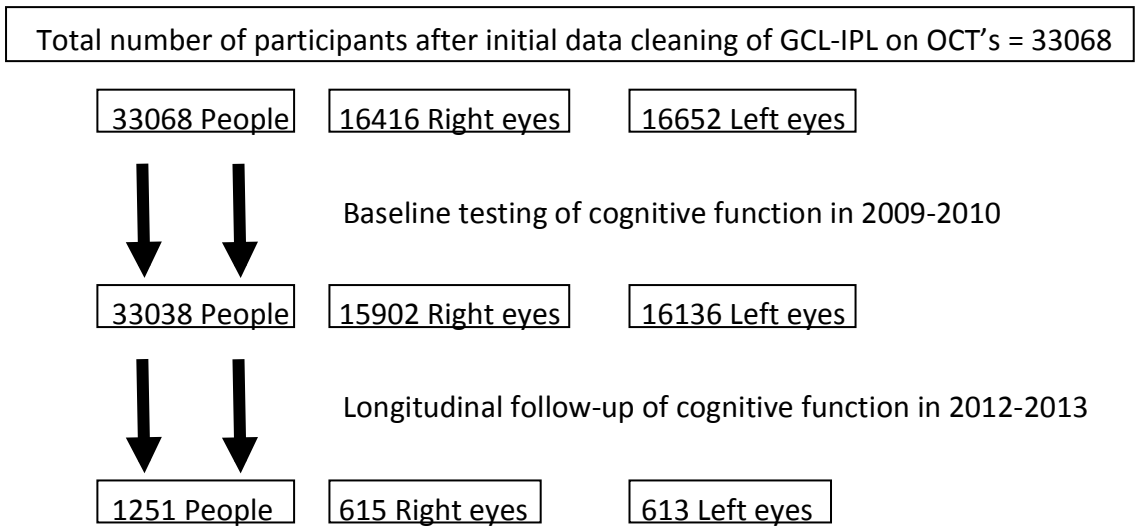

Table 4.35. Characteristics at baseline (2009-2010) of all participants recruited with baseline OCT available for analysis, of those included in baseline analysis, and of the subset with follow-up cognitive function assessment in 2012-2013.

		All participants recruited with OCT available in 2009-2010			Participants with OCT included in this study			Participants with follow-up in 2012-2013		
		N=67316	95% CI		N=32038	95% CI		N=1251	95% CI	
* Age (years)		57.3	57.2	57.3	56.0	55.9	56.1	58.1	57.7	58.5
+ Female sex		54.4%	54.8	54.0%	53.6%	53.0	54.1%	51.1%	53.9	48.3%
+ Ethnicity	White	90.6%	90.4	90.8%	92.7%	92.4	92.9%	98.6%	97.8	99.2%
	Chinese	4.6%	4.1	5.2%	0.4%	0.3	0.4%	0.2%	0.0	0.6%
	Asian	3.3%	3.1	3.4%	2.2%	2.1	2.4%	0.2%	0.0	0.6%
	Black	3.2%	3.1	3.3%	2.6%	2.4	2.8%	0.2%	0.1	0.7%
	Mixed/Other	2.5%	2.3	2.6%	2.1%	2.0	2.3%	0.8%	0.4	1.5%
* Townsend deprivation index		-1.01	-1.03	-0.99	-1.18	-1.21	-1.14	-2.49	-2.63	-2.36
+ Education	College degree	35.7%	35.3	36.0%	37.6%	37.1	38.1%	47.7%	45.0	50.5%
	Prof. qual. or A-level	23.4%	23.1	23.7%	23.6%	23.1	24.1%	23.2%	21.0	25.6%
	O-level	21.1%	20.8	21.4%	21.7%	21.2	22.1%	20.3%	18.1	22.6%
	CSE	5.6%	5.4	5.8%	5.8%	5.6	6.1%	3.1%	2.3	4.2%
	Lower than CSE	14.3%	14.0	14.6%	11.3%	11.0	11.7%	5.7%	4.5	7.1%
+ Laterality = right eye		N/A	N/A	N/A	49.6%	49.1	50.2%	49.2%	46.4	51.9%
* Visual acuity (logMAR)		° 0.02	0.02	0.03	-0.04	-0.04	-0.04	-0.05	-0.06	-0.04
* Intraocular pressure (mmHg)		° 15.8	15.8	15.8	15.0	15.0	15.1	15.2	15.0	15.4
* Refraction (diopters)		° -0.37	-0.39	-0.35	-0.07	-0.1	-0.05	-0.1	-0.21	0.02
* Height (mean cm)		168.7	168.6	168.8	169.3	169.2	169.4	170	169.5	170.5
	Women	162.7	162.6	162.8	163.2	163.1	163.3	163.5	163.1	164.0
	Men	175.8	175.7	175.9	176.4	176.3	176.5	176.7	176.2	177.2
+ Smoker	No	90.3%	90.1	90.5%	90.6%	90.3	90.9%	94.6%	93.2	95.8%
	Occasional	2.9%	2.7	3.0%	3.0%	2.8	3.2%	1.6%	1.0	2.5%
	Yes	6.8%	6.6	7.0%	6.4%	6.1	6.6%	3.8%	2.8	5.0%

* Mean

+ Percentage

° For those excluded, random selection of right/left eyes was not performed; thus, for the "all participants recruited" category, visual acuity, intraocular pressure, and refraction were calculated for right eyes only.

95% CI = 95% confidence interval.

SD = standard deviation

Prof. qual. = Professional or vocational qualification (including higher national diploma)

A-Level = General Certificate of Education Advanced Level, typically taken at age 18

O-Level = General Certificate of Education Ordinary Level, typically taken at age 16

CSE = Certificate of Secondary Education, a less demanding exam usually taken at age 16

A thinner baseline RNFL measure was associated with worse performance on baseline cognitive tests (Figures 4.50 – 54). For each cognitive test (prospective memory, pairs matching, numeric & verbal reasoning, and reaction time) there was worse performance for each quintile of RNFL thinner (Figures 4.50 – 53). Of those in the thinnest RNFL quintile 7.4% (95% CI 6.8 – 8.1%) failed at least 2 out of 4 cognitive tests (Figure 4.54), as

compared to 4.2% (95% CI 3.7-4.7%) of those in the thickest RNFL quintile (p<0.001). To quantify the effect and account for other potential confounding, multivariable logistic regression was used to adjust for the effects of age, sex, race, Townsend deprivation index, educational attainment, refractive error, and IOP, and to calculate odds ratio of a cognitive deficit (Table 4.36). Those in the thinnest RNFL quintile were 11% (95% CI 2-21%, p=0.01) more likely to fail one or more cognitive tests (as defined in methods), compared to those in the thickest quintile (Table 4.36).

Figure 4.50. Prospective memory and retinal nerve fibre layer thickness at baseline. Regression coefficient -0.02 (95% CI -0.02 – -0.01, p<0.001). A greater number of attempts indicate worse performance.

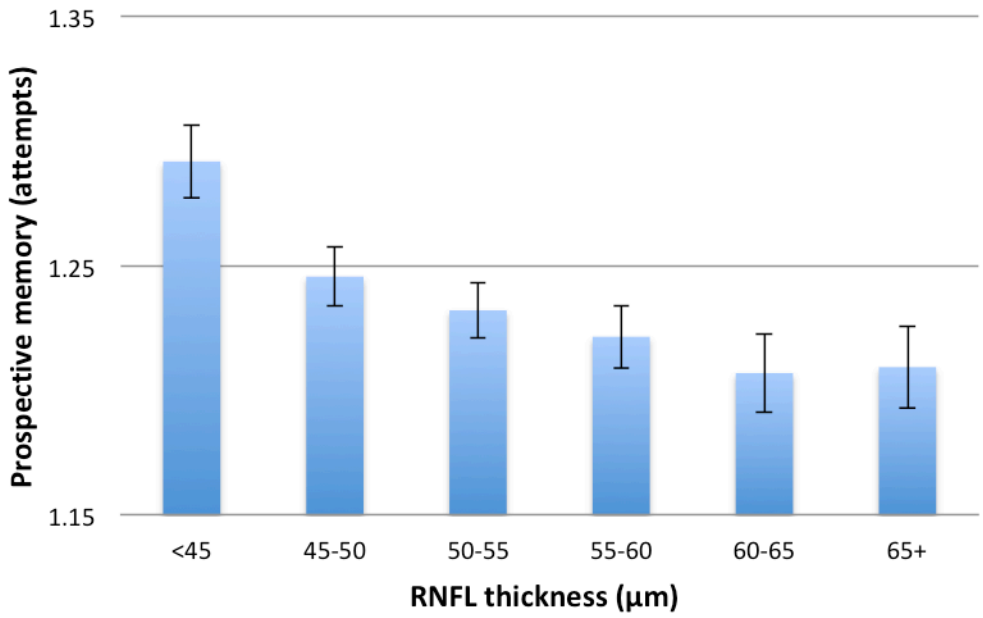

Figure 4.51. Pairs matching and retinal nerve fibre layer thickness at baseline. (A greater number of incorrect matches indicates worse performance.) Regression coefficient -0.03 (95% CI -0.04 – -0.02, p<0.001).

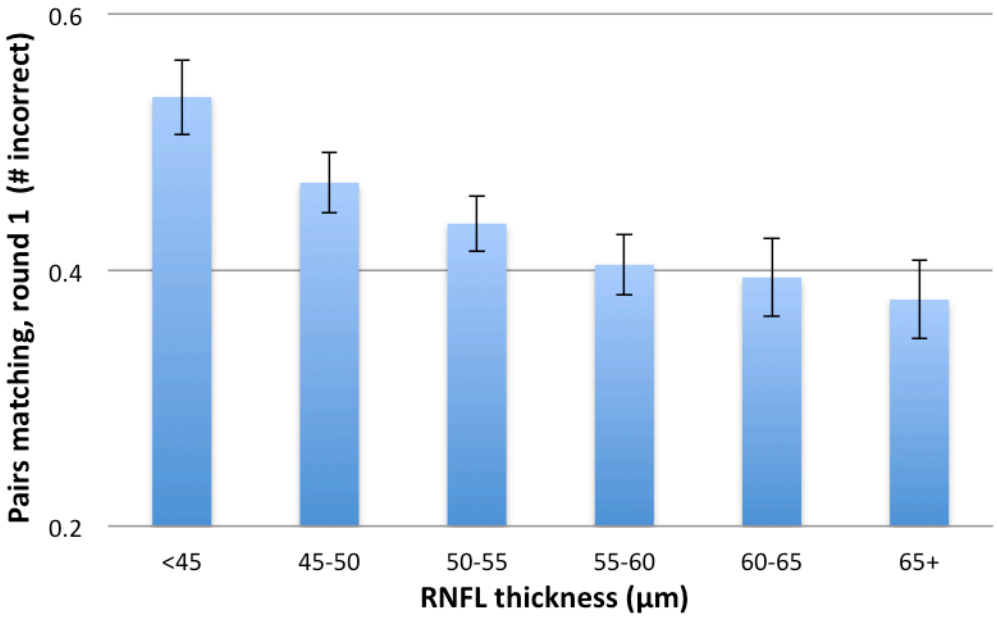

Figure 4.52. Numeric & verbal reasoning and retinal nerve fibre layer thickness at baseline. (Lower score indicates worse performance.) Regression coefficient 0.12 (95% CI 0.11 – 0.14, p<0.001).

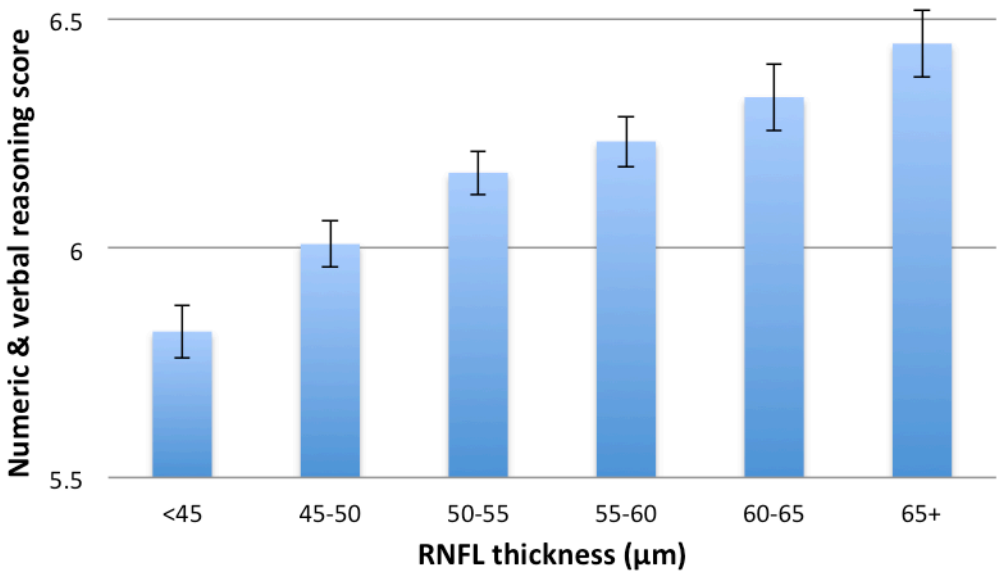

Figure 4.53. Reaction time and retinal nerve fibre layer thickness at baseline. (Longer reaction time indicates worse performance.) Regression coefficient -4.47 (95% CI -5.29 – -3.64, p<0.001).

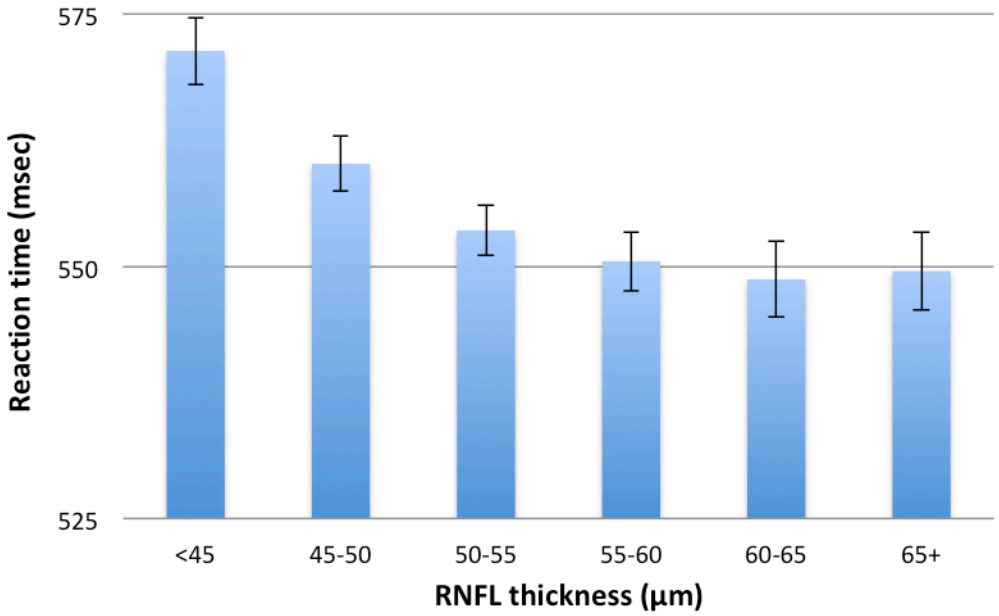

Figure 4.54. Proportion of 32,038 UK Biobank participants with a cognitive deficit (failure of 2 or more of a panel of 4 tests), according to quintile of retinal nerve fibre layer thickness measured in the outer nasal retinal subfield by optical coherence tomography (OCT). Error bars represent 95% confidence intervals.

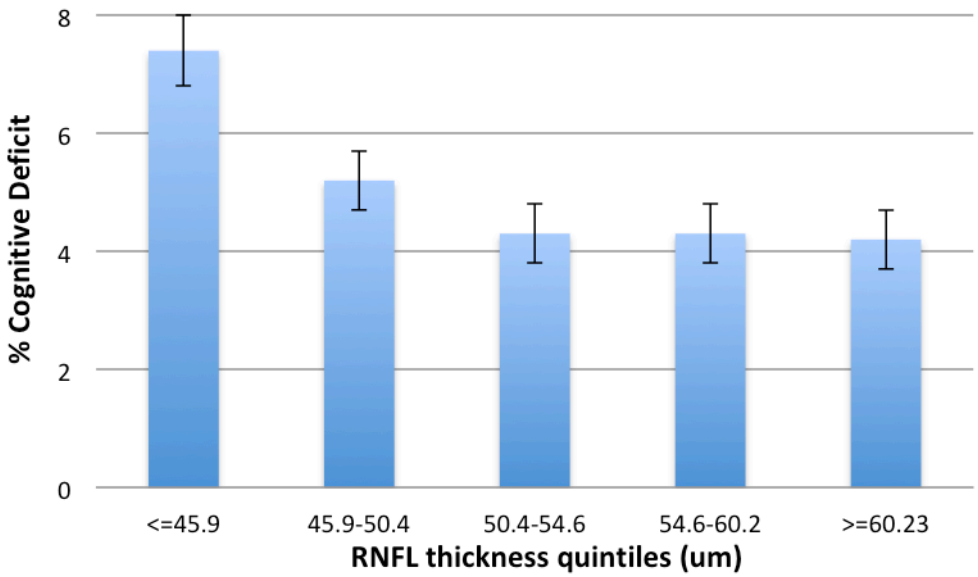

Table 4.36. Multivariable logistic regression modeling of association between RNFL thickness and risk of failing 1 or more tests (compared to 0 tests) at baseline, controlled for age, sex, height, race, refraction, IOP, socioeconomic deprivation, and education.

RNFL (µm)	Odds Ratio	95% CI		P-value
<=45.9	1.11	1.02	1.21	0.01
45.9 - 50.4	0.99	0.90	1.07	0.74
50.4 – 54.6	1.00	0.92	1.09	0.96
54.6 – 60.2	1.02	0.94	1.11	0.67
>=60.2	reference			reference

Baseline RNFL thickness was compared with total number of cognitive tests with worse scores on follow-up testing – i.e., whether a participant did worse on zero, one, two, three, or four tests (Figure 4.55). Thinner baseline RNFL was significantly associated with a future decline in a greater number of cognitive tests (linear regression $p<0.001$), even after controlling for potential confounders (Figure 4.55).

Figure 4.55. Number of cognitive tests worse on follow-up testing is significantly associated with baseline RNFL. Regression coefficient 1.2 µm per each test failed, $p<0.001$. After controlling for potential confounders, including age, sex, race, Townsend deprivation index, height, refraction, and intraocular pressure, regression coefficient 1.1 µm per each test failed, $p<0.001$.

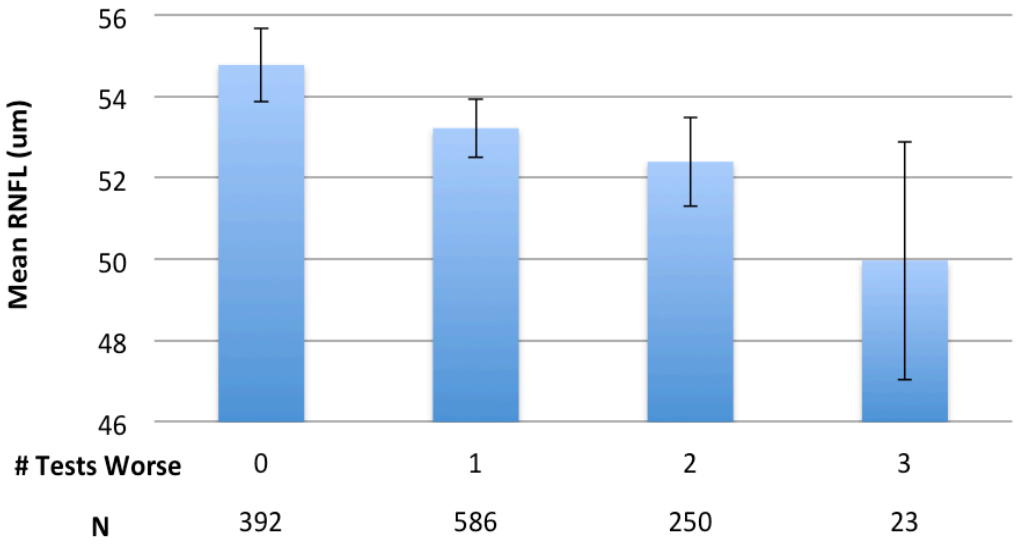

Multivariable regression modeling of association between RNFL thickness and future worsening on one or more follow-up cognitive tests was performed, controlling for age, sex, height, race, refraction, IOP, Townsend deprivation index, and education (Table 4.37). Compared to those in the thickest RNFL quintile, those in the two thinnest quintiles were almost twice as likely (odds ratio 1.92, 95% CI 1.29-2.85, p<0.001) to score worse on at least one cognitive test at follow-up (Table 4.37). Per quintile of RNFL thinning, there was 18% increased risk of cognitive decline at 3-year follow-up (95% CI 8-29%, p<0.001, Table 4.37).

Table 4.37. Multivariable logistic regression modeling of association between RNFL thickness and risk of worsening on 1 or more follow-up cognitive function tests (compared to 0 tests), controlled for age, sex, height, race, refraction, IOP, socioeconomic deprivation, and education.

RNFL Quintile (µm)	Odds Ratio	95% CI		P-value
<=45.9	1.92	1.29	2.85	<0.001
45.9 - 50.4	2.08	1.40	3.08	<0.001
50.4 – 54.6	1.48	1.01	2.18	0.05
54.6 – 60.2	1.51	1.05	2.19	0.03
>=60.2	reference			reference

RNFL (µm)	Odds Ratio	95% CI		P-value
Per quintile	1.18	1.08	1.29	<0.001

SECTION V:

CONCLUSIONS

5.1 Discussion

5.1.1 Retinal Pigment Epithelium

Using the largest known dataset of macular SD-OCT measurements, this study shows novel findings relating to RPE-BM thickness, and its distribution by demographic, ocular, and systemic indices. RPE-BM is significantly thicker in the nasal and temporal subfields as compared to superior or inferior subfields, with greatest thickness in the inner nasal subfield (figure 4.2b). This remains true regardless of sex (figure 4.2c), age (figure 4.3, table 4.2), race (figure 4.4), refraction (figure 4.5, table 4.3), IOP (figure 4.8), blood pressure (figure 4.9, table 4.5), and BMI (figure 4.10, table 4.6).

RPE-BM becomes thinner with each year of age over 46, decreasing 0.1 μm/year (figure 4.3a, tables 4.2 & 4.8). This trend persists across subfields (figure 4.3b-c, tables 4.2 & 4.8). Our findings are in contrast to other studies that have indicated RPE-BM thickness increases with age (Karampelas M et al 2013, Demirkaya et al 2013). However, the numbers included in at least one of these studies was too small to be conclusive (Karampelas M et al 2013). In the other study, numbers were marginally larger; but the age range was wider (18-81 years) and the proportion of people of comparable age to the participants included in the current study (40-69 years) was relatively few (Demirkaya et al 2013). Although the Demirkaya study controlled the analysis for sex, race was not adjusted for and this is a potential confounder, particularly since the

current study found that ethnicity was significantly associated with RPE-BM thickness. Others have examined histologic sections of retina, and suggested increasing deposition of material in the basement membrane with age (Okubo et al 1999, Ramrattan RS et al 1994). If this were indeed true, then my finding of thinner RPE-BM complex would suggest that the effect of RPE thinning is even more dramatic. It may be that histology studies report focal changes, whereas OCT has the potential to provide averaged estimates of change within an entire section or subfield of the retina. A possible explanation for these findings is that age-related loss of RPE cells may lead to remaining cells spreading horizontally to take up space freed by loss of neighboring cells. This process would lead to loss of vertical height of RPE cells with age and resultant reduced RPE-BM thickness with age.

Men and women appeared to have different distributions of RPE-BM thickness, but these were no longer significant after controlling for other variables in multivariable regression modeling.

Black people have significantly thicker RPE-BM than any other race — 3 to 4 µm (approximately 12%) more than white (table 4.8). Some might attribute this finding to skin pigmentation; however, race was self-reported and may be a cultural classification. Further, there was no significant difference between Chinese and whites, and possibly a trend in opposite direction among Asians and whites. To our knowledge, this is the first time this finding has been demonstrated, and may hold clues to the variable phenotypes of macular degeneration in different populations (Wong WL et al 2014).

Refraction is notable in that there appears to be a trend toward thicker RPE-BM with each diopter increase in refraction – i.e., higher hyperopia or less myopia (figure 4.5, table 4.3). This effect may be partially explained by ethnic differences in refraction, as figure 4.6 demonstrates. Nevertheless, the effect persists in multivariable modeling, with RPE-BM thickness increasing 0.28 μm per diopter increase in hyperopic refraction (or each decrease in myopic refraction) (table 4.8). A recent meta-analysis has attempted to identify associations between refractive error and macular degeneration, but any association appears weak (Li et al 2014).

Intraocular pressure is associated with thinner RPE-BM (figure 4.8). Multivariable regression modeling suggests this effect is not significant until after 45 years of age (table 4.8). The association is small, and its clinical relevance is unclear. Nevertheless, this is a new and unexpected finding, as there have been no reported associations between RPE-BM thickness and intraocular pressure, and this warrants further investigation.

The relationship with smoking is complex and must be interpreted with care, given the potential for bias if participants are unwilling to admit to undesirable lifestyle habits. Among those older than age 45, regular smokers showed potentially thinner central RPE-BM as compared to non-smokers (difference -0.27 μm, $p=0.02$, Table 4.8b), but this did not meet the pre-set threshold of $p<0.001$. Many have attempted to explore the association between smoking with oxidative stress and damage to the RPE (Liang FQ et al 2003, Kunchithapautham K et al 2014, Woodell A and Rohrer B 2014). The current findings support a role for smoking in the induction of RPE damage and subsequent loss.

Given the large number of participants in this study, the negative findings are meaningful. There is no clinically significant association between RPE-BM thickness and systolic blood pressure, diastolic blood pressure, or body mass index (figures 4.9 & 4.10, tables 4.5 & 4.6). One might be misled by the small p-values in regression analysis of individual variables; however, the slope of regressions is small, and the low p-value likely represents the lack of fluctuation around a flat line.

Conclusions relating to RPE-BM thickness necessarily rely on interpretation of SD-OCT imaging. Optical reflectivity changes to identify inner and outer RPE boundaries were used to infer changes in thickness. However if optical reflectivity changes occur for other reasons within the RPE cell other than shortening of cells then there could be decoupling between optical reflectivity changes and true thickness change within the RPE/BM complex. Even if OCT based measures of RPE-BM thickness are indeed valid, they may be due to changes in structural, morphological, and density indices. It is not possible to be certain of any direct relationship with function.

This experiment's strengths include its standardized methodology, inclusion of multiple ethnicities across the United Kingdom, and unprecedented number of high-quality SD-OCT images of the macula. This study is limited in that UK Biobank is not population-based, and thus people with fewer resources to attend community research sites are likely under-represented. Nevertheless, it remains possible to make correlations between various biological factors.

Novel findings and associations from this study show RPE-BM thickness is dynamic, with greater thickness nasally and temporally as compared to superiorly and inferiorly; it becomes thinner with older age, myopia, and black ethnicity as compared to all others; furthermore, potential associations with gender and intraocular pressure were identified. These findings hold implications for new directions of research to understand the RPE-BM and disease at this level of the retina.

5.1.2 Photoreceptor inner and outer segments

Photoreceptors are critical for visual function, and thus have been extensively studied for decades, both *in vitro* and *in vivo* (Marshall et al 1979, Tucker GS 1986, Inomata 1988, Curcio et al 1993, Panda-Jonas et al 1995). More recent studies have explored the link between changes in photoreceptor structure and function (Asaoka et al 2017), but with limited understanding of the numerous factors contributing to photoreceptor thickness, a major flaw that limits the validity of existing work. The current study is the largest in vivo study of its kind, and demonstrates the changes visible in both physiological and pathological states.

One existing question is whether older age results in increased photoreceptor thickness due to nodular swelling and accumulation of refractile bodies and lipofuscin by-products (Marshall et al 1979, Tucker GS 1986, Iwasaki and Inomata 1988), or thinning because of

loss of cells and decreased density (Curcio et al 1993, Panda-Jones et al 1995). Indeed, imaging studies have reported conflicting results (Kenmochi et al 2017, Wei et al 2017). A study of 74 people examined mean photoreceptor thickness, and found that those in the oldest group showed significantly thicker photoreceptor complexes than those in the youngest group (Wei et al 2017). However, the study was limited by sample size as well as by its statistical methodology, which did not allow for the correlation between measurements made in the right and left eyes of the same individuals, thereby reducing statistical power (Wei et al 2017). Another study of 127 normal eyes found age-related thinning in the layer between the RPE and the cone outer segment tip, as well as the segment between the inner segment outer segment junction to the external limiting membrane, but not in the segment from cone outer segment tip to the inner segment outer segment junction (Kenmochi et al 2017). While the methodology of this study appeared sound, and determined thickness through a manual count of pixels, the study was limited by its selection of participants (Kenmochi et al 2017). Specifically, among the 127 "normal" eyes, 101 had disease in the fellow eye (including branch retinal vein occlusion, epiretinal membrane, central serous choroiretinopathy, microaneurysms). Whilst these diseases may occur as isolated monocular presentations, the question remains as to whether those participants can truly be representative of a "normal" healthy state.

In the current study, there was a statistically significant association between thinner photoreceptor layer and older age (-0.06 µm/year, $p<0.001$, Table 4.19). Further, when the relationship was examined graphically, there appeared to be a slight positive trend between the ages of 40 to 55, after which the curve appeared to decline steadily (Figure

4.14, Table 4.10). These findings support both theories, that refractile bodies and lipofuscin build up occurs with swelling of photoreceptors (Marshall et al 1979, Tucker GS 1986, Iwasaki and Inomata 1988), but ultimately decreased total density results in decreased overall thickness (Curcio et al 1993, Panda-Jones et al 1995).

There was no identifiable sex-related difference in photoreceptor thickness at central subfield (Figure 4.13c-d, Table 4.19). This analysis adjusted for the effect of height, which was significant in single variable analysis, but not significant after controlling for confounders (Figure 4.18, Table 4.19). This is consistent with the existing literature (Ooto et al 2011).

Surprisingly little has been described regarding the variation in photoreceptor thickness between people of different racial and ethnic backgrounds. There were significant differences among Chinese and blacks, as compared to whites (Figure 4.15, Table 4.11). After controlling for confounders (Table 4.19), photoreceptor thickness at central subfield was 1.84 µm thicker among Chinese as compared to whites ($p<0.001$), and -3.76 µm thinner among blacks as compared to whites ($p<0.001$). Mixed/other ethnicities were also significantly thinner than whites (-0.87 µm, $p<0.001$). Asian ethnicity showed no significant association. The difference between Chinese and Blacks, after controlling for confounders, was almost 6 µm. When considering whether this is clinically significant, one could compare this to age-related differences in thickness of 0.6 µm/year. Intrinsic ethnic differences in photoreceptor layer may contribute to risk factors of retinal disease, and should be considered in future research.

Likewise, little has been published regarding the relationship between IOP and photoreceptor thickness. There was a positive statistically significant association (Figure 4.16, Table 4.12), which remained significant even after controlling for confounders (+0.05 µm/mmHg, p<0.001, Table 4.19). The clinical significance of this is unclear, but may be interesting for future research, to determine whether there is any clinical or pathological significance.

Others have sought and not identified an association between axial length and photoreceptor thickness (Ooto et al 2011). 256 participants were analyzed, with refractive error between -6.0 and +5.0 diopters, and no association identified with photoreceptor thickness. In contrast, the current data showed significant association between refraction and photoreceptor thickness, showing greater photoreceptor thickness with greater ametropia (Figure 4.17, Table 4.13). But if refraction is treated as a single continuous variable, and then controlled for other factors, there was no significant association with photoreceptor thickness.

A recent study of 150 people found significantly thinner photoreceptor layer among those who have ever smoked compared to those who have never smoked (Harris et al 2017). I also found a significant association between smoking and thinner photoreceptor layer, both in single variable analysis (Figure 4.19, Table 4.15), as well as in multivariable regression (-0.87 µm among those who smoked all or most days compared to non-smokers, p<0.001, Table 4.19). Possible explanations for this finding may be due to oxidative stress, inflammatory changes, or altered vascular blood flow (Peluffo et al 2009, Krogh et al, 2017, Garhofer et al 2011, Tamaki et al 1999).

While there initially appeared to be an association between blood pressure, especially diastolic blood pressure, and photoreceptor thickness (Figures 4.20-21, Tables 4.16-17), the association was not significant after controlling for potential confounders (Table 4.19). Given the size of the current study, this is a pertinent negative.

To my knowledge, there are no published data relating to the association between BMI and photoreceptor thickness. The current study finds a negative association between BMI and photoreceptor thickness (Figure 4.22, Table 4.18). This was significant in multivariable regression (-0.12 µm per kg/m^2, $p<0.001$, Table 4.19). This is interesting, as one might expect the opposite, with retinal oedema occurring at higher BMI. I excluded all people who reported diabetes. Furthermore, the trend was visible even at normal BMI.

BMI and smoking are both modifiable risk factors associated with photoreceptor thickness. This novel finding is important as it indicates that lifestyle changes might mitigate or be protective against photoreceptor thinning.

5.1.3 Ganglion Cell Layer – Inner Plexiform Layer Complex

GCL-IPL complex has been well-studied, both in the context of glaucoma as well as cognitive function (Francoz et al 2014, Kim et al 2015, Jiang et al 2018, Liu et al 2016, Cheung et al 2015). However, a literature search identified no other study of the size and scope of the current analysis. I showed GCL-IPL thinning with age, consistent with existing literature (Gao et al 1992, Wei et al 2017, Demirkaya et al 2013, Harwerth and Wheat 2008, Zhang et al 2016, Altay et al 2017, Bloch et al 2017). Advanced Imaging for Glaucoma Study (AIGS) found -0.17 ± 0.05 µm thinner GCL-IPL per year of baseline age ($P < 0.001$) in cross-sectional analysis (Zhang et al 2016). A separate smaller study of 74 people showed -0.14 µm per year difference in GCL-IPL thickness (Wei et al 2017). This correlates well with current findings, which shows a range of -0.07 µm per year at outer temporal subfield to -0.22 µm per year at inner nasal subfield ($p<0.001$) (Figure 4.25). A multivariate analysis was carried out adjusting for potential confounders, and found thinner GCL-IPL ranging from -0.11 µm per year at outer temporal subfield to -0.24 µm per year at inner nasal subfield ($p<0.001$) (Table 4.26a). It is interesting that the differences in GCL-IPL thickness between age groups was more pronounced after controlling for other factors.

To date, the study most comparable to the current study involves the TwinsUK cohort, with 1657 individuals, 1432 of whom were either monozygous or dizygous twin pairs (Bloch et al 2017). They found age ($\beta = -0.14$, $P < 0.001$), refractive spherical equivalence ($\beta = 0.70$, $P <0.001$), and BMI ($\beta = -0.15$, $P = 0.001$) were significantly associated with GCL-IPL thickness in multivariable modeling (Bloch et al 2017). These findings are

consistent with those of this study.

Sex was not found to be significantly associated with GCL-IPL in the TwinsUK cohort, but it was underpowered due to a small number of men (174 or 10.5%) (Bloch et al 2017). Several other studies were not able to find a significant association with sex and GCL-IPL thickness (Wang et al 2016, Mwanza et al 2011). The current analysis did find sex-associated differences in GCL-IPL thickness, though the direction of the effect differed depending on the subfield (Figure 4.24d-e, Table 4.26a-b), potentially reflecting a variation in distribution of cells related to sex. Of note, there was a significant association between GCL-IPL and height at inner subfields (range +0.05 – +0.08 μm/cm after controlling for potential confounders, $p<0.001$) (Figure 4.29, Table 4.23, Table 4.26a). This is important to take into account when adjusting for sex, as women and men have different mean heights (mean 163.1 cm among women, 95% CI 163.0-163.2; mean 176.3 cm among men, 95% CI 176.2 – 176.4; Table 4.20).

TwinsUK study only consisted of white people of British ancestry which is a major limitation of that study, in light of our findings of significant differences among ethnicities (Bloch et al 2017). The current analysis found that at all inner subfields, Asians and black people had significantly thinner GCL-IPL than whites (Table 4.26a). At outer subfields, GCL-IPL among Asians was significantly thinner than whites at 2 out of 4 subfields (Table 4.26b). In contrast, blacks had *thicker* GCL-IPL at outer inferior subfield (Table 4.26b). Chinese people tended to have thicker GCL-IPL as compared to whites (Table 4.26a-b). This should be taken into account, both in academic research involving GCL-IPL thickness, and also in considering diseases where ethnicity is a risk factor.

TwinsUK did not find a significant association between IOP and the ganglion cell complex in any statistical model (Bloch et al 2017). In contrast, in the current analysis there was a significant association at outer subfields, but not inner subfields (range -0.05 µm/mmHg to -0.09 µm/mmHg after controlling for potential confounders, $p<0.001$) (Figure 4.27, Table 4.22, Table 4.26b). This highlights an important weakness in Bloch et al's work, in that the ganglion cell complex was treated as a single structure, and only mean thickness was reported. An important result of the current analysis is the difference in relationships seen in central, inner, and outer GCL-IPL subfields with IOP. The AIGS Study found no association with IOP (Zhang et al 2016), but again, they treated GCL-IPL as a static structure measured as one number, mean thickness, rather than a structure that varies depending on subfield.

Refractive error is another example of the nature and variability of the GCL-IPL complex, with inner subfields appearing to have different trends from outer subfields on single variable analysis (Figure 4.28). Multivariable regression, which controlled for numerous confounders, resulted in much more similar results between inner and outer subfields, although regression coefficients for inner subfields (range +0.11 – +0.48 µm, $p<0.001$, Table 4.26a) were much lower than for outer subfields (range +0.89 – +1.12 µm, $p<0.001$, Table 4.26b). I was not able to control for the effects of magnification and the projected scan length in myopic eyes. Thus, there may be a slight underestimation of thickness among people with myopia. This may partially account for the appearance of an inflection point at emmetropia (Figure 4.28), as the effects of magnification interact with those of physiologic thinning due to changes in axial length or refractive error. My

results are supported by previous studies, which have shown that eyes with longer axial lengths tend to have thinner GCL-IPL (Kim et al 2011, Wu et al 2008, Luo et al 2006). Whilst the absence of axial length measurement is a potential weakness of this study, it is also often the reality in clinical practice, where refractive error is measured as part of a routine exam but axial length measurement is usually ordered as an additional test (i.e., for biometric measurement prior to cataract surgery).

The central subfield showed rather different results from remaining subfields (Table 4.26). This may be the effect of the relative overall thinness of the central subfield (Figure 4.24), increasing any influences from artifact.

A literature search suggests that this study is the first to compare OCT measurements of GCL-IPL with educational attainment and socioeconomic deprivation. The EPIC-Norfolk Eye Study did consider education, but the imaging technology used was Heidelberg Retinal Tomography, and they largely focused on RNFL (Khawaja et al 2013 Oct). The current study shows that lower educational attainment and greater socioeconomic deprivation are significantly associated with thinner GCL-IPL, with the effect most visible at inner subfields (range -0.12 – -0.17 µm per category lower education and –0.16 – -0.20 µm per quintile greater deprivation, after controlling for confounders, $p<0.001$) (Figures 4.30-31, Tables 4.24-26). Some might argue that the effects of education may be due to associations with myopia (Mountjoy et al 2018). However, the current analysis controls for refractive error. Among UK Biobank participants, the youngest age included was 40 years old; thus, educational attainment was most likely achieved several decades prior to participation in the current study. Whether the relationship between education

and GCL-IPL thickness is a reflection of healthier nerve tissue corresponding to greater academic achievement, or whether there is an intrinsic cause and effect between education and nerve development requires further research. Socioeconomic deprivation reflects more current circumstances of participants, but may still carry a component of past exposures. It may be that early factors, such as education, as well as ongoing factors, such as socioeconomic deprivation attribute to the health or attrition of the GCL-IPL.

5.1.4 Retinal Nerve Fibre Layer

This analysis presents novel findings in a dataset of unprecedented size, demonstrating the variation of macular RNFL (mRNFL) and its associations in healthy people. In this cross-sectional analysis, there was an association between older age and thinner mRNFL. This is a reasonable starting point, but it is possible that cohort effects may be masking or exaggerating the observed trends. Thinner RNFL in older people is consistent with existing literature from macula and peripapillary OCT (Vianna et al 2015, Sung et al 2009, Girkin et al 2011, Parikh et al 2007, Varma et al 2003, Vianna et al 2015). The outer nasal subfield showed the largest age-related difference, of 0.06 µm thinner per year of older age, after controlling for other factors in multivariable modeling (Table 4.31). Interestingly, central subfield measurements appear to be thicker with age. Jampel has previously noted that height of the parafoveal annulus relative to the foveal

pit does not differ with age (Jampel et al 2009). It is possible that the central subfield demonstrates a different trend from remaining subfields due to some yet undefined characteristic about the anatomic location. However, it is more likely that the positive association at the central subfield is due to artifact – as central subfield is the thinnest of all subfields (mean 8.3 μm, SD 4.2 μm), it may be more likely to be susceptible to artifactual errors.

RNFL thicknesses at inner subfields are in the predicted range as compared to histologic studies (Varma et al 1996). Histologic studies found inferior subfield to be thickest; in contrast, it was found that of the inner subfields, superior subfield was thickest. These measurements were acquired ex vivo from only 10 eyes and were not classified according to ETDRS subfields, rendering direct comparison to our study problematic. Furthermore, histologic measurement of RNFL thickness is prone to processing artifact, so may not accurately mirror in vivo measurements.

In the outer subfields, women have significantly thicker average mRNFL as compared to men (Figure 4.33d-e). This difference persists after accounting for height in multivariable modeling (Table 4.31). Women have a thinner central subfield mRNFL than men. Recent evidence from studies using deep learning computer algorithms suggests that there are probably fundamental (but largely unquantified and currently unclear) differences in retinal anatomy between women and men (Poplin et al 2017). Given the size of the dataset in the current study, the statistical significance is high ($p<0.001$). Ooto reported a similar finding in a smaller study (Ooto et al 2011). The reproducibility of this finding

suggests further investigation may be warranted to identify the precise location and nature of these differences.

People of different ethnicities have different mRNFL thickness. Specifically, black people have significantly thinner mRNFL than whites in all subfields (Figure 4.35, Table 4.28, and Table 4.31). Asians also have thinner mRNFL than whites, although the statistical probability of this difference is weaker (Figure 4.35, Table 4.28, and Table 4.31). Axial length was not available for analysis; however, the analysis did adjust for refractive error (Tables 4.37 and 4.31). Thinner baseline mRNFL may indicate an increased susceptibility to glaucoma among people of African descent (Quigley 2006).

In contrast, intraocular pressure (IOP_G), the sole modifiable risk factor for glaucoma (Coleman and Miglior 2008, Leske et al 2003, Kass et al 2002, Anderson 2003), is not associated with mRNFL thickness in the range 5 to 21 mmHg. The results were also tested with IOP_{CC}, and found to be consistent. This is a surprising and unexpected negative finding, especially since this study previously showed a small but highly significant trend towards thinner retinal pigment epithelium (RPE) measures in those with higher IOP in this same cohort with identical selection criteria (Figures 4.8 & 4.36, Tables 4.8 & 4.31, Ko et al 2017). Regression lines are either 0.0 or approach 0.0 (Figure 4.36, Table 4.29), and findings persist in multivariable regression modeling (Table 4.31). In particular, it appears that in people without prior glaucoma and $IOP_G \leq 21$, there is no cross-sectional association between mRNFL thickness and IOP_G. It has always been assumed that glaucomatous risk factors exerted an effect across the full spectrum of their distribution. Lowering of intraocular pressure is beneficial in people with

established glaucoma who have always had normal IOPs (Anderson 2003). Our findings offer evidence among the normal population, simply having lower IOP may not offer additional protective effects for preserving mRNFL. Continuing this idea, it does raise questions about the use of macular RNFL for diagnosis and monitoring of glaucoma.

Refraction is significantly associated with mRNFL thickness, being thicker in myopia and thinner in hyperopia (Figure 4.37). One might expect the opposite to be true, as increased axial length may stretch intraocular structures or result in atrophic changes. Certainly, assessment of peripapillary RNFL is more difficult in people with high refractive errors, due to unpredictable changes in anatomy (Rauscher et al 2009, Guedes et al 2003). This study shows good predictability of mRNFL thickness, supporting the potential of mRNFL in diagnosis of glaucoma among people with higher myopia. Axial length was not collected as part of UK Biobank, which is a potential weakness as correction for magnification changes cannot be made. Nevertheless, given the large numbers of participants in the study, having a normative database of such size has the potential for clinical significance. It may allow valid comparisons of mRNFL thickness to be made even where refractive errors exist.

There was a significant association between lower education and thinner RNFL (Figure 4.39 and Table 4.31). This is particularly interesting when taken together with reports that RNFL may be a biomarker for dementia (Garcia-Martin 2014, Coppola et al 2015). One may consider whether educational attainment offers an index of “potential cognitive reserve,” and also may help risk stratify the individual risk of glaucoma. The fact that having higher than average educational attainment is broadly equivalent to a

decade's difference in age, and that this difference persists after adjustment for refractive error and height, points to either genetic heritage and/or early life experiences and exposures as important factors in the glaucoma risk profile. As all participants were at least 40 years of age, and it was assumed that the vast majority of educational exposure occurred prior to enrolment, education may reflect neural development or early life neural health. Townsend deprivation index is a marker for more recent socioeconomic deprivation, and also shows an association between greater deprivation and thinner RNFL (Figure 4.39 and Table 4.31). This supports the previous finding of a strong inverse association between income and self-reported glaucoma in this cohort (Shweikh et al 2015), which extends across the full spectrum of the range. Socioeconomic deprivation is a complex and challenging concept to quantify, interpret and influence. However, these data show that both early and later life markers of educational and material advantage are linked to the thickness of mRNFL.

This study's strengths include its large sample size, use of standardized techniques, and rigorous selection scans of mRNFL thickness. The current study is 40-80 times larger than any other previous study (Le et al 2015, Ooto et al 2011), allowing one to include only people who have the highest-quality OCT scans. Weaknesses of the study include the effectively voluntary nature of participation, potentially biasing the study toward healthier younger people who are able to travel to testing centers, and preventing population-based estimates of prevalence. These will have implications for the representativeness of the absolute values observed, but should have minimal influence on the identification of important aetiological relationships. With such a large study, small associations can be identified, but care must be taken to differentiate statistical

versus clinical significance. Even as the large size of the study is a potential weakness, in that even small associations are identified, it is also a strength of the study, as the negative findings (egg, IOP_G) are likely to be reliable and may have clinical impact.

The study used a large high-quality dataset to describe novel findings in the mRNFL, including quantification of cross-sectional relationships between mRNFL and age, demonstration of sex differences in mRNFL distribution, significantly thinner mRNFL in blacks and Asians as compared to whites, thicker macular mRNFL measurements in people with myopia, and importantly, showed the significant lack of association between macular mRNFL thickness and IOP in the normal range. These findings provide increased understanding of the mRNFL and may inform future investigations into diseases states.

5.1.5 Cognitive Function

5.1.5.1 GCL-IPL and Cognitive Function

Some have argued that GCL-IPL thickness is related to mild cognitive impairment, and may be more sensitive than RNFL for assessing cognitive decline (Cheung et al 2015). Histologic studies have linked retinal ganglion cell degeneration with Alzheimer's disease (Blanks et al 1989). There were significant associations with all baseline

cognitive tests, including prospective memory (Figure 4.41), pairs matching (Figure 4.42), numeric and verbal reasoning (Figure 4.43), and reaction time (Figure 4.44). When considered together, the total number of tests with poor performance was significantly associated with GCL-IPL thickness (-0.03 tests/quintile, $p<0.001$, Figure 4.45). However, after controlling for potential confounders (age, sex, height, race, refraction, IOP, socioeconomic deprivation, and education), all associations lessened, reflected by lower regression coefficients, and two out of four baseline tests were no longer statistically significantly associated with GCL-IPL thickness.

To better quantify risk, modeling was performed to determine the percentage of people who failed either ≥1 or ≥2 baseline cognitive tests with GCL-IPL thickness (Table 4.33, Figure 4.46). Figure 4.46 appears to show a trend of greater cognitive deficit with thinner GCL-IPL (OR 1.04 at threshold of ≥1 cognitive tests, $p<0.001$; OR 1.07 at threshold of ≥2 cognitive tests, $p=0.001$) after controlling for potential confounders. When examined per quintile (Table 4.33), there appears to be a 14% increased risk of failing at least one cognitive test, and 27% increased risk of failing at least two cognitive tests between the thinnest and thickest quintiles of GCL-IPL thickness, but it did not meet threshold for significance ($p=0.003$ and 0.007, respectively).

Longitudinal cognitive testing results were also considered together with baseline GCL-IPL thickness, including number of people with worse performance on 1 or more cognitive tests (Figure 4.47A, Table 4.34A), 2 or more cognitive tests (Figure 4.47B, Table 4.34B), and total number of cognitive tests worse on follow-up (Figure 4.48). None of these were significant at any threshold.

Taken together, one might understand why previous work (Cheung et al 2015) have suggested GCL-IPL thickness was a marker for cognitive function, as there were some significant associations at baseline. The current study shows the complexity of interpreting GCL-IPL thickness, and the importance of controlling for relevant variables when interpreting results.

One could argue that perhaps these findings were not significant because of small numbers, or inadequate follow-up time. The former critique would not be valid for baseline results, as the current study is the largest of its kind, with 33,040 participants. Indeed, longitudinal results included only 1251 participants with follow-up of 3 years. Further, participants of UK Biobank were relatively healthy. Future work may attempt to recall a greater number of participants for follow-up at a future time frame, when the effects of cognitive decline would be more obvious.

5.1.5.2 RNFL and Cognitive Function

UK Biobank is the largest study of its kind, and for the first time, identifies that future decline in cognitive function is associated with thinner retinal nerve fibre layer (RNFL) in a large, healthy community cohort. Those in the lowest two quintiles of baseline RNFL distribution had double the likelihood of a decline in cognitive function over a three year follow-up interval, compared with those in the top RNFL quintile (Table 4.37). As was expected, there was a strong, consistent relationship between thinner RNFL and poorer

cognition in cross-sectional data. A further novel finding was of an incremental relationship between thinner RNFL and poorer cognition in the longitudinal data (Figure 4.37). The findings show that thinner RNFL is a potential indicator for current impaired cognition, and may predict an increased risk of future decline in cognitive function. These cognitive deficits and decline spanned a range of functional domains.

An important limitation of the current study is that although UK Biobank participants were enrolled from a sample representing a cross section of the UK population, the response rate was low. Consequently, the representativeness of the study is limited, participants were more white, middle class and educated. This means that rates of cognitive impairment identified here will not necessarily be the same as those in the UK population, or of another Western European or North American population. However, while the study may not reflect the full UK population, the associations that have been identified are unlikely to be the result on an intrinsic bias in the data, and the overall conclusions should be taken seriously, particularly among those of Western European descent.

The vast number of participants enrolled in UK Biobank required that a balance be struck between detailed, in-depth full clinical testing and the need to complete a cognitive assessment efficiently on hundreds of thousands of participants. Whether the resultant, very large cognitive dataset is strengthened or weakened by this approach is unclear. The individual tests used in this study have been validated by a separate group (Lyall et al 2016). By using tests sensitive to the population range of performance, decline across the population can be detected. This increases the sensitivity of the study

to detect change, and its relevance to population-based early disease stage screening. From an aetiological perspective, this study does not attempt to identify specific cognitive domains linked with RNFL thickness. The range of tests available to test the hypothesis include basic mechanisms such as processing speed (reaction time) and high level functions such as intelligence (reasoning). As such they are suitable for investigating an overall association between cognition and retinal thickness measures. Further work would be required to identify the underlying mechanisms linking RNFL thickness to specific cognitive domains

Findings from the current study are consistent with those from several previous studies of people with established disease. Hinton described an association between dementia and thinner RNFL (Hinton et al 1986). Others have made similar observations in mild, moderate and severe cognitive impairment in cases series (Moreno-Ramos et al 2013, Garcia-Martin et al 2014, Shi et al 2014, Kesler et al 2011, Whitson et al 2015, Gao et al 2015). Thinner RNFL has been recorded in Parkinson's disease (Inzelberg et al 2004), and Lewy body dementia (Moreno-Ramos et al 2013).

Although the bulk of previous data suggesting an association between RNFL thickness and cognition comes from case series, two studies have identified a cross-sectional association between thinner RNFL and poorer cognitive function in community based cohorts, one in a geographically- and genetically-isolated population in the Netherlands (van Koolwijk et al 2009), the other in the EPIC Norfolk cohort in the UK (Khawaja et al 2016). In the EPIC cohort of 8,623 people, thinner RNFL was associated with poorer scores from cognitive tests assessing global function, recognition, learning, episodic

memory, and premorbid intelligence. While EPIC Norfolk described a similar relationship as the current study, the cross-sectional associations were of small effect size, with RNFL thickness appearing to be of little use as a predictive test for cognitive function (Khawaja et al 2016). In contrast, the relationship between baseline RNFL and future cognitive decline in the current study is stronger. A possible explanation for this is that RNFL measurements in EPIC were generated using scanning laser ophthalmoscopy, which is less precise than OCT, as it does not directly measure RNFL thickness. Another recent community-based study assessed a cohort of Chinese people linked poorer cognitive function to thinner sub-foveal choroidal thickness.[29] Choroidal thickness measures were not available in this study because of differences in scanning technology, but it adds weight to the concept that ophthalmic imaging can detect features associated with poorer cognitive function.

Of particular interest and relevance are results from a small, prospective study which examined the longitudinal trends in RNFL thickness in a mixed group of 78 people with normal or mildly impaired cognition over a two year period in Shanghai, Peoples' Republic of China (Shi et al 2014). Sixty retained stable cognitive function, while 18 (23%) suffered a cognitive decline and were then diagnosed as suffering mild cognitive impairment (n=8) or AD (n=10). Using retinal OCT to measure RNFL (as I have done), they observed greater reduction of RNFL thickness among those showing a cognitive decline than the stable participants (−11.0 ± 12.8 (mean ± SD) μm versus -0.4 ± 15.7 μm ($p = 0.009$).

In this study, participants who reported neurological, diabetic, and ocular diseases were excluded, and only people with good visual acuity were included, because of the well-recognised impact these conditions have on RNFL measurements. Consequently, the results are more representative of a pre-morbid population, further strengthening the principle of an association between a thin RNFL and cognitive decline. Others have reported that markers of ill-health, particularly cardiovascular, are risk factors for future cognitive decline – such risk factors include atrial fibrillation, diabetes, heart failure, intermittent claudication, previous stroke and frailty markers such as poor exercise tolerance (Tilvis et al 2004, Marquis et al 2002, Liew et al 2009). The current study does not take these risk factors into account, but they could potentially be considered in future studies.

There was an incremental relationship between a progressively thinner baseline RNFL and a future decline spanning different cognitive domains. Gao, et al. sought, but did not find such a correlation between retinal features and severity of cognitive impairment (Gao et al 2015). One possible explanation is that they used the Mini-Mental State Examination (MMSE) as the index of cognitive impairment, which is likely to be insensitive to subtle early changes (Hinton et al 1986). The association between baseline RNFL and baseline cognitive scores appears to be curvilinear, showing a threshold effect with greater deficit shown in RNFL quintiles one and two (Figure 4.54). Evidence for a curvilinear association between baseline RNFL and future cognitive decline was less convincing (Figure 4.55), although the number of observations was smaller by a factor of 30.

One potential concern with the current study is that multiple statistical tests may lead to significant findings purely by chance; however, our work is supported by results from the Rotterdam Study, published in the same issue as our work (Mutlu et al 2018). 3289 people were analyzed over 5 years, among whom 41 people (1.2%) had existing dementia and 86 people (2.6%) developed dementia over a 5-year time period. A significant association was found between thinner baseline RNFL and incident dementia, but not prevalent dementia, consistent with our findings. While the size of the Rotterdam study was smaller than UK Biobank, the screening methods for dementia were more extensive, including the Mini Mental Status Examination, Geriatric Mental State organic level, and the Cambridge Examination for Mental Disorders of the Elderly, as well as continuous monitoring through electronic linkage with medical records (Mutlu et al 2018). The repeatability of results between two separate longitudinal studies among different populations supports the idea that the findings are not a statistical anomaly, but a significant finding worth further investigation.

Some have argued against there being retinal involvement in generalised neurodegenerative disease (Curcio et al 2993, Davies et al 1995, Parisi et al 2001, Kergoat et al 2001a, Kergoat et al 2001b). Van Koolwijk *et. al.* proposed that while there may be an association between RNFL thickness and cognitive function, it is not sufficient to explain variance in cognitive test scores, and therefore is not a useful predictor of cognitive ability (van Koolwijk et al 2009). UK Biobank cohort benefits from large numbers of participants, and consequently has greater statistical power. Statistical significance is not equivalent to clinical relevance. However, while the bulk of previous research has focused on later stage cognitive impairment and on older participants, my

findings suggest the predictive potential of RNFL thickness measurement in a relatively younger and healthier group of people. Furthermore, the preponderance of white people of relative socioeconomic prosperity (as demonstrated by the favourable mean Townsend deprivation index, Table 4.35) suggests that these results are even more applicable to a "low risk" group, and provide a conservative estimate of the association. More recently, preclinical and translational data revealed that in at least one of the neurodegenerative dementias, frontotemporal dementia caused by progranulin haploinsufficiency, retinal layer changes are indeed related to a demonstrable pathological substrate (Ward et al 2017). Nevertheless, in response to Van Koolwijk *et. al.*, it would be unlikely for any single predictive test to be used in isolation. This study adds weight to the argument of an association between neurodegenerative processes affecting the brain and the eye, and indicates that OCT measurement of the RNFL could provide a non-invasive, relatively low-cost and time-efficient predictive tool.

There can now be little doubt that thinner RNFL is associated with adverse cognitive function. These data also suggest that RNFL thinning precedes cognitive decline in many people, and predicts cognitive deterioration. Wide availability of OCT technology in ophthalmic and optometric practices may be beneficial for general uptake of this potential predictive test. However, one must be careful in its interpretation, to avoid an unnecessary psychological burden to people who may not ultimately experience cognitive decline. Further, attempting to risk-stratify people would be most appropriate if there is a viable treatment or preventative measure. Additional research is required to define a possible role for these observations in health policy and to determine the relevance at an individual level. It is unclear whether RNFL thinning continues even as

cognitive decline occurs, or whether it is a precursor to cognitive deterioration. While UK Biobank did perform follow-up OCT testing, later retinal measures were not available for this analysis. Future research may focus on longitudinal RNFL changes relative to cognitive function. It may be that RNFL imaging is more useful for certain demographic, racial or medical sub-groups. I believe it is plausible that a thinner RNFL is a marker of a currently ill-defined clinical syndrome, which includes cognitive decline.

The finding that a thinner RNFL is associated with significant future cognitive decline in a large cohort of people aged 40 to 69 years, drawn from communities around the UK, consolidates the case for regarding retinal anatomical measures as a useful predictive tool for identifying those at risk of future cognitive loss. The potential for OCT measurement of retinal layers as a predictor of cognitive decline is particularly attractive because it is rapid, non-invasive and widely available, with high potential for uptake.

5.2 Summary

The major conclusions from this body of research may be summarized as follows:

1. OCT can be used to analyse a large number of eyes. UK Biobank obtained OCT measurements from eyes of 67,321 people. This study used OCT to image a large cohort, and through use of automated segmentation, the images were analysed to generate novel findings. Over 33,000 images were selected for analysis. The exact number of scans varied depending on the sub-layer analysed, due to quality issues and varying levels of difficulty using automated segmentation. Manual re-grading rejected <1% of images (range 288 of 34572 RPE images to 2 of 33070 RNFL images), a testimony to the reliability of the automated segmentation algorithm that was selected. There are certain layers that remain difficult to segment on OCT, such as the boundary between the ganglion cell layer and inner plexiform layer, which is why they were analysed as a single complex. Nevertheless, OCT proved itself to be a powerful tool for retinal studies of large cohorts.
2. Retinal sub-layers show variations according to demographic factors such as age, ethnicity, and gender. For all layers analysed, there is an age-related association between thinner retinal sub-layers and older age. Ethnicity affects retinal thickness differently for different sub-layers, with black people having thicker RPE than white people, but showing the opposite result for the remaining sub-layers analysed. This may explain the higher prevalence of disease among certain

ethnicities, such as macular degeneration (higher among white people, who tend of have thinner RPE) and glaucoma (higher among black people who have thinner RNFL). Sex-related differences are a bit more complex. In the photoreceptor layer, women appear to have thinner photoreceptor layers than men at all except two subfields (central and outer superior). However, for the remaining subfields analysed, there is not a consistent difference across all subfields; rather there appears to be variation in distribution. RPE is thicker at central and inner superior subfields among women, but thinner or the same at remaining subfields. GCL-IPL and RNFL appears thicker among women at outer subfields, but thinner at inner subfields. Height was also included in the analysis, as a potential confounder with sex, and results remained consistent. The significance of distribution differences of retinal thickness at different subfields is unclear. However, one needs to take this into account if selecting a single subfield for analysis.

3. Physiological and lifestyle differences are also associated with variation in retinal thickness. An interesting finding was that higher IOP was significantly associated with thinner RPE, but was not associated with thickness of GCL-IPL or RNFL. This is counterintuitive regarding expected relationships between IOP, glaucoma and the retinal layers affected. Whether this finding has clinical significance remains to be seen, but is certainly an interesting area for future research. Additionally, it appears that refractive status affects retinal thickness, with inner retinal layers thicker and outer retinal layers thinner with higher myopia. Possible explanations include differences in axial length-related compression of inner layers and stretching of outer layers, versus magnification-related differences. Smoking,

blood pressure, and BMI were analysed to assess for association with RPE and photoreceptor layers thickness. None of these variables showed a statistically significant association with RPE thickness. In contrast, regular smoking and higher BMI were significantly associated with thinner photoreceptor layer. Blood pressure was not significant after controlling for other variables in multivariable analysis of photoreceptor layer. For GCL-IPL and RNFL layers, associations with smoking/blood pressure/BMI were sought in preliminary analysis, but for the purposes of main analysis, interest shifted to education and socioeconomic deprivation, given the interest in a potential relationship with cognitive function. For GCL-IPL, inner subfields were significantly thinner in those with lower education and greater socioeconomic deprivation. This effect was present at outer subfields, but did not reach statistical significance, possibly because the outer subfields are thinner than inner, so changes may be more subtle. Likewise, RNFL was thinner in those with lower educational attainment. In contrast, socioeconomic deprivation was not significantly associated with RNFL thickness.

4. The relationships with cognitive function are likely to be the most important aspects of this work, with RNFL being associated not only with current cognitive function, but also potentially being predictive of future cognitive decline. The relationship between GCL-IPL and cognitive function was also examined; while results were consistent, much of it was either not statistically significant, or was not significant after adjusting for potential confounders. All cognitive tests were significantly associated with RNFL thickness, and remained consistent after adjusting for potential confounders (demographic, ocular, physiologic, and lifestyle factors). People with the thinnest RNFL were 11% more likely to fail at

least one test at baseline, and almost twice as likely to have a cognitive deficit (fail 2 or more tests). Further, those in the two thinnest RNFL quintiles were twice as likely to have worsening on at least one cognitive test after 3 years, with an 18% increased risk per each quintile thinner RNFL. This is a major finding, and could potentially guide future research into cognitive function as our population ages.

5.3 Future Work

UK Biobank is a massive database, with huge potential. It's main design and function is to identify associations among common disorders. Obviously, one could analyze additional variables such as glucose levels, HA1c, and food logs, together with retinal thickness. These variables could be analyzed using similar algorithm as current work, making further analysis relatively rapid.

Alternatively, separate study could address questions raised by the current analysis. For instance, a significant association was identified between IOP and RPE thickness, but no association between IOP and RNFL thickness among people without ocular disease. To our knowledge, this is the first report of an association between IOP and RPE thickness. Validation of the current work could be attempted using data excluded from the current study (i.e., random selection of opposite eye). If results are confirmed, further study of the relationship between RPE thickness and glaucoma would be to measure RPE thickness among healthy individuals, normal tension glaucoma, and primary open angle glaucoma to detect differences amongst groups.

Macular degeneration is another important area for future research, as it is the leading cause for blindness in developed countries. I found thinner RPE among whites as compared to black people. This is consistent with risk of macular degeneration among the two groups. To my knowledge, no one has demonstrated that thinner baseline RPE is associated with future risk of macular degeneration. As 10 years have passed since UK

Biobank began collecting macular OCT, one could potentially answer this question now, by re-assessing this population for development of macular degeneration through fundus imaging (OCT or photos) or questionnaire, and comparing with baseline RPE thickness. If thinner baseline RPE is associated with future risk of macular degeneration, this could have implications for prevention and treatment. Work is already being conducted to treat macular degeneration by transplanting RPE stem cells (Mehat et al 2018, Takagi et al 2019). Researchers could potentially transplant stem cells into the retinas of those at highest risk of blindness from macular degeneration as a preventative measure.

Cognitive function is arguably the most interesting finding of this body of work. Within UK Biobank, future work may consider follow-up OCT analysis together with future cognitive decline. At the time of writing, these data were collected, but not yet available for analysis. Outside of UK Biobank, the current study informs future research, with RNFL being a potential marker for predicting cognitive decline.

An interesting study would be analyzing RNFL thickness measurements in a high-risk group; specifically, football players, both American and European (soccer), where there has been concern and media attention related to the risk of concussive brain injury and early-onset dementia (Schneider 2019, Ling et al 2017). The former is particularly suited for study, as college- and professional-level players are filmed both in practice and in competition, so impacts to the head can be recorded. The American National Football League has committed $100 million toward the study of concussions and head injuries (Maske 2016). There is an existing concussion protocol including evaluation by a

neurologist during games (Stites 2018). One could measure RNFL thickness on OCT at baseline, as well as yearly follow-up, together with cognitive function testing. Age and gender matched controls could be recruited from lower-impact sports such as baseball. Weight matching will be important, and analysis needs to be controlled for BMI. The potential for such work is exciting – if one day we could predict people at risk for cognitive decline, prevent further decline through behavior modification (such as "benching" a player for a few games), or even develop therapeutics.

This work with UK Biobank has been exciting and may lead to further work to explore the relationship between retina and ocular disease, and could potentially be applied toward improving future cognitive function.

SECTION VI:

REFERENCES

Adhi M, Aziz S, Muhammad K, Adhi MI. Macular thickness by age and gender in healthy eyes using spectral domain optical coherence tomography. PLoS One. 2012;7(5):e37638.

Akashi A, Kanamori A, Nakamura M, et al. The ability of macular parameters and circumpapillary retinal nerve fiber layer by three OCT instruments to diagnose highly myopic glaucoma. Invest Ophthalmol Vis Sci. 2013;54(9):6025-32.

Alamouti B, Funk J. Retinal thickness decreases with age: an OCT study. Br J Ophthalmol. 2003;87(7):899 –901.

Alasil T, Wang K, Keane PA, et al. Analysis of normal retinal nerve fiber layer thickness by age, sex, and race using spectral domain optical coherence tomography. J Glaucoma. 2013;22(7):532–541.

Alencar LM, Medeiros FA & Weinreb R (2007): Progressive localized retinal nerve fiber layer loss following a retinal cotton wool spot. Semin Ophthalmol 22: 103–104.

Altay L, Jahn C, Arikan Yorgun M, Caramoy A, Schick T, Hoyng CB, den Hollander AI, Fauser S. Alteration of retinal layers in healthy subjects over 60 years of age until nonagenarians. Clin Ophthalmol. 2017 Aug 16;11:1499-1503.

Anderson DR. Collaborative normal tension glaucoma study. Current opinion in ophthalmology. 2003: 86-90.

Arcinue CA, Bartsch DU, El-Emam SY, Ma F, Doede A, Sharpsten L, Gomez ML, Freeman WR. Retinal Thickening and Photoreceptor Loss in HIV Eyes without Retinitis. PLoS One. 2015 Aug 5;10(8):e0132996.

Asaoka R, Murata H, Yanagisawa M, Fujino Y, Matsuura M, Inoue T, Inoue K, Yamagami J. The association between photoreceptor layer thickness measured by optical coherence tomography and visual sensitivity in glaucomatous eyes. PLoS One. 2017 Oct 12;12(10):e0184064.

Baek MJ, Kim K, Park YH, Kim S. The validity and reliability of the min-mental stae examination-2 for detecting mild cognitive impairment and Alzheimer's disease in a Korean population. PLoS One. 2016 Sep 26;11(9):e0163792.

Bakrania K, Edwardson CL, Khunti K, Bandelow S, Davies MJ, Yates T. Associations Between Sedentary Behaviors and Cognitive Function: Cross-Sectional and Prospective Findings From the UK Biobank. Am J Epidemiol. 2018 Mar 1;187(3):441-454.

Balazsi AG, Rootman J, Drance SM, Schulzer M, Douglas GR. The effect of age on the nerve fiber population of the human optic nerve. Am J Ophthalmol. 1984;97(6):760 – 766.

Barry Cense, Nader Nassif, Teresa Chen, Mark Pierce, Seok-Hyun Yun, B. Park, Brett Bouma, Guillermo Tearney, and Johannes de Boer. Ultrahigh-resolution high-speed

retinal imaging using spectral-domain optical coherence tomography. Opt. Express 2004;12: 2435-2447.

Bateman RJ, Xiong C, Benzinger TL, Fagan AM, Goate A, et al. Clinical and biomarker changes in dominantly inherited Alzheimer's disease. N Engl J Med. 2012 Aug 30;367(9):795-804.

Blanks JC, Hinton DR, Sadun AA, Miller CA. Retinal ganglion cell degeneration in Alzheimer's disease. Brain Res 1989; 501(2): 364–372.

Bloch E, Yonova-Doing E, Jones-Odeh E, Williams KM, Kozareva D, Hammond CJ. Genetic and Environmental Factors Associated With the Ganglion Cell Complex in a Healthy Aging British Cohort. JAMA Ophthalmol. 2017 Jan 1;135(1):31-38.

Bowd, C., Weinreb, R.N., Williams, J.M. and Zangwill, L.M. The retinal nerve fiber layer thickness in ocular hypertensive, normal, and glaucomatous eyes with optical coherence tomography. Archives of ophthalmology. 2000;118(1), pp.22-26.

Bourne RRA, Jonas JB, Bron AM, Cicinelli MV, Das A, et al. Prevalence and causes of vision loss in high-income countries and in Eastern and Central Europe in 2015: magnitude, temporal trends and projections. Br J Ophthalmol. 2018 May;102(5):575-585.

Bourne R, Resnikoff S, Ackland P. Vision 2020: Right to Sight. GBVI – Global Cause Estimates. Available at: http://atlas.iapb.org/global-burden-vision-impairment/gbvi-global-cause-estimates/. Accessed June 19, 2018.

Breteler MM, van Swieten JC, Bots ML, Grobbee DE, Claus JJ, et al. Cerebral white matter lesions, vascular risk factors, and cognitive function in a population-based study: the Rotterdam Study. Neurology. 1994 Jul;44(7):1246-52.

Brookmeyer R, Johnson E, Ziegler-Graham K, Arrighi HM. Forecasting the global burden of Alzheimer's disease. Alzheimer's Dement 2007;3(3):186–91.

Cabrera Fernández D, Salinas HM, Puliafito CA. Automated detection of retinal layer structures on optical coherence tomography images. Opt. Express. 2005;13(25):10200–10216.

Cajal, S.R. (1892) The Structure of the Retina. (Transl. Thorpe, S.A. and Glickstein, M.), Thomas, Springfield, Il. 1972.

Canny J. A computational approach to edge detection. IEEE Trans. Pattern Anal. Mach. Intell. 1986;8(6):679–698.

Caramoy A, Droege KM, Kirchhof B, Fauser S. Retinal layers measurements in healthy eyes and in eyes receiving silicone oil-based endotamponade. Acta Ophthalmol. 2014;92(4):e292–e297.

Caramoy A, Foerster J, Allakhiarova E, et al. Spectral-domain optical coherence tomography in subjects over 60 years of age, and its implications for designing clinical trials. Br J Ophthalmol. 2012;96(10): 1325–1330.

CATT Research Group, Martin DF, Maguire MG, Ying GS, Grunwald JE, Fine SL, Jaffe GJ. Ranibizumab and bevacizumab for neovascular age-related macular degeneration. N Engl J Med. 2011 May 19;364(20):1897-908.

Chan A, Duker JS, Ko TH, Fujimoto JG, Schuman JS. Normal macular thickness measurements in healthy eyes using Stratus optical coherence tomography. Arch Ophthalmol. 2006;124(2): 193–198.

Chan CM, Yu JH, Chen LJ, et al. Posterior pole retinal thickness measurements by the retinal thickness analyzer in healthy Chinese subjects. Retina. 2006;26(2):176 –181.

Chan MP, Grossi CM, Khawaja AP, Yip JL, Khaw KT, Patel PJ, Khaw PT, Morgan JE, Vernon SA, Foster PJ; UK Biobank Eye and Vision Consortium. Associations with Intraocular Pressure in a Large Cohort: Results from the UK Biobank. Ophthalmology. 2016 Apr;123(4):771-82.

Cheung CY, Ong YT, Hilal S, Ikram MK, Low S, Ong YL, et al. Retinal ganglion cell analysis using high-definition optical coherence tomography in patients with mild cognitive impairment and Alzheimer's disease. J Alzheimer's Dis 2015;45(1):45–56.

Cheung, C.Y., Ong, S., Ikram, M.K., Ong, Y.T., Chen, C.P., Venketasubramanian, N., Wong, T. Retinal vascular fractal dimension is associated with cognitive dysfunction. J. Stroke Cerebrovasc. Dis. 2014;23:43-50.

Chui TY, Song H, Clark CA, Papay JA, Burns SA, Elsner AE. Cone photoreceptor packing density and the outer nuclear layer thickness in healthy subjects. Invest Ophthalmol Vis Sci. 2012 Jun 14;53(7):3545-53.

Chui TY, Thibos LN, Bradley A & Burns SA. The mechanisms of vision loss associated with a cotton wool spot. Vision Res. 2009;49:2826–2834.

Cioffi GA, Durcan FJ, Girkin CA, Gross RL, Netland PA, Samples JR, Samuelson TW, O'Connell SS, Barton K. Basic and Clinical Science Course Section 10: Glaucoma. San Francisco, CA: American Academy of Ophthalmology, 2010. Print.

Coleman AL, Miglior S. Risk factors for glaucoma onset and progression. Surv Ophthalmol. 2008;53 Suppl1:S3-10.

Comas-Herrera A, Wittenberg R, Pickard L, Knapp M, MRC-CFAS. Cognitive impairment in older people: its implications for future demand for services and costs. PSSRU Discussion Paper 2005; 1728.

Coppola G, Di Renzo A, Ziccardi L, Martelli F, Fadda A, Manni G, et al. Optical Coherence

Tomography in Alzheimer's Disease: A Meta-Analysis. PLoS One 2015;10(8):e0134750.

Cruz-Herranz A, Balk LJ, Oberwahrenbrock T, Saidha S, Martinez-Lapiscina EH, et al. The APOSTEL recommendations for reporting quantitative optical coherence tomography studies. Neurology. 2016 ;86:2303-2309.

Tewarie P, Balk L, Costello F, Green A, Martin R, Schippling S, Petzold A. The OSCAR-IB consensus criteria for retinal OCT quality assessment. PLoS One. 2012;7(4):e34823.

Cunea A, Powner MB, Jeffery G. Death by color: differential cone loss in the aging mouse retina. Neurobiol Aging. 2014 Nov;35(11):2584-2591.

Curcio CA, Drucker DN. Retinal ganglion cells in Alzheimer's disease and aging. Ann Neurol 1993;33(3):248–57.

Curcio CA, Messinger JD, Sloan KR, Mitra A, McGwin G, Spaide RF. Human chorioretinal layer thicknesses measured in macula-wide, high-resolution histologic sections. Invest Ophthalmol Vis Sci. 2011 June;52(7):3943-54.

Curcio CA, Millican CL, Allen KA, Kalina RE. Aging of the human photoreceptor mosaic: evidence for selective vulnerability of rods in central retina. Invest Ophthalmol Vis Sci. 1993 Nov;34(12):3278-96.

Davies DC, McCoubrie P, McDonald B, Jobst KA. Myelinated axon number in the optic nerve is unaffected by Alzheimer's disease. Br J Ophthalmol 1995;79(6):596–600.

de Jong, F.J., Schrijvers, E.M., Ikram, M.K., Koudstaal, P.J., de Jong, P.T., Hofman, A., Vingerling, J.R., Breteler, M.M. Retinal vascular caliber and risk of dementia: the Rotterdam study. Neurology. 2011;76:816-821.

Delcourt C, Le Goff M, von Hanno T, Mirshahi A, Khawaja AP, et al. The Decreasing Prevalence of Nonrefractive Visual Impairment in Older Europeans: A Meta-analysis of Published and Unpublished Data. Ophthalmology. 2018 Aug;125(8):1149-1159.

Demirkaya N, van Dijk HW, van Schuppen SM, Abràmoff MD, Garvin MK, Sonka M, Schlingemann RO, Verbraak FD. Effect of age on individual retinal layer thickness in normal eyes as measured with spectral-domain optical coherence tomography. Invest Ophthalmol Vis Sci. 2013 Jul 22;54(7):4934-40.

Ding, J., Strachan, M.W., Fowkes, F.G., Wong, T.Y., Macgillivray, T.J., Patton, N., Gardiner, T.A., Deary, I.J., Price, J.F. Association of retinal arteriolar dilatation with lower verbal memory: the Edinburgh Type 2 Diabetes Study. Diabetologia. 2011;54:1653-1662.

Dorey CK, Wu G, Ebenstein D, Garsd A, Weiter JJ. Cell loss in the aging retina. Relationship to lipofuscin accumulation and macular degeneration. Invest Ophthalmol Vis Sci. 1989;30(8):1691–1699.

Eriksson U, Alm A. Macular thickness decreases with age in normal eyes: a study on the

macular thickness map protocol in the Stratus OCT. Br J Ophthalmol. 2009;93(11):1448–1452.

Farsiu S, Chiu SJ, O'Connell RV, Folgar FA, Yuan E, Izatt JA, Toth CA; Age-Related Eye Disease Study 2 Ancillary Spectral Domain Optical Coherence Tomography Study Group. Quantitative classification of eyes with and without intermediate age-related macular degeneration using optical coherence tomography. Ophthalmology. 2014 Jan;121(1):162-172.

Ferri CP, Prince M, Brayne C, Brodaty H, Fratiglioni L, et al. Global prevalence of dementia: a Delphi consensus study. Lancet. 2005 Dec 17;366(9503):2112-7.

Figueiredo S and Salter K. Zeltzer L, Korner-Bitensky N, Sitcoff E, editors. Stroke Engine: Cambridge Cognition Examination (CAMCOG). 2009 Mar 18. Available at: https://www.strokengine.ca/en/assess/camcog/. Accessed 16 July 2018.

Firth J, Firth JA, Stubbs B, Vancampfort D, Schuch FB, et al. Association Between Muscular Strength and Cognition in People With Major Depression or Bipolar Disorder and Healthy Controls. JAMA Psychiatry. 2018 Jul 1;75(7):740-746.

Fisher DE, Klein BE, Wong TY, Rotter JI, Li X, Shrager S, Burke GL, Klein R, Cotch MF. Incidence of Age-Related Macular Degeneration in a Multi-Ethnic United States Population: The Multi-Ethnic Study of Atherosclerosis. Ophthalmology. 2016 Jun;123(6):1297-308.

Fisher JB, Jacobs DA, Markowitz CE, Galetta SL, Volpe NJ, et al. Relation of visual function to retinal nerve fiber layer thickness in multiple sclerosis. Ophthalmology. 2006;113(2):324-32.

Forte R, Cennamo GL, Finelli ML, de Crecchio G. Comparison of time domain Stratus OCT and spectral domain SLO/OCT for assessment of macular thickness and volume. Eye (Lond). 2009 Nov;23(11):2071-8.

Francoz M, Fenolland JR, Giraud JM, El Chehab H, Sendon D, May F, et al. Reproducibility of macular ganglion cell-inner plexiform layer thickness measurement with cirrus HD-OCT in normal, hypertensive and glaucomatous eyes. Br J Ophthalmol. 2014;98(3):322–8.

Friedman DS, O'Colmain BJ, Muñoz B, Tomany SC, McCarty C, et al. Prevalence of age-related macular degeneration in the United States. Arch Ophthalmol. 2004 Apr;122(4):564-72.

Friedman E, Ts'o MO. The retinal pigment epithelium. II. Histologic changes associated with age. Arch Ophthalmol 1968;79:315–320.

Gao H, Hollyfield JG. Aging of the human retina: differential loss of neurons and retinal pigment epithelial cells. Invest Ophthalmol Vis Sci. 1992;33(1):1–17.

Gao L, Liu Y, Li X, Bai Q, Liu P. Abnormal retinal nerve fiber layer thickness and macula lutea in patients with mild cognitive impairment and Alzheimer's disease. Arch Gerontol Geriatr. 2015;60(1):162–7.

Garcia-Martin ES, Rojas B, Ramirez AI, de Hoz R, Salazar JJ, Yubero R, et al. Macular thickness as a potential biomarker of mild Alzheimer's disease. Ophthalmology 2014;121(5):1149–1151.e3.

Garvin MK, Abramoff MD, Kardon R, Russell SR, Wu X, Sonka M. Intraretinal layer segmentation of macular optical coherence tomography images using optimal 3-D graph search. IEEE Trans. Med. Imaging. 2008;27(10):1495–1505.

GBD 2015 Neurological Disorders Collaborator Group. Global, regional, and national burden of neurological disorders during 1990-2015: a systematic analysis for the Global Burden of Disease Study 2015. Lancet Neurol. 2017;16(11):877-897.

Girkin CA, McGwin G Jr, Sinai MJ, Sekhar GC, Fingeret M, et al. Variation in optic nerve and macular structure with age and race with spectral-domain optical coherence tomography. Ophthalmology. 2011;118(12):2403-8.

Gobel W, Hartmann F, Haigis W. Determination of retinal thickness in relation to the age and axial length using optical coherence tomography. Ophthalmologe. 2001;98(2):157–162.

Gomez ML, Mojana F, Bartsch DU & Freeman WR (2009): Imaging of long-term retinal damage after resolved cotton wool spots. Ophthalmology 116: 2407–2414.

Guedes V, Schuman JS, Hertzmark E, Wollstein G, Correnti A, et al. Optical coherence tomography measurement of macular and nerve fiber layer thickness in normal and glaucomatous human eyes. Ophthalmology. 2003 Jan;110(1):177-89.

Harwerth RS, Wheat JL. Modeling the effects of aging on retinal ganglion cell density and nerve fiber layer thickness. Graefes Arch Clin Exp Ophthalmol. 2008;246:305–314.

Hamer M, Sharma N, Batty GD. Association of objectively measured physical activity with brain structure: UK Biobank study. J Intern Med. 2018 May 18. [Epub ahead of print]

Hammes, H.P., Feng, Y., Pfister, F., Brownlee, M. Diabetic retinopathy: targeting vasoregression. Diabetes 2011;60:9-16.

Healey PR, Mitchell P, Smith W, Wang JJ. The influence of age and intraocular pressure on the optic cup in a normal population. J Glaucoma. 1997 Oct;6(5):274-8.

Hebert LE, Scherr PA, Bienias JL, Bennett DA, Evans DA. Alzheimer disease in the US population: prevalence estimates using the 2000 census. Arch Neurol 2003;60(8):1119–22.

Hebert LE, Weuve J, Scherr PA, Evans DA. Alzheimer disease in the United States (2010-2050) estimated using the 2010 census. Neurology 2013;80(19):1778–83.

Hinton DR, Sadun AA, Blanks JC, Miller CA. Optic-nerve degeneration in Alzheimer's disease. N Engl J Med. 1986;315(8):485–7.

Hood DC, Harizman N, Kanadani FN, Grippo TM, Baharestani S, Greenstein VC, Liebmann JM, Ritch R. Retinal nerve fibre thickness measured with optical coherence tomography accurately detects confirmed glaucomatous damage. Br J Ophthalmol. 2007;91:905-907.

Horn FK, Kaltwasser C, Jünemann AG, Kremers J, Tornow RP. Objective perimetry using a four-channel multifocal VEP system: correlation with conventional perimetry and thickness of the retinal nerve fibrelayer. Br J Ophthalmol. 2012; 96:554-559.

How low-coherence interferometry works. Available at: https://www.novacam.com/technology/how-lci-works/. Accessed 29 May 2018.

Huang D, Swanson EA, Lin CP, Schuman JS, Stinson WG, et al. Optical coherence tomography. Science. 1991 Nov 22;254(5035):1178-81.

Huppert FA, Brayne C, Gill C, Paykel ES, Beardsall L. CAMCOG--a concise neuropsychological test to assist dementia diagnosis: socio-demographic determinants in an elderly population sample. Br J Clin Psychol. 1995 Nov;34 (Pt 4):529-41.

Inzelberg R, Ramirez JA, Nisipeanu P, Ophir A. Retinal nerve fiber layer thinning in Parkinson disease. Vision Res. 2004;44(24):2793–7.

Iseri PK, Altinas O, Tokay T, Yuksel N (2006) Relationship between cognitive impairment and retinal morphological and visual functional abnormalities in Alzheimer disease. J Neuroophthalmol 26: 18–24.

Ishikawa H, Stein DM, Wollstein G, Beaton S, Fujimoto JG, Schuman JS. Macular segmentation with optical coherence tomography. Invest. Ophthalmol. Vis. Sci. 2005;46(6):2012–2017.

Iwasaki M, Inomata H. Lipofuscin granules in human photoreceptor cells. Invest Ophthalmol Vis Sci. 1988 May;29(5):671-9.

Jampel H, Vitale S, Ding Y, Knezevich F 3rd, Quigley H, Zeimer R. Retinal thickness in eyes of older normal individuals and its implication for the diagnosis of glaucoma. J Glaucoma. 2009;18(1):37-43.

Jiang H, Liu Y, Wei Y, Shi Y, Wright CB, Sun X, Rundek T, Baumel BS, Landman J, Wang J. Impaired retinal microcirculation in patients with Alzheimer's disease. PLoS One. 2018;13(2):e0192154.

Jonas JB. Global prevalence of age-related macular degeneration. Lancet Glob Health. 2014 Feb;2(2):e65-6.

Jonas JB, Schmidt AM, Muller-Bergh JA, Schlotzer-Schrehardt UM, Naumann GO. Human optic nerve fiber count and optic disc size. Invest Ophthalmol Vis Sci. 1992;33(6):2012–2018.

Jonas JB, Wang YX, Wei W Bin, Zhu LP, Shao L, Xu L. Cognitive Function and Subfoveal Choroidal Thickness: The Beijing Eye Study. Ophthalmology 2016;123(1):220–2.

Kajifi V, Považay B, Hermann B, Hofer B, Marshall D, Rosin PL, Drexler W. Robust segmentation of intraretinal layers in the normal human fovea using a novel statistical model based on texture and shape analysis. Opt. Express. 2010;18(14):14730–14744.

Kanai K, Abe T, Murayama K, Yoneya S. Retinal thickness and changes with age. Nippon Ganka Gakkai Zasshi. 2002;106(3): 162–165.

Kantarci, K. Magnetic resonance markers for early diagnosis and progression of Alzheimer's disease. Expert Rev. Neurother. 2005;5:663-670.

Karampelas M, Sim DA, Keane PA, Papastefanou VP, Sadda SR, Tufail A, Dowler J. Evaluation of retinal pigment epithelium-Bruch's membrane complex thickness in dry age-related macular degeneration using optical coherence tomography. Br J Ophthalmol. 2013 Oct;97(10):1256-61.

Kass MA, Heuer DK, Higginbotham EJ, Johnson CA, Keltner JL, et. al. The Ocular Hypertension Treatment Study: a randomized trial determines that topical ocular hypotensive medication delays or prevents the onset of primary open-angle glaucoma. Archives of ophthalmology. 2002;120(6):701-13.

Keane PA, Grossi CM, Foster PJ, Yang Q, Reisman CA, Chan K, Peto T, Thomas D, Patel PJ; UKBiobank Eye Vision Consortium. Optical Coherence Tomography in the UK Biobank Study - Rapid Automated Analysis of Retinal Thickness for Large Population-Based Studies. PLoS One. 2016 Oct 7;11(10):e0164095. eCollection 2016.

Kenmochi J, Ito Y, Terasaki H. Changes of outer retinal thickness with increasing age in normal eyes and in normal fellow eyes of patients with unilateral age-related macular degeneration. Retina. 2017 Jan;37(1):47-52.

Kergoat H, Kergoat MJ, Justino L, Chertkow H, Robillard A, Bergman H. An evaluation of the retinal nerve fiber layer thickness by scanning laser polarimetry in individuals with dementia of the Alzheimer type. Acta Ophthalmol Scand 2001;79(2):187–91.

Kergoat H, Kergoat MJ, Justino L, Robillard A, Bergman H, Chertkow H. Normal optic nerve head topography in the early stages of dementia of the Alzheimer type. Dement Geriatr Cogn Disord 2001;12(6):359–63.

Kesler A, Vakhapova V, Korczyn AD, Naftaliev E, Neudorfer M. Retinal thickness in

patients with mild cognitive impairment and Alzheimer's disease. Clin Neurol Neurosurg. 2011;113(7):523–6.

Khawaja AP, Chan MP, Broadway DC, Garway-Heath DF, Luben R, Yip JL, Hayat S, Khaw KT, Foster PJ. Laser scanning tomography in the EPIC-Norfolk Eye Study: principal components and associations. Invest Ophthalmol Vis Sci. 2013 Oct 9;54(10):6638-45.

Khawaja AP, Chan MP, Garway-Heath DF, et al. Associations with retinal nerve fiber layer measures in the EPIC-Norfolk Eye Study. Invest Ophthalmol Vis Sci. 2013;54(7):5028-5034.

Khawaja AP, Chan MPY, Yip JLY, Broadway DC, Garway-Heath DF, Luben R, et al. Retinal Nerve Fiber Layer Measures and Cognitive Function in the EPIC-Norfolk Cohort Study. Investig Opthalmol Vis Sci 2016;57(4):1921.

Khawaja AP, Cooke Bailey JN, Wareham NJ, Scott RA, Simcoe M, et al. Genome-wide analyses identify 68 new loci associated with intraocular pressure and improve risk prediction for primary open-angle glaucoma. Nat Genet. 2018 May 21. [Epub ahead of print]

Kim KE, Yoo BW, Jeoung JW, Park KH. Long-term reproducibility of macular ganglion cell analysis in clinically stable glaucoma patients. Invest Ophthalmol Vis Sci. 2015;56(8):4857–64.

Kim NR, Kim JH, Lee J, Lee ES, Seong GJ, Kim CY. Determinants of perimacular inner retinal layer thickness in normal eyes measured by Fourier-domain optical coherence tomography. Invest Ophthalmol Vis Sci. 2011 May 18;52(6):3413-8.

Kingman S. Glaucoma is second leading cause of blindness globally. Bull World Health Organ. 2004 Nov;82(11):887-8.

Klaver CC, Wolfs RC, Vingerling JR, Hofman A, de Jong PT. Age-specific prevalence and causes of blindness and visual impairment in an older population: the Rotterdam Study. Arch Ophthalmol. 1998;116:653-658.

Knight OJ, Girkin CA, Budenz DL, et al. Cirrus OCT Normative Database Study Group. Effect of race, age, and axial length on optic nerve head parameters and retinal nerve fiber layer thickness measured by Cirrus HD-OCT. Arch Ophthalmol. 2012;130:312–318.

Koh JW, Park KH, Kim MS & Kim JM. Localized retinal nerve fiber layer defects associated with cotton wool spots. Jpn J Ophthalmol. 2010;54:296–299.

Koh VT, Tham YC, Cheung CY, et al. Determinants of ganglion cell-inner plexiform layer thickness measured by high definition optical coherence tomography. Invest Ophthalmol Vis Sci. 2012;53:5853–5859.

Kolb H, Fernandez E, Nelson R, editors. Webvision: The Organization of the Retina and Visual System. Salt Lake City (UT): University of Utah Health Sciences Center; 1995-2005

May 01 [updated 2012 Feb 28]. Available at: http://webvision.med.utah.edu/book/part-ii-anatomy-and-physiology-of-the-retina/. Accessed June 19, 2018.

Koozekanani D, Boyer K, Roberts C. Retinal thickness measurements from optical coherence tomography using a Markov boundary model. IEEE Trans. Med. Imaging. 2001;20(9):900–916.

Kunchithapautham K, Atkinson C, Rohrer B. Smoke exposure causes endoplasmic reticulum stress and lipid accumulation in retinal pigment epithelium through oxidative stress and complement activation. J Biol Chem. 2014 May 23;289(21):14534-46.

Lam DS, Leung KS, Mohamed S, et al. Regional variations in the relationship between macular thickness measurements and myopia. Invest Ophthalmol Vis Sci. 2007;48(1):376–382.

Langa KM, Chernew ME, Kabeto MU, et al. National estimates of the quantity and cost of informal caregiving for the elderly with dementia. J Gen Intern Med. 2001;16:770–78.

Lavinsky F, Wollstein G, Tauber J, Schuman JS. The Future of Imaging in Detecting Glaucoma Progression. Ophthalmology. 2017 Dec;124(12S):S76-S82.

Le PV, Zhang X, Francis BA, Varma R, Greenfield DS, Schuman JS, Loewen N, Huang D; Advanced Imaging for Glaucoma Study Group. Advanced Imaging for Glaucoma Study: Design, Baseline Characteristics, and Inter-site Comparison. Am J Ophthalmol.

2015;159(2):393-403.

Lee HM, Lee WH, Kim KN, Jo YJ, Kim JY. Changes in thickness of central macula and retinal nerve fibre layer in severe hypertensive retinopathy: a 1-year longitudinal study. Acta Ophthalmol. 2017 Oct 4.

Leske MC, Heijl A, Hussein M, Bengtsson B, Hyman L, Komaroff E. Factors for glaucoma progression and the effect of treatment: the early manifest glaucoma trial. Archives of ophthalmology. 2003;121(1):48-56.

Leung CK, Yu M, Weinreb RN, et al. Retinal nerve fiber layer imaging with spectral-domain optical coherence tomography: a prospective analysis of age-related loss. Ophthalmology. 2012;119(4):731–737.

Li Y, Wang J, Zhong X, Tian Z, Wu P, Zhao W, Jin C. Refractive error and risk of early or late age-related macular degeneration: a systematic review and meta-analysis. PLoS One. 2014 Mar 6;9(3):e90897.

Liew G, Wong TY, Mitchell P, Cheung N, Wang JJ. Retinopathy predicts coronary heart disease mortality. Heart 2009;95(5):391–4.

Liu S, Ong YT, Hilal S, Loke YM, Wong TY, Chen CL, Cheung CY, Zhou J. The Association Between Retinal Neuronal Layer and Brain Structure is Disrupted in Patients

with Cognitive Impairment and Alzheimer's Disease. J Alzheimers Dis. 2016 Sep 6;54(2):585-95.

Ling H, Morris HR, Neal JW, Lees AJ, Hardy J, Holton JL, Revesz T, Williams DD. Mixed pathologies including chronic traumatic encephalopathy account for dementia in retired association football (soccer) players. Acta Neuropathol. 2017 Mar;133(3):337-352.

Loduca AL, Zhang C, Zelkha R, Shahidi M. Thickness mapping of retinal layers by spectral-domain optical coherence tomography. Am J Ophthalmol. 2010 Dec;150(6):849-55

Luo HD, Gazzard G, Fong A, et al. Myopia, axial length, and OCT characteristics of the macula in Singaporean children. Invest Ophthalmol Vis Sci. 2006;47(7):2773–2781.

Lyall DM, Cullen B, Allerhand M, Smith DJ, Mackay D, et al. Cognitive test scores in UK Biobank: Data reduction in 480,416 participants and longitudinal stability in 20,346 participants. PLoS One. 2016 Apr 25;11(4):e0154222.

Manassakorn A, Chaidaroon W, Ausayakhun S, Aupapong S, Wattananikorn S. Normative database of retinal nerve fiber layer and macular retinal thickness in a Thai population. Jpn J Ophthalmol. 2008;52(6):450–456.

Marina G. Falleti, Paul Maruff, Alexander Collie & David G. Darby. Practice Effects Associated with the Repeated Assessment of Cognitive Function Using the CogState

Battery at 10-minute, One Week and One Month Test-retest Intervals. Journal of Clinical and Experimental Neuropsychology. 2006; 28(7):1095-1112.

Marshall J, Grindle J, Ansell PL, Borwein B. Convolution in human rods: an ageing process. Br J Ophthalmol. 1979 Mar;63(3):181-7.

Maske M. 2016 Sept 14. NFL to Launch New $100 million Concussion Initiatives to Improve Player Safety. Available at: https://www.washingtonpost.com/news/sports/wp/2016/09/14/nfl-to-launch-new-100-million-concussion-initiatives-to-improve-player-safety/?noredirect=on. Accessed 7 Sept 2019.

McKibbin M, Farragher TM, Shickle D. Monocular and binocular visual impairment in the UK Biobankstudy: prevalence, associations and diagnoses. BMJ Open Ophthalmol. 2018 Jan 31;3(1):e000076. eCollection 2018.

Mehat MS, Sundaram V, Ripamonti C, Robson AG, Smith AJ, et al. Transplantation of Human Embryonic Stem Cell-Derived Retinal Pigment Epithelial Cells in Macular Degeneration. Ophthalmology. 2018 Nov;125(11):1765-1775.

Messenio D, Marano G, Gerosa S, Iannelli F, Biganzoli EM. The influence of age on the recovery of the ERG photostress test. Doc Ophthalmol. 2013;126(2):87–97.

Miglior S, Riva I, Guareschi M, et al. Retinal sensitivity and retinal nerve fiber layer thickness measured by optical coherence tomography in glaucoma. Am J Ophthalmol. 2007;144:733–740

Miller BL, Bigio E, Mesulam MM, Bogyo MS, Mackenzie IR, Staropoli JF, Cotman SL, Huang EJ, Gan L, Green AJ. Individuals with progranulin haploinsufficiency exhibit features of neuronal ceroid lipofuscinosis. Sci Transl Med. 2017;9(385).

Mitry D, Zutis K, Dhillon B, Peto T, Hayat S, Khaw KT, Morgan JE, Moncur W, Trucco E, Foster PJ; UK Biobank Eye and Vision Consortium. The Accuracy and Reliability of Crowdsource Annotations of Digital Retinal Images. Transl Vis Sci Technol. 2016 Sep 21;5(5):6.

Marquis S, Moore MM, Howieson DB, Sexton G, Payami H, Kaye JA, et al. Independent Predictors of Cognitive Decline in Healthy Elderly Persons. Arch Neurol 2002;59(4):601.
Mishra A, Wong A, Bizheva K, Clausi DA. Intra-retinal layer segmentation in optical coherence tomography images. Opt. Express. 2009;17(26):23719–23728.

Moreno-Ramos T, Benito-Leon J, Villarejo A, Bermejo-Pareja F. Retinal nerve fiber layer thinning in dementia associated with Parkinson's disease, dementia with Lewy bodies, and Alzheimer's disease. J Alzheimers Dis 2013;34(3):659–64.

Mormino EC, Betensky RA, Hedden T, Schultz AP, Amariglio RE, Rentz DM, Johnson KA, Sperling RA. Synergistic effect of β-amyloid and neurodegeneration on cognitive

decline in clinically normal individuals. JAMA Neurol. 2014 Nov;71(11):1379-85.

Mountjoy E, Davies NM, Plotnikov D, Smith GD, Rodriguez S, Williams CE, Guggenheim JA, Atan D. Education and myopia: assessing the direction of causality by mendelian randomisation. BMJ. 2018 Jun 6;361:k2022.

Mujat M, Chan R, Cense B, Park B, Joo C, Akkin T, Chen T, de Boer J. Retinal nerve fiber layer thickness map determined from optical coherence tomography images. Opt. Express. 2005;13(23):9480–9491.

Munoz B, West SK, Rubin GS, et al. Causes of blindness and visual impairment in a population of older Americans: the Salisbury Eye Study. Arch Ophthalmol. 2000;118:819-825.

Mutlu U, Colijn JM, Ikram MA, Bonnemaijer PWM, Licher S, et al. Association of retinal neurodegeneration on optical coherence tomography with dementia: a population-based study. JAMA Neurol. 2018 Oct 1;75(10):1256-1263.

Mwanza JC, Durbin MK, Budenz DL, et al; Cirrus OCT Normative Database Study Group. Profile and predictors of normal ganglion cell–inner plexiform layer thickness measured with frequency-domain optical coherence tomography. Invest Ophthalmol Vis Sci. 2011;52(11):7872-7879.

Myers CE, Klein BE, Meuer SM, et al. Retinal thickness measured by spectral-domain optical coherence tomography in eyes without retinal abnormalities: the Beaver Dam Eye Study. Am J Ophthalmol. 2015;159(3):445.e1–456.e1.

Na JH, Sung KR, Baek S, et al. Detection of glaucoma progression by assessment of segmented macular thickness data obtained using spectral domain optical coherence tomography. Invest Ophthalmol Vis Sci. 2012;53(7):3817-3826.

Naghizadeh F, Garas A, Vargha P, et al. Detection of early glaucomatous progression with different parameters of the RTVue optical coherence tomograph. J Glaucoma. 2014;23(4):195-198.

Nassif N, Cense B, Park B, Pierce M, Yun S, Bouma B, Tearney G, Chen T, and de Boer J. In vivo high-resolution video-rate spectral-domain optical coherence tomography of the human retina and optic nerve. Opt. Express 2004;12: 367-376.

Nevado-Holgado AJ, Kim CH, Winchester L, Gallacher J, Lovestone S. Commonly prescribed drugs associate with cognitive function: a cross-sectional study in UK Biobank. BMJ Open. 2016 Nov 30;6(11):e012177.

Okubo A, Rosa RH Jr, Bunce CV, Alexander RA, Fan JT, Bird AC, Luthert PJ. The relationships of age changes in retinal pigment epithelium and Bruch's membrane. Invest Ophthalmol Vis Sci. 1999 Feb;40(2):443-9.

Ooto S, Hangai M, Sakamoto A, et al. Three-dimensional profile of macular retinal thickness in normal Japanese eyes. Invest Ophthalmol Vis Sci. 2010;51(1):465– 473.

Ooto S, Hangai M, Tomidokoro A, Saito H, Araie M, et al. Effects of age, sex, and axial length on the three-dimensional profile of normal macular layer structures. Invest Ophthalmol Vis Sci. 2011 Nov 11;52(12):8769-79.

Panda-Jonas S, Jonas JB, Jakobczyk-Zmija M. Retinal photoreceptor density decreases with age. Ophthalmology. 1995 Dec;102(12):1853-9.

Panter J, Mytton O, Sharp S, Brage S, Cummins S, Laverty AA, Wijndaele K, Ogilvie D. Using alternatives to the car and risk of all-cause, cardiovascular and cancer mortality. Heart. 2018 May 21. [Epub ahead of print]

Paquet C, Boissonnot M, Roger F, Dighiero P, Gil R, Hugon J. Abnormal retinal thickness in patients with mild cognitive impairment and Alzheimer's disease. Neurosci Lett 2007;420(2):97–9.

Parikh RS, Parikh SR, Sekhar GC, Prabakaran S, Babu JG, Thomas R. Normal age-related decay of retinal nerve fiber layer thickness. Ophthalmology. 2007;114(5):921-6.

Parisi V, Restuccia R, Fattapposta F, Mina C, Bucci MG, Pierelli F. Morphological and functional retinal impairment in Alzheimer's disease patients. Clin Neurophysiol 2001;112(10):1860–7.

Patel PJ, Foster PJ, Grossi CM, Keane PA, Ko F, Lotery A, Peto T, Reisman CA, Strouthidis NG, Yang Q; UK Biobank Eyes and Vision Consortium. Spectral-Domain Optical Coherence Tomography Imaging in 67 321 Adults: Associations with Macular Thickness in the UK Biobank Study. Ophthalmology. 2016 Apr;123(4):829-40.

Piumatti G, Moore SC, Berridge DM, Sarkar C, Gallacher J. The relationship between alcohol use and long-term cognitivedecline in middle and late life: a longitudinal analysis using UK Biobank. J Public Health (Oxf). 2018 Jun 1;40(2):304-311.

Poplin R, Varadarajan AV, Blumer K, Liu Y, McConnell MV, Corrado GS, Peng L, Webster DR. Predicting cardiovascular risk factors from retinal fundus photographs using deep learning. ArXiv e-prints: https://arxiv.org/abs/1708.09843; 2017 accessed 17.11.07.

Quigley H.The number of people with glaucoma worldwide in 2010 and 2020. Br J Ophthalmol. 2006; 90(3):262-7.

Ramrattan RS, van der Schaft TL, Mooy CM, de Bruijn WC, Mulder PG, de Jong PT. Morphometric analysis of Bruch's membrane, the choriocapillaris, and the choroid in aging. Invest Ophthalmol Vis Sci. 1994 May;35(6):2857-64.

Rao HL, Kumar AU, Babu JG, Kumar A, Senthil S, Garudadri CS. Predictors of normal optic nerve head, retinal nerve fiber layer and macular parameters measured by spectral domain optical coherence tomograph. Invest Ophthalmol Vis Sci. 2011;52(2):1103–

1110.

Rauscher FM, Sekhon N, Feuer WJ, Budenz DL. Myopia affects retinal nerve fiber layer measurements as determined by optical coherence tomography. J Glaucoma. 2009 Sep;18(7):501-5.

Regillo C, Holekamp N, Johnson MW, Kaiser PK, Schubert HD, Spaide R, Griggs PB, Schmidt-Erfurth UM, editors. Basic and Clinical Science Course Section 12: Retina and Vitreous. San Francisco, CA: American Academy of Ophthalmology, 2010. Print.

Rougier MB, Korobelnik JF, Malet F, et al. Retinal nerve fibre layer thickness measured with OCT in a population-based study of French elderly subjects: the Alienor study. Acta Ophthalmol. 2015; 93(6):539–545.

Rudnicka AR, Jarrar Z, Wormald R, Cook DG, Fletcher A, Owen CG. Age and gender variations in age-related macular degeneration prevalence in populations of European ancestry: a meta-analysis. Ophthalmology. 2012 Mar;119(3):571-80.

Saint Martin M, Sforza E, Barthélémy JC, Roche F, Lefèvre P, Liénard G, Thomas-Anterion C; PROOF group study. Long-lasting active lifestyle and successful cognitive aging in a healthy elderly population: The PROOF cohort. Rev Neurol (Paris). 2017 Dec;173(10):637-644.

Schneider JA. Multiple Pathologic Pathways to Dementia in Football Players With

Chronic Traumatic Encephalopathy. JAMA Neurol. 2019 Aug 5. [Epub ahead of print]

Schrijvers, E.M., Buitendijk, G.H., Ikram, M.K., Koudstaal, P.J., Hofman, A., Vingerling, J.R., Breteler, M.M. Retinopathy and risk of dementia: the Rotterdam Study. Neurology. 2012;79:365-370.

Schuman JS, Hee MR, Puliafito CA, et al. Quantification of Nerve Fiber Layer Thickness in Normal and Glaucomatous Eyes Using Optical Coherence Tomography: A Pilot Study. Arch Ophthalmol. 1995;113(5):586–596.

Schuman JS, Pedut-Kloizman T, Hertzmark E et al. Reproducibility of nerve fiber layer thickness measurements using optical coherence tomography. Ophthalmology. 1996;103:1889-1898.

Shahidi M, Wang Z, Zelkha R. Quantitative thickness measurement of retinal layers imaged by optical coherence tomography. Am. J. Ophthalmol. 2005;139(6):1056–1061.

Shi Z, Wu Y, Wang M, Cao J, Feng W, Cheng Y, et al. Greater attenuation of retinal nerve fiber layer thickness in Alzheimer's disease patients. J Alzheimers Dis. 2014;40(2):277–83.

Shweikh Y, Ko F, Chan MP, Patel PJ, Muthy Z, Khaw PT, Yip J, Strouthidis N, Foster PJ; UK Biobank Eye and Vision Consortium. Measures of socioeconomic status and self-reported glaucomain the U.K. Biobank cohort. Eye (Lond). 2015 Oct;29(10):1360-7.

Smith, J.J., Sorensen, A.G., Thrall, J.H. Biomarkers in imaging: realizing radiology's future. Radiology. 2003;227:633-638.

Song WK, Lee SC, Lee ES, Kim CY, Kim SS. Macular thickness variations with sex, age, and axial length in healthy subjects: a spectral domain-optical coherence tomography study. Invest Ophthalmol Vis Sci. 2010;51(8):3913–3918.

Spaide RF and Curcio CA, Anatomical correlates to the bands seen in the outer retina by optical coherence tomography. Retina. 2011 Sep;31(8):1609-19.

Staurenghi G, Sadda S, Chakravarthy U, Spaide RF; International Nomenclature for Optical Coherence Tomography (IN•OCT) Panel. Proposed lexicon for anatomic landmarks in normal posterior segment spectral-domain optical coherence tomography: the IN•OCT consensus. Ophthalmology. 2014 Aug;121(8):1572-8.

Stites A. 2018 Feb 4. How Does the NFL's Concussion Protocol Work? Available at: https://www.sbnation.com/nfl/2016/9/18/12940926/nfl-concussion-protocol-explained. Accessed 7 Sept 2019.

Strauss, Olaf. The retinal pigment epithelium in visual function. Physiol Rev. 2005 Jul;85(3):845-81.

Sung KR, Kim DY, Park SB, Kook MS. Comparison of Retinal Nerve Fiber Layer Thickness Measured by Cirrus HD and Stratus Optical Coherence Tomography. Ophthalmology. 2009;116(7):1264-70.

Sung KR, Sun JH, Na JH. Progression detection capability of macular thickness in advanced glaucomatous eyes. Ophthalmology. 2012;119(2):308-313.

Sung KR, Wollstein G, Bilonick RA, Townsend KA, Ishikawa H, et al.
Effects of age on optical coherence tomography measurements of healthy retinal nerve fibre layer, macula, andoptic nerve head. Ophthalmology. 2009;116(6):1119-24.

Takagi S, Mandai M, Gocho K, Hirami Y, Yamamoto M, et al. Evaluation of Transplanted Autologous Induced Pluripotent Stem Cell-Derived Retinal Pigment Epithelium in Exudative Age-Related Macular Degeneration. Ophthalmol Retina. 2019 Apr 26. (Epub ahead of print)

Tan O, Chopra V, Lu AT, Schuman JS, Ishikawa H, Wollstein G, Varma R, Huang D. Detection of macular ganglion cell loss in glaucoma by Fourier-domain optical coherence tomography. Ophthalmology. 2009;116(12):2305-14.e1-2.

Tan O, Li G, Lu AT, Varma R, Huang D. Advanced Imaging for Glaucoma Study Group. Mapping of macular substructures with optical coherence tomography for glaucoma diagnosis. Ophthalmology. 2008;115(6):949–956.

Tilvis RS, Kahonen-Vare MH, Jolkkonen J, Valvanne J, Pitkala KH, Strandberg TE. Predictors of Cognitive Decline and Mortality of Aged People Over a 10-Year Period. Journals Gerontol Ser A Biol Sci Med Sci. 2004;59(3):268–74.

Tomita Y, Kubis N, Calando Y, Tran DA, Meric P, Seylaz J, Pinard E. Long-term in vivo investigation of mouse cerebral microcirculation by fluorescence confocal microscopy in the area of focal ischemia. J.Cereb. Blood Flow. Metab. 2005;25:858-867.

Tucker GS. Refractile bodies in the inner segments of cones in the aging human retina. Invest Ophthalmol Vis Sci. 1986 May;27(5):708-15.

Tuulonen A, Airaksinen PJ. Initial glaucomatous optic disk and retinal nerve fibre layer abnormalities and their progression. Am J Ophthalmol. 1991 Apr 15;111(4):485-90.

van Dijk HW, Kok PH, Garvin M, Sonka M, Devries JH, et al. Selective loss of inner retinal layer thickness in type 1 diabetic patients with minimal diabetic retinopathy. Invest. Ophthalmol. Vis. Sci. 2009;50(7):3404–3409.

van Koolwijk LME, Despriet DDG, Van Duijn CM, Oostra BA, van Swieten JC, et al. Association of cognitive functioning with retinal nerve fiber layer thickness. Invest Ophthalmol Vis Sci 2009;50(10):4576–80.

Vanderbeek BL, Zacks DN, Talwar N, Nan B, Musch DC, Stein JD. Racial differences in age-related macular degeneration ratesin the United States: a longitudinal analysis of a managed care network. Am J Ophthalmol. 2011 Aug;152(2):273-282.e3.

Varma R, Bazzaz S, Lai M. Optical Tomography–Measured Retinal Nerve Fiber Layer Thickness in Normal Latinos. Invest Ophthalmol Vis Sci. 2003;44(8):3369-73.

Varma R, Skaf M, Barron E. Retinal Nerve Fiber Layer Thickness in Normal Human Eyes. Ophthalmology. 1996;103(12):2114-9.

Vermeer SE, Hollander M, van Dijk EJ, Hofman A, Koudstaal PJ, et al. Silent brain infarcts and white matter lesions increase stroke risk in the general population: the Rotterdam Scan Study. Stroke. 2003;34:1126-1129.

Vetter C, Dashti HS, Lane JM, Anderson SG, Schernhammer ES, et al. Night Shift Work, Genetic Risk, and Type 2 Diabetes in the UK Biobank. Diabetes Care. 2018 Apr;41(4):762-769.

Vianna JR, Danthurebandara VM, Sharpe GP, Hutchison DM, Belliveau AC, et al. Importance of Normal Aging in Estimating the Rate of Glaucomatous Neuroretinal Rim and Retinal Nerve Fibre Layer Loss. Ophthalmology. 2015 Dec;122(12):2392-8.

Vision 2020: Right to Sight. GBVI – Regional Summaries. Available at: http://atlas.iapb.org/global-burden-vision-impairment/regional-summaries/#western-europe. Accessed June 19, 2018.

Wakitani Y, Sasoh M, Sugimoto M, Ito Y, Ido M, Uji Y. Macular thickness measurements in healthy subjects with different axial lengths using optical coherence tomography. Retina. 2003;23(2): 177–182.

Wang J, Gao X, HuangW, et al. Swept-source optical coherence tomography imaging of macular retinal and choroidal structures in healthy eyes. BMC Ophthalmol. 2015;15(15):122.

Wang JJ, Foran S, Mitchell P. Age-specific prevalence and causes of bilateral and unilateral visual impairment in older Australians: the Blue Mountains Eye Study. Clin Exp Ophthalmol. 2000;28:268-273.

Wang M, Hood DC, Cho JS, Ghadiali Q, De Moraes GV, Zhang X, Ritch R, Liebmann JM. Measurement of local retinal ganglion cell layer thickness in patients with glaucoma using frequency-domain optical coherence tomography. Arch. Ophthalmol. 2009;127(7):875–881.

Ward ME, Chen R, Huang HY, Ludwig C, Telpoukhovskaia M et al. Reproducibility of nerve fiber layer thickness measurements using optical coherence tomography. Ophthalmology. 1996;103:1889-1898.

Wei Y, Jiang H, Shi Y, Qu D, Gregori G, Zheng F, Rundek T, Wang J. Age-Related Alterations in the Retinal Microvasculature, Microcirculation, and Microstructure. Invest Ophthalmol Vis Sci. 2017 Jul 1;58(9):3804-3817.

Weil RS, Schrag AE, Warren JD, Crutch SJ, Lees AJ, Morris HR. Visual dysfunction in Parkinson's disease. Brain 2016;139: 2827–43.

Whitson HE, Farsiu S, Stinnett S, Lee S, Kwark L, Potter G, et al. Retinal imaging biomarkers for early diagnosis of Alzheimer's disease. Invest Ophthalmol Vis Sci. 2015;56(7):389.

Wirth M, Villeneuve S, Haase CM, Madison CM, Oh H, Landau SM, Rabinovici GD, Jagust WJ. Associations between Alzheimer disease biomarkers, neurodegeneration, and cognition in cognitively normal older people. JAMA Neurol. 2013 Dec;70(12):1512-9.

Woodell A, Rohrer B. A mechanistic review of cigarette smoke and age-related macular degeneration. Adv Exp Med Biol. 2014;801:301-7. doi: 10.1007/978-1-4614-3209-8_38.

Wong AC, Chan CW, Hui SP. Relationship of gender, body mass index, and axial length with central retinal thickness using optical coherence tomography. Eye (Lond). 2005;19(3):292–297.

Wong WL, Su X, Li X, Cheung CM, Klein R, Cheng CY, Wong TY. Global prevalence of age-related macular degeneration and disease burden projection for 2020 and 2040: a systematic review and meta-analysis. Lancet Glob Health. 2014 Feb;2(2):e106-16.

World Health Organization. Prevention of blindness and visual impairment: Causes of blindness and visual impairment. Available at http://www.who.int/blindness/causes/en/. Accessed September 15, 2018.

World Health Organization. World Health Report 2003—Shaping the future. Geneva: WHO, 2003.

Wu PC, Chen YJ, Chen CH, et al. Assessment of macular retinal thickness and volume in normal eyes and highly myopic eyes with third-generation optical coherence tomography. Eye (Lond). 2008; 22(4):551–555.

Yang Q, Reisman CA, Chan K, Ramachandran R, Raza A, Hood DC. Automated segmentation of outer retinal layers in macular OCT images of patients with retinitis pigmentosa. Biomed Opt Express. 2011 Sep 1;2(9):2493-503.

Yang Q, Reisman CA, Wang Z, Fukuma Y, Hangai M, et al. Automated layer segmentation of macular OCT images using dual-scale gradient information. Opt Express. 2010;18(20):21293-307.

Zhang X, Francis BA, Dastiridou A, et al. Longitudinal and cross-sectional analyses of age

effects on retinal nerve fibre layer and ganglion cell complex thickness by fourier-Domain OCT. Trans Vis Sci Tech. 2016;5(2):1.

Zou H, Zhang X, Xu X, Yu S. Quantitative in vivo retinal thickness measurement in chinese healthy subjects with retinal thickness analyzer. Invest Ophthalmol Vis Sci. 2006;47(1):341–347.

Zhou A, Taylor AE, Karhunen V, Zhan Y, Rovio SP, et al. Habitual coffee consumption and cognitive function: a Mendelian randomization meta-analysis in up to 415,530 participants. Sci Rep. 2018 May 14;8(1):7526.

Zhu Z, Lee PH, Chaffin MD, Chung W, Loh PR, Lu Q, Christiani DC, Liang L. A genome-wide cross-trait analysis from UK Biobank highlights the shared genetic architecture of asthma and allergic diseases. Nat Genet. 2018 May 21. [Epub ahead of print]